

TECHNISCHE UNIVERSITÄT MÜNCHEN

Lehrstuhl für Experimentelle Genetik

# **Screen to identify the novel pancreatic gene *Synaptotagmin 13 (Syt13)***

Stefanie Julia Willmann

Vollständiger Abdruck der von der Fakultät Wissenschaftszentrum Weihenstephan für Ernährung, Landnutzung und Umwelt der Technischen Universität München zur Erlangung des akademischen Grades eines

Doktor der Naturwissenschaften

genehmigten Dissertation.

Vorsitzender: Univ. Prof. Dr. E. Grill

Prüfer der Dissertation:

1. Univ. Prof. Dr. M. Hrabe de Angelis
2. Univ. Prof. Dr. H. Lickert

Die Dissertation wurde am ....16/03/2016.... bei der Technischen Universität München eingereicht und durch die Fakultät Wissenschaftszentrum Weihenstephan für Ernährung, Landnutzung und Umwelt am ....22/06/2016.... angenommen.



## Danksagung

Ich möchte mich auf dieser Seite bei allen bedanken die mich auf diesem Weg begleitet haben. Insbesondere will ich hier einige beim Namen nennen.

Insbesondere will ich mich bei Herrn Professor Dr. Heiko Lickert bedanken, für die Möglichkeit meine Promotion in seiner Arbeitsgruppe anzufertigen. Die Begeisterung für die Wissenschaft und dein Wissen hat mich stark beeindruckt. Ausserdem will ich mich natürlich noch bei Professor Dr. Martin Hrabe de Angelis bedanken, für die Unterstützung und fachliches Wissen.

Bei Herrn Professor Dr. Grill bedanke ich mich herzlich für den Vorsitz in meiner Prüfungskommission.

Bei dem Team der Arbeitsgruppe Lickert will ich mich für die langjährige Unterstützung bedanken. Besonders Dr. Ingo Burtcher für das offene Ohr bei allen Fragen, die Einführung in konfokale Mikroskopie, Immunhistochemische Färbungen und ES Zellkultur. Bei Dr. Aurelia Raducanu für die Unterstützung in dem nicht immer leichten Screening Projekt und die anschliessende Mausearbeit. Zusätzlich noch bei Dr. Mostafa Bahkti für die Unterstützung und Übernahme im Syt13 Projekt. Ausserdem will ich Aimee Bastidas-Ponce viel Erfolg bei der Weiterführung wünschen – es ist ein vielversprechendes Projekt.

Insbesondere gilt mein Dank an Dr. Bomi Jung, Heide Oller und Dr. Alexander Korostylev für die Unterstützung und hilfreichen Tipps. Auch geht ein herzlicher Dank an Dr. Silvia Engert für die Unterstützung in manchmal schwierigen Situationen. Donna Thompson – du bist eine Perle und dir gebührt extra Dank für deinen besonderen Einsatz in der Arbeitsgruppe. Anne, Wenke, Bianca und Kerstin haben wundervoll geholfen bei alltäglichen Problemen und Arbeiten wie PCRs, Maushausbesuche, Bestellungen und andere kleine Dinge im Laboralltag. Ausserdem noch zu erwähnen sind Dr. Nikola Müller, Steffen Sass, Dr. Martin Irmeler und Dr. Harald Staiger für die gute Zusammenarbeit und Austausch in den verschiedenen Projekten.

Ausserdem will ich mich noch bei dem IDR Team bedanken für die Unterstützung und Informationen die das Projekt vorangetrieben haben. Hier geht mein besonderer Dank an Daniela Padula, Martin Preusse, Esra Karaköse, Anika Böttcher, Noah Mozurri, Lisann Heyner und Felizitas Schmid und natürlich nicht zu vergessen Erik Bader.

Aber der größte Dank geht an meine Familie für die Unterstützung in der Zeit – Danke das ihr für mich da wart und immer ein offenes Ohr hattet. Danke auch an Alex, Alex, Manu, Dani, Alex, Elke und nicht zu vergessen Rainer!

# Contents

<b>1</b>	<b>Abstract</b> .....	7
1.1	The early embryonic development .....	10
1.2	Development of endodermal derived organs .....	11
1.3	Development of the pancreas .....	13
1.4	Regulatory networks of pancreas development .....	15
1.5	The model of endocrine formation .....	18
1.6	Establishment of epithelial asymmetry .....	20
1.7	The family of <i>Synaptotagmins (Syt)</i> .....	22
1.8	Aim of this thesis .....	24
<b>2</b>	<b>Results</b> .....	25
2.1	Generation of the <i>Foxa2<sup>Venus</sup></i> mouse line.....	25
2.1.1	Design and generation of the <i>Foxa2<sup>Venus</sup></i> (FVF) targeting vector .....	25
2.1.2	Analysis of the <i>Foxa2<sup>Venus</sup></i> mouse line in the pancreas .....	27
2.2	Genome-wide expression profile of the pancreas in the secondary transition.....	32
2.2.1	Bioinformatic analysis of pathways in the secondary transition.....	33
2.2.2	Bioinformatic analysis of genes in the secondary transition.....	36
2.3	Identification and characterization of pancreatic genes.....	39
2.3.1	Temporal and spatial progression of pancreatic genes .....	44
2.3.2	Temporal and spatial progression of unknown pancreatic genes .....	48
3.4	Analysis of the novel pancreas gene <i>Synaptotagmin 13 (Syt13)</i> .....	52
3.4.1	Bioinformatic analysis of <i>Syt13</i> .....	52
3.4.1.1	The family of <i>Synaptotagmins</i> .....	52
3.4.1.2	Interaction partner of SYT13 .....	55
3.4.1.3	Target gene prediction of SYT13 .....	56

---

3.4.2 Functional analyses of <i>Syt13</i> .....	57
3.4.2.1 The gene <i>Syt13</i> .....	57
3.4.2.2 The amino acid (aa) sequence of <i>Syt13</i> .....	58
3.4.3 Generation of the genetically modified mouse line <i>Syt13</i> .....	60
3.4.3.1 Design, generation and verification of the <i>Syt13<sup>GT</sup></i> targeting vector.....	60
3.4.4 <i>Syt13</i> mutant mice illustrate expression in diverse ciliated tissues.....	64
3.4.4.1 <i>Syt13</i> reporter gene expression in the early embryo.....	65
3.4.4.2 Characterization of <i>Syt13</i> reporter gene expression in the crown .....	66
3.4.5 <i>Syt13</i> mutants present defects in the adult pancreas .....	69
3.4.6 <i>Syt13</i> expression in pancreas organogenesis .....	72
3.4.7 <i>Syt13</i> associated SNP reveal T2D susceptibility .....	82
3.4.8 Delamination of endocrine precursors in <i>Syt13</i> mutants is impaired.....	83
3.4.9 <i>Syt13</i> mutants show polarity defects .....	87
<b>4. Discussion</b> .....	94
4.1 <i>FVF</i> marks the multipotent progenitors in the pancreas .....	94
4.2 The <i>FVF</i> mouse line is a valuable tool for genome wide expression profiles.....	94
4.3 Molecular pathways guiding pancreas organogenesis .....	96
4.4 The pancreas gene selection for known and unfamiliar genes.....	98
4.5 Generation of different mouse lines .....	100
4.6 Generation of the <i>Syt13<sup>GT/GT</sup></i> mouse line .....	101
4.7 <i>Syt13</i> expression in a distinct subset of tissue .....	101
4.8 Pancreatic multipotent progenitors and endocrine cells marked by <i>Syt13</i> .....	102
4.9 <i>Syt13</i> initiates morphogenesis in the pancreatic epithelium.....	103
4.10 The subcellular localization of <i>Syt13</i> suggests a role in polarity membrane complexes along with BB positioning.....	104
4.11 Potential mechanism of <i>Syt13</i> in endocrine lineage formation.....	106

---

4.12 Hypothetical molecular function of <i>Syt13</i> .....	108
<b>5 Material and Methods</b> .....	<b>110</b>
5.1 Material .....	110
5.1.1 Equipment .....	110
5.1.2 Consumables .....	111
5.1.3 Kits .....	112
5.1.4 Chemicals.....	112
5.1.5 Buffer and solutions .....	115
5.1.6 Enzymes.....	118
5.1.7 Sera and Antibodies.....	119
5.1.8 Oligonucleotides.....	121
5.1.9 Cell lines.....	122
5.1.10 Culture media .....	122
5.1.11 Molecular weight markers .....	123
5.1.12 Mouse lines .....	124
5.2 Methods .....	125
5.2.1 Bioinformatics methods .....	125
5.2.1.1 Affymetrix®Gene 1.0 ST Array.....	125
5.2.1.2 Affymetrix®Gene 1.0 ST Array card .....	125
5.2.1.3 Affymetrix®Gene 1.0 ST Array card quality control.....	125
5.2.1.4 Affymetrix®Gene 1.0 ST Array card analysis .....	126
4.2.1.5 Pancreas gene selection using the digital database Genepaint.org .....	127
5.2.2 Cell culture.....	127
5.2.2.1 Embryonic stem cell culture and spheres culture .....	128
5.2.2.2 Culture of primary murine embryonic fibroblasts .....	128
5.2.2.3 Treatment of MEF with mytomycin .....	128

---

5.2.2.4 Freezing –Thawing of MEFs.....	128
5.3 Molecular biology.....	130
5.3.1 DNA extraction .....	131
5.3.2 RNA preparation.....	131
5.3.3 DNA/RNA concentration .....	132
5.3.4 Reverse transcription .....	132
5.3.5 Gelelectrophorese.....	133
5.3.6 DNA sequencing .....	133
5.4 Protein biochemistry .....	134
5.4.1 Protein extraction from tissue.....	134
5.4.2 Bradford assay for determining protein concentration .....	134
5.4.3 Western blot.....	134
5.4.4 Western blot immunostaining.....	137
5.4.5 Immunohistochemistry .....	137
5.5 Embryology.....	138
5.5.1 Genotyping of mice and embryos .....	138
5.5.2 PCR Programs for genotyping .....	139
5.5.3 Isolation of embryos and organs.....	141
5.5.4 Tissue clearing with BABB .....	141
5.5.5 X-gal (5-bromo-4-chloro-3-indolyl $\beta$ -D-galactoside) staining.....	142
5.6 Histology.....	142
5.6.1 Paraffin sections .....	142
5.6.2 Counterstaining with Nuclear Fast Red (NFR) .....	143
5.6.3 Cryosections .....	143
<b>6 Supplement.....</b>	<b>144</b>
6.1 Abbreviations .....	144

---

6.2 Figures and tables.....	154
6.4 Curriculum Vitae.....	212
6.6 Congresses and Publications .....	213
6.7 Additional Figures.....	214

---

# 1 Abstract

## Screen to identify the novel pancreatic gene *Synaptotagmin 13 (Syt13)*

The multipotent pancreatic progenitors segregate in the secondary transition (E12.5-15.5) into the pancreatic lineages endocrine, ductal and acinar in mouse development. Different signaling pathways as WNT, FGF, Notch, BMP, SHH and RA define anterior-posterior axis and the lineage decision of the organ. The precise mechanism of the formation of the endocrine lineage will allow generation of *in vitro*  $\beta$ -cells for cell-replacement therapy and identify potential disease genes. Thus, we utilized the *Foxa2-Venus fusion (FVF)* knock-in reporter mouse to separate the pancreatic endodermal epithelium (*FVF<sup>+</sup>*) from the surrounding non-endodermal tissue (*FVF<sup>-</sup>*) in the secondary transition. Subsequent global gene expression analyses identified 886 temporal significantly regulated genes in both tissue compartments. By using the public database Genepaint, spatial expression of the genes in the embryo and in the pancreatic region was analyzed in classifying the *in situ mRNA* expression pattern at E14.5 into tip/acinar, epithelium and mesenchyme. In a next step, GO term analyses classified the majority of the genes according to their predicted protein function. The selection of pancreatic genes, yet functionally not described are under the criteria of temporal regulated expression in the secondary transition, lineage prognosis by spatial pancreatic *mRNA* hybridization pattern and predicted protein function. In a next step, we generated Knock in/knock out mice lines to analyze the function and mechanism of these pancreatic candidate genes. Taken together, we successfully accomplished a global gene expression profile during secondary transition of the pancreas, inspected WNT, FGF, Notch, BMP, SHH pathway components and pancreatic lineage determinants. The pancreatic gene candidate, *Synaptotagmin 13 (Syt13)* is expressed in the secondary transition, the trunk *mRNA* hybridization pattern similar to endocrine TF factor *Ngn3* and the gene functionally not described. *Syt13* is a member of the large family of *Synaptotagmins* that are known to regulate vesicle docking and fusion for neurotransmitter and secretory granule release. Expression analysis using the *Syt13 lacZ* reporter gene revealed endocrine-specific expression in pancreas organogenesis and in the adult Islets of Langerhans. In addition, we observe in *Syt13* deficient pancreas delamination defects of endocrine progenitors during secondary transition. Also, we quantified a decline of endocrine differentiated cells characterized through Insulin. In collaboration with Harry Staiger and Hans-Ullrich Häring from the University in Tübingen we identified a single nucleotide polymorphisms (SNP; rs11038374) in *SYT13* that correlates with insulin secretion defects in a cohort of 2100 individuals with increased risk for diabetes. Thus, *Syt13* is expressed and regulates the endocrine lineage in mouse and may present a promising target for diabetes therapy.

---

## Screening und Identifizierung des neuen Pankreas Gen *Synaptotagmin 13 (Syt13)*

In der Pankreasentwicklung differenzieren aus einem Pool von Vorläuferzellen in der sekundären Transition (E12.5-15.5) die endokrine, exokrine und duktales Zelllinien. In dem Prozess selbst sind Gewebeinteraktionen und komplexe Signalwege involviert. Wir haben ein Transkriptionsprofil erstellt um die zeitliche und räumliche Expression regulatorischer und funktioneller Gene zu charakterisieren. Dabei haben wir spezifisch als Zeitpunkt die sekundäre Transition gewählt in der sich die verschiedenen pankreatischen Zelllinien abspalten.

Mit der Forkhead Transkriptionsfaktor *Foxa2<sup>Venus</sup>* (*FVF*) Mauslinie konnten wir pankreatisches Epithelium (*FVF<sup>+</sup>*) von umgebenden Mesenchym (*FVF<sup>-</sup>*) trennen. In dem anschließenden globalen Transkriptionsprofil identifizierten wir 886 signifikant regulierte Gene in beiden Kompartimenten, was auf essentielle Gewebeinteraktionen in der Pankreasentwicklung hinweist. Die Expression aus unserem Profil konnten wir dann mit der öffentlich zugänglichen Datenbank Genepaint für bekannte und unbekannte Gene bestätigen. Mit diesem Ansatz haben wir zudem die unterschiedlichen pankreatischen Linien nach bestimmten Mustern klassifiziert und zwar in Exokrin, Endokrin und Mesenchym. Für bekannte und unbekannte pankreatische Gene konnten wir somit die zeitlich und räumlich begrenzte Expression bei der Abspaltung in unterschiedlichen pankreatischen Linien und die entsprechende Linie aufzeigen. In einem nächsten Schritt generierten wir verschiedene transgene Mauslinien um Funktion und Mechanismus der unbekannt Genen näher zu untersuchen. Zusammengefasst zeigt unser Transkriptionsprofil, dass bekannte und unbekannte Gene in Gewebeinteraktionen und Stoffwechselwegen notwendig sind für die Entwicklung des Pankreas.

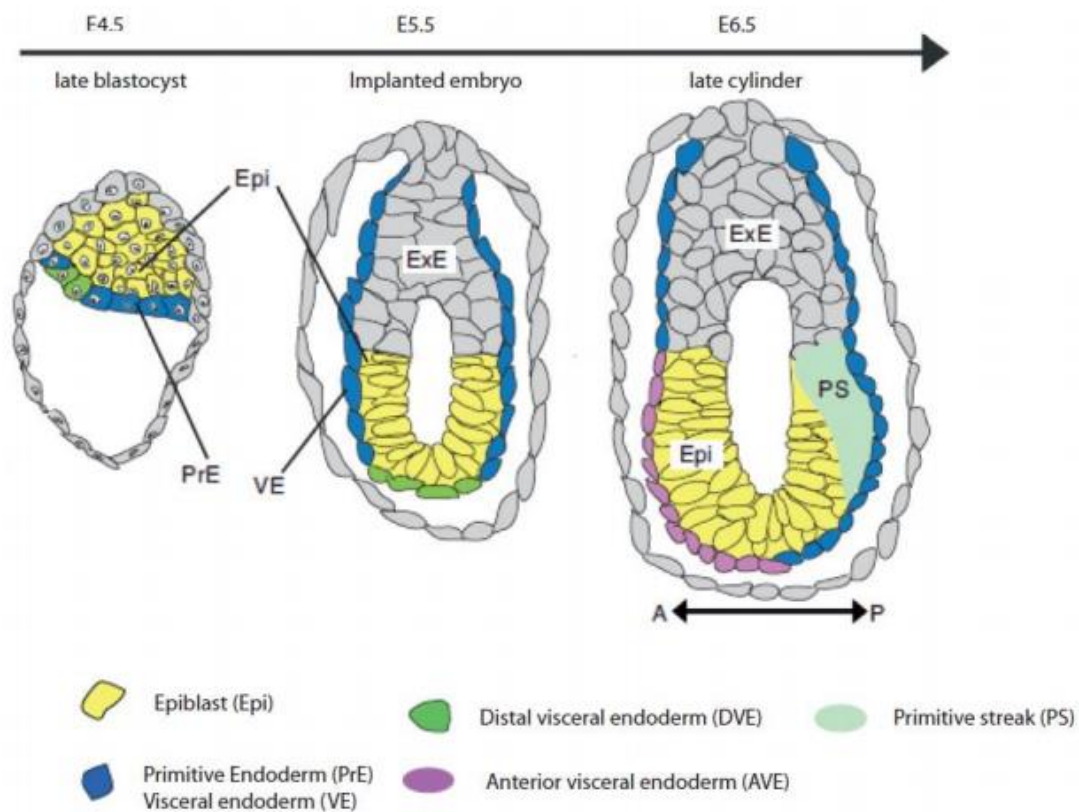
Eines der unbekannt identifizierten Gene ist *Synaptotagmin 13 (Syt13)*, mit räumlich und zeitlich begrenzter Expression in der sekundären Transition. Erste *LacZ* Reporter Gen Expressionsdaten weisen auf *Syt13* in endokrinen Zellen und adulten Langerhans'schen Inseln hin. Wir zeigen, dass *Syt13* im Pankreas notwendig ist für die Abspaltung in die endokrine Linie und für die Bildung der endokrinen Zellmasse. In Kollaboration mit Harry Staiger (Universität Tübingen) konnten wir zudem *Syt13* direkt auf Diabetes beziehen, Genome-wide association studies (GWAS) Studien zeigen auf single nucleotide polymorphism (SNP; rs11038374) in *SYT13* die Defekte in der Insulinsekretion aufweisen. Unsere Daten schlagen vor, dass *Syt13* in der endokrinen Zellentstehung eine Rolle spielt. Die weiteren Aussichten für *Syt13* sind dabei therapeutische Ansätze um endokrine Linien zu expandieren oder um diese zu induzieren.



## Introduction

### 1.1 The early embryonic development

The development of the embryo starts with the formation of the zygote out of the fertilized egg. Thus, the fertilized zygote is capable of producing all the different lineages responsible for the embryo proper. Subsequent cell divisions onwards lead from the zygote to the 8-cell stage, termed as morula (Gardner 2001; Piotrowska and Zernicka-Goetz 2001; Piotrowska-Nitsche and Zernicka-Goetz 2005). These 5 cell cycles are commonly referred to as cleavage decisions, which occur in the absence of cellular growth or in the increase of total cell mass – leading to the blastocyst. At embryonic stage (E) 3.5, a cavity will form in the early blastocyst and will separate the embryo into two cell populations: the outer lining extraembryonic trophoderm (TE) and the inner cell mass (ICM), oriented at one side of the cavity. This lineage segregation process is determined as the first cell fate decision. Further differentiation occurs within the ICM, specifying in the second cell fate decision the primitive Endoderm (PrE) and the Epiblast (Epi) (Figure 2.1 – late blastocyst). The PrE does not contribute to the embryo itself, presumably later as extra-embryonic (ExE) tissue to the yolk sac, whereas the ICM gives rise to the embryo proper (Cockburn and Rossant 2010; Johnson et al. 1986). Prior implantation into the maternal uterus at E4.5, the embryo elongates to an egg-shaped structure. The PrE covers the Epi in the cavity, so that the embryonic lineage will be enclosed by the PrE on one side and by the TE on the other side. In the next step, the PrE expands and lines the luminal surface of the TE and the distal visceral endoderm (DVE) (Figure 2.1 – implanted embryo). Thus, the DVE mediates activity of wingless type MMTV integration family (WNT), fibroblast growth factor (FGF), Bone morphogenetic protein (BMP) and Nodal for the differentiation and patterning of the Epi (Lewis and Tam 2006; Sumi et al. 2013; Sumi et al. 2008; de Sousa Lopes et al., 2004; Beddington and Robertson 1999). In a next step, the Anterior-Posterior (AP) patterning of the body axis is initiated in a dynamic process by variations in the endodermal structure, regionalized gene expression domains and morphogenetic signaling (Tam and Loebel, 2007). At E6.5, the cells of the DVE migrate into the prospective anterior region of the embryo and become the anterior visceral endoderm (AVE) of the late cylinder (Figure 2.1 – late cylinder). In the AVE activity of Wnt and Nodal inhibitors restrict the action of this signaling pathways to the posterior side of the embryo. Thus, formation of the primitive streak (PS) is initiated posterior of the AVE. With the formation of the PS at E6.5, the gastrulation and establishment of the three principal germ layers takes place (Beddington and Robertson 1999; Bartscher and Lickert 2009; Lawson et al. 1986).



modified from Arias et al., 2013

**Figure 2.1: Early stages of mouse embryo development**

In the blastocyst cells get orientated into Epi, distal visceral endoderm (DVE) and primitive endoderm (PrE). The Extraembryonic tissue (ExE) does not contribute to the embryo itself. After implantation Epi cells are immigrating into the primitive streak, egress and displace the AVE. Prior to gastrulation, proximal-distal (PD) and AP are established through morphogenetic signals.

Abbreviations: ExE = Extraembryonic; VE = Visceral endoderm; PrE = Primitive endoderm; Epi = Epiblast; AP = Anterior-Posterior; DVE = Distal visceral endoderm; AVE = Anterior visceral endoderm; PS = Primitive streak; PrE = primitive endoderm.

## 1.2 Development of endodermal derived organs

The gastrulation is initiated through formation of the PS on the opposite side of the AVE. In the steps of gastrulation, Epi cells migrate into the PS and segregate into distinct cell populations. The clonal analysis of Epi fate highlighted that temporal and spatial ingressions of the Epi in the PS defines the three principal germ layers: endoderm, mesoderm and ectoderm.

With this in mind, Epi cells remaining in the blastocyst are still competent of the different embryonic lineages (Morani et al., 2013). As gastrulation is initiated, the Epi cells migrate through the posterior region in the PS and transform into the Exe mesoderm (Kinder et al., 1999). The center and most likely

anterior part of the PS contributes to the mesodermal derived cells as cardiac, cranial, paraxial and axial mesoderm (Kinder et al., 2001). Contrary, the most anterior end of the PS forms the definitive endoderm (DE) (Wells and Melton 1999; Engert et al. 2013). In further steps migrates the DE to the anterior region of the embryo via different routes and displaces the AVE. At the end of gastrulation, the DE covers as a cell-layer sheet the embryo with approximately 500 cells. (Tam and Loebel 2007; Lawson and Pedersen 1987). The DE will form the primitive gut tube through folding of this epithelial sheet. The folding appears at the anterior and posterior ends. Thus, anterior endoderm forms the anterior intestinal portal (AIP) defining the foregut and equally, the posterior endoderm folds to establish the caudal intestine portal (CIP) defining the hindgut region. At the end of folding of the DE, turning of the whole embryo completes internalization as a tube. The derivatives of the gut regions are regionalized in foregut, midgut and the hindgut. The foregut gives rise to the largest number of structures; it forms the pharynx and its derivative as the respiratory part, esophagus, stomach, duodenum and the liver with the pancreas. The midgut is the supplier of the gastrointestinal part of the embryo, with the exception of the upper duodenum. Contrary, the hindgut contributes to the urogenital tract (The atlas of mouse development).

In the ventral foregut endoderm development, organ domains are established through transcription factors and signals from the mesenchyme. The hepatic endoderm is induced by FGF signaling from the mesenchyme and is marked by *Hematopoietically expressed Homeobox (Hhex)* expression, establishing the liver (Zorn and Wells 2010; Zorn and Wells 2009) The first obvious indication of pancreas morphogenesis takes place approximately at embryonic stage E8.0. It is noteworthy that all pancreatic epithelial cells derive from a common pool of pancreatic progenitors that evaginate from the dorsal and ventral section of the foregut/midgut junction. A signaling cascade mainly contributed by mesodermal-derived FGF, BMP, WNT, Activin A, retinoic acid (RA) and repression of sonic hedgehog (SHH) leads to the outgrowth of the pancreatic protrusions (Raducanu and Lickert 2012; Pan and Wright 2011). Upon a gut rotation between E11 and E12, the ventral pancreas switches dorsally and the proximity to the dorsal pancreatic bud leads to the fusion of the two lobes. This period involves tubulogenesis in the ongoing organogenesis which includes micro lumen fusion and the rearrangement of the epithelial sheet into a stratified epithelium (Kesavan et al. 2009). Along with plexus remodeling and proliferation, the pancreatic epithelium (PE) transforms into a branched single luminal ductal system. Simultaneously, in the so called secondary transition, the PE differentiates into the pancreatic lineages Subsequently, the formerly multipotent pancreatic progenitors (MPP) will be specified by lineage commitment through a temporal and spatial restricted transcription factor program. Lineage tracing experiments and Gain/Loss-of function analyses in genetically modified mice further gained

insights into the morphogenetic and transcriptionally mechanism which facilitate maturation of the pancreatic anlagen (Mehta and Gittes 2005; Li et al. 2004; Gittes et al. 1996).

The earliest transcription factors that characterize the pancreatic buds are *Pancreatic and duodenal factor 1 (Pdx1)*, *pancreas transcription factor 1 alpha (Ptf1 $\alpha$ )* and *Homeobox Protein HB9 (Hlxb9)*. In addition, combined ectopic expression of *Pdx1* and *Ptf1 $\alpha$*  converts posterior endoderm into endocrine and exocrine pancreatic tissue, highlighting the importance of both factors for pancreas initiation (Afelik et al. 2006; Sherwood et al. 2009) Although, *winged helix/forkhead box 1/2 (Foxa1/2)*, *NK homeobox x 6-1 (Nkx6-1)* and *Nkx2-2* are co-expressed in the pancreatic initiation stage, but their expression is broadly prevalent in the foregut endoderm. These multipotent cells give later on rise to all the different lineages of the adult pancreas, consisting of exocrine, ductal and endocrine cell. A landmark article by Golosow and Grobstein demonstrated that cytodifferentiation of the PE is promoted by the surrounding non-endodermal tissue. Experiments either stripping of the mesenchyme of the endodermal-derived, as well as pancreatic explants separated by a porous barrier of the non-endodermal part in trans filter experiments, could define the necessity of tissue interactions. In both projections the PE failed to proliferate. Thus, highlighting the tissue interaction in pancreas organogenesis (Golosow et al., 1962; Willmann et al., 2015).

### 1.3 Development of the pancreas

The adult pancreas is a compound gland which is important for the nutrient metabolism and composes of an exocrine compartment with acinar cells and ductal cells and an endocrine compartment composed of  $\alpha$ ,  $\beta$ ,  $\epsilon$ ,  $\delta$  and pancreatic polypeptide (PP) cells organized in structures called the Islets of Langerhans. The acinar cells secrete digestive enzymes which are transported through the ductal system into the duodenum where they catalyze the digestion of nutrients. The endocrine cells secrete hormones such as glucagon, insulin, ghrelin, somatostatin and PP into the blood stream to maintain a fine balanced hormone homeostasis. Understanding the developmental process that leads to the formation of the functional organ is essential to generate potential therapeutic strategies for diabetes (Zorn and Wells 2010; Zorn and Wells 2009).

Pancreas formation appears at around E8.0 likely in the last steps of gastrulation with the separation of the primitive gut tube into foregut and hindgut. In this stage, inductive mesodermal signals including FGFs, BMPs, Activin and RA induce an area in the lateral endoderm and a dorsal domain in the

midline endoderm to become pancreatic tissue as shown by expression of the transcription factor (TF) *Pdx1*, a key regulator of pancreas development (Stanger et al. 2007; Mehta and Gittes 2005; Gittes et al. 1996; Gittes et al., 2009). Continuous signals of Wnt and FGF-signaling from the surrounding tissues activate expansion of the two buds into the surrounding mesenchyme. The stratified epithelium becomes polarized and microlumens are generated throughout the bud which later fuse together to form a luminal epithelial plexus (Figure 2.2). The stratified epithelial bud contains MPP and few differentiated endocrine cells which are mainly glucagon-positive (Herrera et al., 2000). This first differentiation event takes place between E9.0 and E11.5 is called the primary transition. At around E11.5, gut tube rotation brings the two pancreatic buds in close proximity to one another and this event leads to their fusion into a single pancreatic primordium, which shapes the future organ. Massive plexus remodeling leads to the organization of a tubular structure from which branches continue to form through an epithelial branching morphogenesis process. The epithelial cells are still multipotent and capable of differentiation into the three pancreatic lineages: duct, acinar and endocrine. From E12.5 until E15.5, the three pancreatic lineage decisions are subsequently being made in the process of the secondary transition. The segregation of the epithelium initiates patterning into a distal tip region and a proximal trunk. Thereby, the cells representing the tip region will be assigned for the exocrine lineage, which are characterized through expression of *Carboxypeptidase 1 (Cpa1)*, which expresses cells and co-expression of *Ptf1 $\alpha$* . The pattern of the trunk region is commonly represented by ductal/endocrine factors illustrated through *Sry related Homeobox 9 (Sox9)* and *Neurogenin 3 (Ngn3)*. Thus, the ductal cells are bi-potent for either the ductal or endocrine lineage and restricted in the MPP PE. In the secondary transition at E12.5 – 15.5 in the ductal compartment the progenitor pool of the endocrine progenitors marked by *Ngn3*<sup>+</sup> cells delaminate out of the ductal cord through a process which is likely regarded as epithelial-mesenchymal transition (EMT) (Gouzi et al. 2011). Shortly after delamination, the endocrine precursors migrate into the PE and aggregate into the precursor Islets of Langerhans. From E18.5 onwards and in the first days after birth, the Islet of Langerhans morphogenesis takes place, which are indicated through the  $\alpha$ -,  $\delta$ -,  $\epsilon$ -, PP- and  $\beta$ -cells that form clusters, invade the PE and acquire the typical architecture of the adult Islet of Langerhans (Zorn & Wells 2009; Gittes 2009).

In pancreas organogenesis, tubulogenesis is tightly spatio- and temporal regulated, as the lineages including branching morphogenesis develop in the proliferating pancreas (Willmann et al. 2015). The expansion of the pancreas alters compared to branching morphogenesis of different tubular organs as lung, kidney and ureteric bud (Karihaloo et al. 2005). The classical branching morphogenesis suggests that peripheral growth accompanied with epithelial expansion, contrary to the pancreatic branching, implicates plexus formation, proliferation and remodeling and further plexus formation. Postnatal (P), the PE is transformed into a branched single luminal ductal system that is necessary to transporting

digestive enzymes. Currently, tubulogenesis remains widely unknown as the polarity establishment in the different lineages of the pancreas especially affecting the evolving  $\beta$ -cells. This might be an interesting point of research, especially regarding the polarity within the adult Islets of Langerhans, respective  $\beta$ -cells (Kone et al. 2014; Granot et al. 2009; Lo et al. 2012; Martin-Belmonte and Perez-Moreno 2011).

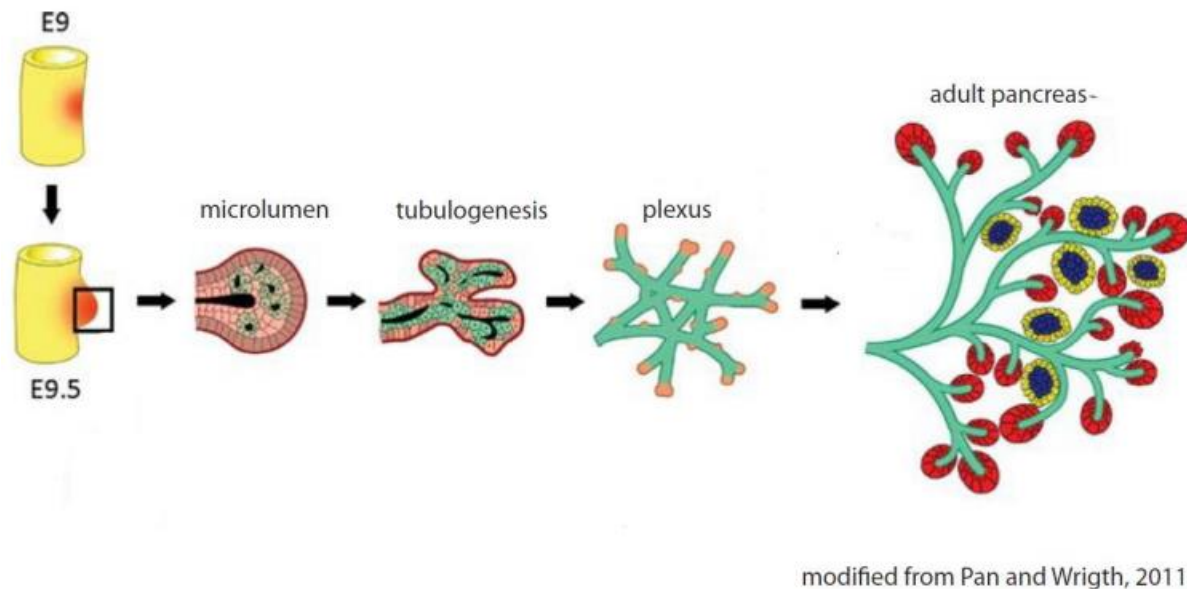


**Figure 2.2: Tubulogenesis of the embryonic pancreas**

The pancreas buds out of the anterior endoderm and at E11, micro lumen within the PE appear. Through a process called tubulogenesis at the beginning of the secondary transition, patterning into the different lineages determines specific regions. Epithelial remodeling (plexus) leads to the adult pancreas including defined compartments as the exocrine lineage (adult pancreas – red ball) and the endocrine Islets of Langerhans (adult pancreas – blue balls with  $\beta$ -cells; outer layer in yellow  $\alpha$ -,  $\delta$ -,  $\epsilon$ - and pp-cells)

Abbreviations: E = embryonic stage; PP = pancreatic polypeptide; PE = pancreatic epithelium

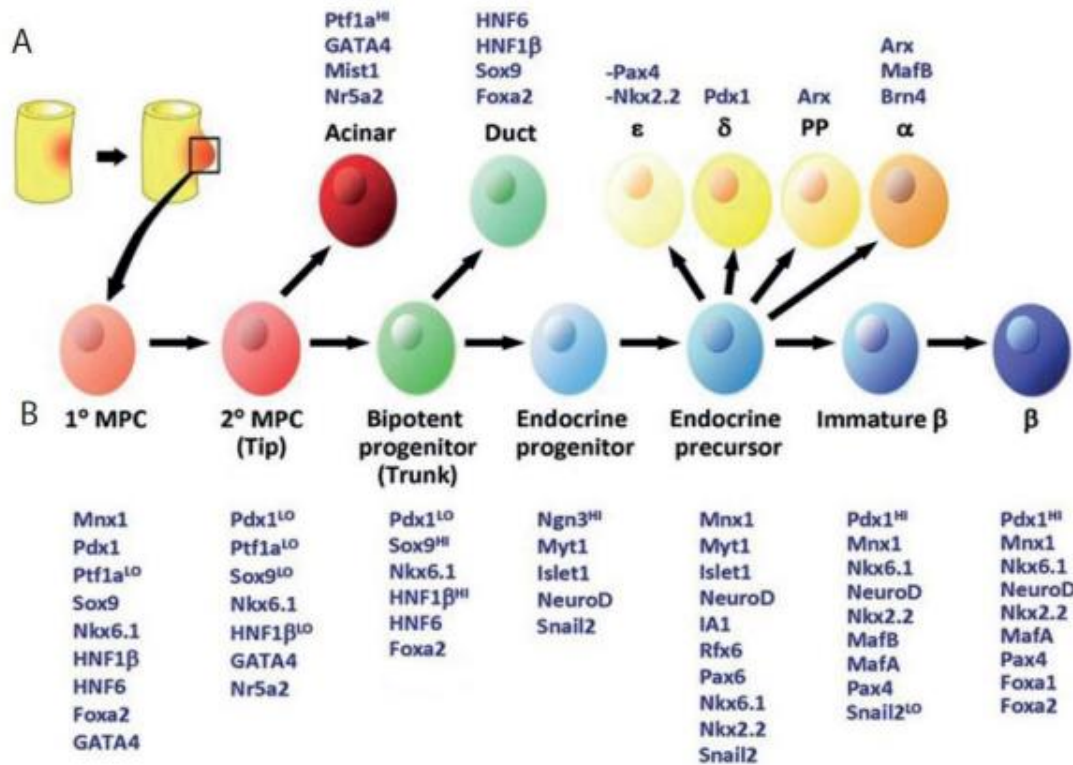
#### 1.4 Regulatory networks of pancreas development

In pancreas organogenesis, a transcription factor hierarchy orchestrates the segregation into the different cell types. The entry point of pancreas initiation is well characterized by the TF *Pdx1*, as in the MPP after pancreas initiation *Pdx1* serves as a marker for the PE (Gao et al. 2008).

Contrary, the adult pancreas consists of different cell types represented in the different lineages: acinar and ductal cells and the endocrine compartment comprising of the Islets of Langerhans which include  $\alpha$ -,  $\delta$ -,  $\epsilon$ - and PP-cells and the  $\beta$ -cells. As the pancreas evolves, the PE is characterized by *Pdx1*

expression, thereby reflecting subpopulations as Pdx1<sup>low</sup> and Pdx1<sup>high</sup>. The Pdx1<sup>low</sup> population is specifically required for the exocrine lineage, whereas the lineage determining factor for the endocrine compartment is represented by the subpopulation Pdx1<sup>high</sup> (Holland et al. 2002). A transcription factor hierarchy is guiding the pancreatic outgrowth, consisting of Pdx1<sup>low</sup> expressing PE within acinar cells represented by Ptf1 $\alpha$ <sup>High</sup> expression, as suppression of *Ptf1 $\alpha$*  induces acinar-to-endocrine formation (Hesselson et al. 2011). In addition, members of the *GATA family* such as *GATA binding protein 4* (*Gata4*) and *basic helix-loop-helix 1* (*Mist1*) regulate acinar cell proliferation (Pan and Wright 2011; Jia et al. 2008). Thus, *Mist1* is scattered on the foregut wall at stage E10.5 and after E13.5 and will be restricted to the acinar progenitors and mature exocrine cells. *Gata4* expression is restricted to the acinar fate in the E, in the adult pancreas *Gata4* expression localizes specifically in the  $\alpha$  - and  $\beta$ -cells of the Islets of Langerhans (Xuan et al. 2012). The factor *nuclear receptor subfamily 5 group a2* (*Nr5a2*) controls the early MPP the progenitor cells in the PE and after separation into tip and trunk pattern the acinar differentiation. It acts directly or through regulatory interactions with the acinar determining factors as *Gata4*, *Ptf1 $\alpha$*  and the *recombining binding protein suppressor of hairless* (*Rbpjl*) (Hale et al. 2014).

In addition, the *SRY related gene 9* (*Sox9*) determines the ductal lineage independently of *Foxa2* and *Hnf6* (Dubois et al. 2011). In the adult pancreas, the ductal lineage is responsible for the transportation of digestive enzymes from the surrounding exocrine tissue into the duodenum. Intercalating blood vessels in the Islets of Langerhans transport the hormones into the blood stream for maintaining the precise blood glucose level in the adult pancreas. Through the use of a gain-of-function, in mice constantly misexpressing *Aristaless related homeobox* (*Arx*),  $\beta$ -cells were converted into pancreatic PP and  $\alpha$ -cells (Courtney et al. 2013). Besides decreasing  $\beta$ -cell mass, mice developed hyperglycemia and died (Figure 2.3 A). There are several more regulatory genes and combinations, thus pointing to a fine-tuned spatio- and temporal network of TF in the secondary transition in pancreas organogenesis.



modified from Pan and Wright et al., 2011

**Figure 2.3: Lineage hierarchy of the pancreatic lineages with cell specific genes for the adult pancreas (A) and the embryonic pancreas from multipotent state at E8.0 to the mature β cell (B).**

**(A)** The adult pancreas consist of acinar cells (Ptf1α<sup>high</sup>, GATA4, Mist1 and Nr5a2), ductal lineage (Hnf6, Hnf1β, Sox9 and Foxa2) and the Islets of Langerhans (α-, δ-, ε- and PP-cells and β-cell).

**(B)** Multipotent progenitors get restricted to the β cell by different lineage commitments.

The transcription factor cascade starts with multipotent pancreatic cells (MPC) (Mnx1, Pdx1, Ptf1α<sup>low</sup>, Sox9, Nkx6-1, Hnf1β, Hnf6, Foxa2, GATA4), the second multipotent state is illustrated in a classical tip pattern (Pdx1<sup>low</sup>, Ptf1α<sup>low</sup>, Sox9<sup>low</sup>, Nkx6-1, Hnf1β<sup>high</sup>, Hnf6 and Foxa2). Bi-potent progenitors are although characterizing the trunk pattern (Pdx1<sup>low</sup>, Sox9<sup>high</sup>, Nkx6-1, Hnf1β<sup>high</sup>, Hnf6, Foxa2). In the next step, endocrine progenitors segregate in the PE (Ngn3<sup>high</sup>, Myt1, Isl1, NeuroD, Snail2). Endocrine progenitors will led to endocrine precursors (Mnx1, Myt1, Isl1, NeuroD, Rfx6, Pax6, Nkx6-1, Nkx2-2, Snail2) and to immature β cells (Pdx1<sup>high</sup>, Mnx1, Nkx6-1, NeuroD, Nkx2-2, MafB, MafA, Pax4, Snail2<sup>low</sup>) to β cells (Pdx1<sup>high</sup>, Mnx1, Nkx6-1, NeuroD, Nkx2-2, MafB, Pax4, Foxa1 and Foxa2)

Abbreviations: Ptf1α = pancreas specific transcription factor 1 α; Gata4 = Gata binding protein 4; Mist1 = basic helix-loop-helix protein; Nr5a2 = nuclear receptor subfamily 5 group a; Hnf6 = Hnf homeobox 6; Hnf1β = Hnf homeobox 1β; Sox9 = Sry related homeobox 9; Foxa2 = winged helix/forkhead box 2; Foxa1 = winged helix/forkhead box 1; PP = pancreatic polypeptide; MPC = multipotent pancreatic cells; Mnx1 = Mox and pancreas homeobox 1; Pdx1 = pancreatic and duodenal homeobox 1; Nkx6-1 = Nk homeobox 6-1; Nkx2-2 = Nk homeobox 2-2; Ngn3 = Neurogenin 3; Myt1 = Myelin transcription factor 1; Isl1 = Isl im homeobox 1; NeuroD = Neuronal Differentiation 1; Snail2 = Snail family Zinc Finger 2; Rfx6 = regulatory factor x 6; MafA = V-maf musculoaponeurotic fibrosarcoma oncogene homolog A; MafB = V-maf musculoaponeurotic fibrosarcoma oncogene homolog B; Pax4 = paired homeobox x 4.

In the development of the pancreas, in conjunction with *Ptf1α* and *Foxa2*, *Pdx1* facilitates the expansion of the PE (Stanger et al. 2007). Thereby in later stages, it acts as an glucose-responsive regulator of insulin gene expression, likely for *glucagon-like peptide-1 (GLP-1)* (Hay et al. 2005). *Ptf1α* and *Foxa2* act upstream of *Pdx1* with the combined expression in the MPP of the PE as early as the pancreatic formation is initiated at E8.0. In the later steps of pancreas organogenesis and finally in the adult pancreas, the total pancreatic cell mass depends strikingly on these marker onset (Stanger et al., 2007). The first lineage segregation appears as early as E9.5 which does not affect the adult pancreas. After the first lineage segregation, a second lineage segregation arises with a typical expression pattern that is described as a tip and trunk. The typical tip pattern represents the MPP at E14.5. The marker onset illustrating the typical bi-potent trunk pattern for the ductal and endocrine lineage in the PE at E14.5 is illustrated by the TF  $Pdx1^{low}$ ,  $Ptf1α^{low}$ ,  $Sox9^{low}$ ,  $HNF1β^{low}$ , NK homeobox, family 6- 1 ( $Nkx6-1$ ), *Gata4* and *Nr5a2* (Zhou et al., 2007). The compartmentalization of the ductal and endocrine lineage leads to a subset of *Neurogenin3<sup>high</sup>* ( $Ngn3^{high}$ ), *Myelin transcription factor 1* (*Myt1*), *ISL LIM homeobox 1* (*Isl1*), *neuronal differentiation 1* (*NeuroD*) and *Snail Family Zinc Finger 2* (*Snail2*) expressing cells (Figure 2.3 B). Thus, the endocrine progenitors still maintain the MPP state of the endocrine lineage, meaning that all the different subcells in the mature Islets of Langerhans derive out of this progenitor pool. In a next step in pancreas organogenesis, the immature  $\beta$ -cells will develop in the precursor Islets of Langerhans to the final mature  $\beta$ -cells. Factors that determine this specific lineage commitment include  $Pdx1^{high}$ , *motor neuron and pancreas homeobox 1* (*Mnx1*), *Nkx6-1*, *NeuroD*, *Nkx-2*, *V-Maf Avian Musculoaponeurotic Fibrosarcoma Oncogene Homolog B* (*MafB*), *MafA*, *Paired Box 4* (*Pax4*) and  $Snail2^{low}$  (Figure 2.3 B). As Snail factors determine the process of EMT, in the mature Islets of Langerhans *Snail2* is no longer expressed (Schaffer et al. 2013; Seymour et al. 2012; Herrera 2000).

### 1.5 The model of endocrine formation

In line with pancreas development, the endocrine lineage at approximately E13.5 will be restricted. Specific factors that drive the endocrine lineage are described as trunk pattern in the PE and is reflected by an epithelial cord pattern, which is illustrated by *Sox9* expression. Within this cord-like structure, the expression of the *Ngn3*-transient population represents the endocrine progenitors (Gradwohl et al. 2000; Gu et al. 2002; Schwitzgebel et al. 2000; Jensen 2004; Zhou et al. 2007). Mainly, lineage tracing experiments implicated that *Ngn3* as a basic helix-loop-helix transcription factor is necessary for the establishment of all endocrine cells as glucagon, Insulin, somatostatin and PP which first assemble into the Islets of Langerhans at E18.5 (Gradwohl et al. 2000; Herrera 2000). The latest attempts showed that *Sox9* deficient mice illustrate a severe reduction in endocrine progenitors marked by *Ngn3*, which

implicates that *Sox9* acts upstream of the endocrine lineage (Seymour et al. 2012). Furthermore, Lynn and Seymour proposed a cell-autonomous role for *Sox9* in *Ngn3* induction, which suggests a negative feedback-loop for co-related expression of *Sox9* and *Ngn3* (Shih et al. 2012; Seymour et al. 2012). These results further determine the importance of *Ngn3* as a key TF for the endocrine progenitor. In addition, upstream TF as *Sox9* and *Pdx1*, specifically in the duct, regulate expression of endocrine precursor *Ngn3*. The signal cascade for the regulation of *Ngn3* is still controversial, as there might be extrinsic and intrinsic signals that affect the proliferation of the endocrine lineage. Interestingly, signals from mesenchyme might not play a role in endocrine formation - as close proximity of epithelium to the mesenchyme accelerates the exocrine fate, whereas missing contact of epithelium to the mesenchyme leads to the endocrine lineage (Li et al. 2004).

In the 1970s, Pictet and Rutter already postulated that these endocrine progenitors delaminate out of the epithelial sheet and cluster to precursor Islets of Langerhans. This delamination process accompanies with alteration in contact to other cells. In the neuron crest system, delamination is well studied and described as transcriptionally controlled by the *Snail* family of TF (Sanitarías et al. 2002; Pictet et al. 1972).

In the process itself, *Snail family Zinc finger* TF are involved and members of the *Rho subfamily of GTPases*. Recently published by Rukstalis, *Snail2/Slug* is co-expressed with endocrine progenitor *Ngn3* and still maintained in a subset of differentiated endocrine cells (Rukstalis et al. 2006; Rukstalis and Habener 2007). These results link to epithelial and to EMT of endocrine progenitors as they leave the ductal cord. In development, cancer cells and metastases the mechanism of EMT is well studied. In the mechanism of EMT the epithelial cells remodel their polarity as they change from epithelial state to mesenchyme. The characteristic of the epithelium is described as apical-basal (AB) polarity including a polarized actin cytoskeleton. As cells change into a mesenchymal state, polarity changes from AB to front-rear and cell junction remodel as the cell moves out of the epithelial sheet. Main TF of EMT are *Snail2*, *Zinc Finger E-Box Binding Homeobox (Zeb)* and *Twist family BHLH transcription factor (Twist)*. Another hallmark of EMT is described as the switch of *E-cadherin (Ecad)* to *N-cadherin*. The loosening of the epithelial character includes the down regulation of *E-cad*. Graphin-Botton had already published that *Ngn3* overexpression leads to endocrine differentiation. Further work by Gouzi showed that *Ecad* is transcriptionally down regulated in endocrine precursors with *Snail2* under the control of *Ngn3*. These results suggest that endocrine progenitors undergo delamination with at least partial EMT. Which mechanism regulates endocrine formation remains elusive and is in focus in the field of diabetes research, as it will help trigger the endocrine commitment *in vivo* (Johansson et al. 2007; Gouzi et al. 2011).

## 1.6 Establishment of epithelial asymmetry

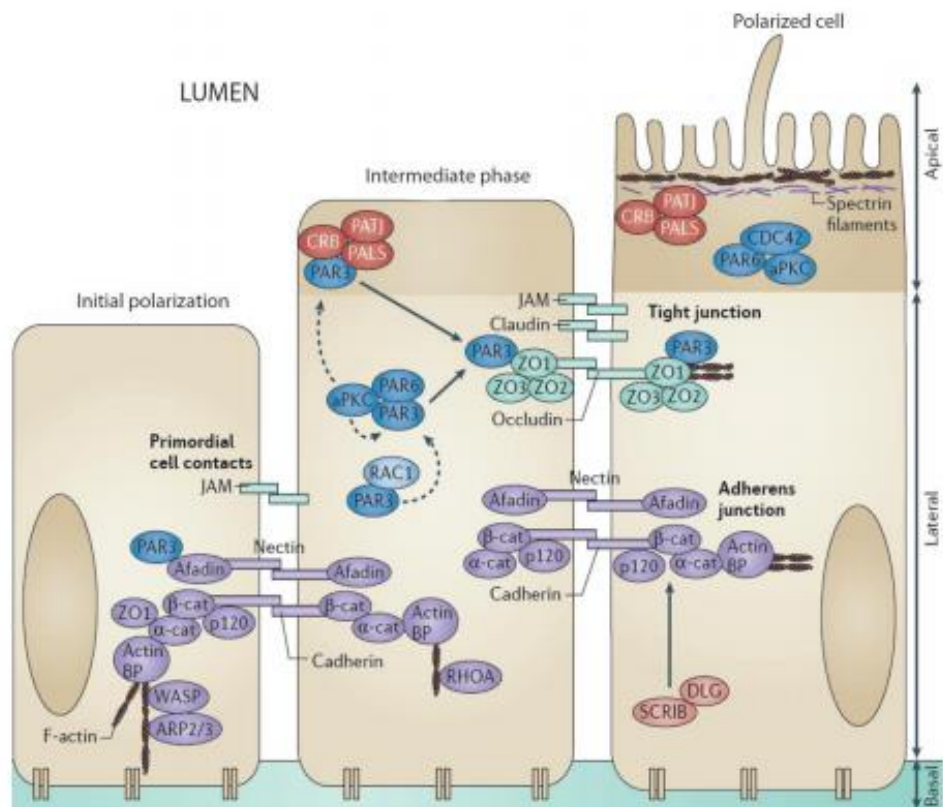
Epithelial sheets are the boundary between the extracellular matrix (ECM) and the epithelial tissue itself. The junctional complexes in the membrane surface participate in the establishment and maintenance of the epithelial asymmetry that separates cellular compartments (Rodriguez-Fraticelli et al. 2012). Thus, organization of polarity complexes, the cytoskeleton, vesicle-trafficking and adhesive junctions are coordinated within the cytoplasm and between neighboring cells. (Figure 2.4) (Apodaca et al. 2012).

The adhesion and barrier functions are carried out through Tight junctions (TJ) and adherens junctions (AJ). In the initiation of polarization mainly junctional adhesion molecules (JAMs), nectin and cadherins define the basolateral surface. A Nectin-Afadin complex mediates via homophilic adhesion receptor domains calcium dependent intercellular adhesion. Thus, they form the first junctional connection to neighboring cells (Figure 2.4). The cytoskeleton illustrates dynamic patterning of actin by the cadherin/ $\beta$ -catenin complexes, which generates a pool of  $\alpha$ -catenin that drives along with p120 (Figure 2.4). Actin-Related Protein 2/3 Homolog (Arp2/3) nucleates actin filaments and establishes an extensive array of branched actin filaments. The interaction to neuronal Wiskott-Aldrich Syndrome Protein (N-WASP), a target of cell division control protein 42 (Cdc42) and Ras-Related C3 Botulinum Toxin Substrate 1 (Rac1), regulates the junctional architecture and cortical tension as demonstrated in vertebrate model systems (Otani et al. 2006). Next, Afadin associates with the cytoplasmic domain of nectins and JAM are recruited to the AJ through an interaction with  $\alpha$ -catenin where it directly interacts with actin filaments (Mandai et al. 1997; Tachibana et al. 2000) (Figure 2.4). Thus, Afadin is a major organizer of the apical junctional complex (AJC), and is essential for the development of AB polarity in vertebrate embryogenesis (Zhadanov et al. 1999; Ikeda et al. 1999). In further steps, the partitioning defective protein 3 (PAR3), a member of the PAR polarity complex, incorporates with the Nectin-Afadin adhesion complex and initiates at the JAM that the primordial cell contacts.

In the intermediate phase of cellular polarization, PAR3 dissociates and localizes to RAC1, which is followed by subapical association to the Par3-Par6- atypical protein kinase C ( $\alpha$ PKC) polarity complex. Besides AJ, TJ are also structurally and functionally linked to the actin cytoskeleton (Figure 2.4). At TJ, TJ proteins (ZO-1, ZO-2, ZO-3) interact with Par3 and stabilize the AB complex through association to actin (Figure 2.4). Cells depleted of ZO-1 show defects in the barrier to larger molecules, and changes in the junctional complexes associated actin, indicating that ZO-1 forms a stabilizing link between the barrier and the junctional actomyosin through PAR3 binding (Li et al. 2005; Wittchen et al. 1999; D'Atri

and Citi 2001). In line with these results, depletion of *zonula occurrence 2* (ZO-2) does not lead to either actin reorganization or altered plasma membrane permeability, whereas a depletion of either ZO-1 and ZO-2 leads to a drastic expansion of the actomyosin associated with AJ (Nomme et al. 2011; Li et al. 2005). Thus, junctional complexes maintain the AB polarity within the cells and in the epithelial sheet.

The protein network establishing AB polarity includes Crumbs (CRB), partitioning defective (PAR, respective Par3-Par6- $\alpha$ PKC) and the Scribble (SCRIB)-lethal (2) giant larvae homologue (DLG) complex. In the initial stage of polarization, it is reported that Par3 forms the primordial cell contacts through interaction with JAM (Ebnet 2003). Par3 dissociates from the junctional primordial complex and forms a ternary complex of Par3 and Par6 linked through  $\alpha$ PKC (Lin et al., 2000). Dissociation of Par3 is initiated through the  $\alpha$ PKC phosphorylation step, which leads to relocalization of Par3 at TJ and the CRB complex. Simultaneously, the CDC42-Par6-  $\alpha$ PKC complex localizes apically, determining the AB polarity in the cell. Thus, the CRB complex defines the apical plasma membrane domain, the PAR complex establishes AB surfaces and the SCRIB-DLG basolateral domains, restricted to epithelial cells (Figure 2.4). As described above, the polarity proteins are ultimately linked to intracellular protein complexes, which make the AJ and TJ (Martín-Belmonte et al. 2008).



modified from Belmonte et al., 2012

**Figure 2.4: The epithelial polarity program players**

The TJ and AJ associate to the PAR complex member PAR3 for establishment of lateral and AB polarity in the initial polarization. Subsequently, establishment and persistence of the polarity within the cell is determined by structural components at the apical and apical-lateral (AL) plasma membrane domains. TJ are represented by TJ protein ZO 1-3 which binds to F-Actin. The AJ are illustrated by Afadin, respectively  $\beta$ -catenin. The intracellular localization of the polarity proteins complexes in a mature AB polarized epithelial cells is achieved through 3 different complexes. The crumbs (CRB) complex (in red), the PAR complex (in blue) and the Scribble (SCRIB)-lethal (2) giant larvae homologue (DLG) complex cooperate to form AJC.

Abbreviations: PAR = partitioning defective protein; PAR3 = partitioning defective protein 3; ZO = zonula occludens; AB = apical-basal; CRB = crumbs; SCRIB = Scribble; DLG = giant larvae homologue; AJC = adherens junction complex; TJ = tight junctions; AJ = adherens junctions; AL = apical-lateral; AJC = adherens junctions complexes.

**1.7 The family of *Synaptotagmins* (Syt)**

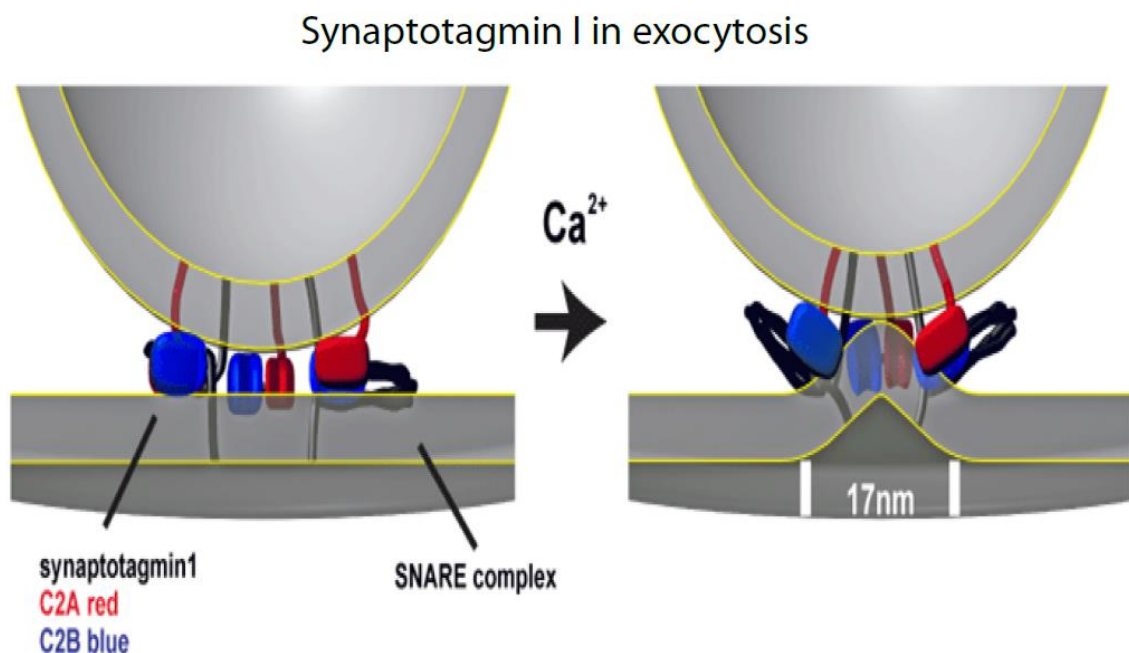
*Synaptotagmins* are commonly known as synaptic vesicle membrane proteins. Representative family member *Synaptotagmin 1* (*Syt1*) undergoes calcium-dependent interaction for neurotransmitter release and vesicle exocytosis (Yoshihara & Littleton 2002). Thus, it may characterize the large family of *Syts*, with at least 19 member in *mammals* (Adolfson and Littleton, 2001). In general, *Syts* are composed of a Transmembrane domain (TMD) including a preceding N-terminal sequence and 2C2 domains, which are defined as  $Ca^{2+}$  binding sites (Ullrich and Südhof 1995; Südhof et al., 2002).

The family can be separated into  $Ca^{2+}$  binder and  $Ca^{2+}$  non-binder, suggesting that different *Syt* isoforms have distinct functions. *Syt1* thereby triggers the  $Ca^{2+}$  release of the soluble trans-soluble N-ethylmaleimide-sensitive-factor attachment receptor (tSNARE) complex. SNARE complexes are membrane trafficking vesicles that establish polarity within the cells. In a developmental context, apical/basolateral SNARE sorting coordinates epithelial morphogenesis (Rodriguez-Fraticelli et al., 2015). Best studied are SNARE-Synaptotagmin complexes in neurons. *Syt1* acts as a membrane binding machine likely due to the fact that the C2 domains interact with the plasma membrane. Upon  $Ca^{2+}$  binding, the plasma membrane is restrained by the C2 domains and in a further step leads the tension to membrane-fusion and exocytosis of neurotransmitters in neurons and neuroendocrine cells (Figure 2.5).

Similar molecular characteristics of members in the *Syt* family are shown by *Synaptotagmin 7* (*Syt7*). Thus, *Syt7* presents a higher affinity to  $Ca^{2+}$  and deletion leads to the partial reduction in  $Ca^{2+}$  triggered release. Remarkably, deletion of *Syt7* along with *Syt1* nearly abolishes exocytosis (Wen et al. 2010).

Also, *Syt7* is expressed in  $\beta$ -cells,  $\alpha$ -cells and insulin-responsive tissues as fat. With this in mind, the protein is involved in  $\text{Ca}^{2+}$  triggered exocytosis of insulin and glucagon and in glucose uptake (Li et al., 2007)

The non-calcium binder in the family of *Synaptotagmins* are currently in focus due to its diverse function. Until now the isoforms *Syt4*, *8* and *13* are unlikely able to bind calcium and for *Syt4* published data shows broad expression in non-neuronal tissues (Fukuda and Mikoshiba 2001; Tsuboi and Rutter 2003). The gene *Syt13* may be regarded as atypical *Syt*, as the TMD is missing the preceding N-terminal sequence and the 2C2 domains lacks of the  $\text{Ca}^{2+}$  binding pockets (Fukuda and Mikoshiba 2001; Poser et al., 2001). Moreover, previous results suggest expression in non-neuronal tissue. Therefore, we are interested in expression, function and mechanism of *Syt13* in transgenic mouse models.



modified from Martens et al.,2007

**Figure 2.5: Model of *Synaptotagmin 1* promoting membrane fusion**

The classical *Syt* is represented by *Syt1*. *Syt1* is transported to the  $\text{Ca}^{2+}$  channel by presumably a member of the kinesin motor family. In a docked stage, the synaptic vesicles are primed for the release of the neurotransmitter. This is indicated through the tSNARE complex. Upon  $\text{Ca}^{2+}$  influx, the C domains frame the plasma membrane, resulting in a buldge pointing towards the vesicle. The close proximity of the membranes leads to fusion and finally to exocytosis of the vesicle content into the channel (17nm pore).

Abbreviations: *Syt* = Synaptotagmin; tSNARE = trans-soluble N-ethylmaleimide-sensitive-factor attachment receptor

## 1.8 Aim of this thesis

*Foxa2* is an important player in the organizer tissue with protein expression in the embryo already at the early stage E6.5. During gastrulation, the endoderm germ layer forms and covers the egg-shaped embryo past emerging out of the PS. Endodermal-derived organs are the glandular structures of the pharynx, the entire gastrointestinal tract, respiratory tract and associated organs such as the liver and the pancreas. Taking the advantage of the recently in our laboratory generated *Foxa2<sup>Venus</sup>* mouse line, we focused on pancreas organogenesis. By accomplishing an expression profile of the endodermal and non-endodermal tissue compartment during the secondary transition, we wanted to enlarge the knowledge of pancreatic regulatory mechanism and single gene expression in pancreas organogenesis. Thus, we separated both tissue compartments and identified conserved pathways and genes in pancreas development.

In addition, novel pancreatic related genes were selected and analyzed for predicted molecular function and mechanism. In using the digital database Genepaint.org, pancreatic candidate genes had been sorted by *in silico in situ hybridization pattern* into the different pancreatic lineages.

Our interest lies in the identified gene *Syt13*, as the *in situ* reflects a trunk pattern, respective endocrine lineage segregation in the secondary phase at E12.5-15.5 in pancreas organogenesis. In generating a knock-in/knock-out mouse line (*Syt13<sup>GT/GT</sup>*) we analyzed the function and molecular mechanism of *Syt13*. Restricted expression pattern during pancreas organogenesis and subcellular localization lead us to the hypothetical model of *Syt13* in endocrine lineage segregation in the secondary transition phase in pancreas organogenesis.

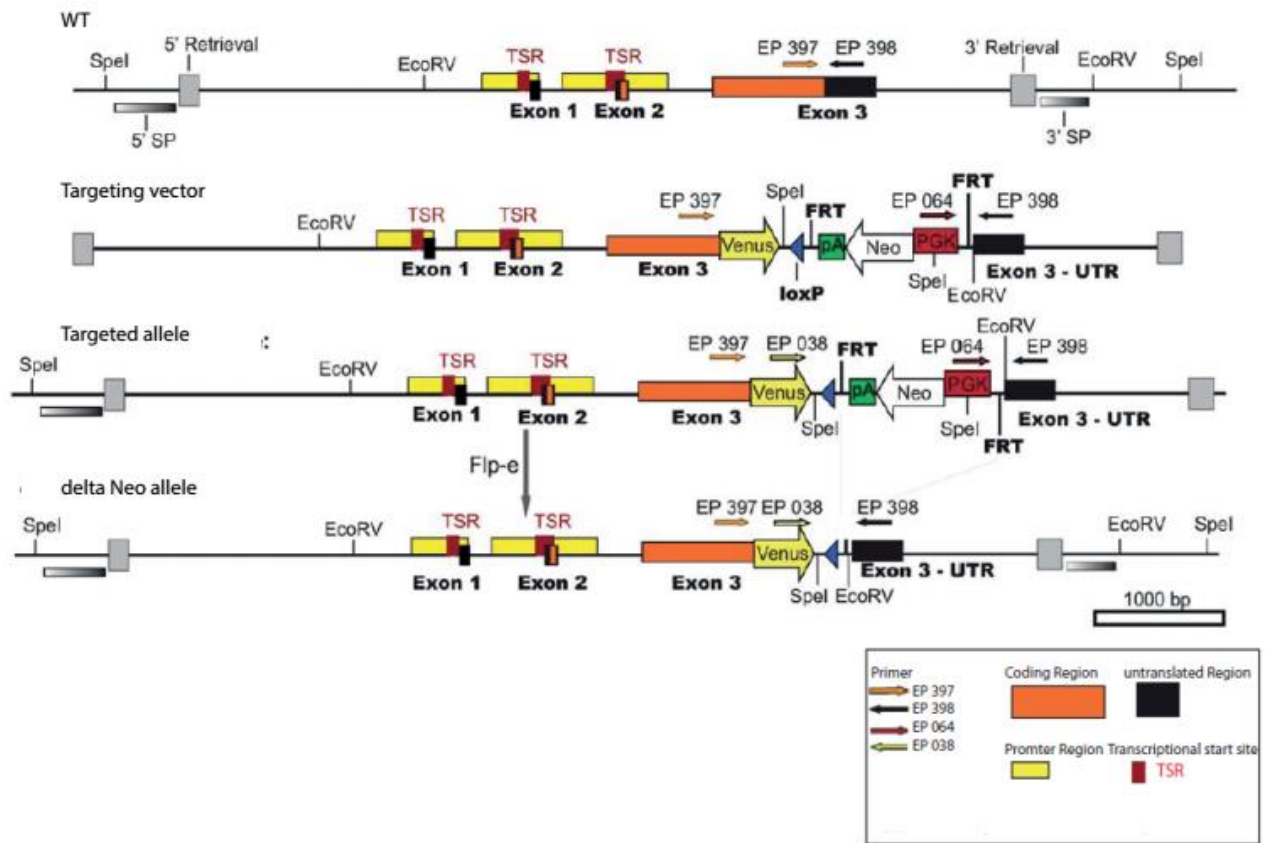
## 2 Results

### 2.1 Generation of the *Foxa2*<sup>Venus</sup> mouse line

In the gastrulation of the mouse embryo at E6.5 the three principal germ layers evolve: the ectoderm, the mesoderm and the endoderm (Ichikawa et al., 2013). Subsequently, the family of Fox TF is required for the formation of the DE, as well as the organs which develop out of the epithelial squamous cell sheet lining the egg-shaped embryo. Thus, *Foxa2* plays a master role in the formation of endoderm and *Foxa2*<sup>-/-</sup> mice already show lethality at E10-11 with severe defects in node, notochord, neural tube and closure of the gut tube (Burtscher et al., 2009; Uetzmann et al., 2008; Weinstein et al., 1994). Also, the family members *Foxa1* and *Foxa2* are key TF in metabolism, mutant mice reflect an absent of the liver and *Cre* mediated deletions leads to hypoglucagonemia, respective hypoglycemia in the adult Islets of Langerhans (Lee et al., 2005). Further analysis of *Foxa2* in the pancreas will determine lineage allocation and metabolic impact of the gene in endocrine lineage segregation, clustering of precursor Islet of Langerhans and in the mature Islets of Langerhans. Hence, by using a knock-in strategy to express a Venus reporter protein under the control of *Foxa2* expression, we generated in our laboratory the *Foxa2*<sup>Venus</sup>(FVF) mouse line to investigate these processes.

#### 2.1.1 Design and generation of the *Foxa2*<sup>Venus</sup> (FVF) targeting vector

For the FVF targeting strategy, we generated a targeting construct and replaced the Stop-Codon in the Exon 3 in the open reading frame (ORF) of the *Venus* reporter gene, followed by the original *Foxa2* 3'-untranslated region (3'-UTR) (Figure 3.1, yellow arrow). Downstream of the *Venus* reporter gene the inserted *polyadenylation site* (*pA*) represents a translational stop codon (Figure 3.1, green box). The stop codon insertion followed the *phosphor-glycerate kinase* (*PGK*) driven *neomycin* (*neo*) resistance gene flanked by the *Flippase* (*Flp*) recognition target (*FRT*) (Figure 3.1, white arrow and red box).



modified from Burtscher et al., 2013

**Figure 3.1: Targeting strategy of the *FVF* allele**

The *WT* allele consists of 3 Exons. In the stop codon of Exon 3 the targeting vector with the Venus-tag was fused. The targeting allele can be distinguished from the *WT* allele by using the Primer EP 397 and 398 for genotyping. Mice carrying the *FVF-Neo* allele were crossed with *Flp-e* mice for excision of the *PGK* driven *neo*-resistant cassette. Targeting and verification was accomplished by Dr. Ingo Burtscher.

Abbreviations: TSR = transcriptional start site/region; En2 = engrailed homeobox; SA = splice acceptor; pA = SV40 large T gen; neo = neomycin, PGK = phospho-glycerate-kinase; UTR = untranslated region; EP = Primer; FRT = Flipase (Flp) recognition target; *Flp-e* = enhanced Flipase; *FVF* = *Foxa2-Venus* fusion; *WT* = wild type; *loxP* = Site-specific recombinase Cre; bp = base pair.

IDG3.2 embryonic stem (ES) cells were electroporated after linearization of the targeting construct with *Ascl* and neoresistant clones selected upon 300µg/ml G418. The chimeras were generated by diploid aggregation of the recombinant ES cells with *CD1* morula (Nagy et al., 2000) and chimerism was scored by coat colour. Upon removal of the *neo* cassette by using *Flp-e* (enhanced Flipase) mediated excision (Dymecki et al., 1996) the *FVF* mice had been mated for eighth generations into the C57Bl/6 background and also on a mixed background including *CD1/D57Bl/6/129Sc*. The targeting was accomplished by Dr. Ingo Burtscher and Wenke Barkey.

For genotyping of the *FVF* allele using polymerase chain reaction (PCR) the following primer (EP) were designed to distinguish between the *WT* allele with 207 base pairs (bp) (EP397, EP398), the *FVF Neo* allele at 317bp (EP64, EP398) and the *FVF delta Neo* allele with 506bp (EP38, EP398) (Figure 3.1). For further utilizing the *FVF* mouse line, heterozygous intercrosses were generated.

### 2.1.2 Analysis of the *Foxa2<sup>Venus</sup>* mouse line in the pancreas

In the initial stage of pancreas organogenesis at E8.0, the pancreatic primordia buds out into the surrounding mesenchyme. Thereupon, the pancreatic cell population is assigned as MPP until in the secondary transition the MPP segregate into the different lineages (Koop et al., 2011). With this in mind, lineage segregation of the PE at E14.5 may be illustrated by a specified marker lineage analysis. Thus, we were interested in the MPP characteristics of the *FVF positive (FVF<sup>+</sup>)* PE and lineage specification within the PE in the secondary transition at E14.5 (Burtscher et al., 2009).

A Tamoxifen inducible promoter of *Cpa1* determines lineage segregation of the formerly MPP at E14.5 into the exocrine compartment illustrated by a typical expression pattern in the PE referred to as tip (Zhou et al., 2007). Interestingly, we observed expression of *FVF* in the PE along with co-expression of *Cpa1* in these tip epithelial boundaries (Figure 3.2, A-D). Also, *FVF<sup>+</sup>* cells are represented to a larger extend in the PE, all *Cpa1<sup>+</sup>* cells co-localize to *FVF<sup>+</sup>* cells at E14.5 in the tip compartment of the PE (Figure 3.2, C – D; C \*). This co-localization not only illustrates cytoplasmic distribution of *Cpa1* compared to the nuclear localization of the endogenous *FVF* protein. In addition, rosette-like structures represent the branching morphogenesis in pancreas organogenesis at E14.5 (Figure 3.2, D') (Villasenor et al. 2010). Remarkably, *Cpa1<sup>+</sup>* cells co-express *FVF<sup>high</sup>* to a lesser extend compared to *FVF<sup>low</sup>* expression within the cells (Figure 3.2, D', red arrow *CPA1<sup>+</sup>* and *FVF<sup>+</sup>*, yellow arrow *CPA1<sup>-</sup>* and *FVF<sup>+</sup>*). In summary, our previous results do not only confirm the tip pattern of the formerly MPP in the PE, we characterized the lineage segregation into the exocrine lineage at E14.5, identified 2 subpopulations of endogenous *FVF*, stated as *FVF<sup>high</sup>*, respective *FVF<sup>low</sup>* and directly categorized a *FVF<sup>low</sup>CPa1<sup>+</sup>* cell population likely as protrusions at the ceiling of the PE.

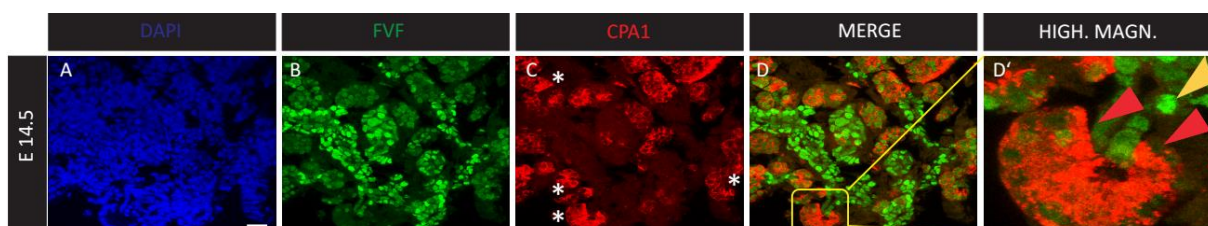


Figure 3.2: *FVF* and *Cpa1* co-localize in the PE

## Results

**(A-D')** The 4',6-Diamidin-2-phenylindol (DAPI) counterstain and immunohistochemistry (IHC) against FVF and Cpa1 on a coronal PE section at E14.5 (A-D'). All FVF<sup>+</sup> expressing cells in the PE express Cpa1 at the onset of pancreas lineage segregation in the tip region (C, \*). Cpa1<sup>+</sup> expressing cells are mainly in the tip region of the PE (D). The FVF<sup>+</sup> area is broader since it is also expressed within the PE, illustrating the subpopulations FVF<sup>high</sup> and FVF<sup>low</sup> (D', FVF<sup>high</sup> yellow arrow and FVF<sup>low</sup> (red arrow) .

Scale is set for 25µm

Abbreviations: DAPI = 4',6-Diamidin-2-phenylindol; FVF = Foxa2-Venus-Fusion; CPA1 = Carboxypeptidase 1; HIGH. MAGN. = Higher Magnification; PE = pancreatic epithelium; IHC = Immunohistochemistry.

Similar to *Cpa1*, the paired homeodomain *Pax6* is present as early as E9.0 in the dorsal and ventral pancreatic primordia, suggesting a crucial role in pancreas organogenesis. Contrary to *Cpa1*, *Pax6* is required for endocrine cell development and mutations in the gene of *PAX6* are associated to diabetic diseases in respect to  $\alpha$ -cells (Gosmain et al., 2010; St-Onge et al., 1997; Zorn and Wells, 2011). Hence, we performed further analysis of *Pax6* in the secondary transition at E14.5.

Whereas FVF<sup>+</sup> expressing cells represent the PE, Pax6<sup>+</sup> cells are restricted to certain territories combined in clusters in the PE (Figure 3.3, A-C). More precise, the Pax6<sup>+</sup> regions are within the PE, compared to the tip pattern of FVF<sup>low</sup>Cpa1<sup>+</sup> expressing compartments. Also, FVF<sup>high</sup> co-localizes to Pax6, these regions suggest to represent the trunk pattern and thereby endocrine cell fate (Figure 3.3, D) (Zhou et al., 2007; Shih et al., 2013). We could observe the direct correlation of FVF<sup>low</sup>Pax6<sup>-</sup> (Figure 3.3, D' red arrow) and FVF<sup>high</sup>Pax6<sup>+</sup> (Figure 3.3, D' yellow arrow) and thereby define the different subpopulations in the PE at E14.5 in more detail.

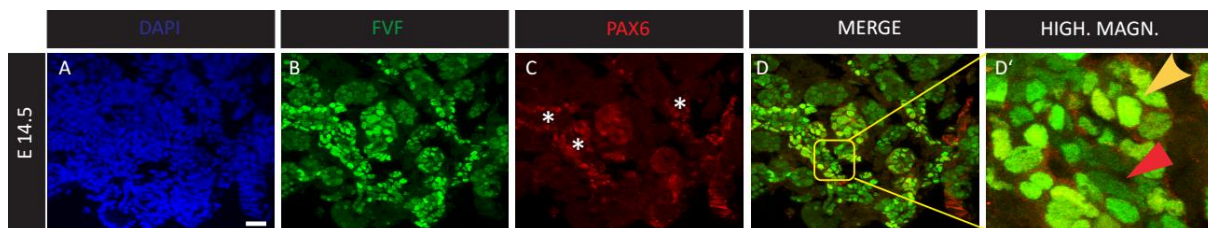


**Figure 3.3: FVF and Pax6 co-localize in the PE**

**(A-D')** IHC on PE and mesenchyme (DAPI counterstain) at E14.5 on a coronal pancreatic section against FVF and Pax6 at E14.5(A-D'). Pax6<sup>+</sup> expressing cells are restricted to the trunk region of the PE (C, \*). Contrary, the FVF<sup>+</sup> compartment represents the PE. Consistently, the PE illustrates the subpopulations FVF<sup>high</sup> and FVF<sup>low</sup> (D', FVF<sup>high</sup> yellow arrow and FVF<sup>low</sup> red arrow).

Scale is set for 25µm

Abbreviations: DAPI = 4',6-Diamidin-2-phenylindol; FVF = Foxa2-Venus-Fusion; Pax6 = paired homeodomain x 6; HIGH. MAGN. = Higher Magnification; PE = pancreatic epithelium; IHC = Immunohistochemistry; E = embryonic stage.

Likewise the endocrine progenitor Pax6, the endocrine precursor Nkx6-1 becomes restricted to the particular endocrine trunk compartment in the secondary transition at E14.5 (Kopp et al., 2011; Pan et al., 2013; Shih et al., 2013). We confirmed the FVF<sup>+</sup> expressing cell population, representing the PE and a regionalized *Nkx6-1*<sup>+</sup> cell subpopulation illustrated by a typical trunk pattern (Figure 3.4; A-D; C \*). The observation of the FVF<sup>high</sup>Nkx6-1<sup>+</sup>, respective FVF<sup>low</sup>Nkx6-1<sup>-</sup> verified previous results of endocrine versus exocrine lineage segregation (Figure 3.4, B-D, D red arrow, see also Figure 3.3). Remarkably, different subpopulation characterized by FVF<sup>high</sup>Nkx6-1<sup>-</sup> and FVF<sup>-</sup>Nkx6-1<sup>+</sup>, (Figure 3.4, D', FVF<sup>high</sup>Nkx6-1<sup>-</sup> yellow arrow and FVF<sup>-</sup>Nkx6-1<sup>+</sup> black arrow) suggesting a competence windows for the generation of the different endocrine cell types along with different protein expression levels of FVF and Nkx6-1.

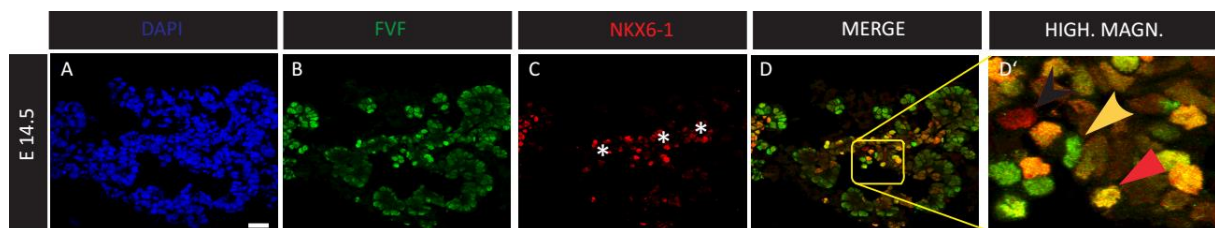


**Figure 3.4: FVF and Nkx6-1 co-localize in the PE**

**(A-D')** In the PE at E14.5 on coronal sections IHC illustrates FVF and Nkx6-1 (DAPI counterstain). The PE is marked with a FVF<sup>+</sup> expressing cell compartment, Nkx6-1<sup>+</sup> expressing cells are restricted to the trunk compartment of the PE (C \*). Interestingly, the PE illustrates the subpopulations FVF<sup>high</sup>Nkx6-1<sup>-</sup> and FVF<sup>high</sup>Nkx6-1<sup>+</sup>, (D', FVF<sup>high</sup>Nkx6-1<sup>-</sup> yellow arrow, FVF<sup>high</sup>Nkx6-1<sup>+</sup> red arrow and FVF<sup>-</sup>Nkx6-1<sup>-</sup> yellow arrow).

Scale is set for 25µm

Abbreviations: DAPI = 4',6-Diamidin-2-phenylindol; FVF = Foxa2-Venus-Fusion; NKX6-1 = NK homeobox 6-1; HIGH. MAGN. = Higher Magnification; PE = pancreatic epithelium; IHC = Immunohistochemistry; E = embryonic stage.

In the next step, we determined the regionalized compartmentalization of the ductal and endocrine lineage commitment in the bi-potent trunk pattern at E14.5. The gene *Hnf1β* consequently forms the duct in the secondary transition and on the mRNA level in the regulatory transcriptional network that regulates *Ngn3* expression (Solar et al., 2009; Oliver-Krasinski et al., 2009). Thus, in the FVF<sup>+</sup> PE, *HNF1β*<sup>+</sup> cells are expressed in the trunk pattern (Figure 3.5, C \*) – interestingly, our observation suggesting rather a FVF<sup>low</sup>HNF1β<sup>+</sup> subpopulation as the expected FVF<sup>high</sup>HNF1β<sup>+</sup> expressing cells (Figure 3.5, A-D). The co-localization of FVF<sup>low</sup>HNF1β<sup>+</sup> characterizes the duct, endocrine lineage segregation of the formerly bi-potent precursors is marked through FVF<sup>high</sup>HNF1β<sup>-</sup> protein levels (Figure 3.5, D', FVF<sup>low</sup>HNF1β<sup>+</sup> yellow arrow and FVF<sup>high</sup>HNF1β<sup>-</sup> red arrow).

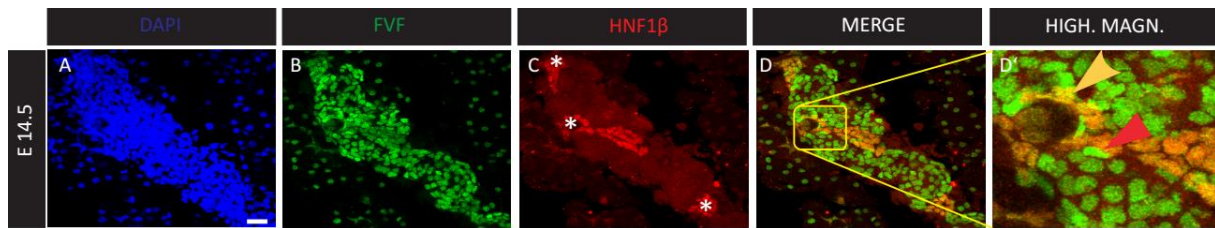


**Figure 3.5: FVF and Hnf1 $\beta$  co-localize in the PE**

**(A-D')** In coronal sections at E14.5, the PE is represented by FVF IHC, respective a regionalized trunk compartment by HNF1 $\beta$  IHC (DAPI counterstain). The HNF1 $\beta$ <sup>+</sup> cell population co-localizes to the FVF<sup>+</sup> cell population (A-D; C \*). It is to note, that the FVF<sup>low</sup> cells are characterized through HNF1 $\beta$ <sup>+</sup> regionalized expressing cells. On that account, FVF<sup>high</sup> cells are HNF1 $\beta$ <sup>-</sup> (D; D', FVF<sup>low</sup> HNF1 $\beta$ <sup>+</sup> yellow arrow and FVF<sup>high</sup> HNF1 $\beta$ <sup>-</sup> red arrow).

Scale is set for 25 $\mu$ m

Abbreviations: DAPI = 4',6-Diamidin-2-phenylindol; FVF = Foxa2-Venus-Fusion; HNF1 $\beta$  = HNF1 Homeobox  $\beta$ ; HIGH. MAGN. = Higher Magnification; PE = pancreatic epithelium; IHC = Immunohistochemistry; E = embryonic stage.

We further focused on the ductal compartment in respect to *Sox9*. The *Sox9* gene expression is excluded from the MPP cells at the beginning of the secondary transition and localized in the trunk pattern (Seymour et al., 2007). Notably, we confirmed previous results of the FVF<sup>+</sup> PE, FVF<sup>low</sup>Sox9<sup>+</sup> and FVF<sup>high</sup>Sox9<sup>-</sup> and FVF<sup>low</sup>Sox9<sup>-</sup> cell populations in the PE at E14.5 (Figure 3.6, A-D, C \*). The co-localization of Sox9 and FVF<sup>low</sup> is restricted to the cord-like structure, defining the common progenitor pool of the formerly bi-potent trunk precursors (Figure 3.6, D' red arrow). Thus, the endocrine committed cells are represented by FVF<sup>high</sup>Sox9<sup>-</sup> expression (Figure 3.6, D' yellow arrow; Figure 3.1-3.5).

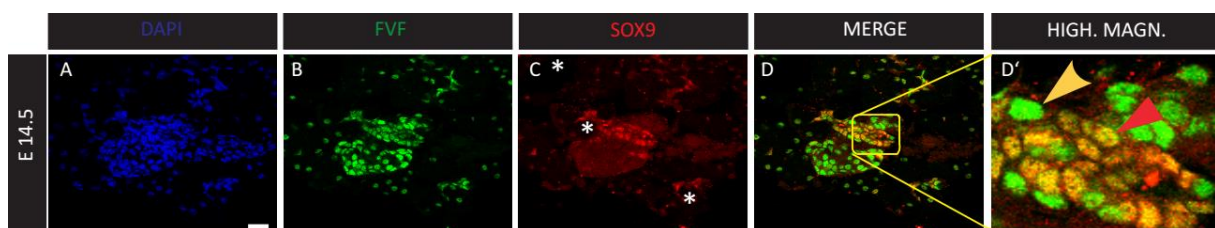


**Figure 3.6: Figure 3.5: FVF and Sox9 co-localize in the PE**

**(A-D')** Repetitive coronal sections at E14.5 of the PE and IHC of FVF and Sox9 identified the PE with a FVF<sup>+</sup> cell population and the trunk compartment as a Sox9<sup>+</sup> cell population (DAPI counterstain) (A-D, C \*). The Sox9<sup>+</sup> cells co-localizes to the FVF<sup>low</sup> cell population (A-D, C \*, D'). Contrary, FVF<sup>high</sup> does not contribute to Sox9<sup>+</sup> PE regions (D; D', FVF<sup>low</sup>Sox9<sup>+</sup> red arrow and FVF<sup>high</sup>Sox9<sup>-</sup> yellow arrow).

Scale is set for 25 $\mu$ m

Abbreviations: DAPI = 4',6-Diamidin-2-phenylindol; FVF = Foxa2-Venus-Fusion; Sox9 = SRY related gene 9; HIGH. MAGN. = Higher Magnification; PE = pancreatic epithelium; IHC = Immunohistochemistry; E = embryonic stage.

Previous results suggest that the  $FVF^{high}$  cell subpopulation segregates into the endocrine lineage, also we were interested at which E the MPP of the PE will become restricted, mainly described at  $FVF$  expression levels. Our first observation indicated lineage segregation of  $FVF$  between E18.5 and P1, the formerly  $FVF^{+}Ecad^{+}$  PE at P1 is specified as  $FVF^{-}Ecad^{+}$  PE (Figure 3.7, A-B and D). As opposed to this, the  $Pdx1^{+}$  cell population illustrates  $FVF^{+}Ecad^{-}$  and more detailed  $FVF^{high}Ecad^{-}Pdx1^{low}$  expression, respective a  $FVF^{low}Ecad^{-}Pdx1^{high}$  cell subpopulations (Figure 3.7, B-D; D',  $FVF^{high}Ecad^{-}Pdx1^{low}$  red arrow and  $FVF^{low}Ecad^{-}Pdx1^{high}$  yellow arrow). At E18.5 the  $FVF^{high}$  expressing cell population lining the outer edge of the precursor Islets of Langerhans, suggesting that this progenitor cell pool will give rise to  $\alpha$ -cells (Figure 3.7, E18.5, B; D',  $FVF^{high}Ecad^{-}Pdx1^{low}$  red arrow). Contrary,  $Pdx1^{high}$  marked cells are expressed in the inner perimeter indicating  $\beta$ -cell commitment (Figure 3.7, E18.5, B; D',  $FVF^{low}Ecad^{-}Pdx1^{high}$  yellow arrow) (Willmann et al., 2015; Wang et al., 2010; Wang et al., 2005). In later E at P1, precursor Islets of Langerhans mature as indicated in regionalized  $FVF^{high}$  expression, respective  $Pdx1^{high}$  and the PE will become compartmentalized into the different lineages (Figure 3.7, P1, D',  $FVF^{high}Ecad^{-}Pdx1^{low}$  red arrow and  $FVF^{low}Ecad^{-}Pdx1^{high}$  yellow arrow). Also in the adult Islets of Langerhans  $FVF$  co-localized to  $Pdx1$  with a slight number of  $FVF^{high}$  cell population which may represent the  $\alpha$ -cells (Figure 3.7, P36, D',  $FVF^{high}Ecad^{-}Pdx1^{low}$  red arrow and  $FVF^{low}Ecad^{-}Pdx1^{high}$  yellow arrow).

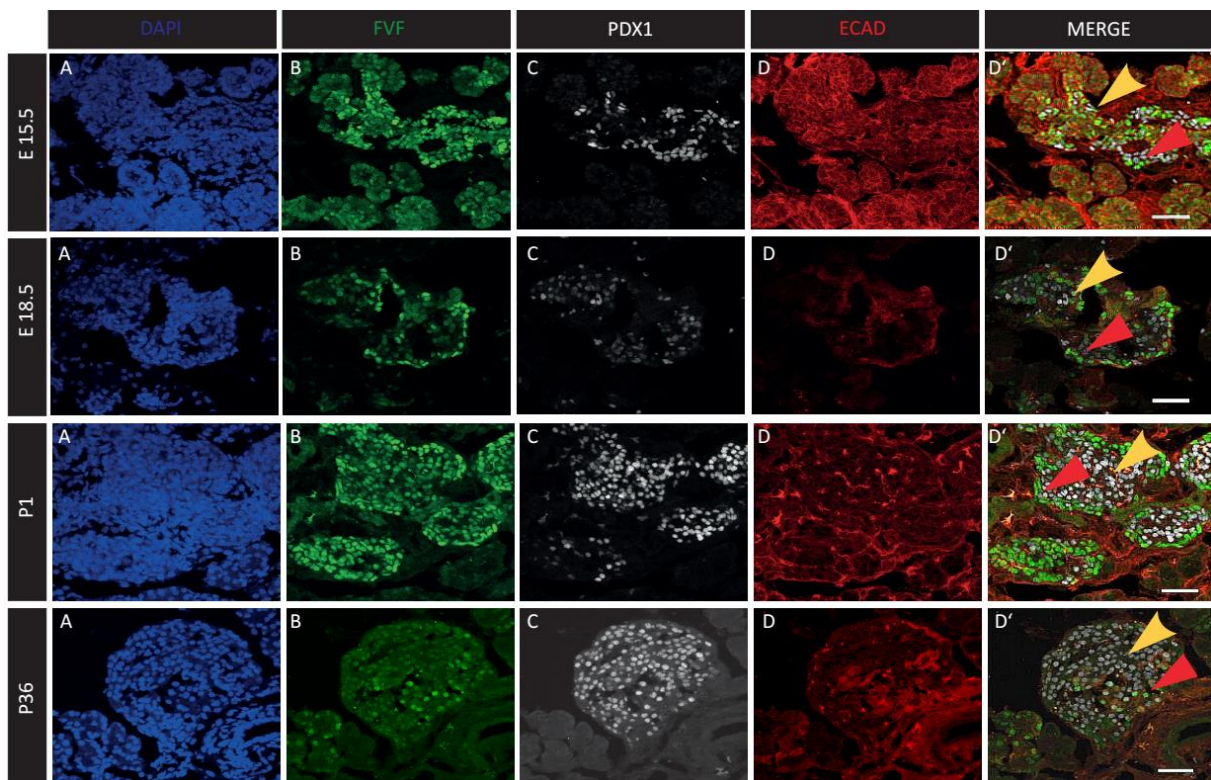


Figure 3.7: FVF expression after secondary transition correlates to the endocrine lineage commitment.

**(A-D')** Consecutive pancreatic coronal sections and IHC after secondary transition (E15.5, E18.5, P1 and P36) identified lineage restriction of the formerly MPP PE (DAPI for counterstain). The *FVF*<sup>+</sup> expression will become restricted to regionalized compartments in the PE (E15.5 – P36, A-B). Thus, the PE is characterized through *Ecad*; contrary the endocrine progenitors, precursors and mature endocrine cells are illustrated by *Pdx1* (E15.5 – P36, C; E15.5 – P36, D). The different subpopulations of FVF anti-correlate to *Pdx1*, by means *FVF*<sup>high</sup> cells are *Pdx1*<sup>-</sup>, whereas the *FVF*<sup>low</sup> cell population represents the *Pdx1*<sup>+</sup> cell pool (E15.5 – P36, D', *FVF*<sup>high</sup> red arrow and *Pdx1*<sup>+</sup> yellow arrow).

Scale is set for 50µm

Abbreviations: DAPI = 4',6-Diamidin-2-phenylindol; IHC = Immunohistochemistry; FVF = Foxa2-Venus-Fusion; *Pdx1* = pancreatic and duodenal homeobox 1; E = embryonic stage; PE = pancreatic epithelium, P = postnatal, *Ecad* = E-cadherin, MPP = multipotent pancreatic progenitors.

Taken together, this analysis reveals that FVF co-localizes to the MPP in the secondary transition at E14.5. Interestingly, PE patterning and FVF levels indicate the different lineages in pancreas organogenesis. Thus, the *FVF*<sup>low</sup> cell compartment is characterized through a *Cpa1*<sup>+</sup>*Hnf1b*<sup>+</sup>*Sox9*<sup>+</sup>*Ecad*<sup>+</sup> marker onset likely describing the exocrine and ductal progenitor pool. On the other hand, endocrine lineage segregation in the PE at E14.5 is illustrated by *Nkx6-1*<sup>+</sup>*Pax6*<sup>+</sup>*Ecad*<sup>-</sup> expressing cells. Although the subpopulations of FVF follows different expression cascades, our results emphasize the *FVF*<sup>+</sup> cell population within the PE and thus utilizing the *FVF* knock-in reporter mouse for a global gene expression profile of the PE and surrounding tissue in the secondary transition.

## 2.2 Genome-wide expression profile of the pancreas in the secondary transition

The TF factor Foxa2 is the key regulator of early development, previous work in Heiko Lickerts laboratory (Tamplin et al., 2008) identified in an *in situ* hybridization screen novel nodal genes selected by their specific mRNA expression in the organizer region in the node at E7.5. These first results indicated for two of the selected genes, *Pitchfork (Pifo)* and *Flattop (fltp)*, a role in left-right asymmetry, cilium disassembly and basal body (BB) docking (Tamplin et al., 2008; Gegg et al., 2014; Kinzel et al., 2010). Thus, in the global gene expression profile of *FVF*<sup>+</sup> PE and *FVF*<sup>-</sup> non-endodermal derived tissue we aimed to characterize regulatory and functional genes in the secondary transition of the pancreas by utilizing the *FVF* knock-in reporter mouse. (Burtscher and Lickert, 2013).

In general, different global gene expression analysis of the pancreas focuses on the endocrine lineage, although exocrine lineages determine pancreatic endocrine fate in the first secondary transition phase. This is illustrated by knockdowns of exocrine determined TF as *Ptf1a*, *Cpa1*, *Nr5a2* which will led to hypoplasia and/ or failure in pancreas organogenesis (Kawaguchi et al., 2002; Krapp et al., 1996; Zhou et al., 2007). Hence, we analyzed tissue interactions in the secondary transition and identified known

and yet functionally not described pancreatic genes, metabolic pathways and dissected classical EMT factors in the PE and non-endodermal derived tissue compartment.

### 2.2.1 Bioinformatic analysis of pathways in the secondary transition

For generating a global transcriptional expression profile during secondary transition, we dissected the pancreata of endodermal ( $FVF^+$ ) and non-endodermal ( $FVF^-$ ) derived tissue compartment at consecutive stages from E12.5 until E15.5 of  $FVF$  mice, respective  $WT$ . Analysis of lineage allocations is mandatory during secondary transition, in earlier E established endocrine progenitors will be depleted (Heller et al. 2004) and from E16.5 onwards segregation into precursor Islets of Langerhans indicates maturation (Gradwohl et al. 2000; Herrera et al., 2000). Thus, the total RNA of three biological replicates for each stage of two the distinct cell populations, the pancreatic epithelium ( $FVF^+$ ) and the  $FVF^-$  population, was used to generate the gene regulatory network (GRN) of the pancreas in the secondary transition. The application of the Affymetrix® array card (GeneChip® Gene 1.0 ST Array Card), subsequent processing of the probe set (GeneChip® Scanner 3000 7G Whole-Genome Association System) lead to the probe set outcome. The Affymetrix® Expression console normalized the robust multichip-analyses (RMA) on gene-level (ratio >200 compared endodermal and non-endodermal). Comprehensive R based microarray analyses web frontend (CARMAweb) inducted genewise testing by Limma t-test and Benjamini-Hochberg multiple testing correction with a false discovery rate (FDR<5%) offered statistically significant differential expression of 2921 probe sets. The statistical Principal component (PC) analysis thereby linearized the different E for both tissue compartments. The first PC (PC1) shows the spatial distant difference between the endodermal, respective non-endodermal tissue compartment with a variance of 68.7% variance Whereas PC2 describes the different E with a total variance of 13.3%. (See Figure 3.8 B) (Willmann et al., 2015).

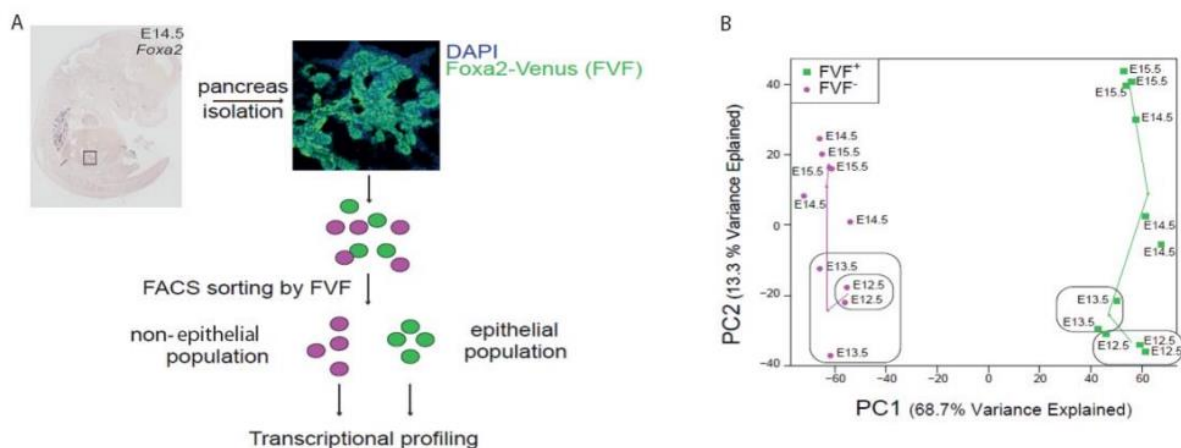


**Figure 3.8: Experimental setup for the GRN.**

- (A)** The GenePaint *in silico in situ* demonstrates mRNA expression of *Foxa2* at E14.5, the black box indicates the pancreatic region in the whole mount embryo. The *FVF*<sup>+</sup> cell population represents the PE, contrary the *FVF*<sup>-</sup> cell population is marked through DAPI IHC at E14.5. After pancreas dissection and single cell suspension, fluorescent-activated cell sorting (FACS) sorting separated the endodermal (*FVF*<sup>+</sup>) of the non-endodermal (*FVF*<sup>-</sup>) cell compartment. Global transcriptional profiling was accomplished by Affymetrix® GeneChip® Gene 1.0 ST Array Card and statistical analyses through the Affymetrix® Expression console.
- (B)** The Affymetrix® Expression console was used for statistical analysis, thereby using PC analysis separated the different E. In taking triplicates of the RNA samples, each sample in the different embryonic stage was referenced against each other. The results are blotted with variances between 68.7% (PC1) and 13.3% (PC2).

Abbreviations: RNA = ribo nucleotide acid; E = embryonic stage; FACS = fluorescent activated cell sorting; PC = principal component; DAPI = 4',6-Diamidin-2-phenylindol; PE = pancreatic epithelium; IHC = immunohistochemistry; *FVF*<sup>+</sup> = *Foxa2*-Venus-Fusion positive; *FVF*<sup>-</sup> = *Foxa2*-Venus-Fusion negative.

First of all, we determined the quantity of dysregulated genes at each E for both tissue compartments (Figure 3.9, A). In total, 7346 genes at E14.5 are differentially expressed, indicating increasing morphogenetic alterations within the PE (Pan and Wright, 2011a; Pictet et al., 1972). Due to lower sample sizes and less concordant ribonucleotide acid (RNA) in the *FVF*<sup>-</sup> at E13.5, the number of significantly regulated genes was reduced by multiple testing corrections (Willmann et al., 2015).

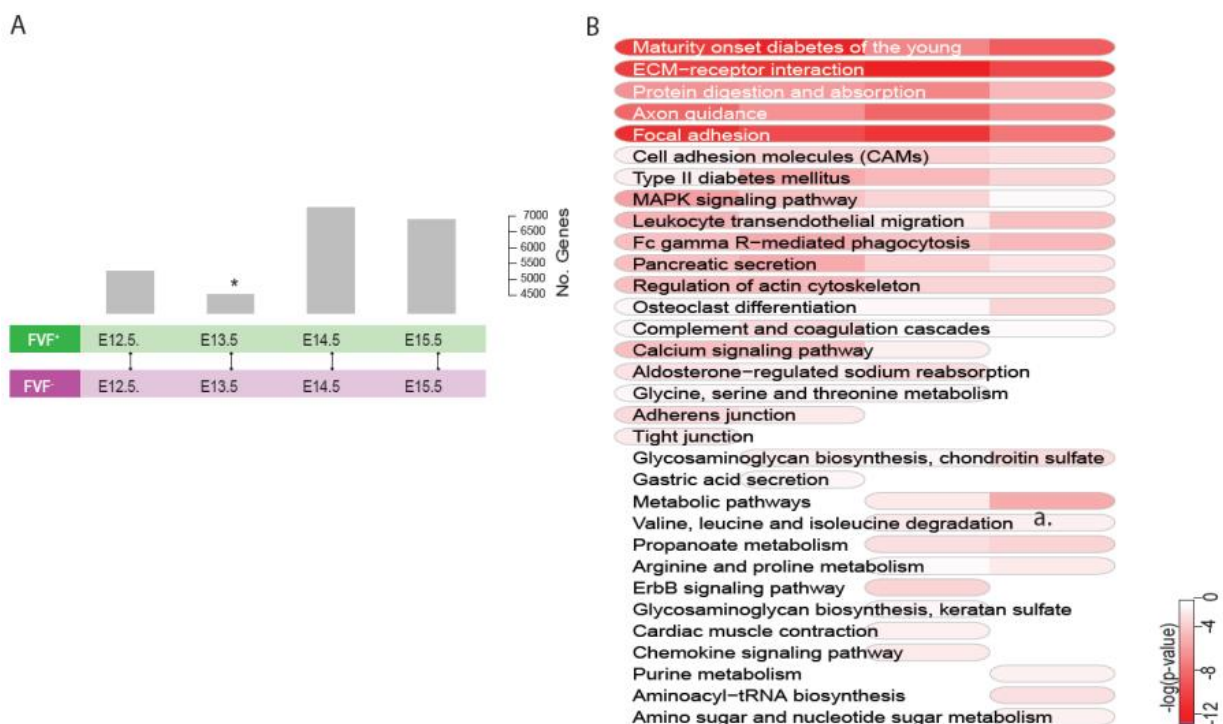


**Figure 3.9 : The GRN in the pathway analysis.**

- (A) The Histogramm describes the quantity of dysregulated genes of each developmental stage (p-value < 0.01). At E13.5 sample size represent duplicates (\*, n=2); E12.5 – E15.5 are represented in triplicates (n=3, exception E13.5 n=2).
- (B) The Kyoto Encyclopedia of Genes and Genomes (KEGG) pathway analysis was performed with indicated hierarchical pathway enrichments in the different E of the secondary transition. Significant differences in *FVF<sup>+</sup>* to *FVF<sup>-</sup>* compartment are color-coded (red color-code illustrates for the terms high dysregulated number of genes in comparison of both tissue populations, respectively ( $\log_{10}(p) < 1$  with  $p < 0.1$ )).

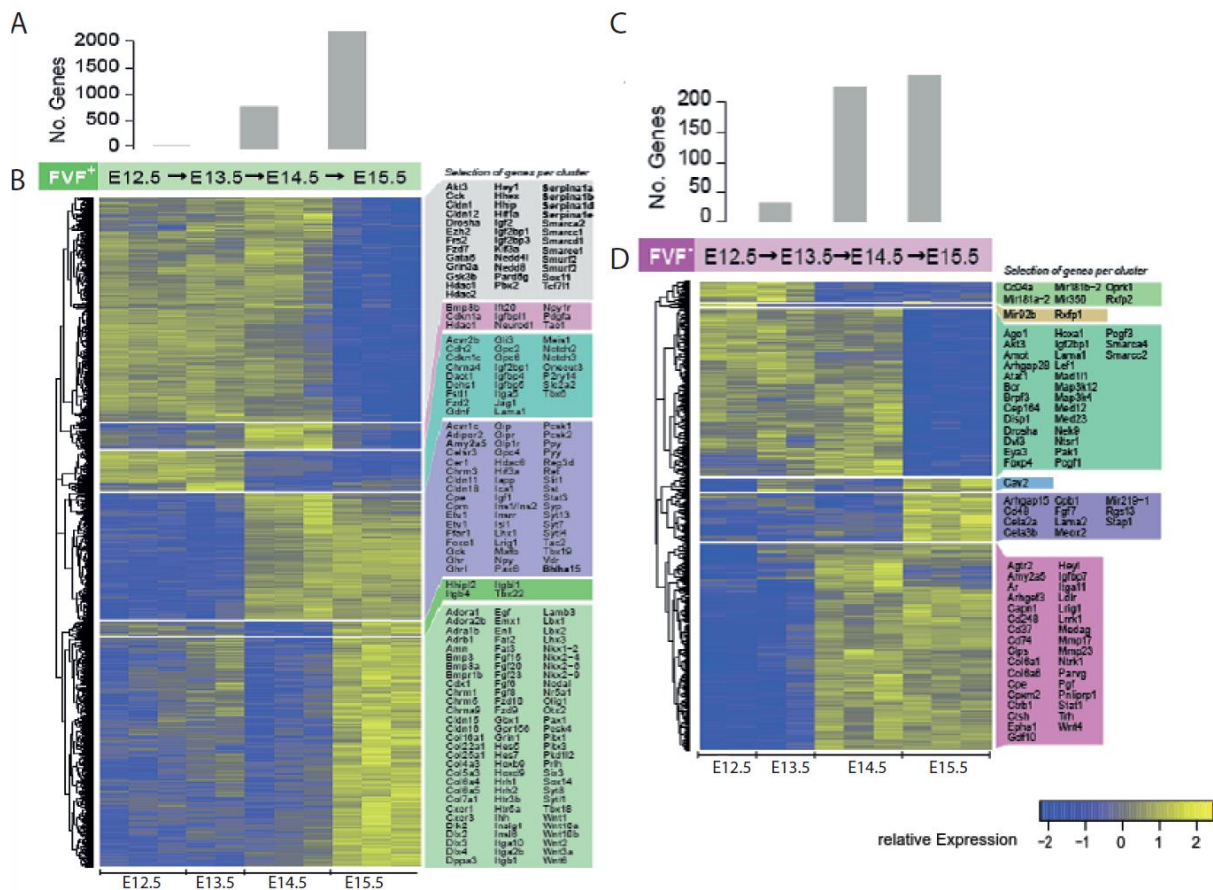
Abbreviations: n = number; E = embryonic stage; KEEG = Kyoto Encyclopedia of Genes and Genomes; E = embryonic stage; log = logarithm; *FVF<sup>+</sup>* = Foxa2-Venus-Fusion positive; *FVF<sup>-</sup>* = Foxa2-Venus-Fusion negative; ECM = extracellular matrix; tRNA = transfer ribo nucleid acid; No/n = number.

The endodermal population shows discrepancy compared to the non-endodermal population in metabolic pathways mainly due to diverse assignments in both tissue compartments. Functional pathway analysis was performed by using the database resource Kyoto encyclopedia of genes and genome (KEGG). We wanted to achieve a more comprehensive understanding of high-level functions and pathways which differ in both populations (Figure 3.9 B). The key pathway as maturity onset diabetes of the young (MODY) and type 2 diabetes (T2D) are upregulated, indicating the ongoing organogenesis of the pancreas. Interestingly, ECM-receptor interaction (ECM) and cell adhesion molecules (CAM) are highly deregulated. This result is in line with already published data by Kesavan for Laminin-1 inhibition, which leads to failure in branching morphogenesis and differentiation. It may reflect the importance of ECM and mesenchyme for proper proliferation of the pancreas during secondary transition (Kesavan et al., 2014). Mitogen-activated protein kinases (MAPK kinases) indicate a role in lineage formation by MAPK/ERK pathway and transcriptional activation of lineage specific factors. Recently published by Morris might suggest for the pathway regulation of actin cytoskeleton and AJ/TJ remodeling of the epithelial polarity sheet as the endocrine lineage establishes (Morris et al., 2015). Which mechanism as classical EMT or delamination occurs, is still controversial. More interestingly, axon guidance within the epithelial population is dysregulated, indicating the correlation of the gene activity program of endocrine cells in neural tissue and in the pancreas. Our results confirm published data by Arensbergen, in which insulin-producing  $\beta$ -cells adopt a neural gene activity program by repressing the Polycomb complex (Van Arensbergen et al., 2010). Thus, highlighting again the close relationship of neuronal and pancreatic derived progenitors. One more point to mention might be the pathways for amino-acid related biosynthesis and the metabolic pathway which are regulated from E14.5 onwards. This may implicate ongoing differentiation of the different lineages and expansion and branching of the pancreas. As the KEGG pathway analysis only offers pathways and does not reflect

single gene expression in a spatial-temporal manner, in the next step we wanted to elucidate specific gene expression (Willmann et al., 2015).

### 2.2.2 Bioinformatic analysis of genes in the secondary transition

The KEGG pathway analysis illustrates dysregulated pathways in correlation between the *FVF*<sup>+</sup> - and the *FVF*-cell population, respective endodermal versus non-endodermal tissue compartment. In the next step, the GRN was utilized for deciphering single gene expression of a selected subset of genes. Therefore, the selected genes were arranged in clusters due to their expression profile in terms of the *FVF*<sup>+</sup> - and the *FVF*-cell compartment, spatio-temporal separated in the E of the secondary transition (Willmann et al., 2015).



modified from Willmann et al., 2015

**Figure 3.10: The GRN in endodermal and non-endodermal tissue populations**

(A) The Column reflects the quantity of dysregulated genes in the endodermal-derived tissue compartment peaking in at E15.5 with 2196 genes, respective the *FVF*<sup>+</sup> cell population (FDR adjusted p-value < 0.01).

- (B)** Hierarchical clustering in the heatmap identifies 6 different clusters with characteristic molecular profiles for the endodermal cell compartment, respective FVF<sup>+</sup> cell population..
- (C)** The Column reflects the regulated genes in the the non-endodermal tissue compartment, peaking in with 246 genes in the non-epithelial population at E15.5, respective FVF<sup>-</sup> cell population(FDR adjusted p-value < 0.01).
- (D)** The heatmap reflects clustered genes due to their expression profile in the secondary transition in the non-endodermal population with 6 different clusters (FDR adjusted p-value < 0.01).

Abbreviations: E = embryonic stage; FVF = Foxa2-Venus Fusion; No = number; GRN = gene regulatory network; FDR = false discovery rate.

Interestingly, genes in the epithelial population are higher regulated with a maximum of 2169 genes at E15.5. This might indicate, that the MPP in the secondary transition already segregated into the different lineages as endocrine, duct and acinar and suggests to reflect a higher quantity of transcriptional changes. Thus, the endodermal compartment illustrates greater changes compared to the non-endodermal tissue compartment (246 in the non-endodermal population).

Hierarchical clustering of the different transcriptional expression over time revealed different clusters for a specific subset of genes. As expected, exocrine progenitors as *Amylase, 2 Alpha 5 (Amy2a5)*, *Mist1/Bhlha* and *Nr5a2* show increased expression in the ongoing secondary transition. Similar result are determined for the endocrine lineage factors (*Ins1, Ins2, Insrr, Isl1, Pax6*) suggesting ongoing proliferation of the pancreas and dedifferentiation at the end of secondary transition. The downregulation of the *Serpina* family represented in the heatmap (*Serpina 1a, 1b, 1d, 1e*) might be due to expression at the tip regions of the pancreas and perdition during pancreas preparation ongoing with FACs inefficiency. The FGF (*Fgf15, 20, 23, 6*) and WNT-pathway (*Wnt1, 2, 3a, 5a, 6, 10b* and *Fzd9,10*) implicate cell dedifferentiation, as the pathway components are commonly known factors for cell junction remodeling (Ciruna et al., 2001; Lickert et al., 2005). *Cela2a* and *Cela3b* had been lately described as microvascular factors involved T2D (Han et al., 2011). Furthermore, factors expressed in mid-hindbrain boundary (*Wnt1, Otx2, Fgf8, En1*), indicating again the relationship of epithelial progenitors in development into different tissues. The pathway of microRNAs (miRs) (*Ago1, Drosha*) show equal expression during secondary transition, escalating at E15.5. The chromatin regulation reflects similar expression pattern with decreasing expression at E15.5 (*Smarca2, Smarca1, Med12, Med23*). Insulin-like growth factor binding proteins (*Igfbp4, Igfbp5*) are highly downregulated at the end of secondary transition. We could detect the same results for *Glypican1* and *Glypican4 (Glp1, Glp4)* as published data showed for these genes a role in canonical Wnt-signaling and BMP signaling for the differentiation of cardiac progenitors into cardiomyocytes (Strate et al., 2015). In addition, planar cell polarity (PCP) pathway components (*Fzd2*), Notch components (*Notch2, Notch3*) and Wnt-signaling

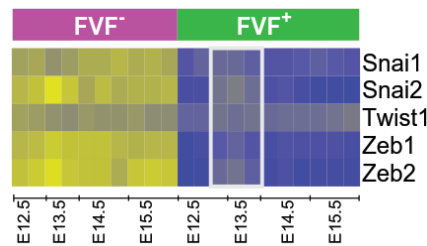
(*Wnt6*, *Wnt3a*, *Wnt10a*, *Wnt10b*, *Wnt1*) indicate a signaling cascade in the PE likely due to the fact that pancreas differentiation relies on paracrine instead of autocrine factors (Pan and Wright, 2011) (Figure 3.10 B). Furthermore, several genes can be depicted in the transcriptome profile by unknown function in pancreas development and arrange into the different expression cluster. Thus, the hierarchical clustering might represent similar function of genes yet functionally not described in pancreas organogenesis.

In the non-endodermal compartment, lesser amount of cells are dysregulated between the different E. This might be explained by the more stable character of the mesenchyme compared to the differentiating epithelium. The miR pathway (*Mir181a-2*, *Mir181b-2*, *Mir350*) shows equal expression compared to the PE. The miRs peaks in at around E12.5 with open chromatin structure and transcriptional changes until E14.5 (*Ago1*). As postulated, classical EMT might initiate endocrine formation (Gouzi et al., 2011; Johansson et al., 2007). Interestingly, EMT factors are expressed in the mesenchyme, suggesting remodelling of this specific tissue compartment. Upon Wnt-/ $\beta$ -catenin signaling, progenitors expressing *small cell lung carcinoma cluster 4<sup>+</sup>* (*Cd24a<sup>+</sup>*) will be integrated by possible EMT mechanism into adult renal, thus highlighting EMT in pancreas organogenesis (Zhang et al., 2015). With peaking expression of *Cd24a* at E12.5 we could identify decreasing expression of *Cav2* at around E15.5. This is in line with already published data, as both are novel marker for EMT, respectively MET (Dragoi et al., 2014). MAPK kinases (*Map3k12*, *Map3k4*) upregulated at E12.5, implicate proliferation and expansion of the endocrine pancreas into the surrounding mesenchyme. ECM proteins (*Col6a1*, *Col6a6*) might be essential in the mesenchyme in later E of the secondary transition as the expression peaks in at around E14.5. As the non-endodermal compartment reflects more stable expression due to lesser number of regulated genes (Peak at E15.5, including 246 genes), similar molecular mechanism might play a role as already described in the PE compartment (Figure 3.10 D).

Taken together, the single gene expression sustain previous results in pancreas organogenesis comprising of PCP, indicating a polarity establishment in pancreas morphogenesis (Cortijo et al., 2012; Gegg et al., 2014)

At latest in the E E13.5 MPP of the PE will be disposed and cells are restricted to the different lineages. Pictet and Rutter already postulated in the 70ies that these endocrine progenitors delaminate out of the epithelial sheet and cluster to precursor Islets of Langerhans. This Delamination process accompanies with alteration in junctional contacts to other cells. In the neuron crest system, delamination is well studied and described as transcriptionally controlled by the *Snail family of transcription factors* (Blanco et al., 2002). Until now, mechanism regarding pancreas organogenesis

are controversial, either delamination, classical EMT or Epithelial-to-epithelial transition (EET) are in discussion (Nieto et al. 2009, Burtscher et al., 2013; Willmann et al., 2015).



modified from Willmann et al., 2015

**Figure 3.11: The TF of EMT in the GRN**

The TF as *Snail/Snai1*, *Snail/Snai2*, *Twist1*, *Zeb1* and *Zeb2* represent EMT expression in the non-endodermal population (FVF<sup>-</sup>) and in the endodermal cell population (FVF<sup>+</sup>). The white box indicates slight upregulation in the pancreatic epithelium at E13.5.

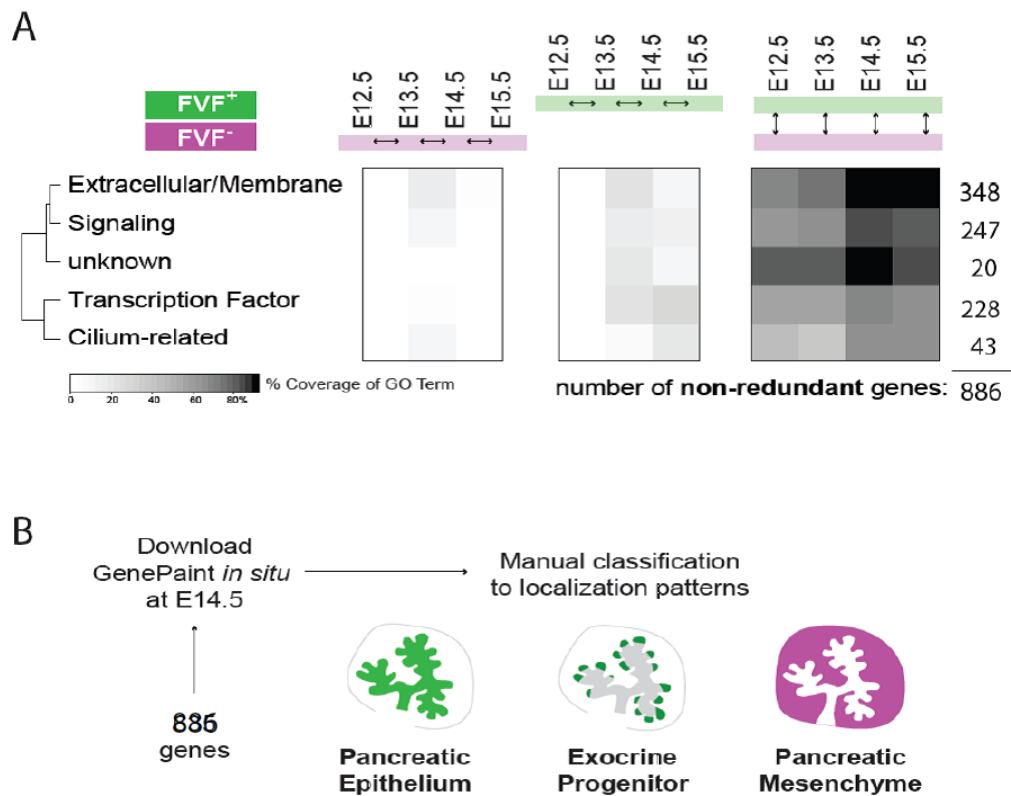
Abbreviations: *Snail/Snai1*= *Snail family Zinc finger 1* ; *Snail/Snai2*= *Snail family Zinc finger 2*; *Twist1* = *Twist Family BHLH Transcription Factor 1*; *Twist2* = *Twist Family BHLH Transcription Factor 2*; *Zeb1* = *Zinc Finger E-Box Binding Homeobox 2*; *Zeb2* = *Zinc Finger E-Box Binding Homeobox 2*; E = embryonic stage; FVF<sup>+</sup> = Foxa2-Venus-Fusion positive; FVF<sup>-</sup> = Foxa2-Venus-Fusion negative; EMT = epithelial-to-mesenchymal transition; GRN = gene regulatory network.

In the process itself are *Snail family Zinc finger* TF involved and members of the Rho subfamily of GTPases. Recently published by Rukstalis et al., *Snail2/Slug* is co-expressed with endocrine progenitor *Ngn3* and still maintained in a subset of differentiated endocrine cells (Rukstalis and Habener, 2007). These results suggest EMT of endocrine progenitors as they leave the ductal cord. To elucidate this question, we looked for classical EMT TF in the non-endodermal, respective mesenchymal population and in the endodermal population. Surprisingly, the EMT TF (*Snail1*, *Snail2*, *Twist1*, *Zeb1* and *Zeb2*) are expressed in the non-endodermal compartment. Whereas in the PE at E13.4 a slight increase, especially in *Snail2* and *Zeb2*, might implicate the process itself (Figure 3.11). From the previous results, we assume that the low detection of the classical EMT factors in the PE suggests rather delamination than EMT (Willmann et al., 2015).

### 2.3 Identification and characterization of pancreatic genes

The GRN profile was further attained for identification of known and yet pancreatic related genes functionally not described. Thus, Gene ontology (GO) term analysis classified the genes into functional

groups by selected terms Extracellular/located at Plasma membrane, Signaling, Transcription factor, cilium-related und unknown by function. E-mapping further reflects non-redundant genes by their GO term in the non-endodermal, PE and in correlation of both tissue compartments to each other, respectively. The non-endodermal expressed genes showed at E13.4 coverage of approximately 40% for the term extracellular/ located at plasma membrane and 20% for the term signaling with GO terms. The term unknown represents genes with yet unspecified protein domains, indicating that the GO database does not reflect all protein domains. The PE compartment covers in maximum of approximately 40% of the genes by GO term at E15.5. It is to mention that a higher amount of genes could be sorted by their GO term in the epithelial population. Comparison between both tissue compartments reflected for the genes a maximum of 100% coverage by GO term analysis for Extracellular/located at plasma membrane. The same coverage could be observed for genes with unknown molecular protein domain peaking in at E14.5 (Figure 3.12 A) (Willmann et al., 2015).



modified from Willmann et al., 2015

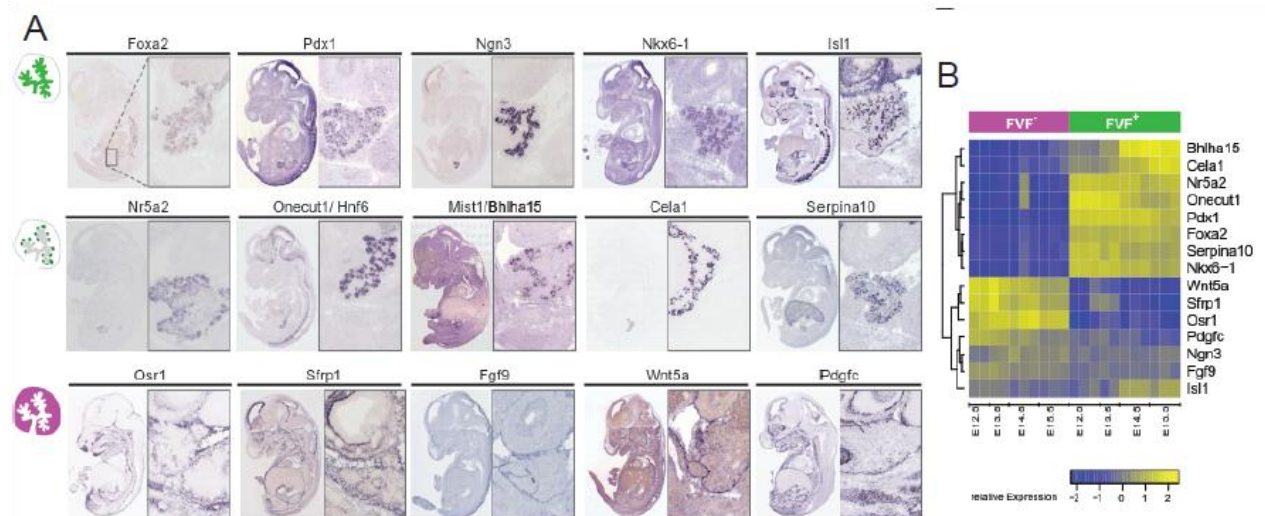
**Figure 3.12: Experimental setup for expression pattern analysis.**

- (A)** Bioinformatic GO term analysis was accomplished for sorting genes in total 886 probe sets for the different GO terms Extracellular/located at Plasma membrane (348), Signaling (247), Transcription factor (228), cilium-related (43) und unknown by function (20) in the PE, non-endodermal and both cell compartments in correlation to each other, respectively.

(B) Furthermore the GenePaint *in silico in situ* database by using embryonic whole mount section at E14.5 classified the 886 probe sets to different localization pattern. For this purpose pictures were captured of the wholemount embryo and a zoom (3x) into the pancreatic region for the selection into either PE, exocrine/tip and mesenchyme lineage.

Abbreviations:GO = gene ontology; PE = pancreatic epithelium; E = embryonic stage; FVF<sup>+</sup> = Foxa2-Venus-Fusion positive; FVF<sup>-</sup> = Foxa2-Venus-Fusion negative; % = percentage.

As we predicted the function of the genes, the next step was determining the lineage of our depicted genes. For this approach the GenePaint *in silico in situ* database offers whole mount *in silico in situs* at the E14.5. In total 886 genes were analyzed by their mRNA expression pattern (Supplement Table 10), thus genes already summarized according to their GO term and thereby offering predicted function and lineage. The PE was classified manually into an PE/trunk pattern, exocrine progenitors with tip pattern and the pancreatic mesenchyme represented in a hybridization pattern at the ceiling of the pancreatic region to assure the right localization of the different probe sets (Willmann et al., 2015).



modified from Willmann et al., 2015

**Figure 3.13: Representative pancreatic genes classified into specific expression patterns**

(A) For classification of the *in situ* expression patterns of the PE we referred to known pancreatic marker as *Foxa2* and *Pdx1*. The trunk pattern is represented by *Ngn3*, *Nkx6-1* and *Isl1*. The tip pattern is illustrated in the pancreatic exocrine progenitors *Nr5a2*, *Onecut/Hnf6*, *Mist/ Bhla15*, *Cela1* and *Serpina10*. In addition, the mesenchymal expression pattern accounts to the genes *Osr1*, *Sfrp1*, *Fgf9*, *Wnt5a* and *Pdgfc*.

(B) The heatmap correlates to the selected genes in the *in situ* expression pattern of (A). The genes *Foxa2*, *Pdx1*, *Ngn3*, *Nkx6-1*, *Isl1*, *Nr5a2*, *Onecut*, *Hnf6*, *Mist/ Bhla15*, *Cela1*, *Serpina10*, *Osr1*, *Sfrp1*,

*Fgf9*, *Wnt5a* and *Pdgfc* are clustered by their expression profile in the *FVF*<sup>+</sup>, respective *FVF*<sup>-</sup> cell population.

Abbreviations: *FVF*<sup>+</sup> = *Foxa2-Venus-Fusion positive*; *FVF*<sup>-</sup> = *Foxa2-Venus-Fusion negative*; *Foxa2* = *winged helix/forkhead box*; *Pdx1* = *Pancreatic and duodenal factor 1*; *Ngn3* = *Neurogenin 3*; *Nkx6-1* = *NK6 homeobox 1*; *Isl1* = *ISL LIM homeobox 1*; *Nr5a2* = *nuclear receptor subfamily 5*; *Onecut1/Hnf6* = *one cut homeobox 1*; *Mist1/Bhlha15* = *Basic Helix-Loop-Helix Family, Member A15*; *Cela1* = *Chymotrypsin-like elastase family member 1*; *Serpina10* = *Serpine peptidase inhibitor, clade A (alpha-1 antiproteinase, antitrypsin), member 10*; *Osr1* = *odd-skipped related 1*; *Sfrp1* = *secreted frizzled-related protein 1*; *Fgf9* = *fibroblast growth factor 9*; *Wnt5a* = *wingless-type MMTV integration site family, member 5A*; *Pdgfc* = *platelet derived growth factor C*; E = embryonic stage.

The MPP in the PE in the beginning of the secondary transition is marked by *Foxa2* and *Pdx1* expression (Gao et al., 2008). Zhou et al described the segregation process in the secondary transition with the tip domain marked by *Ptf1α /c-myc/Cpa1* in addition to *Pdx1* expression, whereas the trunk domain is marked by expression of TF as *Ngn3* and *Nkx6-1* (Bonner-Weir, 2000; Dubois et al., 2011; Schaffer et al., 2013; Seymour et al., 2008; Zhou et al., 2007). This observation implicate that within the trunk domain endocrine progenitors (*Ngn3*<sup>+</sup>) reside next to endocrine precursors (*Nkx6-1*<sup>+</sup>) in pancreas organogenesis. Indeed, we observed for the endocrine determining factor *Ngn3* and late endocrine factor *Isl1* a typical trunk pattern with the *in situ* pattern in the center of the pancreatic region. The expression profile of the specific marker subset clearly detects *Foxa2*, *Pdx1* and *Nkx6-1* in the PE. Interestingly, the mRNA of the endocrine precursor factor *Nkx6-1* is at E14.5 expressed in the whereas protein level indicate expression within the trunk pattern (Schaffer et al., 2013). In the non-endodermal population slight expression of the endocrine progenitors *Isl1* at E12.5 was confirmed by published data (Kim et al., 2000), in line that at consecutive later E *Isl1* expression increases in the PE. As expected *Ngn3* is expressed in the PE, the quantity of *Ngn3*<sup>+</sup> cells is illustrated in low expression levels (Figure 3.13 B). More surprisingly, we could detect expression in the non-endodermal population, suggesting contamination, false positive probe sets or neuronal progenitors in the surrounding mesenchyme account to this result (Willmann et al., 2015).

For the expression patterning of the Genepaint *in silico in situs* categorized into tip, we selected *Nr5a2*, *Onecut/Hnf6*, *Mist1/Bhlha15*, *Cela1* and *Serpina 10*. In the secondary transition, *Nr5a2* controls acinar differentiation as illustrated in the tip pattern. Interestingly, the gene also encodes in the MPP at earlier E. Notch pathway components as *Rbpj* and pancreatic determining TF *Foxa2* and *Ptf1α* through regulator interaction may control *Nr5a2* expression (Hale et al., 2014). The mechanism which finally separates *Nr5a2* into the exocrine lineage is until now not determined. *Onecut/Hnf6* and *Mist1/Bhlha15* are well described TF for the exocrine compartment of the PE. As they show together with *Nr5a2* multipotency at least during the first transition phase in the PE, these factors are later restricted to the

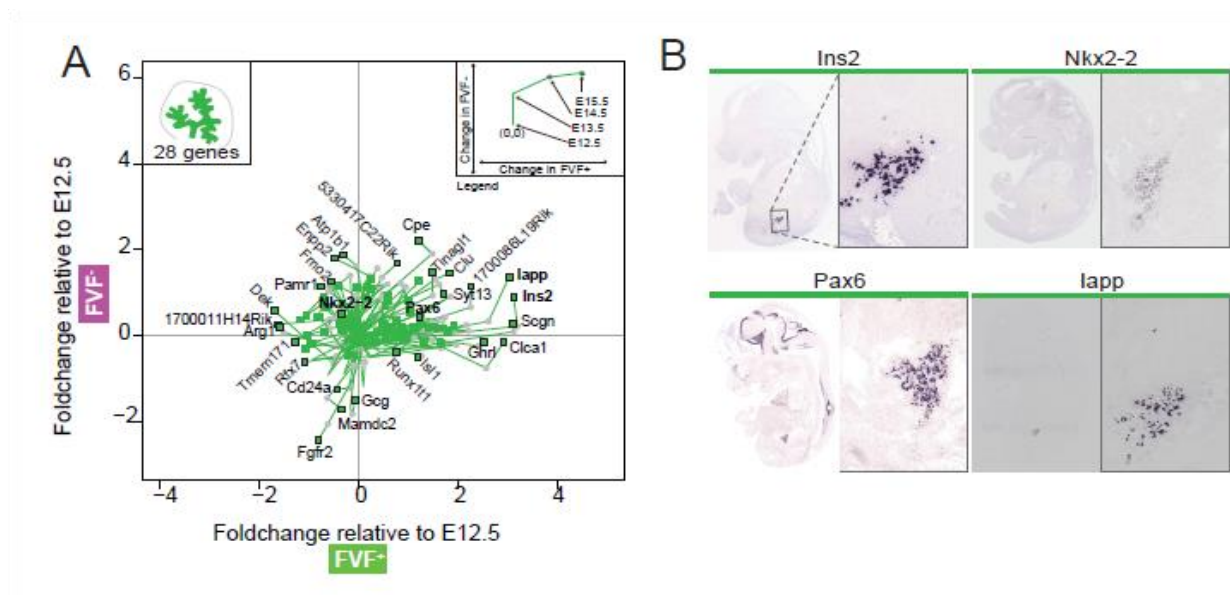
bipotent tip pattern which is determined for the exocrine and ductal lineage segregation (Pan and Wright, 2011). Due to the fact, that the exocrine lineage is not only determined by TF, we selected lipases and amylases as *Cela1* and *Serpina10* for the tip structure. Interestingly, in our expression profile *Mist1/ Bhlal5* and *Cela1* show expression in the PE only from E14.5 onwards, whereas the other factors are already expressed in the beginning of the secondary transition. This might be due to low expression of *Mist1/ Bhlal5* in the multipotent cells. The low mRNA expression the profile in the beginning of the secondary transition for *Cela1* suggests rather active transcription of the acinar lineage determinant at later E in line that the gene rather indicates bipotent tip cells already segregated into the acinar lineage (Figure 3.13 A-B) (Willmann et al., 2015).

E-specific signaling regulates patterning and specification of the pancreas mainly regulated in the non-endodermal compartment of the pancreas (Gittes et al., 2009; Nostro et al., 2011). Mesenchymal cells regulate branching and pancreatic growth of both the exocrine and endocrine compartment. Also, Golosow et al. described that proliferation of precursors and differentiated pancreatic cells failed as the mesenchyme is stripped of from the PE (Golosow et al., 1962). Therefore we classified the *in situ* hybridization patterns for mesenchymal located genes as *odd-skipped related 1 (Osr1)*, *secreted frizzled-related protein 1 (Sfrp1)*, *fibroblast growth factor 9 (Fgf9)*; *wingless-type MMTV integration site family, member 5A (Wnt5a)* and *platelet derived growth factor receptor c (Pdgfc)*. For example *Osr1* suggests expression in lung development including a role in the Wnt/ $\beta$ -catenin pathway by suppression of BMP signaling (Rankin et al., 2012). At E14.5 *Osr1* is clearly detectable in the pancreatic mesenchyme, but we could not identify an *in situ* hybridization expression pattern in the lung. This might suggest Wnt/ $\beta$ -catenin signaling with loss of BMP in the mesenchyme. But there still remain questions as there is only expression in the non-endodermal tissue compartment and we could not detect expression in the profile in the endodermal-derived compartment (Figure 3.13 A-B). Surprisingly, canonical Wnt-member *Wnt5a* is expressed in the mesenchyme as published data suggested by Rodriguez-Seguel for *Wnt5a* facilitation of *Pdx1* expression (Rodriguez-Seguel et al., 2013). In *Wnt5a*<sup>-/-</sup> zebrafish, the Islets of Langerhans failed to organize in a proper way, implicating for *Wnt5a* a role in endocrine formation (Kim et al., 2005). These might be due to low expression within the epithelium, similar to *Sfrp1*, which seems to regulate Wnt-signaling (Gibb et al., 2013). As expected, signaling factors are accumulating in the mesenchyme. The factor *Pdgfc* plays a role in embryogenesis within the mesoderm and on later E in neural crest cells, the knock-in mouse line might be a tool for deciphering mesenchymal interaction in pancreas development (Suzuki et al., 2015). As we found a member of the FGF family (*Fgf9*) in the mesenchyme, signaling via FGF might play a role via autocrine signaling into the PE. In the profile, the mesenchymal factors are clearly expressed in the non-endodermal compartment, with slight expression of *Fgf9* and *Pdgfc* in the PE (Willmann et al., 2015).

Our analysis of the *in silico in situ* expression pattern of known pancreatic genes confirmed common pattern as tip and trunk. We additionally classified the mesenchyme to further determine possible signaling pathways and tissue interactions. Therefore, our approach might be a good tool to further elucidate the dataset for spatial and temporal progression of single genes in the secondary transition.

### 2.3.1 Temporal and spatial progression of pancreatic genes

In the next step spatial and temporal expression of known pancreatic genes was further analyzed. We depicted pancreatic regulatory genes of the GRN and classified the genes in correlation to the specific *in situ* hybridization pattern. Thus, we selectively grouped the genes into epithelial/trunk, tip and mesenchymal pattern at E14.5. In the attached blot, the single gene expression in the different E are illustrated in more detail (Willmann et al., 2015).



modified from Willmann et al., 2015

**Figure 3.14: Temporal and spatial expression of depicted known pancreatic genes and the classical PE/trunk *in silico in situ* pattern obtained by Genepaint.**

- (A) The blot reflects the depicted different genes in each single timepoint in the secondary transition. The genes used in the *in situ* hybridization pattern as *Ins2*, *Nkx2-2*, *Pax6* and *lapp* are highlighted in bold. In total, we included 28 genes for the blot of the PE (*1700011H14Rik*, *Dek*, *Pamr1*, *Fmo2*, *Enpp2*, *Atp1b1*, *5330417C22Rik*, *Cpe*, *Tinag1*, *Clu*, *1700086L119Rik*, *Syt13*, *Pax6*, *lapp*, *Ins2*, *Scgn*, *Cla1*, *Ghrl*, *Isl1*, *Runx1t1*, *Gcg*, *Mamdc2*, *Fgfr2*, *Cd24a*, *Nkx2-2*).

**(B)** In addition, the *in situ* classification annotated the genes into an epithelial/trunk pattern. The genes *Ins2* and *Pax6* represent a pattern related to the PE, whereas the genes *Nkx2.2* and *lapp* illustrate a trunk pattern. It is to note that the described genes mainly present unique expression in the pancreatic region with the exception of *Pax6* (*in situ* pattern in the neurogenic regions of the whole mount embryo).

Abbreviations: : *FVF<sup>+</sup>* = *Foxa2-Venus-Fusion positive*; *FVF<sup>-</sup>* = *Foxa2-Venus-Fusion negative*; *Foxa2* = *winged helix/forkhead box*; E = embryonic stage; *Ins2* = *Insulin 2*; *Nkx2-2* = *NKX homeobox 2-2*; *Pax6* = *paired box 6*; *lapp* = *islet amyloid polypeptide*; *1700011H14Rik* = *RIKEN cDNA 1700011H14 gene*; *Dek*, = *DEK proto-oncogene*; *Pamr1* = *Peptidase Domain Containing Associated With Muscle Regeneration 1*; *Fmo2* = *flavin-containing monooxygenase*; *Enpp2* = *Ectonucleotide Pyrophosphatase/Phosphodiesterase 2*; *Atp1b1* = *Sodium/potassium-transporting ATPase subunit beta-1, 5330417C22Rik = RIKEN cDNA 5330417C22 gen;*; *Cpe* = *Carboxypeptidase E*; *Tinagl1* = *Tubulointerstitial Nephritis Antigen-Like*; *Clu* = *Clusterin*, *1700086L119Rik = RIKEN cDNA 1700086L119 gene*, *Syt13* = *Synaptotagmin 13*, *Pax6* = *paired homeobox x 6*; *Ins2* = *Insulin 2*; *Scgn* = *Secretagogin*; *Clca1* = *Chloride Channel Accessory 1*; *Ghrl* = *Ghrelin*; *Isl1* = *SL LIM Homeobox*; *Runx1t1* = *Runt-Related Transcription Factor 1*; *Translocated To, 1 (Cyclin D-Related)*; *Gcg* = *Glucagon*; *Mamdc2* = *MAM Domain Containing 2*, *Fgfr2* = *Fibroblast Growth Factor Receptor 2*, *Cd24a* = *small cell lung carcinoma cluster 4*.

For the pattern described as PE, we manually depicted *Insulin2* (*Ins2*) with increasing expression in the PE. The same results could be observed for the gene *islet amyloid polypeptide* (*lapp*), which reflects even higher expression in the PE compared to *Ins2*. Furthermore, the *lapp* hybridization pattern reflects a more typical trunk pattern compared to *Ins2*. Both genes are described in the context of diabetes; the gene *Ins2* accounts for MODY4, disruption in the gene leads to the onset of diabetes. Additionally, the gene *lapp* is involved in T2D and Alzheimer disease, but until now not described as MODY gene. The gene *Pax6* illustrated stable expression with characteristically PE pattern in the *in situ*. As *Pax6* and *Nkx2-2* are essential in neuronal differentiation, expression in the GRN indicates again the correlation between midgut-hindbrain formation (Ertaylan et al., 2014; Rudnick et al., 1994; Van Arensbergen et al., 2010; Willmann et al., 2015) (Figure 3.14 A-B).

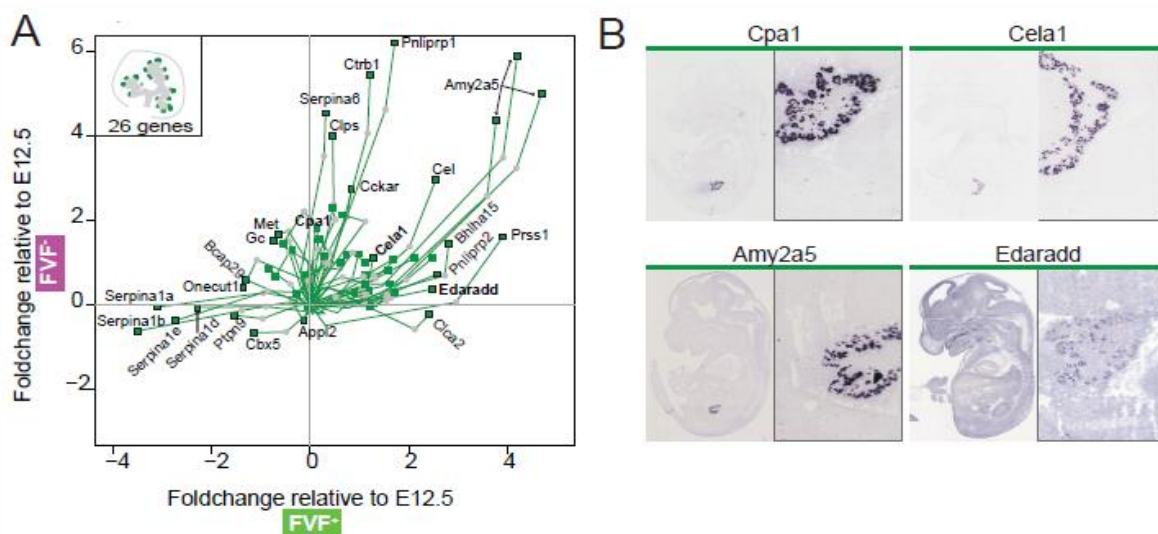
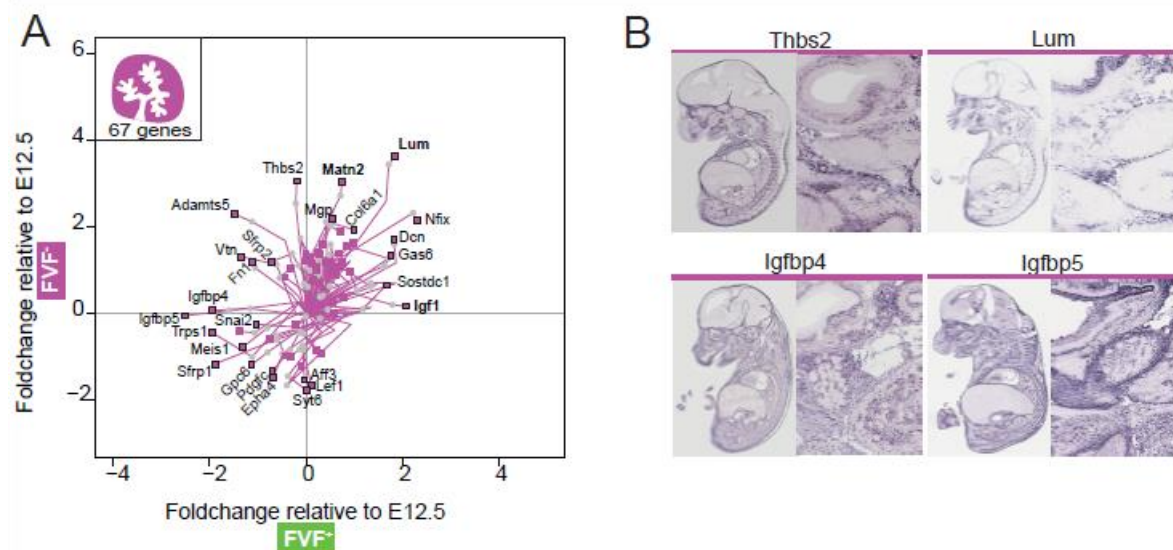


**Figure 3.15: Temporal and spatial expression of depicted known pancreatic genes and the classical trunk *in silico in situ* pattern obtained by Genepaint.**

- (A) The blot reflects in total 26 depicted genes illustrating the tip *in situ* expression pattern, respective exocrine progenitors at consecutive E in the secondary transition of pancreas organogenesis (*Serpina1a*, *Serpina1b*, *Serpina 1e*, *Serpina 1d*, *Ptpn9*, *Cbx5*, *Appl2*, *Clca2*, *Edaradd*, *Prss1*, *Pnliprp2*, *Bhlha15*, *Cel*, *Amy2a5*, *Cela1*, *Cckar*, *Clps*, *Pnliprp1*, *Ctrb1*, *Serpina6*, *Clps*, *Cckar*, *Cpa1*, *Met*, *Gc*, *Bcap29*, *Onecut1*). The genes *Cpa1*, *Cela1*, *Amy2a5* and *Edaradd* are highlighted in bold, indicating the illustration in the *in situ* expression pattern in (B).
- (B) The selected genes used in the *in situ* pattern as *Cpa1*, *Cela1*, *Amy2a5* and *Edaradd* reflect a tip pattern in the PE at E14.5. In addition, the genes have a unique hybridization pattern exclusively in the pancreatic region of the whole mount embryo sections.

Abbreviations: E = embryonic stage; PE = pancreatic epithelium; *Serpina1a* = *Serpin Peptidase Inhibitor, Clade A, Member 1*; *Serpina1b* = *Serpin Peptidase Inhibitor, Clade B, Member 1*; *Serpina 1e* = *Serpin Peptidase Inhibitor, Clade E, Member 1*; *Serpina 1d* = *Serpin Peptidase Inhibitor, Clade D Member 1*; *Ptpn9* = *Protein Tyrosine Phosphatase, Non-Receptor Type 9*; *Cbx5* = *Chromobox protein homolog 5*; *Appl2* = *Adaptor Protein, Phosphotyrosine Interaction, PH Domain And Leucine Zipper Containing 2*; *Clca2* = *Chloride Channel Accessory 2*; *Edaradd* = *EDAR-Associated Death Domain*; *Prss1* = *protease, serine 1*; *Pnliprp2* = *pancreatic lipase related protein2*; *Bhlha15* = *basic helix-loop-helix family, member a15*; *Cel* = *carboxyl ester lipase*; *Amy2a5* = *amylase 2a5*; *Cela1* = *chymotrypsin like elastase family member 1*, *Cckar* = *cholecystokinin A receptor*; *Pnliprp1* = *pancreatic lipase-related protein 1*; *Ctrb1* = *chymotrypsinogen B1*; *Serpina6* = *Serpin Peptidase Inhibitor Member 6*; *Clps* = *colipase*; *Cpa1* = *carboxypeptidase A1*; *Met* = *MET proto-oncogene*; *Gc* = *group specific component*; *Bcap29* = *B-cell receptor associated protein 29*; *Onecut1* = *oncut domain, family member*; *FVF<sup>+</sup>* = *Foxa2-Venus-Fusion positive*; *FVF<sup>-</sup>* = *Foxa2-Venus-Fusion negative*; *Foxa2* = *winged helix/forkhead box*.

A classical tip pattern is reflected by *Cpa1*, the mRNA expression itself seems steady in the secondary transition (Figure 3.15 A-B). *Cpa1* is clearly restricted to the pancreatic region with starting mRNA expression at around E9.5 and protein expression at E10.5 (Zhou et al., 2011; Zhou et al., 2007). The gene marks the MPP in the earlier E and at E14.5 bi-potent tip progenitors co-express *Cpa1/Ptf1a* (Kopp et al., 2011). The gene *Chymotrypsin-like elastase family member 1* (*Cela1*), *Amylase 2a5* (*Amy2a5*) and *Ectodysplasin-A receptor-associated adapter protein* (*Edaradd*) show increasing expression within the secondary transition including a typical tip pattern. Although, these genes have in common a function as lipase or amylase. Interestingly, these genes reflect in the *in situ* exclusively patterning at the tip regions, indicating the pancreas-specificity of these genes (Figure 3.15 A-B) (Willmann et al., 2015).



modified from Willmann et al., 2015

**Figure 3.16: Temporal and spatial expression of depicted known pancreatic genes and the classical mesenchymal *in situ in situ* pattern obtained by Genepaint.**

- (A) The blot shows the selected different 67 genes describing a mesenchymal hybridization pattern, for each single timepoint of secondary transition at E14.5 26 genes are illustrates in the blot (*Thbs2*, *Mgo*, *Matn2*, *Col6a1*, *Lum*, *Nfix*, *Dcn*, *Gas6*, *Sostdc1*, *Igf1*, *Aff3*, *Lef1*, *Syt6*, *Epha4*, *Pdgfc*, *Gpc6*, *Sfrp1*, *Meis1*, *Trps1*, *Snail2*, *Igfbp5*, *Igfbp4*, *Fb1*, *Vtn*, *Sfrp2*, *Adamts5*). In total gene expression of the genes is randomly distributed in the non-endodermal and endodermal cell population.
- (B) The genes used in the *in situ* pattern as *Thbs2*, *Lum*, *Igfbp4* and *Igfbp5* are highlighted in bold (A). The mesenchymal genes illustrate ubiquitous hybridizational patterning in the mouse whole mount embryo at E14.5.

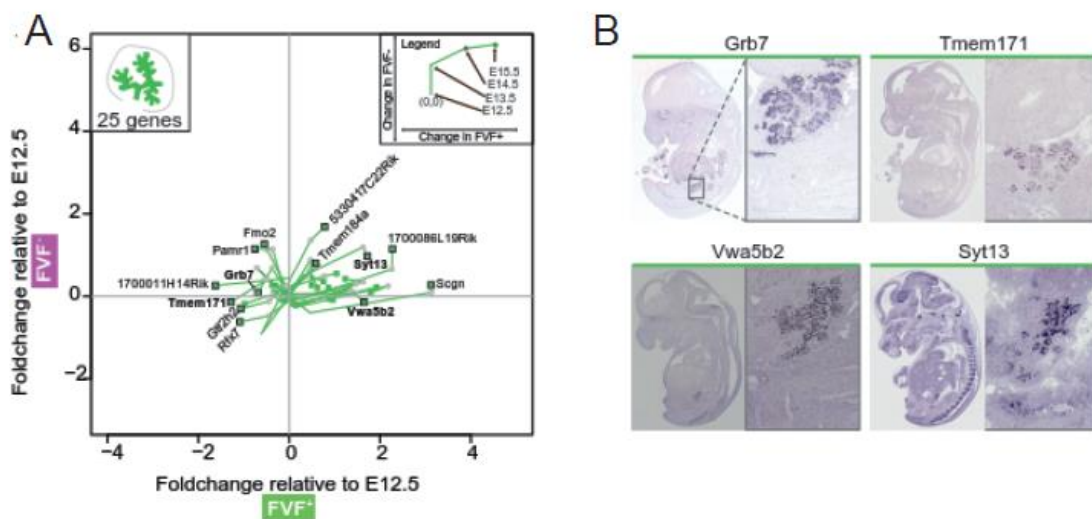
Abbreviations: E = embryonic stage; PE = pancreatic epithelium; *FVF+* = *Foxa2-Venus-Fusion positive*; *FVF-* = *Foxa2-Venus-Fusion negative*; *Foxa2* = *winged helix/forkhead box*; *Thbs2* = *thrombospondin 2*; *Mgo* = *mago nashi-like protein*, *Matn2* = *Matrilin 2*; *Col6a1* = *Collagen type VI alpha 1*; *Lum* = *Lumican*; *Nfix* = *Nuclear Factor I/X*; *Dcn* = *Decorin*; *Gas6* = *Growth-arrest-specific gene-6*; *Sostdc1* = *Sclerostin Domain Containing 1*; *Igf1* = *Insulin-Like Growth Factor 1*; *Aff3* = *AF4/FMR2 Family, Member 3*; *Lef1* = *Lymphoid Enhancer-Binding Factor 1*; *Syt6* = *Synaptotagmin 6*; *Epha4* = *EPH Receptor A4*; *Pdgfc* = *Platelet-derived growth factor C*; *Gpc6* = *Glypican 6*; *Sfrp1/2* = *Secreted Frizzled-Related Protein 1/2*; *Meis1* = *Meis homeobox 1*; *Trps1* = *Trichorhinophalangeal Syndrome I*; *Snail2* = *Snail Family Zinc Finger 2*; *Igfbp4/5* = *Insulin-Like Growth Factor Binding Protein 4/5*; *Fb1* = *fibrillin-1*; *Vtn* = *Vitronectin*; *Adamts5* = *ADAM Metallopeptidase With Thrombospondin Type 1 Motif, 5*.

The mesenchymal *in situ* pattern is represented by *Thrombospondin 2* (*Thbs2*) with strong mRNA expression in the GRN, ubiquitous hybridization pattern in the whole mount embryo and clearly detectable pattern at the ceiling of the pancreatic region (Figure 3.16 A-B). As a homotrimeric glycoprotein, *Thbs2* mediates cell-to-cell and cell-to-matrix interactions and homozygous mice die due to marked structural and functional abnormalities in a variety of connective tissues (Kyriakides et al., 1998) implicating that secreting factors regulate proliferation and expansion of the developing

pancreas. The gene *Lumican (Lum)* shows expression within the PE, but the *in situ* pattern mesenchymal characteristics. This might represent the mesenchyme which progressively invades the PE. Interestingly, the gene itself is involved in ECM organization, suggesting a role in pancreas morphogenesis and tissue interactions (Chakravarti et al., 1998). More interestingly, *insulin-like growth factor binding protein 4 (Igfbp4)* and 5 already show escalating mRNA expression in the mesenchyme with clear *in situ* pattern in the mesenchyme. Which role these members of the insulin-like growth factor in pancreas organogenesis play, remains unclear (Gu et al., 2004; Willmann et al., 2015).

### 2.3.2 Temporal and spatial progression of unknown pancreatic genes

The temporal and spatial selection of familiar pancreatic genes gained the benefit of a scheme for dissection of functionally yet not described genes in pancreas organogenesis. Thus, we selected unknown genes for their expression profile in the different tissue compartments and classified the genes related to the specific *in situ* hybridization pattern. In general, classification of previously unknown genes in pancreatic organogenesis with unique expression pattern in the pancreatic region was the main goal (Willmann et al., 2015).



modified from Willmann et al., 2015

**Figure 3.17: Temporal and spatial expression of depicted genes functionally not described in pancreas organogenesis and the *in silico in situ* pattern classified as PE/trunk obtained by Genepaint.**

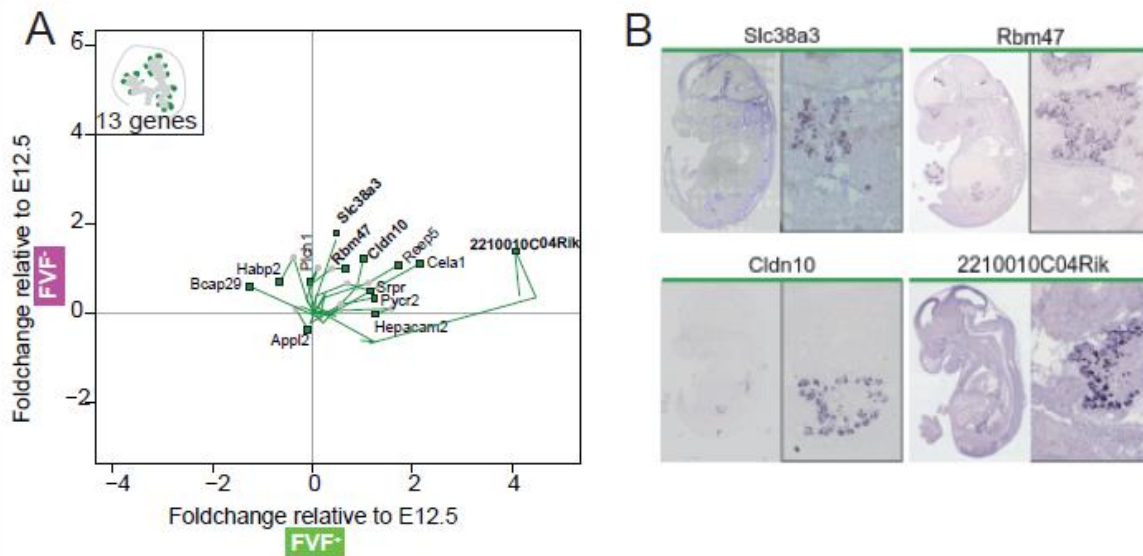
(A) The blot illustrates the selected genes including the gene expression profile at each single timepoint in the secondary transition. In total 25 genes inheriting a PE hybridization pattern were depicted for further analysis, 14 of these genes functionally not described in the context of pancreas

organogenesis (*1700011H14Rik*, *Grb7*, *Pamr1*, *Fmo2*, *5330417C22Rik*, *1700086L119Rik*, *Syt13*, *Tmem184a*, *Scgn*, *Clca1*, *Vwa5b2*, *Rfx7*, *Gtt2h2*, *Tmem171*) - the genes illustrated in bold letters are described more precisely in (B).

- (B)** Genepaint hybridization pattern of the whole mount embryo and the pancreatic region of the depicted genes *Grb7*, *Tmem171*, *Vwa5b2* and *Syt13*. The pancreatic candidates presumably reflect exclusive expression pattern in the pancreatic region with exception of the gene *Syt13*. In addition, *Syt13* illustrates expression pattern in the neurogenic region of the brain and in the precursor ganglions.

Abbreviations: E = embryonic stage; PE = pancreatic epithelium; *FVF*<sup>+</sup> = *Foxa2-Venus-Fusion positive*; *FVF*<sup>-</sup> = *Foxa2-Venus-Fusion negative*; *Foxa2* = *winged helix/forkhead box*; *Fmo2* = *Flavin Containing Monooxygenase 2*; *Grb7* = *Growth Factor Receptor-Bound Protein 7*; *Pamr1* = *Peptidase Domain Containing Associated With Muscle Regeneration 1*; *5330417C22Rik* = *RIKEN cDNA 5330417C22 gene*; *1700086L119Rik* = *RIKEN cDNA 1700086L119 gene*; *Syt13* = *Synaptotagmin 13*; *Tmem184a* = *Transmembrane protein,184a*; *Scgn* = *Secretagogin*; *Clca* = *Chloride Channel Accessory 1*; *Vwa5b2* = *Von Willebrand Factor A Domain Containing 5B2*; *Rfx7* = *Regulatory Factor X, 7*; *Gtt2h2* = *General transcription factor IIH, polypeptide 2*; *Tmem171* = *Transmembrane protein 171*.

For the epithelial *in situ* pattern we identified genes with mainly unique hybridization pattern in the pancreatic region of the mouse whole mount embryo at E14.5 (Figure 3.17 A-B). The yet functionally not described gene in pancreatic context, *growth factor receptor bound protein 7* (*Grb7*) illustrates stable mRNA expression in pancreatic organogenesis and appears to reflect a typical epithelial *in situ* expression pattern. We could observe similar results for the yet pancreatic unknown gene *Transmembrane protein 171* (*Tmem171*), with steady-stable expression in the secondary transition and a hybridization pattern exclusively in the pancreatic region. In addition, the novel putative pancreatic gene *von Willebrand factor A domain containing 2B2* (*Vwa5b2*) appears to be upregulated in the *FVF*<sup>+</sup> cell population, respective PE. Interestingly, we identified the unknown pancreatic gene *Synaptotagmin 13* (*Syt13*) illustrating a hybridization pattern described as trunk and thus suggesting in relation to endocrine progenitor *Ngn3*, respective endocrine progenitor *Nkx6-1*. The gene expression profile reflects escalating expression of *Syt13* in the ongoing pancreas organogenesis, indicating that *Syt13* might be involved in proliferation and morphogenesis of the pancreas. We assume that the PE hybridization pattern will account for genes involved in epithelial tissue interaction, segregation and differentiation. Taken together, the depicted genes which are functionally not described in the pancreas, are interesting gene candidates for deciphering the genes in the process of lineage commitment into the different lineages in pancreas organogenesis (Willmann et al., 2015).



modified from Willmann et al., 2015

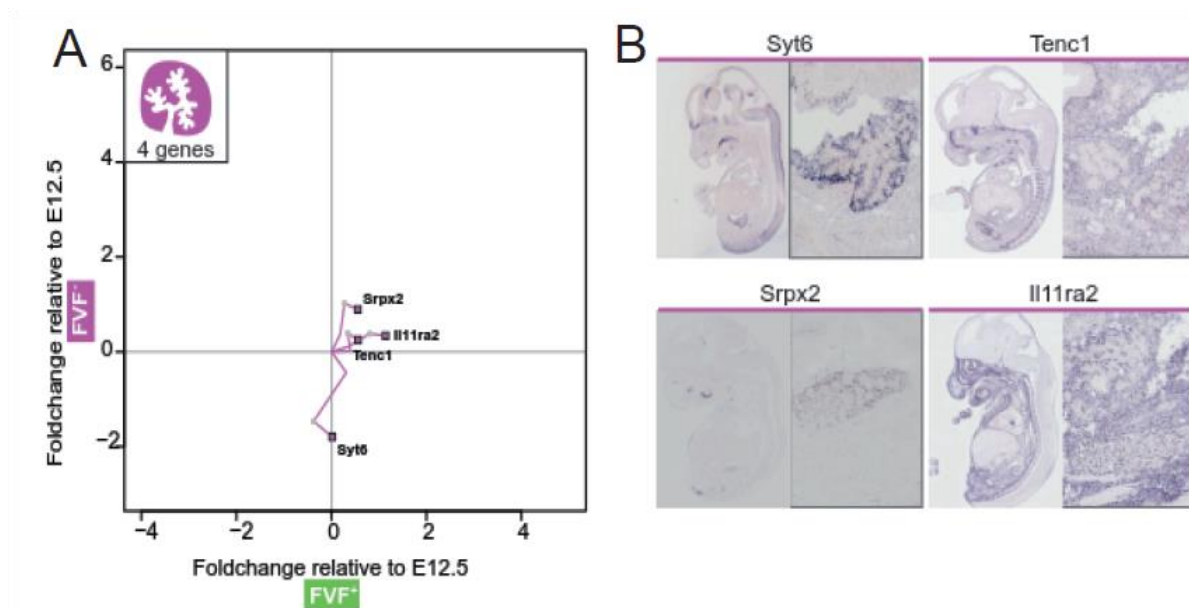
**Figure 3.18:** Temporal and spatial expression of depicted functionally not described genes reflecting a classical tip *in silico in situ* pattern hybridization pattern.

- (A)** In total 13 genes functionally not described in the context of pancreas organogenes were selected including a tip hybridization pattern (*Bcap29*, *Habp2*, *Pch1*, *Slc38a3*, *Rbm47*, *Cldn10*, *Reep5*, *Cela1*, *Srpr*, *Pycr2*, *Hepacam2*, *2210010C04Rik*). In addition, the gene expression profile at the specific consecutive E in the secondary transition describes the genes as differentially regulated. The genes represented in the *in silico in situs* are marked in bold letters.
- (B)** The hybridization pattern of the genes *Slc38a3*, *Rbm47*, *Cldn10* and *2210010C04Rik* illustrated in the wholemount embryo and in the pancreatic region. It is to note that the selected genes mainly illustrate exclusively an *in situ* pattern in the pancreatic region.

Abbreviations: E = embryonic stage; PE = pancreatic epithelium;  $FVF^+$  =  $FVF^+$  = *Foxa2-Venus-Fusion positive*;  $FVF^-$  = *Foxa2-Venus-Fusion negative*; *Foxa2* = *winged helix/forkhead box*; *Bcap29* = *B-Cell Receptor-Associated Protein 29*; *Habp2* = *Hyaluronan Binding Protein 2*; *Pch1/Vrk1* = *Vaccinia Related Kinase 1*; *Slc38a3* = *Solute Carrier Family 38, Member 3*; *Rbm4* = *RNA Binding Motif Protein 47*; *Cldn10* = *Claudin-10*; *Reep5* = *Receptor Accessory Protein 5*; *Cela1* = *Chymotrypsin-Like Elastase Family, Member 1*; *Srpr* = *Signal Recognition Particle Receptor*; *Pycr2* = *Pyrraline-5-Carboxylate Reductase Family, Member 2*; *Hepacam2* = *HEPACAM Family Member 2*; *2210010C04Rik* = *RIKEN cDNA 2210010C04 gene*.

The GRN at the secondary transition of the pancreas accumulates a quantity of genes functionally not describe in the pancreatic context. Hence, selection of genes including the *in situ* hybridization pattern classified as tip presumably determines the bi-potent progenitors in line with ductal/exocrine lineage segregation. In addition, regional specificity of the hybridization pattern in the pancreatic region suggest a unique function in pancreas organogenesis and maturation. In total, 13 genes are categorized (*2210010C04Rik*, *Slc38a3*, *Rbm47*, *Cldn10*, *Reep5*, *Cela1*, *Srpr*, *Pycr2*, *Hepacam2*, *Appl2*, *Bcap29*, *Habp2*, *Appl2* and *Plch1*) (Figure 3.18, A-B). Thus, pancreatic unknown gene *solute carrier family 38 member 3* (*Slc38a3*) showed decreasing expression in the pancreatic epithelium, along with a slightly detectable

hybridization *in situ* expression pattern in the pancreatic region (Figure 3.18 A-B). Almost similar results are obtained for the pancreatic candidate genes *RNA binding motif protein 47 (Rbm47)* and *Claudin-10 (Cldn10)*. Both genes are presumably steady-stable expressed in the PE and present a *in situ* hybridization pattern at the ceiling of the pancreatic region. Contrary, the gene *2210010C04Rik* illustrates in the GRN escalating mRNA expression in line with intense tip hybridization pattern at the ceiling of the pancreatic region (Figure 3.18 A-B). Further analysis regarding these genes will shed light on function and mechanism in pancreas organogenesis. (Willmann et al., 2015).



modified from Willmann et al., 2015

**Figure 3.19: Temporal and spatial expression of genes, functionally not described in pancreas organogenesis, selected due to a comparable mesenchymal hybridization pattern in Genepaint.**

- (A) The mesenchymal hybridization pattern including genes functionally not described in the pancreatic context 4 genes were selected (*SrpX2*, *Il11ra2*, *Tenc1*, *Syt6*). In the consecutive E of the secondary transition the gene expression profile illustrates random expression within the PE, respective the non-endodermal tissue compartment.
- (B) The hybridization pattern of the genes *Syt6*, *Tenc1*, *Il11ra2* and *SrpX2* are illustrated in the wholemount embryo and in the pancreatic region at E14.5. The genes are ubiquitously expressed in the whole mouse embryo, with exception of *SrpX2* with unique pattern in the pancreatic region.

Abbreviations: E = embryonic stage; PE = pancreatic epithelium; *FVF+* = *Foxa2-Venus-Fusion positive*; *FVF-* = *Foxa2-Venus-Fusion negative*; *Foxa2* = *winged helix/forkhead box*; *SrpX2* = *sushi-repeat containing protein, X-linked 2*; *Il11ra2* = *Interleukin 11 Receptor, Alpha 2*; *Tenc1* = *Tensin-like C1 domain-containing phosphatase*; *Syt6* = *Synaptotagmin 6*.

In the classified mesenchymal hybridization pattern, only a small amount of genes with unknown function had been identified. The genes *sushi-repeat-containing protein, X-linked 2 (SrpX2)*, *Interleukin 11 Receptor, Alpha 2 (Il11ra2)*, *tensin like C1 domain-containing phosphatase (Tenc1)* and

*Synaptotagmin 6 (Syt6)* are selected for comparable hybridization pattern. After all, the blot of the different developmental E in the secondary transition offered unexpected results. The transcriptome profile of the classified genes illustrates expression randomly in the PE and surrounding mesenchyme (Figure 3.19, A-B). In addition, the genes are ubiquitous expressed in the whole mouse embryo at the specific E14.5. Regardless of the mentioned points, the unknown pancreatic factor *Syt6* suggest to be an interesting candidate in pancreas organogenesis. Our previous results for *Syt13* along with *Syt6* may indicate that calcium and non-calcium binder in the family of Synaptotagmin are involved in pancreas development. Currently, the other pancreatic unknown candidate genes are not described on the base of pancreas organogenesis and maturation (Willmann et al., 2015).

In summary, we characterized functionally pancreatic genes for their temporal expression in the secondary transition and classified spatial expression in the *in situ* hybridization pattern. Taken this approach, the selected, yet functionally not described pancreatic genes are classified compared to the already characterized pancreatic genes. Thus, pancreatic candidate genes are speculatively classified into a specific lineage and described in the context of a function. Further analysis of the pancreatic gene candidates in the Lickert laboratory will determine the specific lineages, function and mechanism in pancreas organogenesis, morphogenesis and maturation into the adult pancreas, respective Islets of Langerhans (Willmann et al., 2015).

### **3.4 Analysis of the novel pancreas gene *Synaptotagmin 13 (Syt13)***

We identified in the global transcriptome of the pancreas in the secondary transition the gene *Syt13* as yet functionally not described in pancreas organogenesis. In a next step we characterized *Syt13* by its gene and protein.

#### **3.4.1 Bioinformatic analysis of *Syt13***

##### **3.4.1.1 The family of *Synaptotagmins***

The mouse and human genome encodes at least 19 family members of *Synaptotagmin (Syt)* (Adolfson and Littleton, 2001). *Syts* are described in the context of docking to lipid membranes, in particular localization to the apical surface in a phosphatidylserine and phosphatidylinositol-4,5-biphosphate (PtdIns(4,5)P<sub>2</sub>) dependent manner. In sensing the Calcium (Ca<sup>2+</sup>) levels at the surface, *Syts* are involved

in exocytosis processes of the cell (Augustine et al., 2001; Chapman et al., 2008; Koh et al., 2003; Belmonte et al., 2012). Nonetheless isoforms of *Syts* vary in their  $\text{Ca}^{2+}$  dependent lipid binding, the classification into the large family is coupled to a typical N-terminal Transmembrane domain (TMD), a central linker region and 2 C-terminal C2-domains (Xu et al., 2014; Xu et al., 2009; Südhof et al., 2002; Ullrich et al., 1995). Thomas Südhof was awarded the nobel prize in 2013 for elucidating the role of *Synaptotagmin 1 (Syt1)* as a  $\text{Ca}^{2+}$  sensor in synaptic vesicles exocytosis (Geppert et al. 1994; Xu et al. 2009). Thus, we were interested in the role of *Synaptotagmin 13 (Syt13)* in exocytotic processes as the C2-domains lack of the  $\text{Ca}^{2+}$  binding residues, suggesting a different role of *Syt13* on a cellular level (von Poser et al., 2001; Fukuda et al., 2001).

In using the digital database Genepaint, we inspected the hybridization pattern of the *Syt* isoforms in the whole mount embryo and in the region of the pancreas.

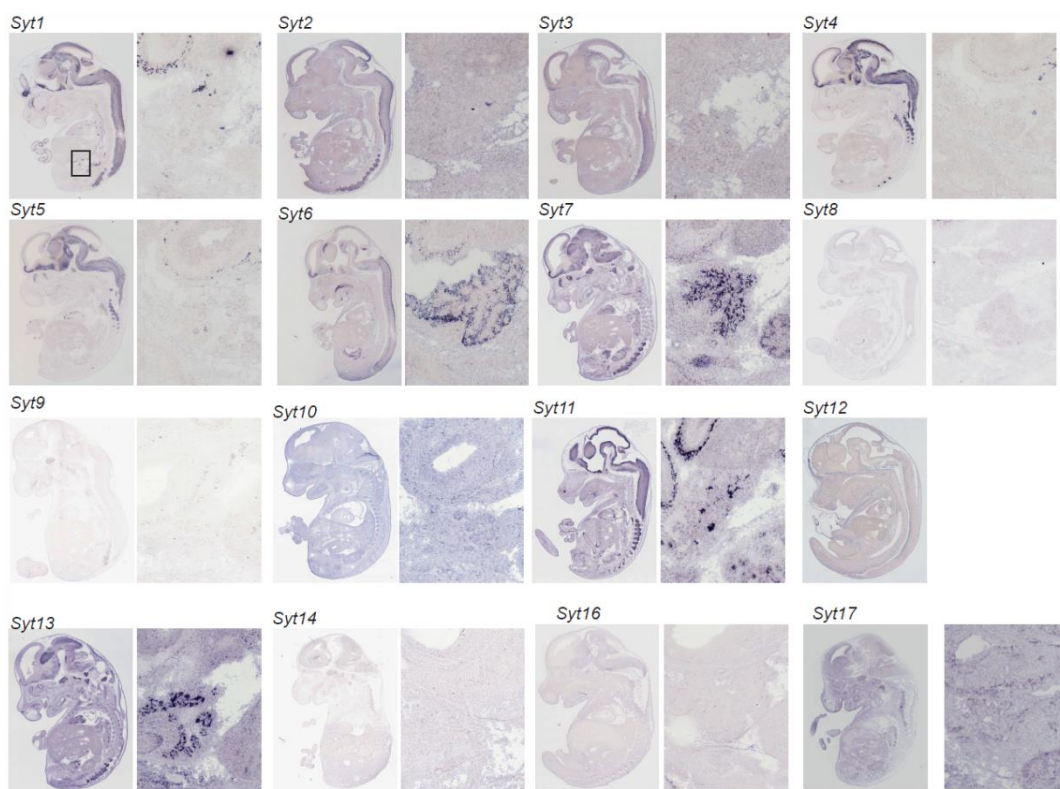
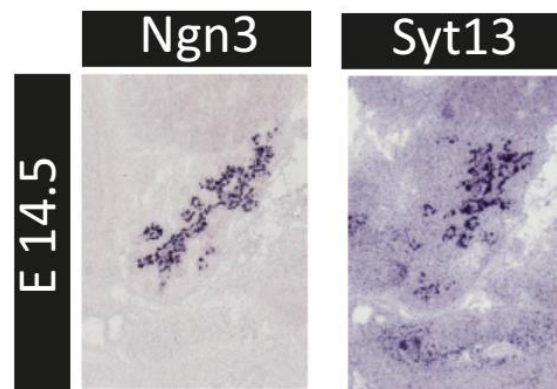


**Figure 3.20: Spatial expression of the *Syt* isoforms (*Syt1-17*) in whole mount embryo and in the pancreatic region.**

The Genepaint *in situ* at E14.5 illustrates for *Syt1-7*, *Syt11*, *Syt13* and *Syt17* patterning in the whole mount embryo and for *Syt6-7*, *Syt13* and *Syt17* localization in the pancreatic region (Zoom 3x). The *Syt* isoforms 8-10, 12, 14 and 16 reflect no hybridization of the probe sets in the whole mount embryo. It is to note that Genepaint did not offer *in silico in situ* of *Syt15*. The black box in the whole mount embryo of *Syt1* indicates the pancreatic region.

Abbreviations: E = embryonic stage; *Syt1* = *Synaptotagmin1*; *Syt2* = *Synaptotagmin2*; *Syt3* = *Synaptotagmin3*; *Syt4* = *Synaptotagmin4*; *Syt5* = *Synaptotagmin5*; *Syt6* = *Synaptotagmin6*; *Syt7* = *Synaptotagmin7*; *Syt8* = *Synaptotagmin8*; *Syt9* = *Synaptotagmin9*; *Syt10* = *Synaptotagmin10*; *Syt11* = *Synaptotagmin11*; *Syt12* = *Synaptotagmin12*; *Syt13* = *Synaptotagmin13*; *Syt14* = *Synaptotagmin14*; *Syt16* = *Synaptotagmin16*; *Syt17* = *Synaptotagmin17*; E = embryonic stage.

The function of *Syts* already described in literature, are mainly in the context of docking/fusion of synaptic vesicles, depolarization and  $Ca^{2+}$  influx in the brain. Hence, *Syt1* hybridization pattern reflects expression in the medulla and neocortex regions at E14.5 (Figure 3.20). For *Syt13* the Genepaint *in situ* illustrates an expression pattern in the thalamus, inner ear (cochlea), cranial ganglion and root ganglion. Next to this we could observe a clear expression pattern of *Syt13* in the pancreatic region. Also, *Syt6* and *Syt7* show a pancreatic expression pattern at E14.5, suggesting a role of these isoforms in pancreas organogenesis. Among these, *Syt7* null mutant mice show impaired insulin secretion and glucose intolerance. The effect is most likely due to a defect in  $Ca^{2+}$  sensing vesicle exocytosis (Gut et al. 2001; Andersson et al. 2012). Taken together, the function of *Syt6* and *Syt13* during pancreas organogenesis has not been addressed yet.



modified from Willmann et al., 2015

**Figure 3.21: Spatial expression of *Ngn3* and *Syt13* in the pancreatic region.**

Genepaint *in silico in situ* of the whole mount embryo at E14.5 with zoom (3x) into the pancreatic region illustrates the trunk pattern of the endocrine progenitor *Ngn3*. The hybridization pattern of *Syt13* correlates to the trunk pattern of *Ngn3*, indicating that *Syt13* is involved in endocrine formation.

Abbreviations: E = embryonic stage; *Ngn3* = *neurogenin 3*; *Syt13* = *Synaptotagmin 13*.

The hybridization expression pattern of *Syt13* correlates to the endocrine progenitor *Ngn3*, suggesting that *Syt13* marks the bi-potent trunk progenitors at E14.5. Thus, the endocrine progenitor in the PE suggest to be characterized by expression of  $Ngn3^+Syt13^+$ . Taken the previous results of the endocrine precursor pool as  $FVF^+$ , respective  $Pdx1^+$  cell population, we further hypothesize of  $Nkx6-1^+Pax6^+Ecad^+$

*Syt13*<sup>+</sup> cells which will aggregate into the surrounding PE into precursor Islets of Langerhans (Section 3.1). Thus, further studies will determine the precise expression pattern of *Syt13* in the secondary transition in pancreas organogenesis (Willmann et al., 2015).

### 3.4.1.2 Interaction partner of SYT13

In the next step profile-to-profile sequence alignment of the sequence of SYT13 scored for molecular pathways and protein-protein interaction partners. As a result Basophilic serine/threonine kinase group members (Baso\_ST\_kin) – more precise Calmodulin dependent Kinase 2 (CAMK2G) and PKCζ (PRKCZ) – and the kinase binding site group (Kin\_bind) with the ERK D-domain (MAPK1) are scored in the range 04056 – 04612 ( Figure 3.22).

<b>Basophilic serine/threonine kinase group (Baso_ST_kin)</b>				
<b>Calmodulin dependent Kinase 2</b>			Gene Card <a href="#">CAMK2G</a>	
<u>Site</u>	<u>Score</u>	<u>Percentile</u>	<u>Sequence</u>	<u>SA</u>
T127	<u>0.4056</u>	0.081 %	<u>SRLKRQVTEELSIRP</u>	1.052
<b>PKC zeta</b>			Gene Card <a href="#">PRKCZ</a>	
<u>Site</u>	<u>Score</u>	<u>Percentile</u>	<u>Sequence</u>	<u>SA</u>
T345	<u>0.4612</u>	0.144 %	<u>QKLKKKQTKRAKHKI</u>	4.533
<b>Kinase binding site group (Kin_bind)</b>				
<b>Erk D-domain</b>			Gene Card <a href="#">MAPK1</a>	
<u>Site</u>	<u>Score</u>	<u>Percentile</u>	<u>Sequence</u>	<u>SA</u>
L130	<u>0.4381</u>	0.010 %	<u>KRQVTEELSIRPQNG</u>	1.043

**Figure 3.22: Profile-profile alignment of SYT13 amino acid (aa) sequences to the references database scansite.org.**

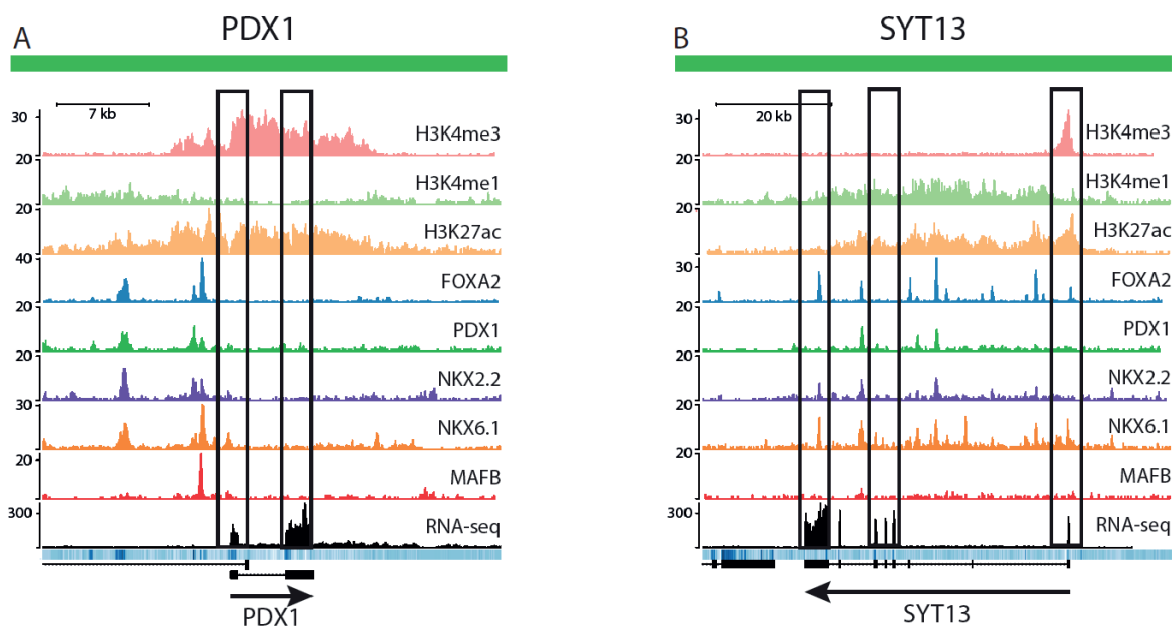
The database scansite.org was acquired for putative interaction partner of SYT13 aa sequences. First, Basophilic serine/threonine kinase group members (Baso\_ST\_kin) and a kinase binding site group (Kin\_bind) was scored in the range 04056 – 04612. In detail, Calmodulin dependent Kinase 2 (CAMK2G), PKCζ (PRKCZ) and the ERK D-domain (MAPK1) at indicated sites show a percentage between 0.01%-0.144%. The affected aa are highlighted in bold in the Gene Card.

Abbreviations: SYT13 = Synaptotagmin 13; Baso\_ST\_kin = serine/threonine kinase group; Kin\_bind = kinase binding site group ; % = percentage; CAMK2G = Calmodulin dependent Kinase 2; PRKCZ = PKCζ; MAPK1 = ERK D-domain; aa = amino acid.

Interestingly, the *Calmodulin dependent kinase 2 (CAMK2G)* plays a role in Insulin secretion (Osterhoff et al., 2003; Gloyn et al., 2002). Additionally, activation of PKC $\zeta$  in  $\beta$ -cells improves glucose tolerance and leads to increased  $\beta$ -cell replication (Velazquez-Garcia et al. 2011). These results are interesting under the perspective of  $\beta$ -cell proliferation *in vivo*. Additionally, *Foxa2* expression decreases through inhibition of glucose-mediated activation of PKC $\zeta$ , pointing to a polarity complex recruitment in  $\alpha$ - and  $\beta$ -cells of the Islets of Langerhans. This is in line with already published data as PKC isoforms in  $\beta$ -cells are variable in their localization induced by glucose dynamics (Kaku et al. 2010). Taken together, we assume Co-expression of *FOXA2* and *SYT13* in the adult Islets of Langerhans and speculate of co-expression in pancreas organogenesis, respective embryogenesis.

### 3.4.1.3 Target gene prediction of SYT13

In a next step, we wanted to confirm previous results in adult Islets of Langerhans by distribution of histone modification and transcription factors at the loci of *PDX1* and *SYT13* (Pasquali et al., 2014; Morán et al. 2012).



modified from Willmann et al., 2015

**Figure 3.23: CHIP-seq of maturity Islet of Langerhans transcription factor (TF) with corresponding RNA seq data of *PDX1* and *SYT13*.**

(A) and (B) The open chromatin configuration is marked by *H3K4me3*, *H3K4me1*, *H3K27ac* indication active transcription of *PDX1* and *SYT13*. The loci of *PDX1* and *SYT13* are bound at least 3 times by

the maturity Islet of Langerhans transcription factors (FOXA2, PDX1, NKX2-2, NKX6-1, MAFB). In addition, RNA-seq data illustrates expression of *PDX1* and *SYT13*.

Abbreviations: H3K4me3 = Histone 3 lysine 4 trimethylation; H3K4me1 = Histone 3 lysine 4 monomethylation; H3K27ac = Histone 3 lysine 27 acetylation; *PDX1* = *Pancreatic and duodenal factor 1*; *SYT13* = *Synaptotagmin 13*; FOXA2 = winged helix/forkhead box 2; NKX2-2 = NK2 homeobox 2, NKX6-1 = (NK6 homeobox 1; MAFB = V-maf musculoaponeurotic fibrosarcoma oncogene homolog B; Chip-seq = Chromatin ImmunoPrecipitation DNA-Sequencing; RNA-seq = ribo nucleotide acid sequencing; kb = kilobyte; TF = transcription factor.

The gene *PDX1* shows on the chromatin level open configuration and thereby active transcription. Recently Boyer and colleagues have shown distinct roles of proximal and distal cis-regulators sequences in *Pdx1* in pancreatic expression. In the 5'- region of *Pdx1* proximal (-52.6 to -1.9 kb in mouse) and distal (-5.67kb to -6.2kb in rat) locus are binding sites for Foxa2, Nkx2-2, L-Maf, Hnf6, Hnf1 and Pdx1 itself (Boyer et al. 2006). As these factors define endoderm and more importantly endocrine lineage segregation, regulatory mechanism controlling the onset of transcriptional regulation are on the main focus. Interestingly, *Foxa2* acts as an upstream regulator of *Pdx1* (Gao et al. 2008), whereas *Nkx6-1* has been suggested to be negatively regulated by Pdx1 (Boyer et al. 2006; Shih et al. 2015). In summary, negative and positive feedback loops orchestrate the transcriptional hierarchy in which the different lineages of the pancreas segregate in the secondary transition (Willmann et al., 2015).

Open chromatin configuration reflected by H3K4me3 and H3K27ac correlates with active transcription of *SYT13*. Also, FOXA2, PDX1, NKX2-2 and especially NKX6-1 show active transcription of *SYT13* in the adult Islets of Langerhans. An interesting point might reflect *NKX6-1*, as the gene in adult Islets of Langerhans is exclusively expressed within the  $\beta$ -cells (Seymour et al. 2008). *MAFB* does not reflect active transcription, probably due the fact, that *MafB* directly regulates expression of *Pdx1* and *Nkx6-1* (Artner et al. 2007). These data suggest for *Syt13* regulation by FOXA2 and NKX6-1 and thereby expression of mRNA in the adult human Islets of Langerhans in the  $\alpha$ - and in the  $\beta$ -cells (Willmann et al., 2015).

### 3.4.2 Functional analyses of *Syt13*

For analysis of the function and mechanism of *Syt13* we characterized gene and protein expression in different organs of adult and E in *mus musculus*.

#### 3.4.2.1 The gene *Syt13*

The gene *mus musculus Syt13* is located on chromosome 2 at the position 92.915.098 – 92.956.058 on the forward strand. The genomic region (including exons and introns) consists of 40.96 kilo bases (kb) and comprises of 6 exons and one promoter (Figure 3.24). The promoter region is located in the 5'-untranslated region next to the first exon of the gene. There is one transcript predicted with a length of 1282bp as illustrated by the cDNA sequence.

```

CCCCGGGGAAGGTGAGCGGCTGCGGGACCCAGCCCCCTCGCCGGGAGCGGGCACCAATGGTGC
TGTCGGGTGCCTGTGATCGCGCTGGGCGCCACGCTGGGCACAGCCACCAGCATCCTCGCGTT
GGTGCGGGGTACCTGCCTGTGTGCGGCACATGCACCCCAAGAAGGGGGCTGCTGCCGCGGGA
CCAGGACCCCGACCTGGAGAAGGCGAAGCCAGCTTGCTCGGGTCTGCACAACAGTTCAAT
TTGTTAAAAAGTCCACGGAACCTGTTTCAGCCCCGTGCCCTCCTCAAGTTCCCAGACATCTA
GGACCCAGGCCAGCTGTGACGGCTCCAGAGGTCATCAACTATGCAGACTATTCACTGAGGT
CTACGGAGGAGCCCACTGCACCTGCCAGCCCCCAACCCCCGAATGACAGTCGCCTCAAGAG
GCAGGTCACAGAGGAGCTGTTTCATCCTCCCTCAGAATGGTGTGGTGAGGATGTCTGTGTC
ATGGAGACCTGGAACCCAGAGAAGGCTGCCAGTTGGAACCAGGCCCCCAAACCTCCACTACT
GCCTGGACTATGACTGTCAGAAGGCAGAATTGTTTGTGACTCGCCTGGAAGCTGTGACCCAG
CAACCACGACGGAGGCTGTGACTGCTACGTCCAAGGGAGTGTGGCCAATAGGACCGGCTCT
GTGGAGGCTCAGACAGCCCTAAAGAAGCGGCAGCTGCACACCACCTGGGAGGAGGGCCTGG
TGCTCCCCCTGGCGGAGGAGGAGCTCCCCACAGCCACCCTGACGCTGACCTTGAGGACCTG
CGACCGCTTCTCCCGTCACAGCGTGGCCGGGGAGCTCCGCCTGGGCCTGGACGGGACATCT
GTGCCCTCTAGGGGCTGCCCAGTGGGGCGAGCTGAAGACTTCAGCGAAGAGCCATCTGCAGG
AGCTGGAGAGGTCCTACTATCCATCAGCTACCTCCCGGCTGCCAACC GCCTCCTGGTGGTG
CTGATTAAAGCCAAGAACCTCCACTCTAACCAGTCCAAGGAGCTCCTGGGGAAGGATGTCT
CTGTCAAGGTGACCTTGAAGCACCAGGCTCGGAAGCTGAAGAAGAAGCAGACTAAACGAGC
TAAGCACAAGATCAACCCCGTGTGGAACGAGATGATCATGTTTGGAGCTGCCTGACGACCTG
CTGCAGGCCTCCAGTGTGGAGCTGGAAGTGTGTTGGCCAGGACGATTCAGGGCAGAGCTGTG
CGCTTGGCCACTGCAGCCTGGGCCTGCACACCTCGGGCTCTGAGCGCAGCCACTGGGAGGA
GATGCTCAAAAACCCTCGCCGGCAGATTGCCATGTGGCACCAGCTGCACCTGTAACCAGCT

```

**Figure 3.24:**The complementary deoxyribonucleine acid (cDNA) sequence of the gene *Syt13 mus musculus*

The first 6 bases of the 6 exons of the *mRNA* sequence are highlighted in bold letters, the *mRNA* sequence itself in blue. The 5' and 3'UTR sites are coloured in orange. In total, the sequence has a length of 1282 bp.

Abbreviations: cDNA = complementary deoxyribonucleid acid; Syt13 = Synaptotagmin 13; bp = base pair; *mRNA* = messenger ribo nucleotide acid; UTR = untranslated region.

### 3.4.2.2 The amino acid (aa) sequence of Syt13

The *mus musculus Syt13* protein itself comprises of 426 aa. The sequence consist of 2 residual splicing sites, suggesting alternative transcripts of the protein.

## Results

MVLSVPVIALGATLGTATSILALCGVTCLCRHMHPPKGLLPRDQDPDEKAKPSLLGSAQQFNVKKSTEPVQPRALLKF  
 PDIYGPRAVTAPEVINYADYSLRSTEEPTAPASPOPPNDSRLKRQVTEELFILPQNGVVEDVCMETWNPKEAASWNQ  
 APKLHYCLDYDCQKAEFLVTRLEAVTSNHDDGGDCYVQGSVANRTGSVEAQTALKKRQLHTTWEEGLVPLAAEEELPTA  
 TLTLTLRTRCDRFSRHSVAGELRLGLDGTSVPLGAAQWGLKTSAKEPSAGAGEVLLSISYLPAAANRLLVLIKAKNLHS  
 NQSKELLGKDVSVKVTLLKHQARKLKKKQTKRAKHKINPVWNEMIMFELPDDLLQASSVELEVLGQDDSGQSCALGHCSL  
 GLHTSGSERSHWEEMLNPRRQIAMWHQLHL

**Figure 3.25: The aa sequence of Syt13 in *mus musculus*.**

In black/blue are alternating exons. Residual overlap splicing sites are marked in red. The amino acid sequence consists of 426 aa.

Abbreviations: aa = amino acid; Syt13 = Synaptotagmin 13.

Protein alignment of different species reveals high conservation between the species. The orthologues of mouse (*mus musculus*; 92.915.098 – 92.956.058) and rat (*ratus norvegicus*; 81.814.261 – 81.854.605) illustrate 100% coverage. Orthologues are found in humans (*H. sapiens*; 45240301 – 45286319); cattle (*Bos taurus*; 76161411 – 76203527) and zebrafish (*D. rerio*; 38444790 – 38466359). The TMD and the C2-domains of the protein Syt13 suggests therefore a conserved mechanism within mammalian orthologs (Figure 3.26).

		TMD	
D. rerio	1	---MLVSAATAL-LGATLGTVSGVLTLCGLSLLCKSC--KKGKLESDEADPEKAKPSILHTLTQFSVHKCTEPIQPOASLKFPQIYRPFKSVTSQEVIN	93
M. musculus	1	---MVLSVPVIALGATLGTATSILALCGVTCLCRHMHPPKGLLPRDREPDPEKARPGVLQAAQFNIKKSTEPVQPRLLKFPDIYGPRAVTAPEVIN	96
R. norvegicus	1	---MVLSVPVIALGATLGTATSILALCGVTCLCRHMHPPKGLLPRDREPDPEKARPGVLQAAQFNVKKSTEPVQPRLLKFPDIYGPRAVTAPEVIN	96
H. sapiens	1	---MVLSVPVIALGATLGTATSILALCGVTCLCRHMHPPKGLLPRDQDPDEKAKPSLLGSAQQFNVKKSTEPVQPRALLKFPDIYGPRAVTAPEVIN	96
B. taurus	1	---MVLSVPVIALGATLGTATSILALCGVTCLCRHMHPPKGLVLRDLEPDPEKAKPSVLRRAAQFNVKKSTEPVQPRALLKFPDIYGPRAVTAPEVIN	96
C2			
D. rerio	94	YKEHG-----ASNDTSAEELDTCNQATEREEVFSLPRQASADETPCTSEQTGAMTSSSILYPKLHFSISLHKESGELHINIVEAENISVEAGCEGYI	186
M. musculus	97	YADYLETTEESAAPASPOAQSDSRLKRQVTEELSIRPQNGVVEDV-CVMETWNPKEAASWNQAPKLFRLDYDQKKAELFVTSLEAVTSDHEGGDCDCYI	195
R. norvegicus	97	YADYLTGTTTEESAAPASPOAQSDSRLKRQVTEELFILPQNGVVEDV-CVMETWNPKEAASWNQAPKLFRLDYDQKKAELFVTSLEAVTSDHEGGDCDCYI	195
H. sapiens	97	YADYSLRSTEEPTAPASPOPPNDSRLKRQVTEELFILPQNGVVEDV-CVMETWNPKEAASWNQAPKLYCLDYDCQKAEFLVTRLEAVTSNHDDGGDCDCYV	195
B. taurus	97	YADYTLKTAEPAPASPOAPNDSRLKRQVTEELFILPQNGVVEDV-CVMETWNPKEAASWNQAPKLYCLDYDRQKAEFLVTRLEAVTSDHDGGDCDCYV	195
C2			
D. rerio	187	SGCVSVSEEQRHAHTAVHKLAVHVQWGEELVFAALPMEGTEEDTDSLDEGEVALSLHCCDRFSHNSTLGMFRKLDVSMMLDADCVLDLQPPKQEVTSSTGE	286
M. musculus	196	QGSVAVKTGSVEAQTALKKRQLHTTWEEGLALPLG-----EELPTATLTLTLRTRCDRFSRHSVIGELRLGLDASVPLGAAQWGLKTTAKEPSAGAGE	290
R. norvegicus	196	QGSVAVKTGSVEAQTALKKRQLHTTWEEGLTLPGL-----EELPTATLTLTLRTRCDRFSRHSVIGELRLGLNGASVPLGTAQWGLKTTAKEPSAGTGE	290
H. sapiens	196	QGSVANRTGSVEAQTALKKRQLHTTWEEGLVPLA-----EELPTATLTLTLRTRCDRFSRHSVAGELRLGLDGTSVPLGAAQWGLKTSAKEPSAGAGE	290
B. taurus	196	QGSVANSMGVSVEAQTALKKRELHTMWEEGLVPLA-----EELPTATLTLTLRTRCDRFSRHSVVGELRLGLDGVSVPLGAAQWGLKTSVKEPSAGTGE	290
C2			
D. rerio	287	LLLSLSYLPAAANRLGVVVMKARGLQSDKRLKDN--DLSVKLTLKHQNAKLRKKQTRRVKHKMNPVWNEMMELPSELAKSSVDLEVLNLASPGTLLPL	384
M. musculus	291	VLLSISYLPAAANRLLVLIKAKNLHSNQSKELLGKDVSVKVTLLKHQARKLKKKQTKRAKHKINPVWNEMIMFELPDDLLRASSVELEVLGQEEGSPSCEL	390
R. norvegicus	291	VLLSISYLPAAANRLLVLIKAKNLHSNQSKELLGKDVSVKVTLLKHQARKLKKKQTKRAKHKINPVWNEMIMFELPDDLLQASSVELEVLGQEEGSPSCEL	390
H. sapiens	291	VLLSISYLPAAANRLLVLIKAKNLHSNQSKELLGKDVSVKVTLLKHQARKLKKKQTKRAKHKINPVWNEMIMFELPDDLLQASSVELEVLGQEEGSPSCEL	390
B. taurus	291	VLLSISYLPAAANRLLVLIKAKNLHSNQSKELLGKDVSVKVTLLKHQARKLKKKQTKRAKHKINPVWNEMIMFELPDDLLRASSVELDVLGAGGQSCVL	390
D. rerio	385	GRCMLGLQTSGLQHWKQLDNPRKQIAMWHPLYT	420
M. musculus	391	GHC SLGLHASGERSHWEEMLNPRRQIAMWHQLHL	426
R. norvegicus	391	GRC SLGLHASGERSHWEEMLNPRRQIAMWHQLHL	426
H. sapiens	391	GHC SLGLHTSGERSHWEEMLNPRRQIAMWHQLHL	426
B. taurus	391	GHC SLGLHASGERSHWEEMLNPRRQIAMWHQLHL	426

**Figure 3.26: The orthologous of the protein Syt13**

The Syt13 typical protein domains are highlighted in blue (TMD) or in red (C2). Selected species are *d. rerio*, *m. musculus*, *r. norvegicus*, *h. sapiens* and *b. taurus*. The aa length differs in the range of 420-426 aa. The protein domains are conserved among the different species, suggesting a conserved mechanism.

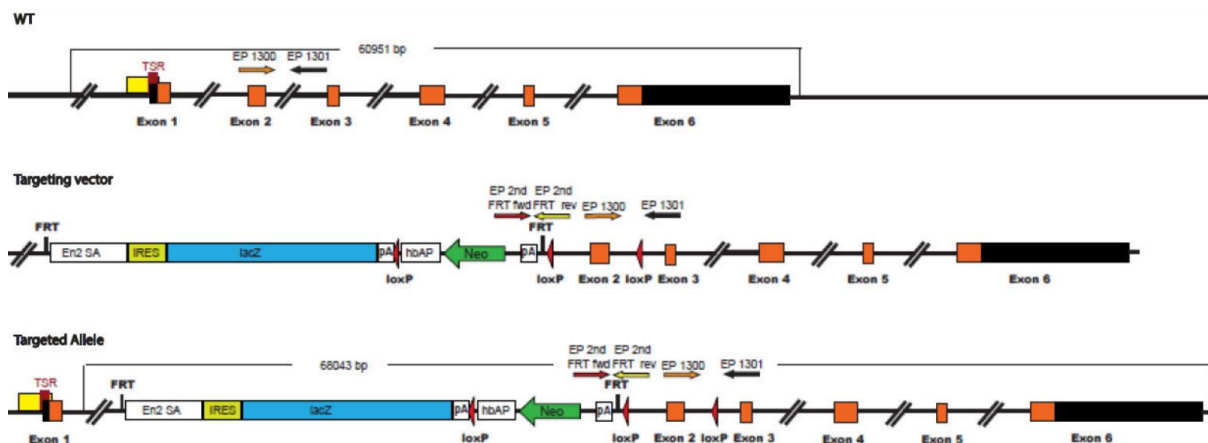
Abbreviations: *m. musculus* = *mus musculus*; *r. norvegicus* = *ratus norvegicus*; *h. sapiens* = *Homo sapiens*; *b. taurus* = *Bos taurus*; *D. rerio* = *danio rerio*; TMD = transmembrane domain; aa = amino acid; Syt13 = Synaptotagmin 13.

### 3.4.3 Generation of the genetically modified mouse line *Syt13*

For knock in/knock out studies of the gene *Syt13* *in vivo*, we generated different mouse lines.

#### 3.4.3.1 Design, generation and verification of the *Syt13*<sup>GT</sup> targeting vector

The targeting vector was designed for the critical Exon2 (CE2) in the *WT* allele of *Syt13*. A frameshift in the transcript would lead to nonsense-mediated decay (NMD) and null allele of *Syt13* (Caveoer 1987). The reporter-tagged knockout allele comprises of an inserted *internal ribosome entry-site (IRES)/lacZ*-promoter driven *Neo* targeting cassette. Insertion takes place upstream of the critical exon by recombination in the 5'- and 3'-homology arms. The cassette contains a *En2 SA* next to the *IRES* (Figure 3.27, white and yellow box). Both elements are fused to a *lacZ*-gene and a *pA* site. The *lacZ*-gene is utilized for  $\beta$ -galactosidase ( $\beta$ -gal) activity and transcription of the Reportergen will be terminated by the *pA* site. The loxP-flanked *human beta act promoter (hbAP)* acts as promoter for the *neo* resistance (white box and green box in Figure 3.27). The transcription of *neo* stops by the loxP-flanked *pA* site in the opposite direction (Figure 3.27, white box). After the loxP-flanked CE2, the 3'UTR encodes for the *WT* allele.



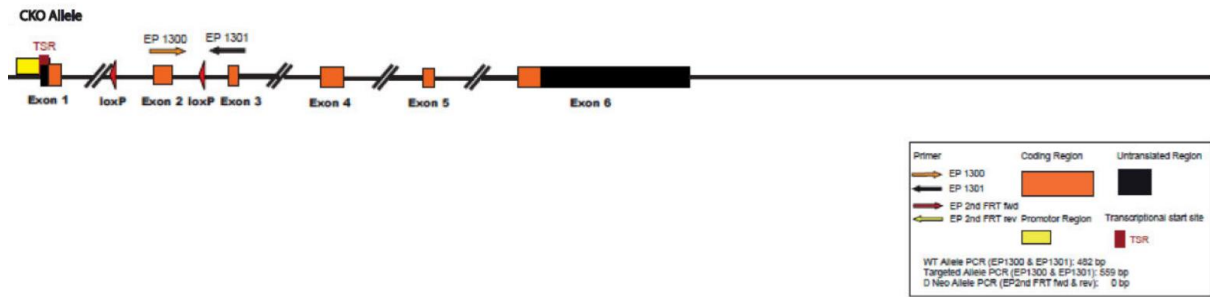


**Figure 3.27: Targeting strategy of the *Syt13* allele**

The *WT* allele comprises of 6 Exons. In the ORF of CE2 the targeting vector was inserted by homologous recombination. The targeted allele can be distinguished between the *WT* allele by genotyping using the EP 1300, 1301, *FRT* fwd and *FRT* rev. The exons are marked by orange boxes, untranslated regions are in black and promoter region in yellow. *Site-specific recombinase Cre* (loxP sites, red arrow) and *Flp-e* will achieve conditional knockout. The figure is on scale.

Abbreviations: *TSR*= transcriptional start site/region; *En2 SA*= splice acceptor of mouse exon 2; *IRES*= internal ribosome entry-site; *lacZ*= $\beta$ -galactosidase; *pA*= polyadenylation site/ *sv40 large t gene*; *hbAP*= human beta act promoter; *neo*=neomycin; *CE2*= critical Exon 2; EP = Primer; *CKO* = conditional knock out; *Syt13* = Synaptotagmin 13..

The *Syt13-D05* targeting vector (PrPGS00039\_A\_D06) had been linearized with *Ascl* and electroparted in IDG3.2 ES cells. Upon neomycin resistance we selected for positive ES cell clones. For chimeric mice we aggregated the positive ES cell clones with *CD1 morula* (Nagy et al., 2000). Chimerism and germline transmission was scored through coat colour. As the ES cell clones had been targeted in *JM8.N4* cells with the genotype *a/a* (Agouti null), chimeras will be either black/agouti or white. In breeding the chimeras with *C57BL/6N*, germline transmission will be indicated by black generation (G) 1 offspring (Pettitt et al. 2009) Furthermore, *conditional knock out (CKO)* mice were generated by intercrossing the *Syt13<sup>GT/GT</sup>* to *Flp-e* (enhanced Flipase), backcrossed to *C57Bl/6J* (Dymecki et al., 1996) and intercrossed to the *ROSA26 (R26R) Cre*-reporter line. Confirmation of the *Syt13-D05* clone was accomplished by Long Range PCR (data not shown). Targeting was done by Dr. Antje Burger and Dr. Andreas Horlein.

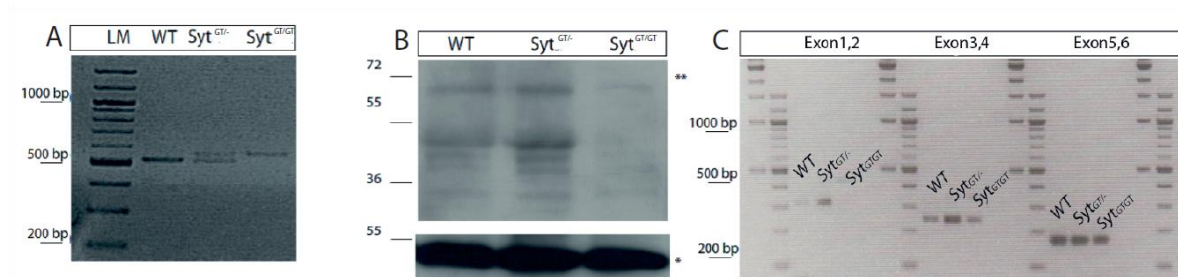


**Figure 3.28: Verification of the *Syt13<sup>GT</sup>* allele by PCR, Western blot and RT-PCR**

- (A) Agarose Gelelectrophorese after PCR amplification of lysed mouse tails from different genotypes illustrates for the *WT* allele a band at 510bp, *Syt13<sup>GT/-</sup>* at 510bp and 550bp for the *Syt13<sup>GT/GT</sup>* at 550bp by PCR using EP 1300 and 1301.
- (B) In the Western blot of brain lysate of *WT* positive signals appear at approximately 47kD and 68 kD (indicated by \*\*), similar results are reflected for the *Syt13<sup>GT/-</sup>*, whereas in the *Syt13<sup>GT/GT</sup>* brain lysate the positive signals appears to be weaker. The lower panel represents the actin loading control at approximately 50 kD (indicated by \*).
- (C) The RT-PCR analysis with Exon-spanning Primer illustrates transcription of Exon 1-2 in *WT* and *Syt13<sup>GT/-</sup>* but none for the *Syt13<sup>GT/GT</sup>*. The Exon 3-4 are transcribed for all genotype including lesser quantity of *Syt13<sup>GT/GT</sup>*. The last Exons (Exon 5-6) are transcribed for all genotypes. This indicates expression of the C2 domains in the *Syt13<sup>GT/GT</sup>*, whereas the transmembrane domain will be deleted.

Abbreviations: PCR = polymerase chain reaction; *WT* = wild type; *Syt13* = *Synaptotagmin 13*; bp = basepair; EP = Primer; kD = kilo Dalton; RT = real time; LM = lengthmarker; GT = gene trap.

To distinguish between *WT* and *Syt13<sup>GT/GT</sup>* allele, genotyping was carried out with the EP1300 and 1301, resulting in a PCR product for the *WT*-allele of 510 bp and for the targeted *Syt13<sup>GT/GT</sup>* allele with 550 bp (Figure 3.28, A). Additionally, *Cre* mediated intercrosses (*Syt<sup>R/-</sup>*) were genotyped with EP 1322,1323 and 1324. The PCR products resulted in a *WT* band at 384bp and for *Syt<sup>R/-</sup>* with 307bp.

Western blot analysis on brain lysate taking the genotype *WT*, *Syt13<sup>GT/-</sup>* and *Syt13<sup>GT/GT</sup>* showed 2 predicted band for *Syt13*. The first band at around 47 kilo Dalton (kD) appears weaker in the *Syt13<sup>GT/GT</sup>*. A second band appears at approximately 68kD (indicated \*\*) which is also attenuated in the *Syt13<sup>GT/GT</sup>* compared to *WT*. The loading control was accomplished with Actin at 50kD (indicated \*) (Figure 3.28, B). For the Real-Time PCR (RT-PCR) we generated exon spanning primer. By means, transcriptional inactivation of Exon1-2 for *Syt13<sup>GT/GT</sup>* indicates frameshift and NMD decay. Exon3-4 and Exon 5-6 in the *Syt13<sup>GT/GT</sup>* are transcribed and might point to exon skipping (Figure 3.28, C). Our results indicate for *Syt13<sup>GT/GT</sup>* an hypomorphic allele. As this might complicate results due to different protein levels of *Syt13*, we crossed the *Syt13<sup>GT/GT</sup>* mouse in the ubiquitous expressing *R26R* Cre-reporter line (Soriano, 1999). The *R26R* mediates excision of the *loxP*- flanked *neo* cassette and *CE2* (*Syt<sup>R/-</sup>*). In the first line, we performed *LacZ* reporter studies using the hypomorphic allele (*Syt13<sup>GT/GT</sup>*), in later sections we are focusing on the *in vivo* analysis of *Syt<sup>R/R</sup>*.

Chimeras were scored for coat colour and positive chimeras either mated with *CD1* or *C57Bl/6J*. Heterozygous intercrosses are determined as second G2. For the *Syt13<sup>GT/GT</sup>* we did not observe severe phenotypic changes compared to the *WT*. Except that in G1 and G2 we noticed a hydrocephalus with

incomplete penetrance (approximately 4%) and cystic structures in the pancreas. Mendelian ratio of *Syt13<sup>GT/-</sup> CD1 G2* intercrosses showed no significant changes to expected ratios.

<b>Syt13 CD1 G2 intercrosses</b>		
WT	<i>Syt13<sup>GT/-</sup></i>	<i>Syt13<sup>GT/GT</sup></i>
40	87	46
23.0%	50%	27.0%

**Table 1: *Syt13<sup>GT/-</sup> CD1 G2* intercrosses**

In total, generation of the *Syt13 CD1 G2* maintained 173 viable mice.

For the heterozygous intercrosses into the background *C57/Bl/6J* for 2 generation Mendelian ratio increased for *Syt13<sup>GT/-</sup>* and declined for *Syt13<sup>GT/GT</sup>* mice.

<b>Syt13 C57Bl/6J G2 intercrosses</b>		
WT	<i>Syt13<sup>GT/-</sup></i>	<i>Syt13<sup>GT/GT</sup></i>
19	35	11
29%	54%	17%

**Table 2: *Syt13<sup>GT/-</sup> C57Bl/6J G2* intercrosses**

Establishment of this mouse line attained 65 mice at weaning age.

Heterozygous intercrosses with *R26R* led to excision of *CE2*. The *R26R* loci for *Syt13* is thereby annotated as the *WT* allele.

<b>Syt13 C57Bl/6J G1 intercrosses</b>		
WT	<i>Syt13<sup>GT/-</sup></i>	<i>Syt13<sup>R/-</sup></i>
50	24	28
49%	24%	26%

**Table 3: *Syt13*<sup>G7/-</sup> C57Bl/6J G1 intercrosses**

Here we generated 102 viable offspring

In the inbreed of the *Syt13*<sup>R/R</sup> allele for G2 we did observe no viable homozygous survivor for the *Syt13*<sup>R/R</sup> allele at weaning age.

<b>Syt13 C57Bl/6J G2 intercrosses</b>		
WT	<i>Syt13</i> <sup>R/-</sup>	<i>Syt13</i> <sup>R/R</sup>
10	15	0
40%	60%	0%

**Table 4: *Syt13* C57Bl/6J G2 intercrosses**

The mouse line generated to this timepoint the total mouse number of 25 mice

Additionally we could observe lethality for the offspring at approximately 2-3 day after birth (P 2-3). Further observations of this strain will either determine the lethality of the *Syt13*<sup>R/R</sup> allele or will bring viable offspring.

<b>Syt13 C57Bl/6J G2 dead pups</b>		
WT	<i>Syt13</i> <sup>R/-</sup>	<i>Syt13</i> <sup>R/R</sup>
0	4	1
0%	80%	20%

**Table 5: *Syt13*<sup>R/R</sup> C57Bl/6J G2 dead pups at P1**

#### 3.4.4 *Syt13* mutant mice illustrate expression in diverse ciliated tissues

We analyzed *LacZ* reporter gene expression in the early mouse embryo and in the adult mouse. The regions of *Syt13* expression implicated first a cilium related phenotype, contradictory to this

observation we could not detect *Syt13* expression in ciliated tissue as lung and kidney (Cano et al. 2006).

### 3.4.4.1 *Syt13* reporter gene expression in the early embryo

We observed *Syt13* reporter gene expression in the embryo at E9.5. At this stage  $\beta$ -gal activity appears to be actively transcribed. In the lateral view of the E9.5 embryo, the distal parts of the oral epithelium showed weak expression pattern. Especially the trigeminal ganglion (tg) and the facio-acoustic ganglia (fag) exhibit a pattern of the *LacZ* reporter gene (Figure 3.29, A-B).

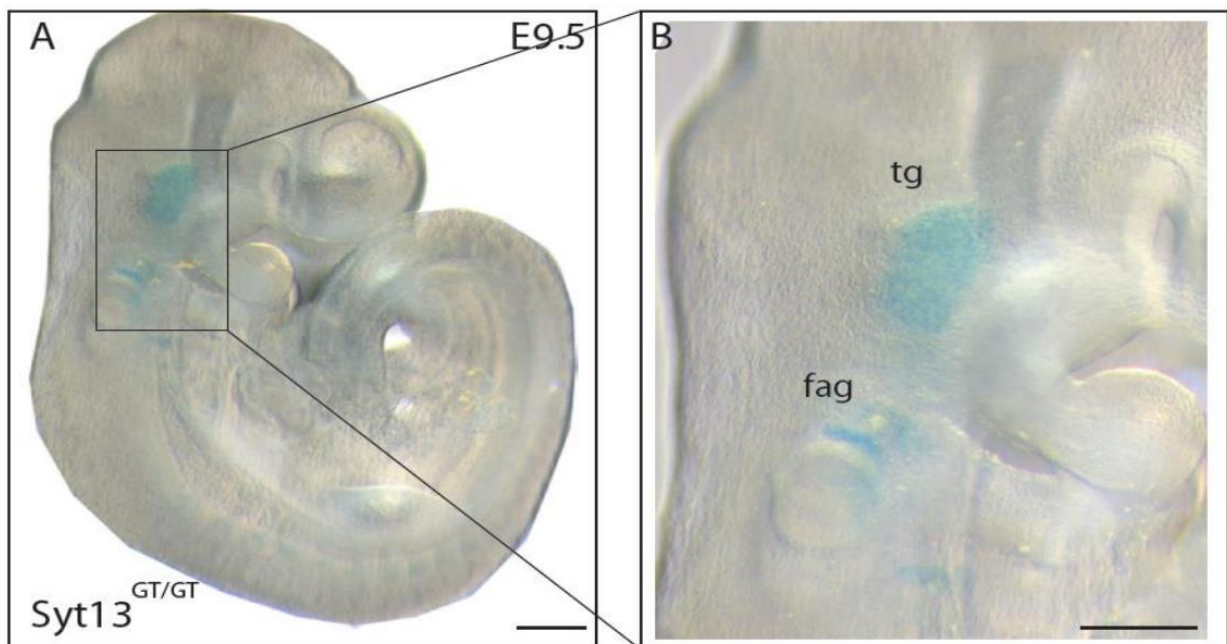


**Figure 3.29: Whole mount *LacZ* staining of the embryo at E9.5**

- (A) *LacZ* expression reflects specific pattern in the distal parts of the oral epithelium, in the trigeminal ganglion (tg) and in the facio-acoustic ganglia (fag).
- (B) Zoom into the region of interest of the whole mount embryo at E9.5

Scale is set on 500  $\mu$ m for A, respective 250  $\mu$ m for B

Abbreviations: tg = trigeminal ganglion; fag = facio-acoustic ganglia; LacZ =  $\beta$ -galactosidase; Syt13 = Synaptotagmin 13; GT = gene trap; E = embryonic stage.

In later stages at E11.5, *lacZ* reporter gene activity was observed at the tg and the dorsal root ganglion (Figure 3.30, B). Also, in a higher magnification into the pancreatic region,  $\beta$ -gal expression in the PE is obvious - not restricted to a subset of pancreatic cells (Figure 3.30, C).

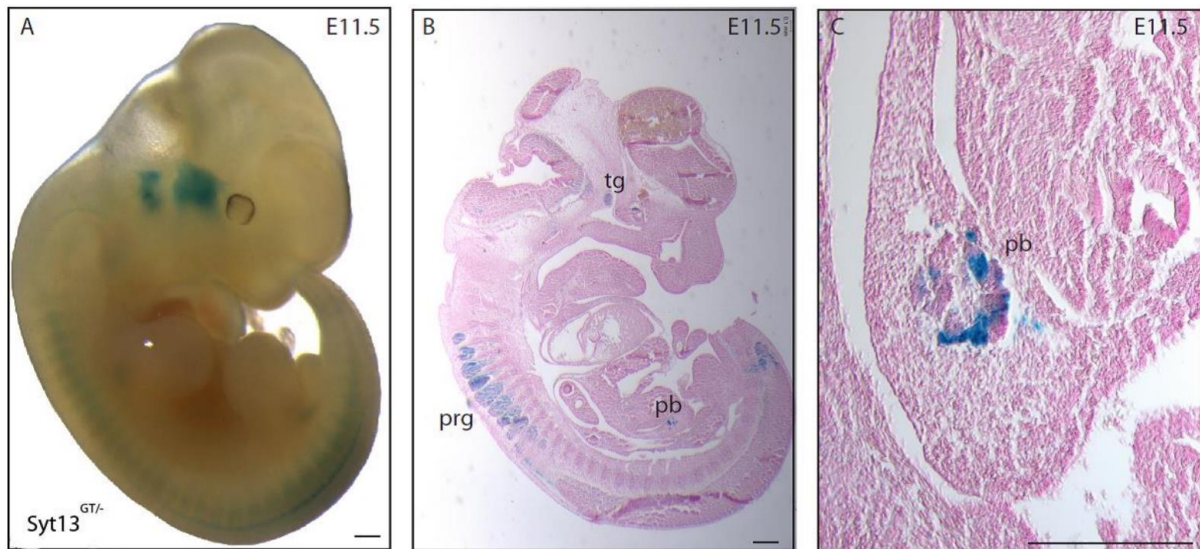


**Figure 3.30: The  $\beta$ -gal activity reflects distinct expression pattern in the early mouse embryo at E11.5.**

- (A) Whole mount *LacZ* staining at E11.5 reflects specific expression pattern in the ganglia precursor epithelium
- (B) In line with previous observation, we could confirm at E11.5 *LacZ* staining in paraffin sections in the tg, with additional pattern in the posterior root ganglions (prg) and in the pancreatic bud (pb).
- (C) In the section of the pancreatic region expression is detected in the PE at the specific E12.5.

Scalebar for all images is set at 50  $\mu$ m.

Abbreviations: tg = trigeminal ganglion; fag = facio-acoustic ganglia; prg = posterior root ganglion; pb = pancreatic bud; E = embryonic stage; *LacZ* =  $\beta$ -galactosidase; PE = pancreatic epithelium; *Syt13* = Synaptotagmin 13; GT = gene trap;  $\beta$ -gal =  $\beta$ -galactosidase.

Taken together, we suggest that *Syt13* is expressed in the ganglion precursor cells. In particular at E9.5 in tg and the fag. In later stages  $\beta$ -gal shows activity in the tg, the prg and the pancreatic primordia (pb). Most likely, *Syt13* is important for cell differentiation into postmitotic tissue. We further speculate about *Syt13* in the development of the inner ear and in pancreas organogenesis, as we could detect strong reporter gene expression in the precursor cells as the tg and the pancreatic bud.

#### 3.4.4.2 Characterization of *Syt13* reporter gene expression in the crown

The  $\beta$ -gal reflected no ubiquitous expression pattern, as it was active in a specific subset of progenitor cells. In later at E14.5 and E15.5 *Syt13*<sup>+</sup>, respective *LacZ*<sup>+</sup> cells are located in the floorplate (fp), cerebral cortex (cc), main olfactory epithelium (moe) and the opticle ventricles (ov) (Figure 33 B). Furthermore, the *Syt13*<sup>GT/GT</sup>-mice indicate in the crown region a distinct reporter gene expression in the hair follicle

(hf) (Figure 3.31 C red arrow). We suggest expression in the choroid plexus, as the cerebral cortex and the choroid plexus are interconnected through the ventricles in the brain (Lun et al. 2015). However, we did not define the precise expression in this organ.

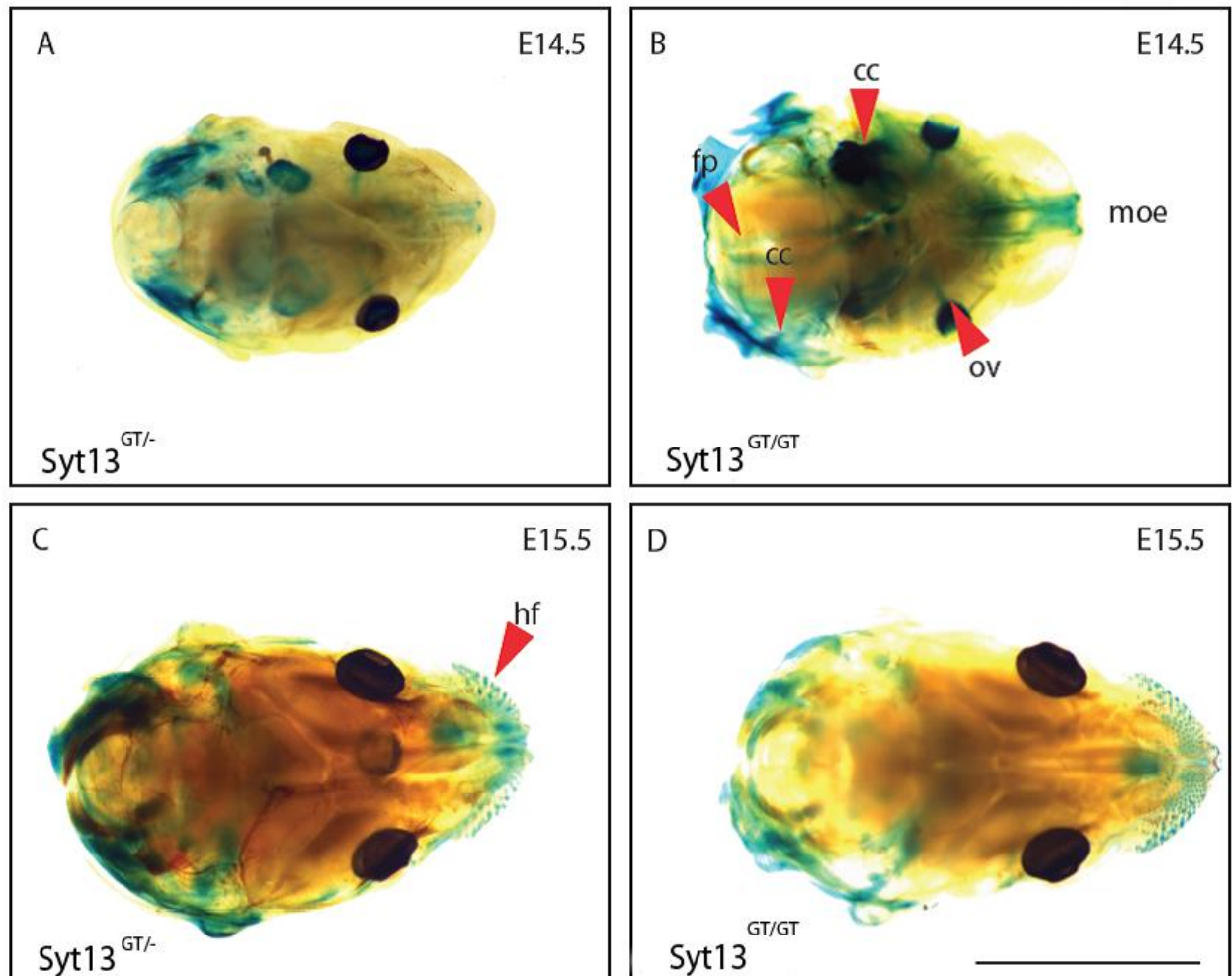


**Figure 3.31: *LacZ*- reporter analyses in the crown at E14.5 (A - B) and E15.5 (C - D).**

- (A) The  $\beta$ -gal activity is widely distributed in the BABB cleared head at E14.5. In heterozygous mice ( $Syt13^{GT/-}$ ) expression pattern correlate to the crown of the homozygous mice (B).
- (B) The homozygous mice ( $Syt13^{GT/GT}$ ) reflect reporter gene expression in the main olfactory epithelium (moe), cerebral cortex (cc) floor plate (fp) and the optic ventricle (ov).
- (C) Additionally, at E15.5 heterozygous mice reflect  $\beta$ -gal expression in the hair follicle (hf), which is also represented in the homozygous mice (D).
- (D) The crown of  $Syt13^{GT/GT}$  embryos at E15.5 illustrate the similar expression pattern as already described in the  $Syt13^{GT/-}$ -embryos.

## Results

Scale is set for 2500  $\mu\text{m}$

Abbreviations: LacZ =  $\beta$ -Galactosidase; E = embryonic stage; *Syt13* = *Synaptotagmin 13*; moe = main olfactory epithelium; cc/c = cerebral cortex; fp = floor plate; ov = optic ventricle; hf = hair follicle; *GT* = *gene trap*.

We investigated the brain compartment P for subsequent *lacZ* reporter gene expression. At 10 weeks (10 w)  $\beta$ -gal activity can be detected in the cc/c, more precise in the 2<sup>nd</sup> and 3<sup>rd</sup> layer. Additionally, in the dentate gyrus (d) *Syt13*<sup>+</sup> cells are detectable, but the precise position of these cells is not clear and thus we could not determine if progenitor stem cells are affected. (Figure 3.31, A - B). Interestingly, at a low percentage, homozygous mice (*Syt13*<sup>GT/GT</sup>) with hydrocephalus are born and alive until approximately 10 w (Figure 3.31, E). The hydrocephalus illustrates defects in ciliogenesis as the cerebrospinal fluid (CSF) in the ventricles will not be moved properly. Besides, several homozygous mutant mice with hydrocephalus went together with a decreased body weight (personal observation). This phenotype might be explained by a defect in ciliogenesis which alters the turnover of the CSF in the ventricles (Liu et al. 2014).

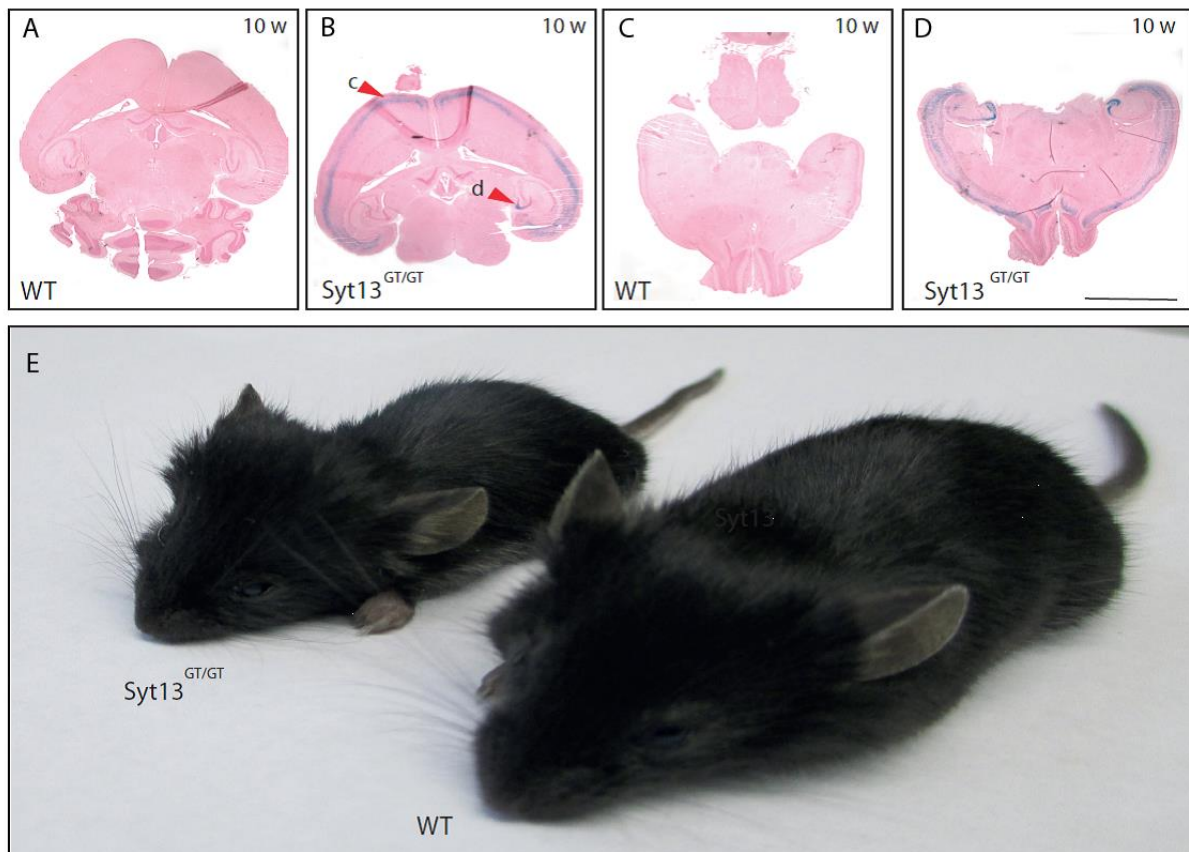


**Figure 3.32: Reporter gene expression in the crown of 10 w mice (A-D), respective *WT* and *Syt13*<sup>GT/GT</sup> illustrating a hydrocephalus (E).**

(A) Paraffin sections of *WT* from 10w brain samples

- (B) Littermate of the 10w mice with the genotype *Syt13<sup>GT/GT</sup>* illustrating reporter gene expression in the cc/c and in the dendrites (d)
- (C) Serial section of the *WT* from the 10 w littermate
- (D) *Syt13<sup>GT/GT</sup>* serial paraffin sections illustrate expression pattern in the 2<sup>nd</sup>, 3<sup>rd</sup> and 4<sup>th</sup> layer of the cc/c region
- (E) Incomplete penetrance in the *Syt13<sup>GT/GT</sup>* illustrated as an occasional incident a hydrocephalus along with insufficient body weight compared to the *WT* at P 10w.

Scale is set for 1000  $\mu$ m

Abbreviations: cc/c = cerebral cortex; d = dentate gyrus/ dendrites; w = weeks; *WT* = wild type; *Syt13* = *Synaptotagmin 13*; *GT* = gene trap; P = postnatal.

In summary, *Syt13* appears to be expressed in the neurogenic regions of the brain. The genes *Syt 1* and *Syt2* are well described in the context of neurons. *Syt4* is ubiquitously expressed in the brain, whereas *Syt3* and *Syt4* are redundant in the hippocampal synapses alike *Syt1* (Ullrich et al. 1994). In the crown of the mouse, *Syt13* implicates to be involved in differentiation of progenitor cells into certain lineages, presumably as a neuro-endocrine factor. The reporter gene expression illustrates a distinct subset of cells which are *LacZ*<sup>+</sup>. We further speculate, that the functional mechanism of *Syt13* in neuro-endocrine cells is conserved in *mammals*.

### 3.4.5 *Syt13* mutants present defects in the adult pancreas

Previous results illustrated *Syt13*<sup>+</sup> cells in the PE at E11.5 (Figure 3.30, C), in a next step P stages were selected for elucidating *LacZ* reporter gene expression in the Islets of Langerhans, respective the PE. Pancreatic paraffin sections of *Syt13<sup>GT/-</sup>* and *Syt13<sup>GT/GT</sup>* mice at the P 30 revealed specific localization of *Syt13*<sup>+</sup> cells in the Islets of Langerhans (Figure 3.33, A-F). Also, in the cluster of the Islets of Langerhans we could not distinguish between  $\alpha$ ,  $\beta$ ,  $\epsilon$ ,  $\delta$  and PP cells (Figure 3.30, B and E). Additionally, the Islets of Langerhans of the genotype *Syt13<sup>GT/GT</sup>* have atypical structures as the Islets of Langerhans differ in size and shape compared to the pancreatic sections of *Syt13<sup>GT/-</sup>* (Figure 3.33, A-B and D-E). For *Syt13<sup>GT/-</sup>* and *Syt13<sup>GT/GT</sup>* cystic structures are embedded in the exocrine tissue, suggesting impairment in ciliogenesis (Figure 3.33 C and F). Thus, we might refer to the *kinesin heavy chain member 3a* (*Kif3a*) mutant mice which exhibit cysts in the pancreas caused to primary cilia deletion in pancreatic ductal cells described by Cano et al. (Cano et al. 2006). We focused our further analysis on the Islets of

Langerhans, respective the endocrine progenitors and precursors in pancreas organogenesis. For this first observations in the adult pancreas we used *Syt13<sup>GT/-</sup>* and *Syt13<sup>GT/GT</sup>* mice crossed into the *CD1* background.

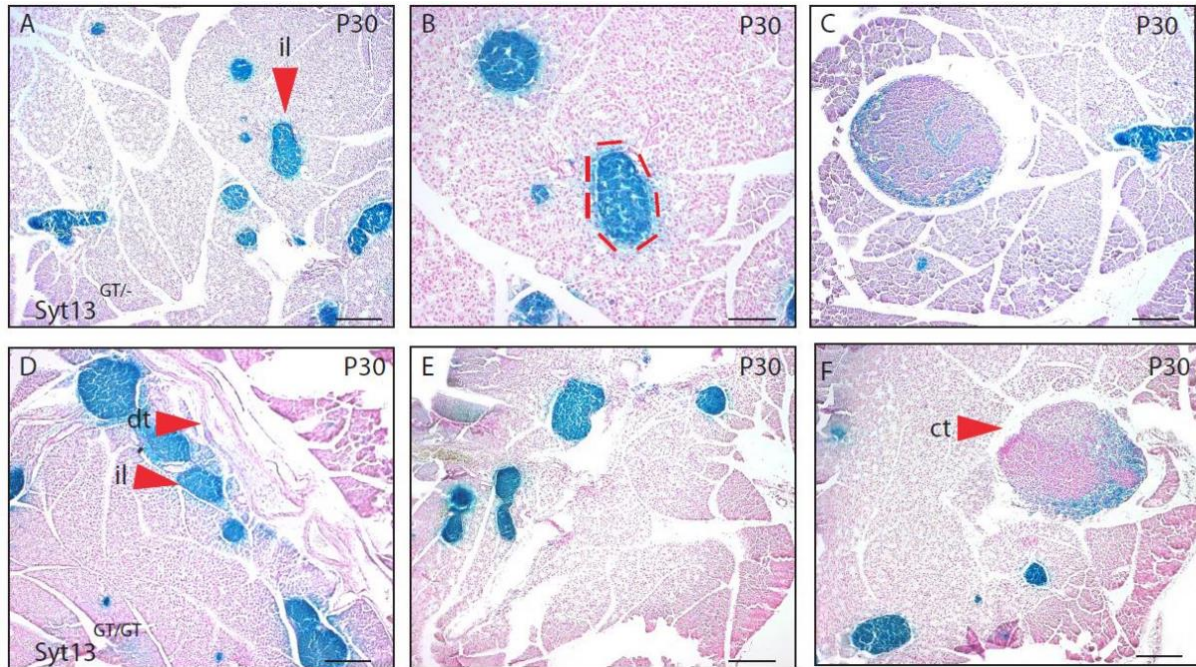


**Figure 3.33: *Syt13* reporter gene expression in the Islets of Langerhans and in cystic structures.**

- (A) Saggital paraffin sections of *Syt13<sup>GT/-</sup>* P30 pancreas tissue (il = Islets of Langerhans)
- (B) In *Syt13<sup>GT/-GT</sup>* pancreatic saggital sections the majority of the il illustrate a typical roundish structure (splitted red lines).
- (C) Although, *LacZ* reporter gene expression is reflected in the cyst-like structures in the paraffin section of the *Syt13<sup>GT/-</sup>* (see also F, ct = cyst structure).
- (D) In the *Syt13<sup>GT/-GT</sup>* serial paraffin sections, the Islets of Langerhans accumulate at the ductal (dt) region.
- (E) By P30, the Islets of Langerhans show atypical structure as they appear branched and enlarged.
- (F) In the paraffin sections of the genotype *Syt13<sup>GT/GT</sup>*, *lacZ* reporter expression is restricted to the cyst-like structures (ct = cyst)

Scale is set at 500µm.

Abbreviations: P= postnatal; il = Islets of Langerhans; ct = cyst-like structure; dt = duct/ductal; P = post natal; *Syt13* = *Synaptotagmin 13*; *GT* = *gene trap*.

To further determine the role of *Syt13* in the adult Islets of Langerhans, area measurment of *WT* and *Syt13<sup>GT/GT</sup>* of 10 w old pancreatic sections was performed. mice. The *Syt13<sup>GT/GT</sup>* pancreatic paraffin

sections illustrate inappropriate clustering of the Islets of Langerhans (il) close to the ductal (dt) region compared to the *WT* (Figure 3.34, A - B). Additionally, the ductal region is enlarged in *Syt13<sup>GT/GT</sup>* pancreas and cavities (cv) are embedded in the PE (Figure 3.34 B red arrow). In summary, the area of the Islets of Langerhans is enlarged in the *Syt13<sup>GT/GT</sup>* pancreas compared to the *WT*. Moreover, *WT* Islets of Langerhans have more compact, roundish structures and the Islets of Langerhans are clearly separated from the ductal compartment. Phenotypic analyses of *Shh<sup>-/-</sup>* mice already illustrates hyperplastic clustered Islets of Langerhans (Kim and Melton 1998). Also, PCP pathway component as *Wnt5a* reflects similar phenotypic characteristics. The Islet of Langerhans formation is not delayed, but in *Wnt5a* mutant mice the Islets of Langerhans remain in ductal proximity at E18.5. Interestingly, equal results are highlighted in the *Syt13* pancreatic paraffin section. The Islets of Langerhans accumulate in the ductal region, are enlarged and surrounded by necrotic tissue. Next to the necrotic tissue, cavities in the exocrine pancreatic tissue may indicate cancerogenesis in the mutant pancreatic sections at 10 w. Most of the exocrine tumors derive of the cells lining the duct, appearance and arrangement of the carcinoma cells most likely are duct-like (or adeno-), given the term adenocarcinoma to pancreatic cancer.

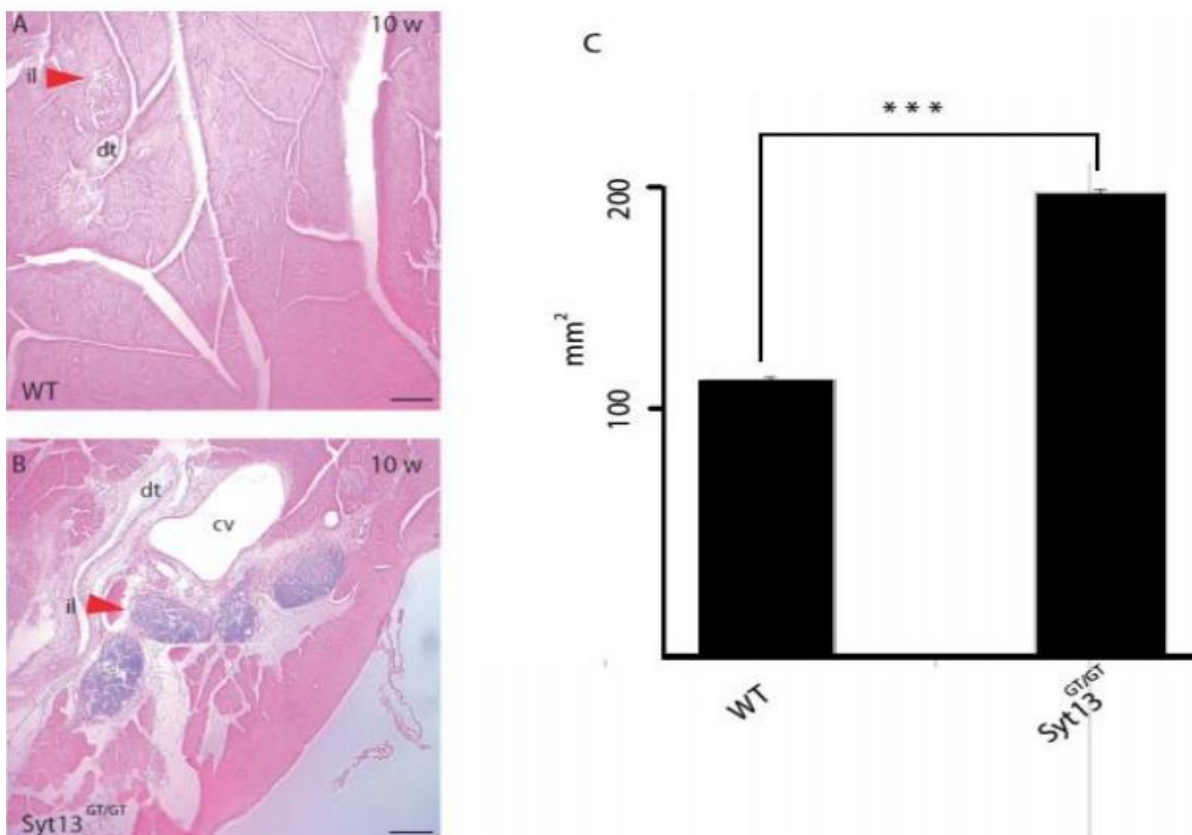


**Figure 3.34:** Islets of Langerhans in *Syt13<sup>GT/GT</sup>* are stretched along the pancreatic duct and enlarged.

- (A) *WT* pancreatic paraffin sections at 10 weeks (w) illustrating Islets of Langerhans (i) and the duct (dt).
- (B) *Syt13<sup>GT/GT</sup>* pancreatic paraffin sections reflect differences in the area and localization of the Islets of Langerhans compared to *WT*. As illustrated above the Islets of Langerhans are proximal to the ductal region in *Syt13<sup>GT/GT</sup>* pancreas. Islets of Langerhans (il) are marked by red arrow. Additionally, the ductal region is enhanced and the pancreatic tissue illustrates cavities (cv).
- (C) Measuring the area of the Islets of Langerhans (mm<sup>2</sup>) shows an increase in cell mass in the genotype of *Syt13<sup>GT/GT</sup>* compared to the *WT* (*WT* n=18 and *Syt13<sup>GT/GT</sup>* n=73 sections/in total for n= 2 mice; (p value < 0.001)).

Scalebar 150  $\mu$ m.

Abbreviations: *WT* = wild type; il = Islets of Langerhans; cv = cavity; dt = duct; w = weeks; *Syt13* = *Synaptotagmin 13*; n = number; w = weeks; GT = gene trap.

Taken together, we could observe that *Syt13* is expressed in the adult Islets of Langerhans. In the *Syt13<sup>GT/GT</sup>* mice pancreata, the Islets of Langerhans are altered by structure, cysts and necrotic tissue appear in the pancreatic exocrine compartment. It might be interesting to elucidate the role of *Syt13* in ciliogenesis-related processes as these previous results refer to published cilia-related phenotypes (McClintock et al., 2008).

### 3.4.6 *Syt13* expression in pancreas organogenesis

Previous results indicate lineage restriction of *Syt13* in the endocrine compartment (section 3.4.5). Further analyses of whole mount pancreata, dissected of mice with genotype *Syt13<sup>GT/-</sup>* *Syt13<sup>GT/GT</sup>* at E16.5 and E17.5 illustrate a distinct expression pattern in the periductal region of the pancreas (Gittes et al., 2009) (Figure 3.35, A-B'). In paraffin sections, the periductal localization of the reporter gene could be confirmed (Figure 3.35, C-D'''). The *Syt13<sup>+</sup>* cells are stretched along the ductal periphery (Figure 3.35, D-D''), delamination defects are indicated through clustering of the endocrine committed cells as a combined aggregate (Figure 3.35, C and D) contrary to immigration into the exocrine tissue compartment in the *WT* (data not shown).

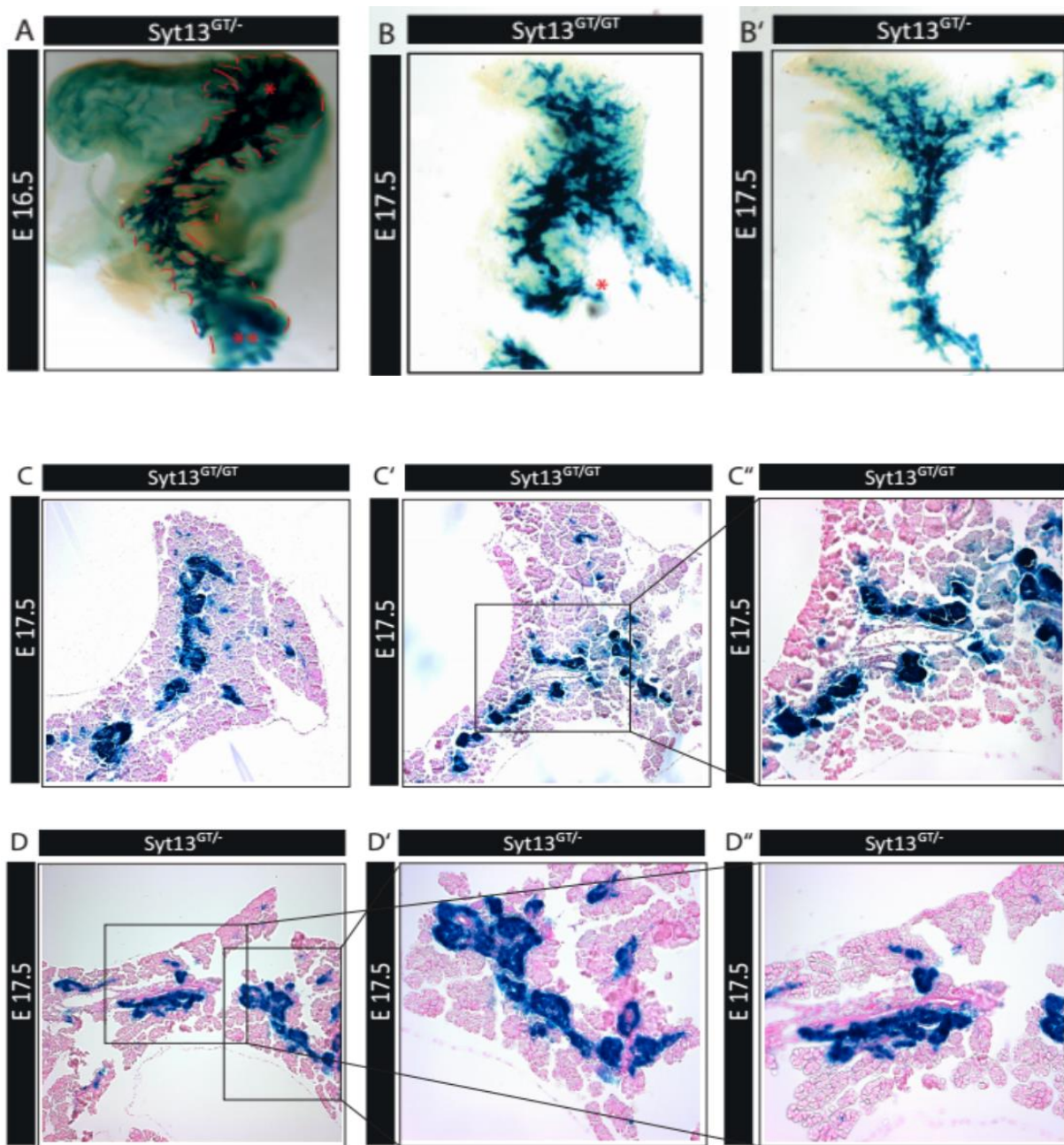


**Figure 3.35: *Syt13* shows periductal accumulation in the pancreas.**

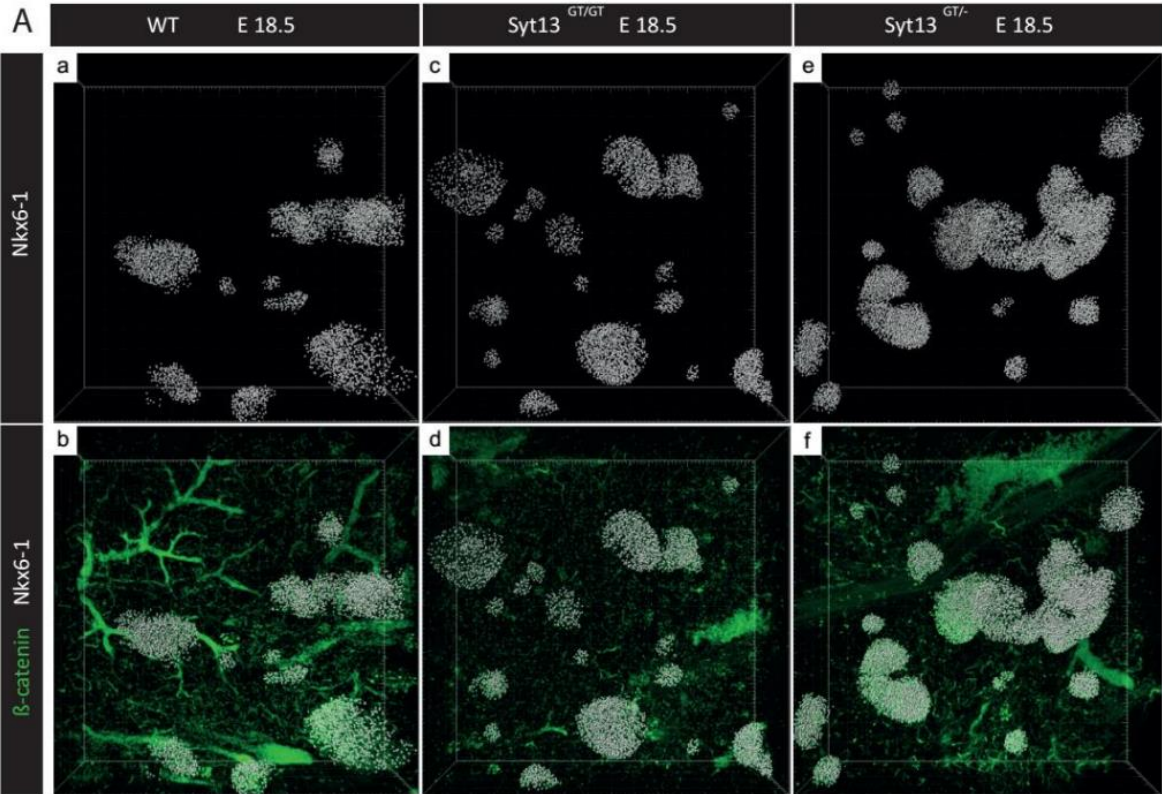
- (A) The pancreas in the whole mount at E16.5 of the *Syt13*<sup>GT/-</sup> genotype is framed in red lines. As illustrated, the pancreas proliferates at the stomach in the tail region (\*), whereas the head region is located next to the duodenum (\*\*).
- (B-B') Whole mount of pancreata at E17.5 for both genotypes (*Syt13*<sup>GT/-</sup> and *Syt13*<sup>GT/GT</sup>) reflects periductal expression pattern of the *LacZ* reporter gene. It is to note, that the tip regions of the pancreas suggest to be *Syt13*<sup>-</sup> after the secondary transition, implicating lineage restriction of *Syt13* to the endocrine lineage.
- (C-C'') The paraffin sections of *Syt13*<sup>GT/GT</sup> at E17.5 show accumulation of *Syt13*<sup>+</sup> cells at the ductal region of the pancreas (C). The Zoom into the indicated region illustrates the streaking of *LacZ*<sup>+</sup> reporter gene cells at the ductal periphery (C'-C'').

**(D-D'')** In the genotype *Syt13<sup>GT/-</sup>* at E17.5 of the presented paraffin section, *Syt13<sup>+</sup>* cells reside along the duct (D) and are aggregated into cluster which are not separated of each other (see Zoom into the indicated regions) (D'-D'').

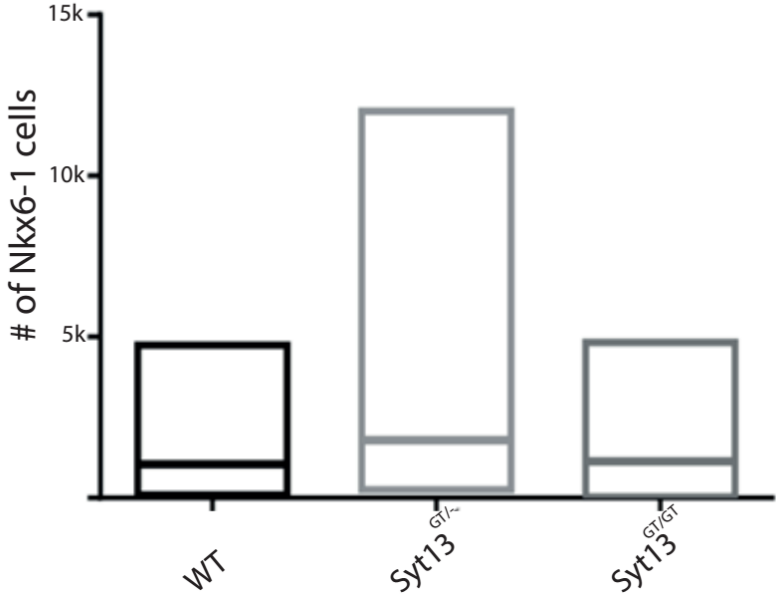
Abbreviations: Syt13 = Synaptotagmin 13; GT = gene trap; E = embryonic stage; LacZ =  $\beta$ -galactosidase.

To specify the  $\beta$  cell mass in the precursor Islets of Langerhans in more detail, whole mount imaging and 3 dimensional modelling was accomplished on pancreata of different genotypes. In the *WT* (22147 *Nkx6-1<sup>+</sup>* cells), *Syt13<sup>GT/GT</sup>* (29892 *Nkx6-1<sup>+</sup>* cells) and *Syt13<sup>GT/-</sup>* (28709 *Nkx6-1<sup>+</sup>* cells) precursor Islets of Langerhans, respective *Nkx6-1<sup>+</sup>* cells - are distributed within the PE (Figure 3.36, Aa-Af; B). Interestingly, we made the observation that in the *Syt13<sup>GT/-</sup>* and *Syt13<sup>GT/GT</sup>* pancreata, vessel marker  $\beta$ -catenin illustrates a slight intensity decrease, implicating impairment in vascular maturation (Figure 3.36, Ad and Af) (Liebner et al. 2008). Additionally, the *Syt<sup>GT/-</sup>* precursor Islets of Langerhans cluster to a higher order as a 'superislet' in line with the observed hydrocephalus (Figure 3.36, Af). Taken together, *Syt13* deficient mice appear to have an enlarged precursor Islets of Langerhans – featured by an increase of the total cell mass in endocrine progenitors (*Nkx6-1<sup>+</sup>*) in the precursor Islets of Langerhans (Figure 3.36, B). This might point to an increase in the subtype as  $\alpha$ ,  $\beta$ ,  $\epsilon$ ,  $\delta$  PP of the cells in the Islets of Langerhans.

Further analysis of whole mount pancreata and 3 dimensional imaging at the P7 stage confirmed the previous observation of the 'Superislets' in the PE (Figure 3.36, *Syt13<sup>GT/-</sup>* A-A'). The Islets of Langerhans are enlarged, clustered and remain in close proxy to each other, implicating delamination and immigration defects during endocrine lineage segregation (Figure 3.36, *Syt13<sup>GT/GT</sup>* A-A', C). Taken together, the results implicate that *Syt13* is involved in endocrine lineage commitment and thus in the metabolic impact of either T1D or T2D.



**B** Nkx6-1 endocrine progenitor cells



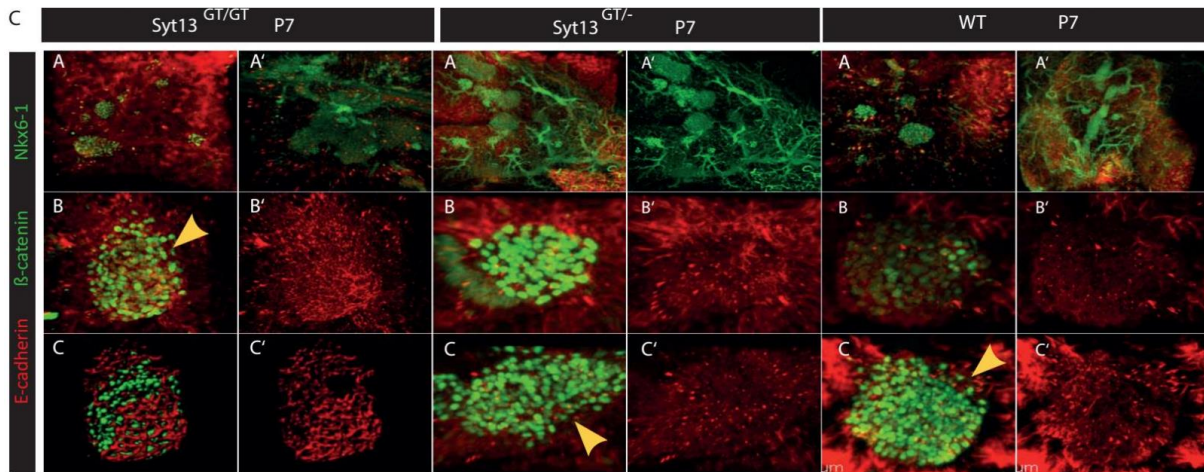


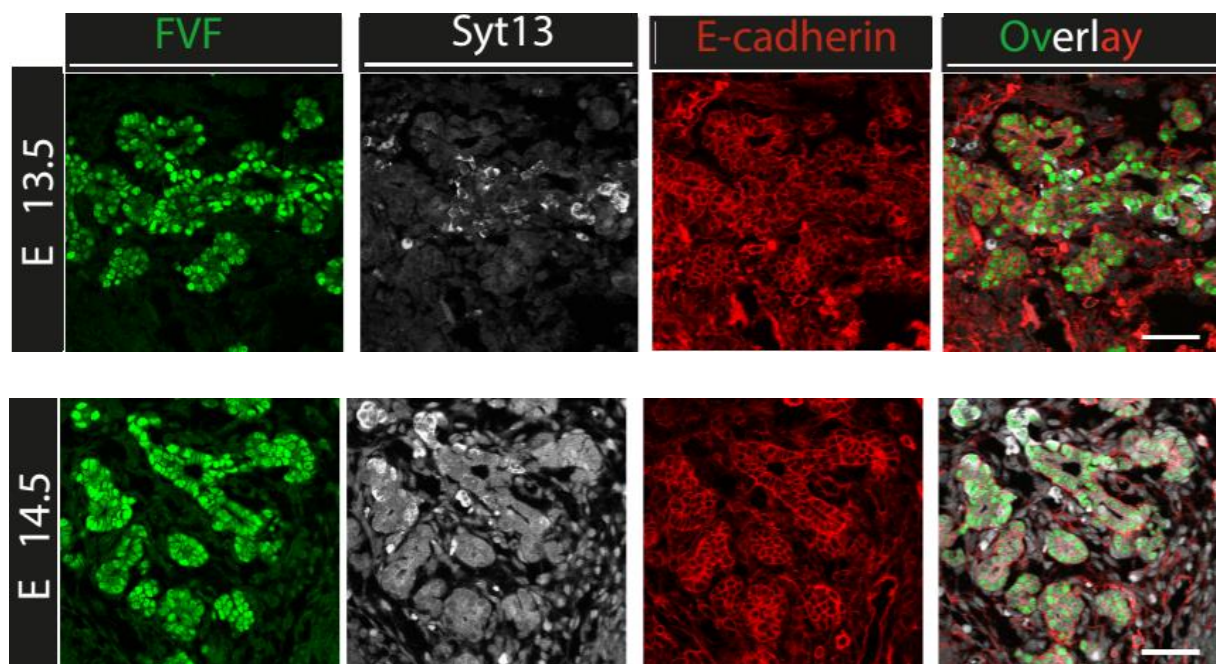
**Figure 3.36: The precursor Islets of Langerhans in *Syt13* deficient mice illustrate Superislets along with a lower quantity of the  $\beta$ -cell mass.**

- (Aa-b)** IHC on whole mount pancreata at E18.5 and 3 dimensional imaging using IMARIS softshell software of the genotype *WT* illustrates distribution of precursor Islets of Langerhans in the PE. It is to note that the precursor Islets of Langerhans are located next to the blood vessels. The *Nkx6-1*<sup>+</sup> expressing cell pool represent the precursor Islets of Langerhans, contrary, IHC on  $\beta$ -catenin indicates the vascularization in the PE.
- (Ac – d)** The genotype *Syt13*<sup>GT/GT</sup> of the E18.5 pancreas shows dispersal localization of the precursor Islets of Langerhans, vessels are indicated to be delayed in organogenesis as the IHC on  $\beta$ -catenin is declined.
- (Ae-f)** Whole mount pancreata of *Syt13*<sup>GT/-</sup> in 3 dimension reflect clustered precursor Islets of Langerhans – stated as ‘Superislets’. The  $\beta$ -catenin expression level is slightly decreased compared to the *WT*. In addition, the mouse of the genotype *Syt13*<sup>GT/-</sup> exhibited a hydrocephalus.
- (B)** In the precursor Islets of Langerhans, the total  $\beta$ -cell mass was calculated by counting *Nkx6-1*<sup>+</sup> cells. For the *WT* (22147 *Nkx6-1*<sup>+</sup> cells – value = 21) and *Syt13*<sup>GT/-</sup> (28709 *Nkx6-1*<sup>+</sup> cells – value = 16) p value was calculated at 0.0029, respective <0.0001. The genotype *Syt13*<sup>GT/GT</sup> (29892 *Nkx6-1*<sup>+</sup> cells – value = 26) showed a p value of 0.0004.
- (C)** Repetitive IHC and 3 dimensional imaging with IMARIS softshell software of whole mount pancreata of different genotypes for the precursor Islets of Langerhans at P7. The genotype *Syt13*<sup>GT/GT</sup> illustrates Islets of Langerhans (*Nkx6-1*<sup>+</sup> cell population) and vascularization ( $\beta$ -catenin<sup>+</sup> cells) in the PE (*E-cadherin*<sup>+</sup> cells) (A-A’). The Islets of Langerhans (B yellow arrow) immigrate into the PE (B’). The 3 dimensional imaging presents the single Islet of Langerhans from (B) and the PE (C-C’). The genotype *Syt13*<sup>GT/GT</sup> showed as an obvious phenotype ‘Superislets’. IHC revealed vascularization and that the Islets of Langerhans are aggregated to clusters in the PE (A-B’). The Islets of Langerhans appear to be enlarged in the length (C yellow arrow) and *Ecad* expression decreased (C’). For the *WT*, vessels and Islets of Langerhans are distributed in the PE (A-A’). The Islets of Langerhans reflect a roundish architecture in the PE (B, C yellow arrow). It is to note, that the IHC on *Ecad* correlates in the *WT* in the 2 samples (B’ *Ecad*<sup>low</sup>, C’ *Ecadherin*<sup>high</sup>).

## Results

Abbreviations: Syt13 = Synaptotagmin 13; Nkx6-1 = NK homeobox x 6-1; *WT* = wild type; *GT* = gene trap; E = embryonic stage; IHC = immunohistochemistry; P = postnatal; PE = pancreatic epithelium; n = number; GT = gene trap.

In a next step we examined endogenous Syt13 in the secondary transition of pancreas organogenesis. At E13.5, the PE segregates into a  $FVF^{high}$  and  $FVF^{low}$  subpopulation, illustrating the lineage commitment of the formerly MPP of the PE. Interestingly, the  $Syt13^+$  cell pool co-localizes to the  $FVF^{high}$  endocrine precursor cells (Figure 3.37, A E13.5 yellow arrow). In addition, a minor subpopulation stated as  $Syt13^{low}$  is expressed at the luminal surface of the ductal compartment (Figure 3.37, A E13.5 \*). At E14.5 the endocrine progenitors expressing  $Syt13^{high}FVF^{high}$  leave the ductal cord, represented by distribution of this specific cell pool in the PE (Figure 3.37, A E14.5). We further characterized the precursor Islets of Langerhans, which cluster and migrate into the PE at E15.5 (Figure 3.37, A E15.5 yellow arrow). The closer examination of the  $Syt13^+$  expressing cells at the end of the secondary transition at E16.5 illustrated a higher quantity of the  $Syt13^{high}$  cells compared to the earlier stages (Figure 3.37, A E16.5), indicating that in the PE and within the endocrine progenitors' lineage restriction. Taken the results in account, Syt13 implicates to characterize the  $FVF^{low}$  cell compartment in the secondary transition in line with a  $Cpa1^+Hnf1\beta^+Sox9^+Ecad^+$  marker onset, respective exocrine and ductal progenitors. In addition, the  $Syt13^{high}$  co-localizes to  $FVF^{high}$ , emphasizing an endocrine precursor pool of  $Syt13^{high}FVF^{high}Nkx6-1^+Pax6^+Ecad^+$  (Figure 3.37, A' E13.5 and E15.5 red arrow).



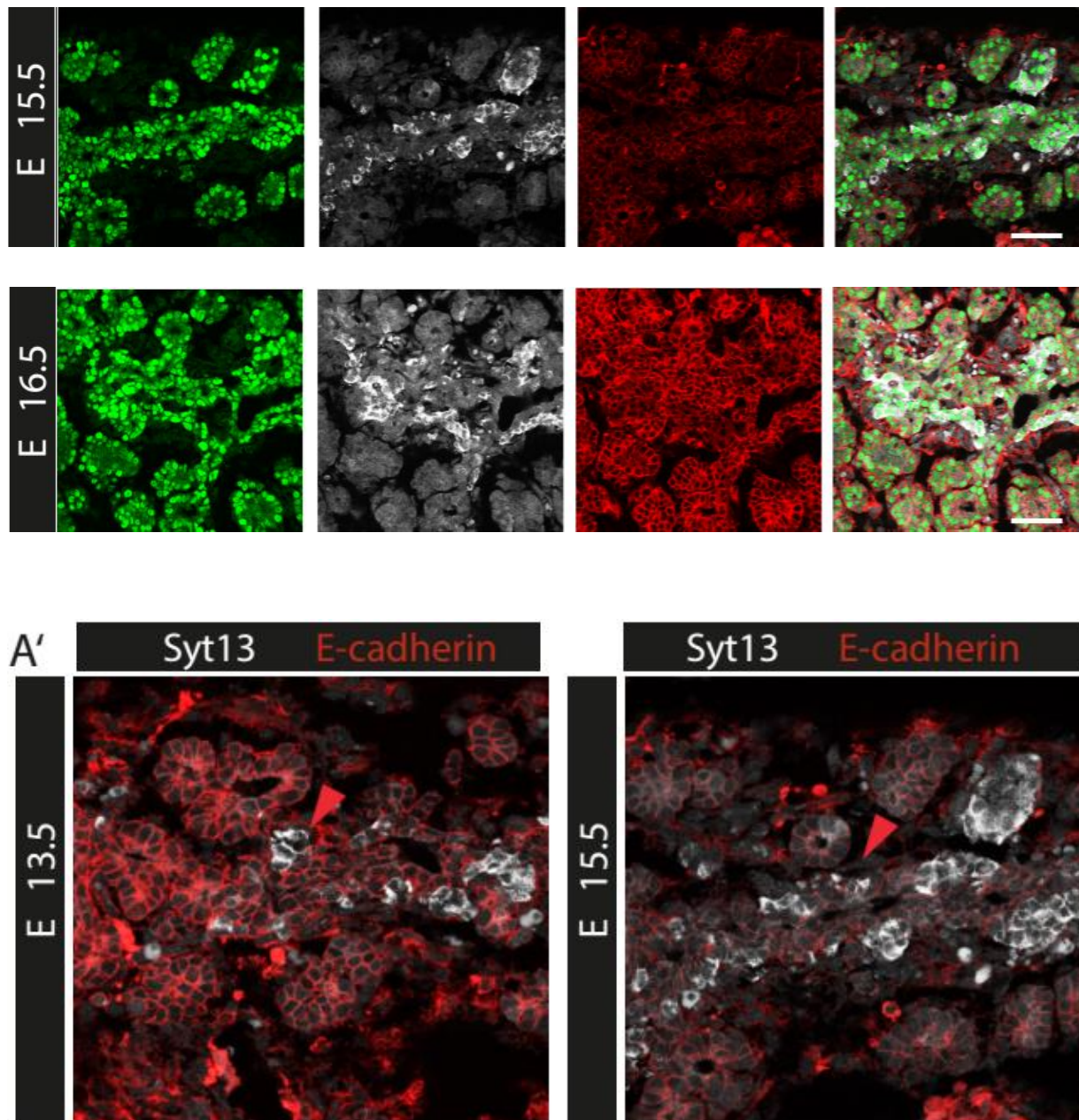


**Figure 3.37: In the secondary transition of the pancreas the endocrine precursor pool is characterized through  $Syt13^{high}$ .**

- (A)** In coronal sections at the different E of the secondary transition (E13.5 – E15.5) and at E16.5, the PE is illustrated by IHC of FVF and Ecad. At E13.5 the  $Syt13^{high}$  cell population co-localizes to the  $FVF^{high}$  cell population (E3.5 yellow arrow). A subpopulation of  $Syt13^{low}FVF^{low}$  is expressed in the ductal cells (E13.5 \*). At E14.5 and E15.5 the  $Syt13^{high}$  cells accumulate in the PE (E15.5 yellow arrow) and after secondary transition the amount of  $Syt13^{high}$  expressing cells increase (n=1) (E16.5).
- (A'')** The  $Syt13^{high}$  regionalized expression illustrates  $Ecad^{low}$  levels (red arrow), in line with the  $Ecad^{high}$   $Syt13^{low}$  in the PE of the secondary transition. On that account the endocrine precursors are characterized through a  $Syt13^{high}FVF^{high}Nkx6-1^{+}Pax6^{+}Ecad^{-}$  marker onset.

Scale is set for 100 $\mu$ m

## Results

Abbreviations: *Syt13* = *Synaptotagmin 13*; n = number; *FVF*<sup>+</sup> = *Foxa2-Venus-Fusion positive*; *FVF*<sup>-</sup> = *Foxa2-Venus-Fusion negative*; *Foxa2* = *winged helix/forkhead box*; *NKX6-1* = *NK homeobox 6-1*; *PAX6* = *paired homeodomain 6*; *PE* = *pancreatic epithelium*; *IHC* = *Immunohistochemistry*; *Ecad* = *E-cadherin*; *E* = *embryonic stage*.

Taken previous results in account, we identified after secondary transition a *Syt13*<sup>+</sup>*Nkx6-1*<sup>+</sup> endocrine progenitor pool in the PE, respective endocrine differentiated cells (Figure 3.38, A) in addition to *Syt13*<sup>+</sup>*Nkx6-1*<sup>-</sup> cells (Figure 3.38, A yellow arrow). As the *Syt13*<sup>+</sup>*Nkx6-1*<sup>-</sup> cell reside next to *Nkx6-1*<sup>+</sup> compartment and reflects *Cd49*<sup>low</sup> (*Itga6*; *Integrin alpha 6*) as an exocrine marker, this might indicate to differentiation into  $\alpha$ ,  $\epsilon$ ,  $\delta$  and PP producing endocrine cells. Additionally, we examined in differentiated endocrine cells (*Ins*<sup>+</sup>) co-localization to *Syt13*<sup>+</sup> cells (Figure 3.38, B) along with *Ins*<sup>-</sup>*Syt13*<sup>+</sup> cells (Figure 3.38, B yellow arrow). Thus, we assume that *Syt13* is expressed in at least 2 different subtypes of the Islets of Langerhans.

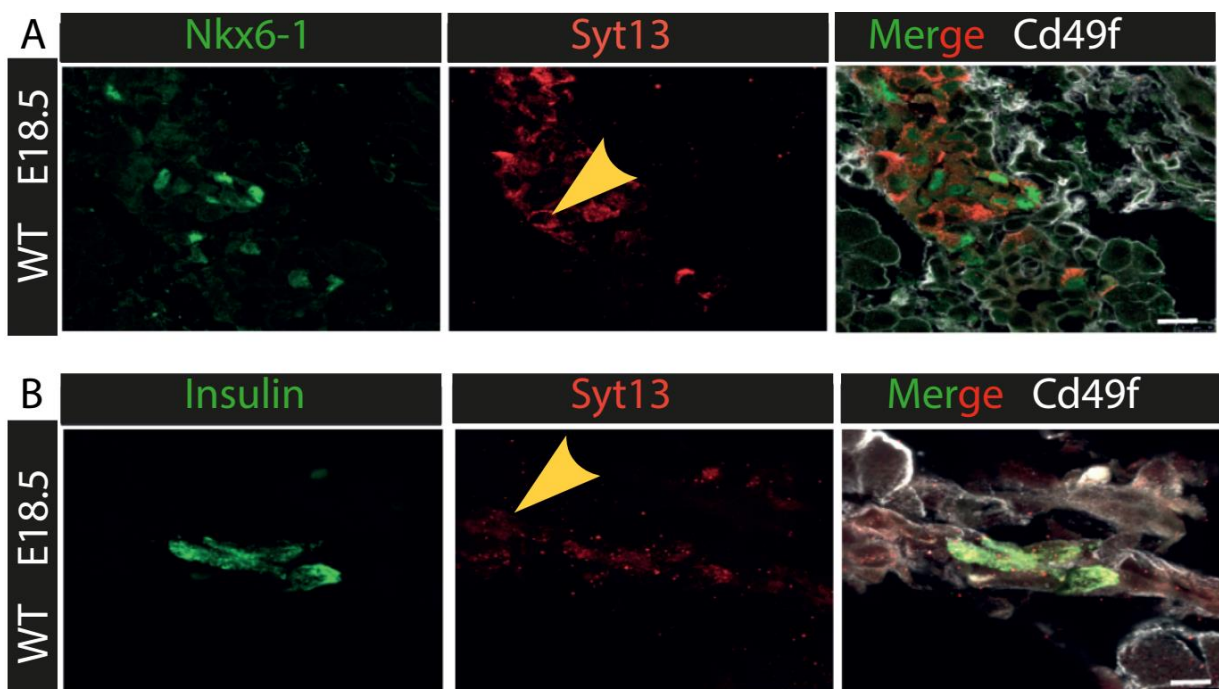


**Figure 3.38: After secondary transition of the pancreas the endocrine progenitors and endocrine cells are expressing *Syt13*.**

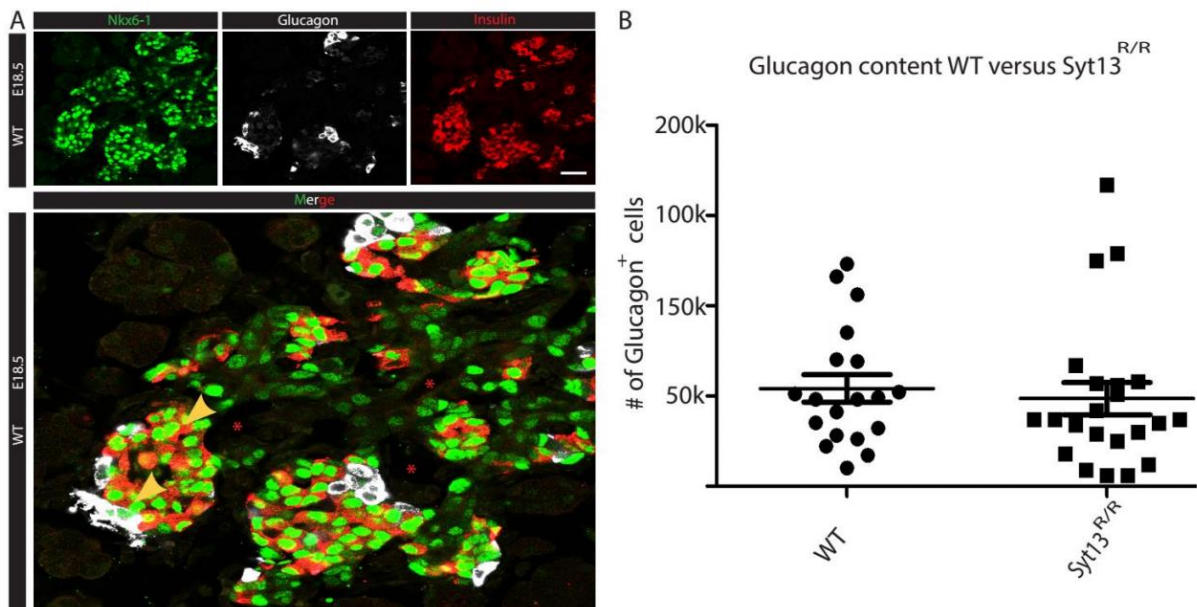
- (A) The endocrine precursors are marked by IHC against *Nkx6-1* on the pancreatic coronal section of *WT* E18.5. It is to note that *Syt13*<sup>+</sup> cells co-localizes to *Nkx6-1*, also *Nkx6-1*<sup>-</sup> cells are *Syt13*<sup>+</sup> (yellow arrow). The PE is characterized through IHC for *Cd49f* (*Itga6*; *Integrin alpha 6*).
- (B) Endocrine differentiated cells represented by *Insulin* co-express *Syt13*; in addition some *Syt13*<sup>+</sup> cells remain *Insulin*<sup>-</sup> (yellow arrow). Also *Cd49*<sup>high</sup> cells are *Syt13*<sup>-</sup> in the PE of the *WT* E18.5 pancreas.

Scale is set at 100 $\mu$ m

## Results

Abbreviations: *Syt13* = *Synaptotagmin 13*; IHC = immunohistochemistry; NKX6-1 = NK homeobox 6-1; Cd49f = Itga6; Integrin alpha 6; PE = pancreatic epithelium; *WT* = *wild type*.

Also, we were interested in the content of endocrine differentiated cells, respective  $\text{Insulin}^+\text{Glucagon}^+$  ( $\text{Ins}^+\text{Gcg}^+$ ) cells in the *Syt13* deficient mice (*Syt13<sup>R/R</sup>*) at E18.5. Thus, the *WT* illustrates typical precursor Islets of Langerhans likely described by the roundish architecture comprising of  $\text{Gcg}^+$  expressing cells at the ceiling and  $\text{Ins}^+$  cells in the inner part of the cluster (Figure 3.39, A yellow arrow) in the ductal compartment. Contrary, we observed for the *Syt13<sup>R/R</sup>* pancreata a randomly distributed  $\text{Ins}^+\text{Gcg}^+$  cell pool in proxy to the duct (Figure 3.39, C yellow arrow and \*). Interestingly, the quantity of  $\text{Gcg}^+$  cells did not differ significantly between the genotypes *WT* and *Syt13<sup>R/R</sup>* (Figure 3.39, B), whereas the differentiated endocrine  $\text{Ins}^+$  cells are remarkably altered by their quantity (Figure 3.39, D \*, p-value 0.0289).



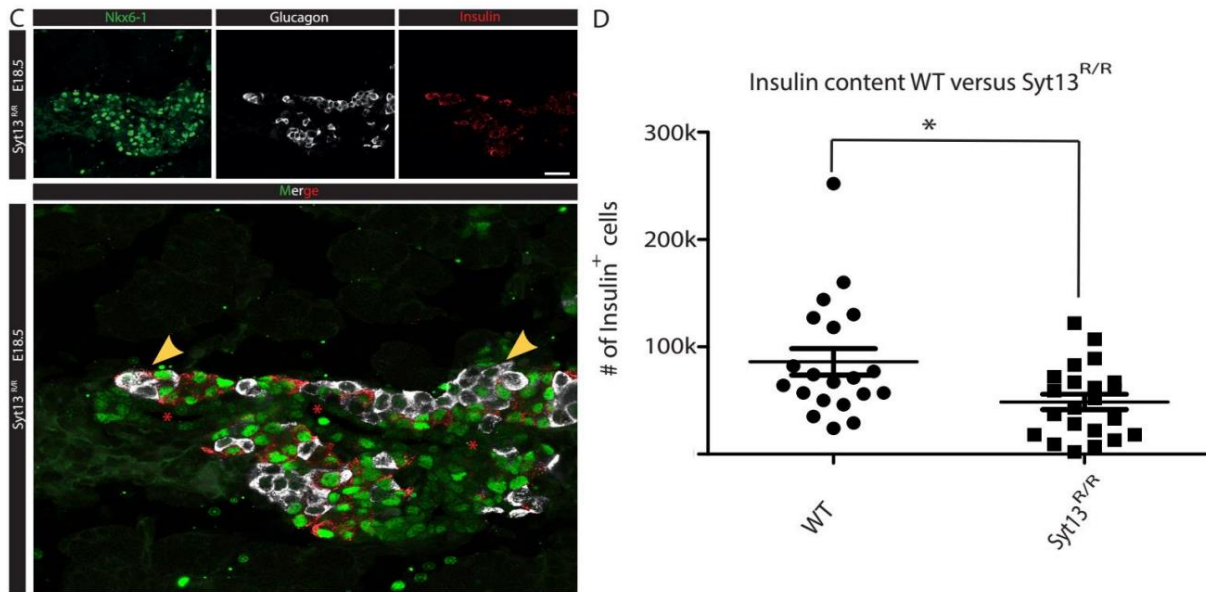


**Figure 3.39: In the *Syt13<sup>R/R</sup>* mutants precursor Islets of Langerhans are disorganized with a decreased quantity of *Ins<sup>+</sup>* cells.**

- (A) Coronal sections of the WT at E18.5 illustrates precursor Islets of Langerhans comprising of polyhormonal *Ins<sup>+</sup>Gcg<sup>+</sup>*, *Ins<sup>+</sup>* and *Gcg<sup>+</sup>* cells (yellow arrow). The precursor Islets of Langerhans are segregating from the ductal compartment (\*), indicating differentiation of endocrine progenitors (*Nkx6-1<sup>+</sup>*) into the different subtypes as  $\alpha$ ,  $\beta$ ,  $\epsilon$ ,  $\delta$  PP.
- (B) The content of *Gcg<sup>+</sup>* in the WT versus *Syt13<sup>R/R</sup>* illustrates a slight decrease in *Gcg<sup>+</sup>* cell pool in the genotype *Syt13<sup>R/R</sup>*. For the two-tailed t-test no significance was calculated (p-value = 0.3240), implemented statistical values are combined in the supplement
- (C) In the genotype *Syt13<sup>R/R</sup>* the precursor Islets of Langerhans at E18.5 are attached to the ductal compartment (\*) and the *Ins<sup>+</sup>Gcg<sup>+</sup>* randomly distributed (yellow arrow). In addition, polyhormonal *Ins<sup>+</sup>Gcg<sup>+</sup>* appear (left yellow arrow). It is to note that an endocrine pool (*Nkx6-1<sup>+</sup>*) may represent the overall endocrine precursor as  $\epsilon$ ,  $\delta$  or pancreatic polypeptide (PP) cells.
- (D) The *Insulin<sup>+</sup>* (*Ins<sup>+</sup>*) cell population decrease in the quantity in the genotype *Syt13<sup>R/R</sup>* compared to the WT. The differences are significant including a p-value of 0.0289, implemented statistical values are combined in the supplement.

Scale bar represents 50 $\mu$ m

Abbreviations: PP = pancreatic polypeptide;  $\epsilon$  = epsilon;  $\delta$  = delta; *Nkx6-1* = NK homeobox x 6-1; *Ins* = Insulin; *Gcg* = Glucagon; E = embryonic stage; WT = wild type, *Syt13* = *Synaptotagmin 13*; R = Rosa; # = number; k = thousand/1000.

Taken together, we confirmed a *Syt13<sup>+</sup>* cell pool in the PE in the secondary transition combined to the *Syt13<sup>+</sup>Nkx6-1<sup>+</sup>* endocrine precursor cells. Furthermore, we detected altered architecture of the adult Islets of Langerhans combined with the altered precursor Islets of Langerhans defined as 'Superislets'. Also, we observed a decrease in *Ins<sup>+</sup>* cells, suggesting that the increase in the cell mass in the Islets of

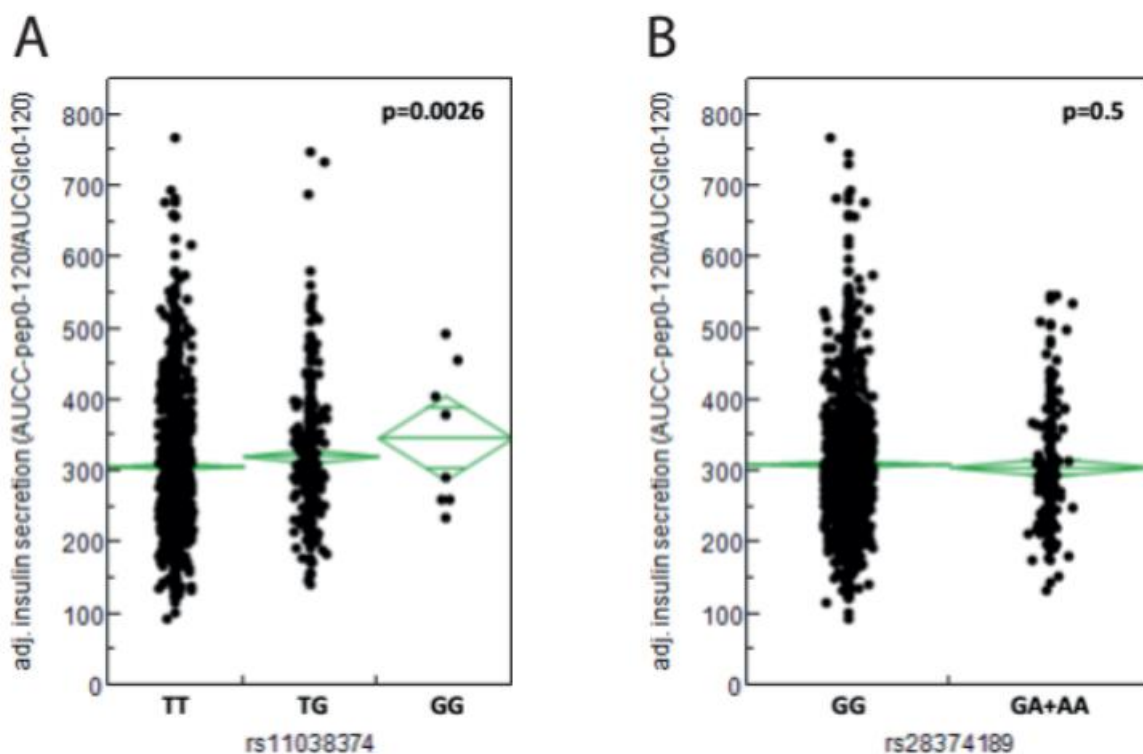
Langerhans is in notion with an increase in either  $\alpha$ ,  $\epsilon$ ,  $\delta$  or PP cells. Additionally, polarity appears to be disturbed as the defined architecture of precursor and adult Islets of Langerhans differs compared to the WT.

### 3.4.7 *Syt13* associated SNP reveal T2D susceptibility

The Genome-wide association study (GWAS) evaluated the influence of polymorphisms of the *Syt13* gene in development of T2D among 2100 individuals. A total of 12 valid Single nucleotide polymorphism (SNP) were genotyped (Table).

SNP rs11038374 showed significant allelic association with T2D patients when compared to normal glucose tolerant (NGT) controls. Multiple linear regression analysis of SNP rs11038374 with adjustment for age, body mass index (BMI), gender and insulin sensitivity indicated that in individuals the G/G genotype was significantly associated with T2D when compared with T/T and T/G (Figure 3.40, A).

A significant difference in allele frequency was found in SNP rs28374189 comparing male and female T2D patients with NGT controls (0.1 versus 0.002) (Figure 3.40, B), A being the major allele present at lower frequency in T2D. Multiple linear regression analysis showed that this SNP is associated with increased risk of T2D in men carrying the genotype G/A and women carrying the A/A and G/A genotype adjusted on gender, age and BMI (Figure 3.40, B'-B'').



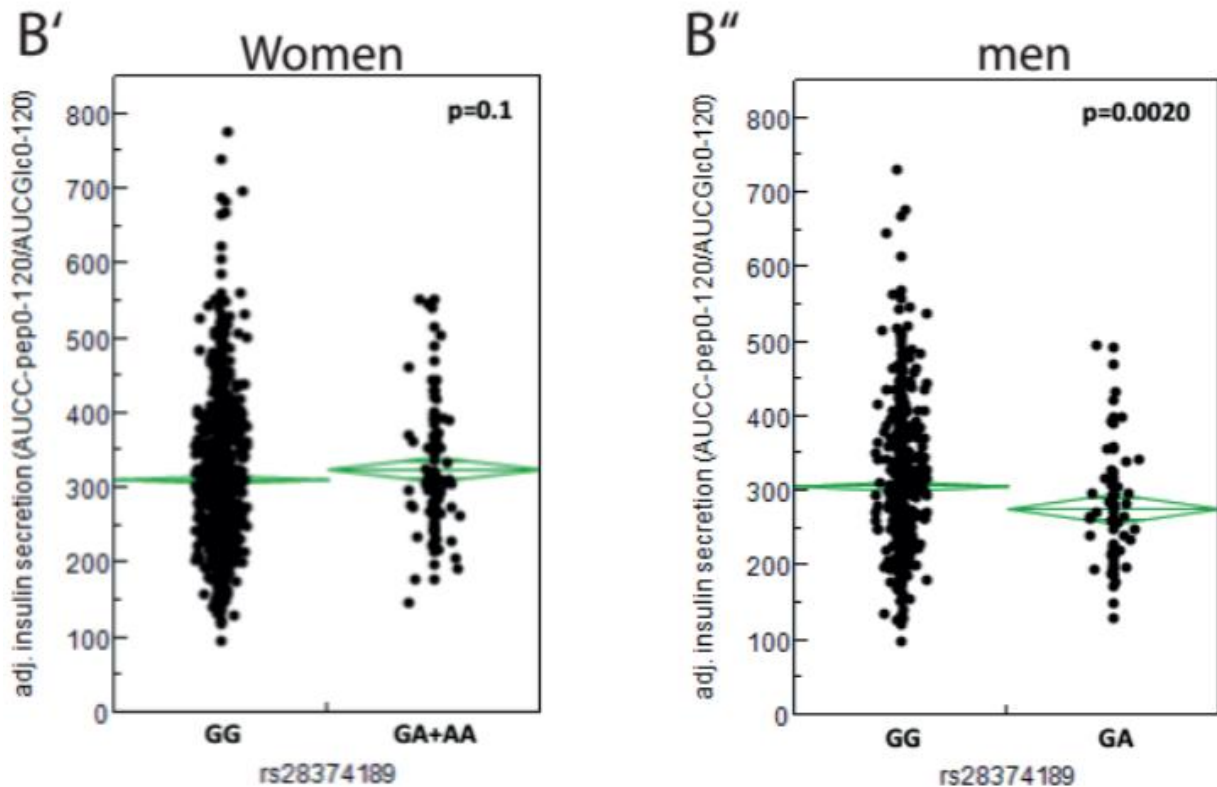


**Figure 3.40: SNP in rs1038374 and rs28374189 correlate to T2D susceptibility**

- (A)** The SNP rs1038374 is associated with impairment in insulin secretion for the genotype G/G (p-value 0.0026). Each individual of the cohort is applied in the scheme, separated by the different SNP variants. The adjusted insulin level ( $AUC_{C-pep0-120}/AUC_{Glc0-120} (*10^{-9})$ ) for T/T ( $313 \pm 101$ ), T/G ( $320 \pm 103$ ) and G/G ( $335 \pm 110$ ) are indicated (green line).
- (A')** Allelic association of SNP rs28374189 to gender biased insulin secretion defects ( $p_{Gender\ interaction}$  0.0005). The genotypes G/A ( $186 \pm 227$ ) and A/A (107) are linked to T2D (p-value 0.5), whereas G/G ( $170 \pm 153$ ) illustrated normal glucose tolerance (NGT).
- (B)** The adjusted insulin secretion ( $AUC_{C-pep0-120}/AUC_{Glc0-120} (*10^{-9})$ ) calculated  $p_{Gender\ interaction}$ . In women in the genotype A/A ( $n=1$ ) with insulinogenic index 107 and G/A  $186 \pm 227$  includes a p value of 0.1 compared to the NGT (G/G).
- (B')** In the gender interaction, allelic frequency of SNP rs28374189 showed in men the genotypes G/G and G/A insulin secretion susceptibility. The genotype A/A is only present in women.

Abbreviations: SNP = single nucleotide polymorphism; adj = adjusted; pep = peptide; GCG = glucagon; c-pep = c-peptide; NGT = normal glucose tolerance; T2D = type 2 diabetes.

### 3.4.8 Delamination of endocrine precursors in *Syt13* mutants is impaired

Our *Foxa2* and *Pdx1* co-localization study revealed that both factors are co-expressed in the PE in the secondary transition, in addition subpopulation stated as  $FVF^{low}Pdx1^{low}$  and  $FVF^{high}Pdx1^{high}$  correlate to

the exocrine/ductal and endocrine lineage segregation in the PE (Willmann et al., 2015; Burtscher and Lickert, 2009; Gao et al., 2008). Thus, we were interested in the co-localization of the  $Syt13^{high}$  endocrine progenitor cell pool in regard to co-expression to the  $FVF^{high}Pdx1^{high}$  subpopulation (Figure 3.41, A-D', \*). And indeed we could confirm previous results, a  $FVF^{high}Pdx1^{high}Syt13^{high}$  subpopulation in the PE at E13.5 indicating endocrine lineage segregation (Figure 3.41, A-D', \* and D, red arrow). Surprisingly, we identified a  $FVF^{high}Pdx1^{low}Syt13^{high}$  cell, suggesting a critical competence window between  $\alpha$ - and  $\beta$ -cell neogenesis in the secondary transition of pancreas organogenesis (Figure 3.41, A-D', yellow arrow).

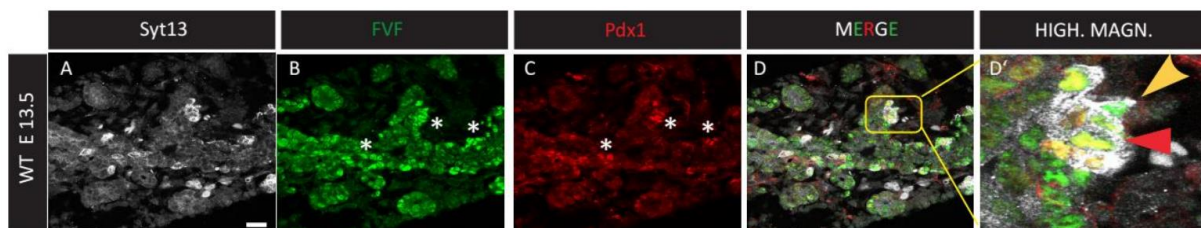


**Figure 3.41: FVF, Pdx1 and Syt13 co-localize in the PE**

**(A-D')** IHC against FVF, Pdx1 and Syt13 on a coronal PE section of at E13.5 (A-D'). All  $FVF^+$  expressing cells in the PE express Pdx1 at the onset of pancreas lineage segregation in the PE (C, \*).  $Syt13^{high}$  expressing cells are mainly in the ductal region of the PE and correlate to  $FVF^{high}$  and  $Pdx1^{high}$  (\*). The endocrine lineage segregation is characterized through  $FVF^{high}Syt13^{high}Pdx1^{low}$  representing the  $\alpha$ -cells (D-D', yellow arrow), contrary the  $FVF^{low}Syt13^{high}Pdx1^{high}$  marks the  $\beta$ -cell pool (D-D', red arrow). Also, it is to note that the precursors of the different subpopulations  $\alpha$ ,  $\epsilon$ ,  $\delta$  or PP suggest to derive out of the  $Syt13^{high}$  cell pool.

Scale is set for 25 $\mu$ m

Abbreviations: FVF = Foxa2-Venus-Fusion;  $FVF^+$  = FVF positive; Pdx1 = pancreatic and duodenal homeobox 1; E = embryonic stage; PE = pancreatic epithelium; HIGH. MAGN. = Higher Magnification; PE = pancreatic epithelium; IHC = Immunohistochemistry, Syt13 = Synaptotagmin 13.

In a next step, we further gained insights into the mechanism regarding the role of *Syt13*. Thus,  $FVF^{high}Nkx6.1^+$  cells are aggregated in clusters at E18.5 in the *WT*, illustrating the precursor Islets of Langerhans (Figure 3.42, A, yellow arrow). The endocrine progenitors delaminate as clusters proxy to the ductal compartment into the exocrine tissue ( $Cd49f^{high}$ ) (Figure 3.42, A, red arrow). Remarkably, the  $FVF^{high}Nkx6.1^+$  cells reside out of the ductal cord ( $Cd49f^{low}$ ), indicating lineage segregation of the formerly MPP in the PE in line that  $FVF^{low}$  expression correlates to the  $Hnf1\beta^+Sox9^+$  trunk pattern (section 3.1.2). Also, the ductal compartment is indicated as a ductal stratified tree with defined polarity ( $Cd49f^+$ ), whereas the endocrine compartment reflects in regard to the basement marker unpolarized cells (Figure 3.42, A, red arrow) (Crisera et al., 2000; Sugiyama et al., 2006). Contrary, the

*Syt13<sup>R/R</sup>* PE at E18.5 illustrates FVF<sup>high</sup>Nkx6.1<sup>+</sup> residing in the ductal compartment (Figure 3.42, A', red arrow), thus implying delamination defect of the endocrine precursors into the PE (Figure 3.42, A, yellow arrow). Taken these first images, the FVF<sup>+</sup> cell population suggests to be increases compared to the Nkx6-1<sup>+</sup> cells and are lining the outer ceiling of the precursor Islets of Langerhans, which might accompanies with an increase in differentiated  $\alpha$ -cells.

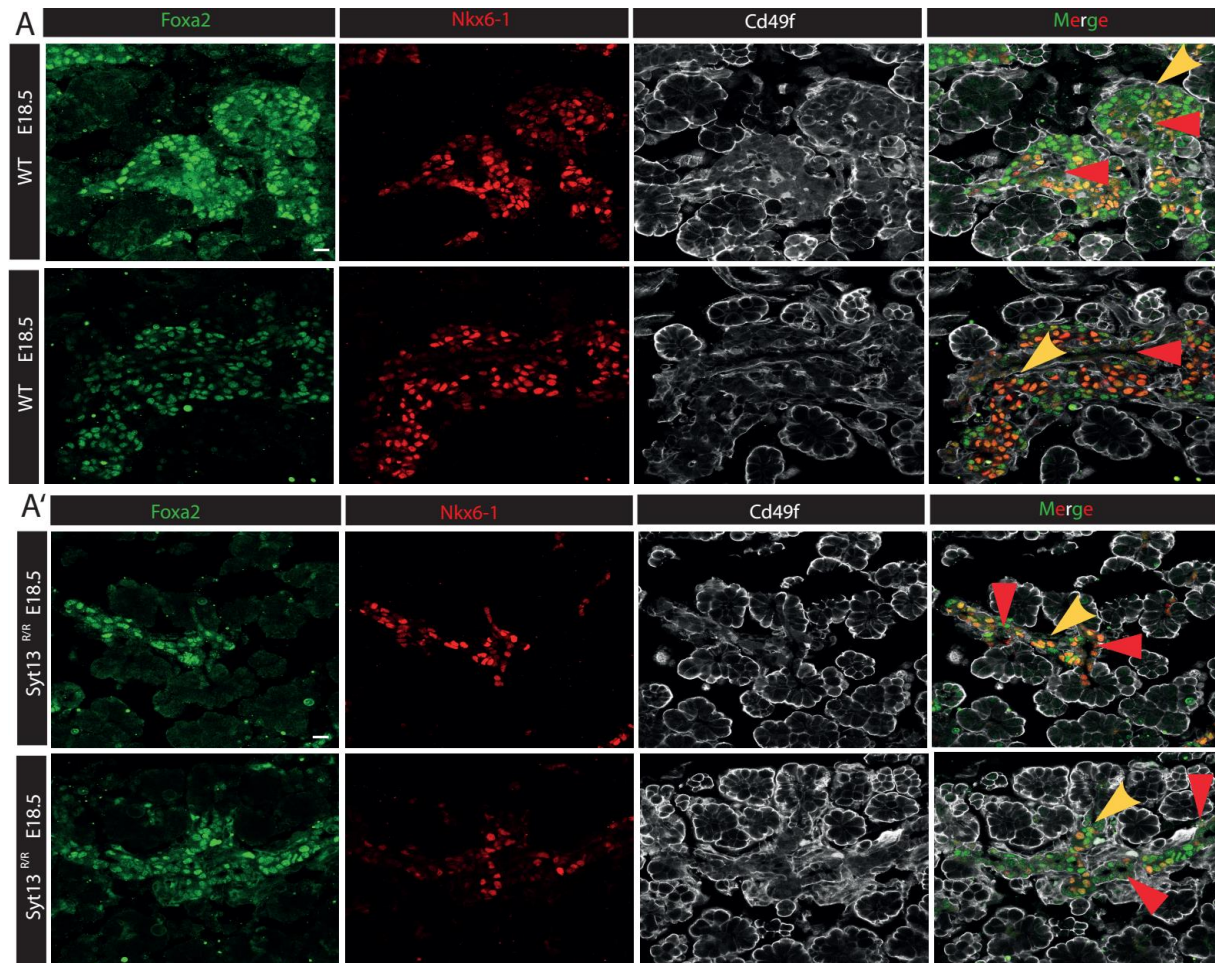


**Figure 3.42: The endocrine precursors fail to delaminate into the PE in *Syt13<sup>R/R</sup>* pancreata**

- (A) WT coronal sections at E18.5 and subsequent IHC of Foxa2 and Nkx6-1 characterizes the endocrine progenitors (Foxa2<sup>+</sup>Nkx6-1<sup>-</sup>Cd49f<sup>-</sup> yellow arrow) and precursor Islets of Langerhans (Foxa2<sup>+</sup>Nkx6-1<sup>+</sup>Cd49f<sup>-</sup> yellow arrow) after lineage segregation. The precursor Islets of Langerhans are aggregated into clusters in the PE (yellow arrow). The ductal and exocrine PE reflects Foxa2<sup>+</sup>Nkx6-1<sup>-</sup>Cd49f<sup>+</sup> expressing cells with AB polarity (basal Cd49f<sup>+</sup>), the endocrine compartment covalent regions (Cd49f<sup>-</sup>)
- (A') Pancreatic coronal sections at E18.5 of litter mate with the genotype *Syt13<sup>R/R</sup>* shows endocrine progenitors (Foxa2<sup>+</sup>Nkx6-1<sup>-</sup>Cd49f<sup>-</sup> yellow arrow) in close proxy to the duct endocrine progenitors (Foxa2<sup>+</sup>Nkx6-1<sup>-</sup>Cd49f<sup>+</sup> red arrow). The Foxa2<sup>+</sup>Nkx6-1<sup>-</sup>Cd49f<sup>-</sup> accumulate at the trunk region (Foxa2<sup>+</sup>Nkx6-1<sup>-</sup>Cd49f<sup>-</sup> yellow arrow), notably the Foxa2<sup>+</sup> cells are reflected in a higher quantity compared to Nkx6-1<sup>+</sup> cell population.

Scale is set for 10µm

Abbreviations: *Foxa2* = winged helix/forkhead box 2; *Foxa2*<sup>+</sup> = winged helix/forkhead box 2 positive; *Nkx6-1* = NK homeobox x 6-1; *Foxa2*<sup>-</sup> = winged helix/forkhead box 2 negative; ; *Nkx6-1*<sup>+</sup> = NK homeobox x 6-1 positive; ; *Nkx6-1*<sup>-</sup> = NK homeobox x 6-1 negative; *Cd49f* = *Itga6*; *Integrin alpha 6*; *Cd49f*<sup>+</sup> = *Itga6*; *Integrin alpha 6* positive; *Cd49f*<sup>-</sup> = *Itga6*; *Integrin alpha 6* negative; WT = wild type; E = embryonic stage; AB = apical-basal; *Syt13* = Synaptotagmin 13; R = *Rosa*; PE = pancreatic epithelium.

Thus, we were further interested if *Syt13* characterizes the endocrine progenitors (Carpino et al., 2016). Previous results suggest *Syt13*<sup>+</sup>*Ngn3*<sup>+</sup> progenitors segregate into endocrine precursors (*Nkx6-1*<sup>+</sup>), in particular the subpopulation *Syt13*<sup>high</sup>. In addition, subpopulations of *Ngn3* were identified at E14.5, *Ngn3*<sup>low</sup>*Syt13*<sup>low</sup> indicating the stratified ductal compartment (Figure 3.43, A' blue arrow), *Ngn3*<sup>high</sup>*Syt13*<sup>low</sup> indicating endocrine progenitor segregation (Figure 3.43, A' red arrow) and a *Ngn3*<sup>high</sup>*Syt13*<sup>high</sup> subpopulation (Figure 3.43, A' yellow arrow), likely illustrates delamination of the endocrine progenitor. Interestingly, subcellular localization of *Syt13* reflects discrepancies in the *Ngn3* subpopulation, in *Ngn3*<sup>low</sup>*Syt13*<sup>low</sup> cells cytoplasmic with apical accumulation, in the *Ngn3*<sup>high</sup>*Syt13*<sup>high</sup> expressing cell basal concentration of endogenous *Syt13* and in endocrine precursors cytoplasmic distribution (Figure 3.41. and 3.43, A' \*). Preliminary data suggests coherence of subcellular localization of *Syt13* to delamination and differentiation of endocrine progenitors into endocrine precursors. We hypothesize in the process of cell division as pre-existing cellular polarity is used to polarized cell fate determinants in a cell-autonomous fashion. During mitosis, cell fate determinants thereby segregate assymmetrically (Frydman and Spradling 2001; Fuller and Spradling 2007).

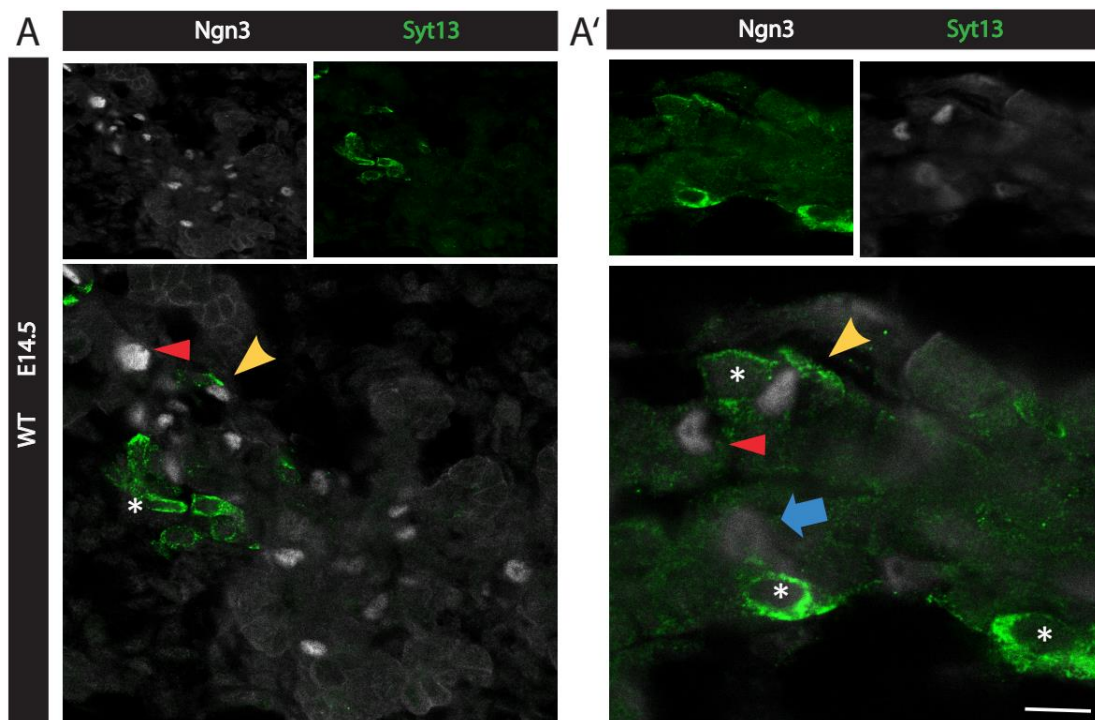


**Figure 3.43: Syt13 co-localizes to Ngn3 in the PE at E14.5**

- (A) IHC on coronal section of the WT at E14.5 with endocrine progenitor  $\text{Ngn3}^+$  and  $\text{Syt13}^+$  cells in the PE identified different subpopulations,  $\text{Ngn3}^{\text{high}}\text{Syt13}^{\text{low}}$  expressing cells (red arrow),  $\text{Ngn3}^{\text{low}}\text{Syt13}^{\text{low}}$  in the ductal region and a  $\text{Ngn3}^{\text{high}}\text{Syt13}^{\text{high}}$  subpopulation lining the outer edge of the ductal compartment. In addition,  $\text{Ngn3}^{\text{high}}\text{Syt13}^{\text{high}}$  cells suggests to be converted in endocrine precursors (\*).
- (A') Repetitive IHC on WT section and higher magnification into the region of interest illustrating  $\text{Ngn3}^{\text{high}}\text{Syt13}^{\text{low}}$  expressing cells (red arrow),  $\text{Ngn3}^{\text{low}}\text{Syt13}^{\text{low}}$  (blue arrow),  $\text{Ngn3}^{\text{high}}\text{Syt13}^{\text{high}}$  (yellow arrow) and  $\text{Ngn3}^{\text{high}}\text{Syt13}^{\text{high}}$  (\*). Thereby, unequal subcellular localization of Syt13 in the different subpopulations of randomly cytoplasmic (\*), basally constriction ( $\text{Ngn3}^{\text{high}}\text{Syt13}^{\text{high}}$ ) and apical ditribution suggest functional mechanism in vesicle trafficking and polarity establishment.

Scale is set on 100 $\mu\text{m}$

Abbreviations: Syt13 = Synaptoagmin 13; Ngn3 = Neurogenin 3; WT = wild type; IHC = immunohistochemistry; E = embryonic stage.

Summarized, Pdx1 illustrates co-localization to Foxa2 in the PE, in notion that Pdx1 is a downstream target of Foxa1 and Foxa2 (Gao et al., 2008). Syt13 shows co-localization to Pdx1 and Foxa2 at E13.5, highlighted by the fact that Pdx1, Foxa2 and Syt13 are strongly upregulated as endocrine precursors leave the ductal epithelium. Also, Syt13<sup>high</sup> co-localizes to some extent to the upregulated Ngn3 endocrine progenitor cell population in the mechanism of delamination and segregation into endocrine precursors. Thus, subcellular localization of Syt13 shifts from apical/cytoplasmic to basal. In line with these observations, in Syt13 deficient pancreata at E18.5, endocrine precursors fail to leave the ductal cord, emphasizing the role of Syt13 in the process of delamination.

### 3.4.9 Syt13 mutants show polarity defects

In the spheres-forming assay, we aimed to elucidate the underlying mechanism in which the gene Syt13 is involved. We isolated pancreata at E14.5 of different genotypes, generated single cell suspension using collagenase treatment and in subsequent tracing of the formerly single cells we observed after 2 days spheres-like structures (Figure 3. 44, A WT, DAY 1 and DAY 2 red arrow, Zoom indicates the sphere). These hollow spheres or cysts are characterized by formation of an central lumen (Galvez-Santisteban et al., 2012). Interestingly, in the spheres forming assay of the genotype Syt13<sup>GT/-</sup> the single cell of Day 0 (Syt13<sup>GT/-</sup>, red arrow) aggregate into a cluster of cells (DAY1, red arrow). At Day 2 the cluster increases in size, if cleavages or accumulation of cells appears remains unclear. However, spheres formation could only be observed once (Figure 3. 44, Syt13<sup>GT/-</sup> DAY 0 – DAY 2 red arrow and Zoom). Replicating results are obtained by capturing traced cells of the genotype Syt13<sup>GT/GT</sup> after 2 days

- contrary to the *WT*, cells cluster contiguously, indicating defects in initiation of a single lumen (Figure 3. 44, A *Syt13<sup>GT/GT</sup>*, DAY 0 – DAY 2 red arrow and Zoom).

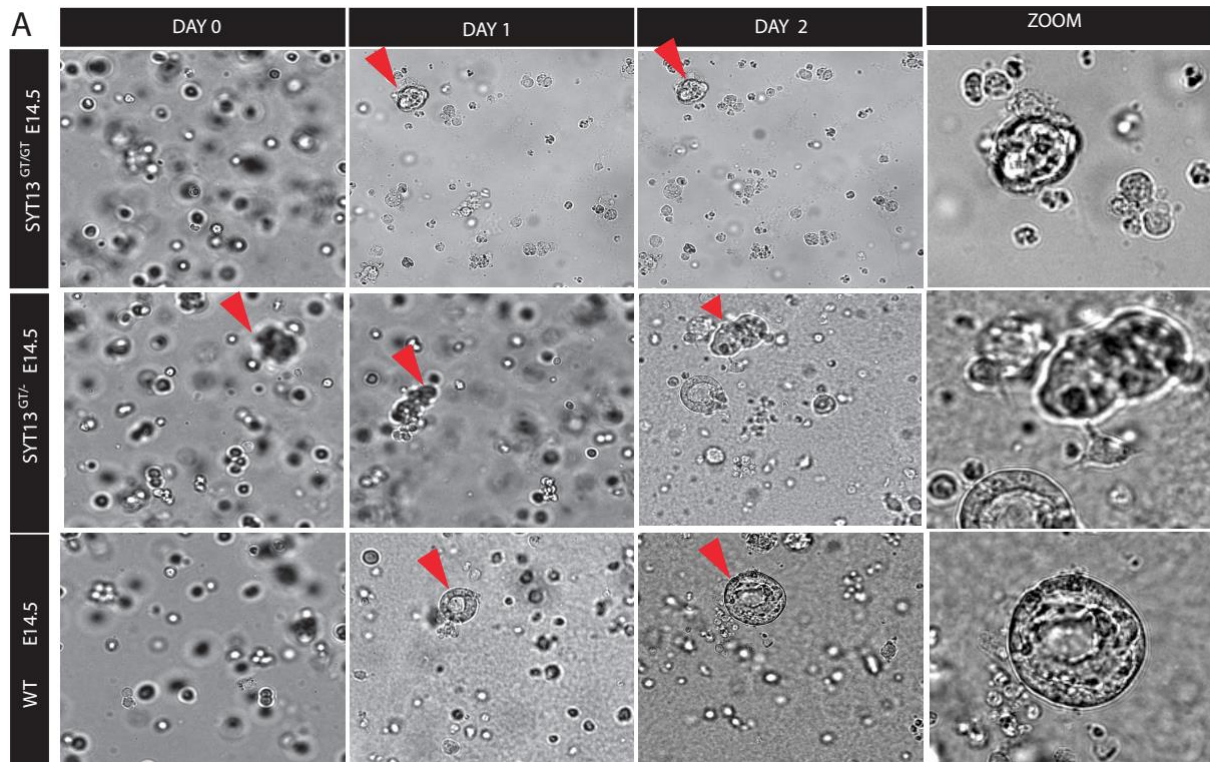


**Figure 3.44: Sphere-forming assay of the different genotypes *WT*, *Syt13<sup>GT/-</sup>* and *Syt13<sup>GT/G</sup>***

**(A)** Isolated and dissociated pancreata at E14.5 of the different genotypes *WT*, *Syt13<sup>GT/-</sup>* and *Syt13<sup>GT/GT</sup>* are analyzed by their sphere-forming activity in the Matrigel-containing culture. The single cells were traced from time point 0 (DAY 0) (red arrow) for 2 days and at last for the region of interest images are acquired in a higher magnification.

Abbreviations: WT = wild type; E = embryonic stage; Syt13 = Synaptotagmin 13; GT = gene trap.

Similar results are obtained in adjacent experiments – in the *WT*, the sphere-forming assay illustrate spheres as round shaped structures including a hollow inside, indicating polarity establishment of the MPP at E14.5 (Figure 3. 44, B *WT*, DAY0 – DAY2 red arrow). It is to note that we observed secreting cells at the surface of the traced sphere (Figure 3. 44, B *WT*, DAY2 red arrow and ZOOM \*). In addition, single cells of the PE suggest to migrate and cluster, though lumen initiation failed as the cluster remains aggregated (Figure 3. 44, B *Syt13<sup>GT/GT</sup>*, DAY0 – DAY2 red arrow and ZOOM). Thus, *Syt13* suggest to be expressed in the PE at E14.5, indicating subpopulations as *Syt13<sup>high</sup>* and *Syt13<sup>low</sup>* in the secondary transition of pancreas organogenesis.

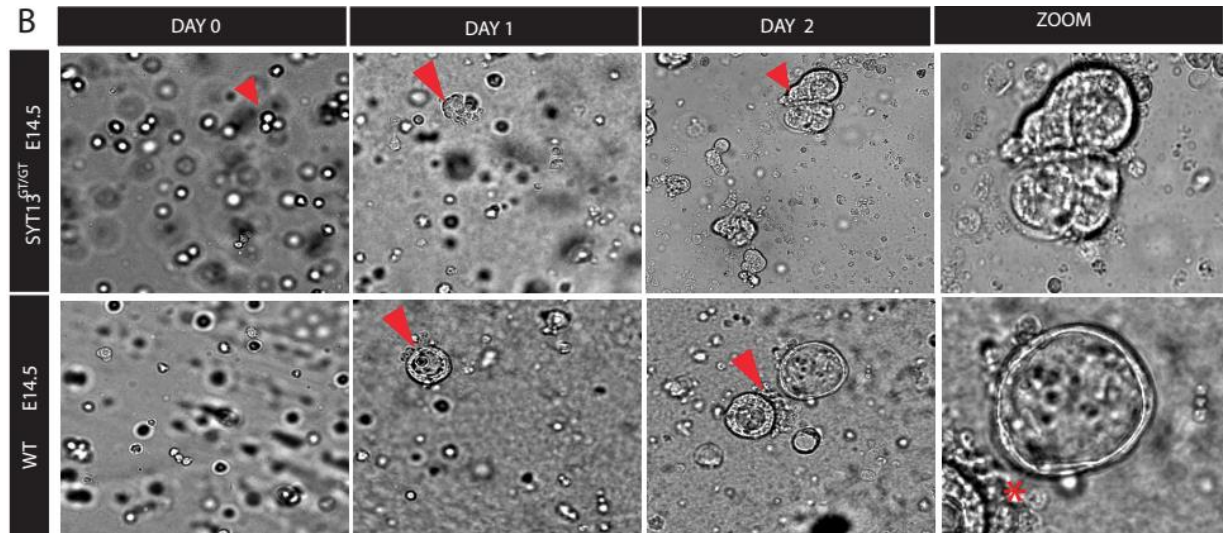


**Figure 3.44: Sphere-forming assay of the different genotypes *WT*, *Syt13<sup>GT/-</sup>* and *Syt13<sup>GT/G</sup>***

**(B)** Single cell suspension was accomplished of isolated pancreata at E14.5 of *WT* and *Syt13<sup>GT/GT</sup>*. Both genotypes illustrate spheres-forming activity and are analyzed by their sphere-forming activity in the Matrigel®-seeded cells. The single cells were traced from time point 0 (DAY 0) (red arrow) for 2 days (DAY 2) and at last for the region of interest images are acquired in a higher magnification (ZOOM).

Abbreviations: WT = wild type; E = embryonic stage; Syt13 = Synaptotagmin 13; GT = gene trap; © = incorporated.

We then examined the morphology of the pancreas at the stage of 2 month (m) in the *WT* compared to *Syt13<sup>GT/-</sup>*, strikingly the PE in *Syt13<sup>GT/-</sup>* mice had abnormal cluster of nuclei, unlike the even distribution of the nuclei in rosette-like structures in the PE of the *WT*. The cells change their intracellular organization relative to the capillaries (Figure 3. 45, A-A' \*), thus implicating vesicular trafficking defects in the PE of *Syt13<sup>GT/-</sup>*. Taken preliminary data, *Syt13* suggest to be expressed within the PE at the indicated stage E14.5 (Figure 3.45) with a defined subpopulation of *Syt13<sup>low</sup>*, contrary the *Syt13<sup>high</sup>* cell pool characterizes endocrine precursors and the  $\beta$ -cells (*Ins<sup>+</sup>*) in the precursor Islets of Langerhans (section 3.4.5 – 3.4.6). Moreover, we suggest a role of *Syt13<sup>+</sup>* in differentiation into  $\alpha$ -cells concerning co-expression of *Syt13<sup>high</sup>* and *FVF<sup>high</sup>*. Thus, in a next step, subcellular localization of endogenous *Syt13* in the PE in line with observations in tubulogenesis during pancreas organogenesis was determined in regard to molecular mechanism of the novel pancreatic gene.

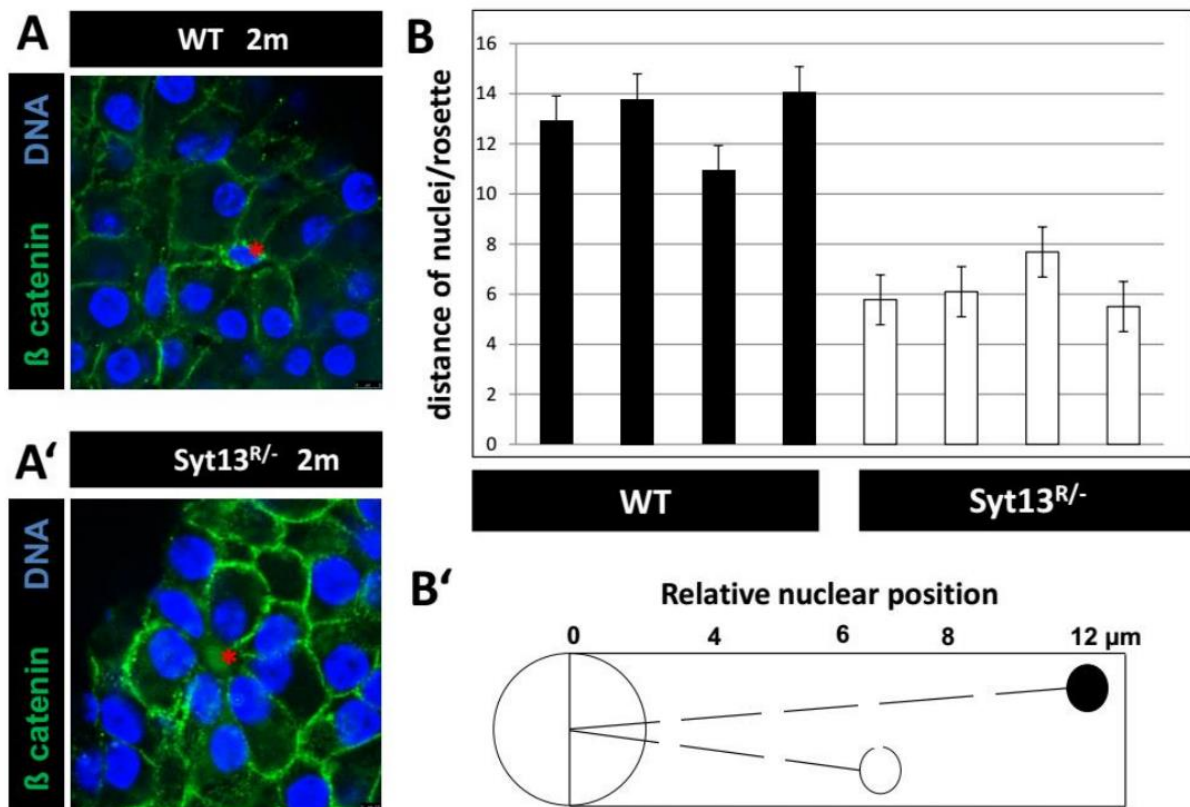


**Figure 3.45: Cell Polarity is altered in the PE of *Syt13* deficient mice.**

- (A) IHC on coronal sections of the PE of 2 m old pancreata highlighting rosette-like structures surrounding capillaries (\*). DNA is highlighted in DAPI, the PE by IHC on  $\beta$ -catenin either on WT coronal sections or *Syt13*<sup>R/-</sup>.
- (B) The position of the nucleus in the rosette-like structures cells was determined relative to the center of rosettes. Black, WT; White *Syt13*<sup>GT/-</sup>; one bar represent a rosette-like structure with calculated standard deviation (SD).
- (B') The relative nuclear position in the PE of *Syt13*<sup>GT/-</sup> is altered, nuclei are shifted to the center of the rosette-like structures. Analysis was performed on the same values as in (B).

Abbreviations: DAPI = 4',6-Diamidin-2-phenylindol, Syt13 = Synaptotagmin 13; R = Rosa; PE = pancreatic epithelium; m = month; WT = wild type; SD = standard deviation; IHC = immunohistochemistry; DNA = desoxy ribo nucleine acid.

In pancreatic morphogenesis, cytodifferentiation of the MPP in the PE initiates trunk, respective primary lumen (PL) formation. The monolayered epithelial sheet remodels to a multilayer PE in line with segregation into the different lineages (Villasenor et al. 2010). Hence, we confirmed the *Syt13*<sup>+</sup> PE at E12.5, indicating that *Syt13* characterizes the MPP in commence of the secondary transition (Figure 3. 46, A). In addition, we identified subcellular localization of *Syt13* at the apical side, which suggests polarization of the PE and formation of the PL already at E12.5 (Figure 3. 4, A yellow arrow) (Kesavan et al., 2009; Villasenor et al., 2010). In a next step, we identified at E14.5 in the *WT*, monolayered

rosette-like structures, characterized by a central apical lumen (Ezrin<sup>+</sup>) and basal orientated nuclei (Cdf49f<sup>+</sup>). Interestingly, previous results are confirmed for the genotype *Syt13<sup>R/R</sup>*. The coordinated polarized vesicle trafficking and cell division implicates to be altered as we observed a multilayered PE (Martin-Belmonte and Perez-Moreno 2011). AB polarity appears to be established to some extent, however nuclei in the rosette-like structures are randomly distributed and even suggest to be multinucleated (Figure 3.46, B *Syt13<sup>R/R</sup>*). Furthermore, we observed asymmetric cell division in the *Syt13<sup>R/R</sup>*, as the division plane appears orthogonal (Figure 3. 46, B *Syt13<sup>R/R</sup>* \*) contrary to the planar spindle orientation (3. 46, B *Syt13<sup>R/R</sup>* \*\*) (Lechler and Fuchs 2005). Thus, deficiency in Syt13 might affect on a cellular level the vesicular trafficking machinery and polarity establishment of the PL, further insights into the subcellular localization of Syt13 was performed by secondary raster electron microscopy (SEM) analysis.

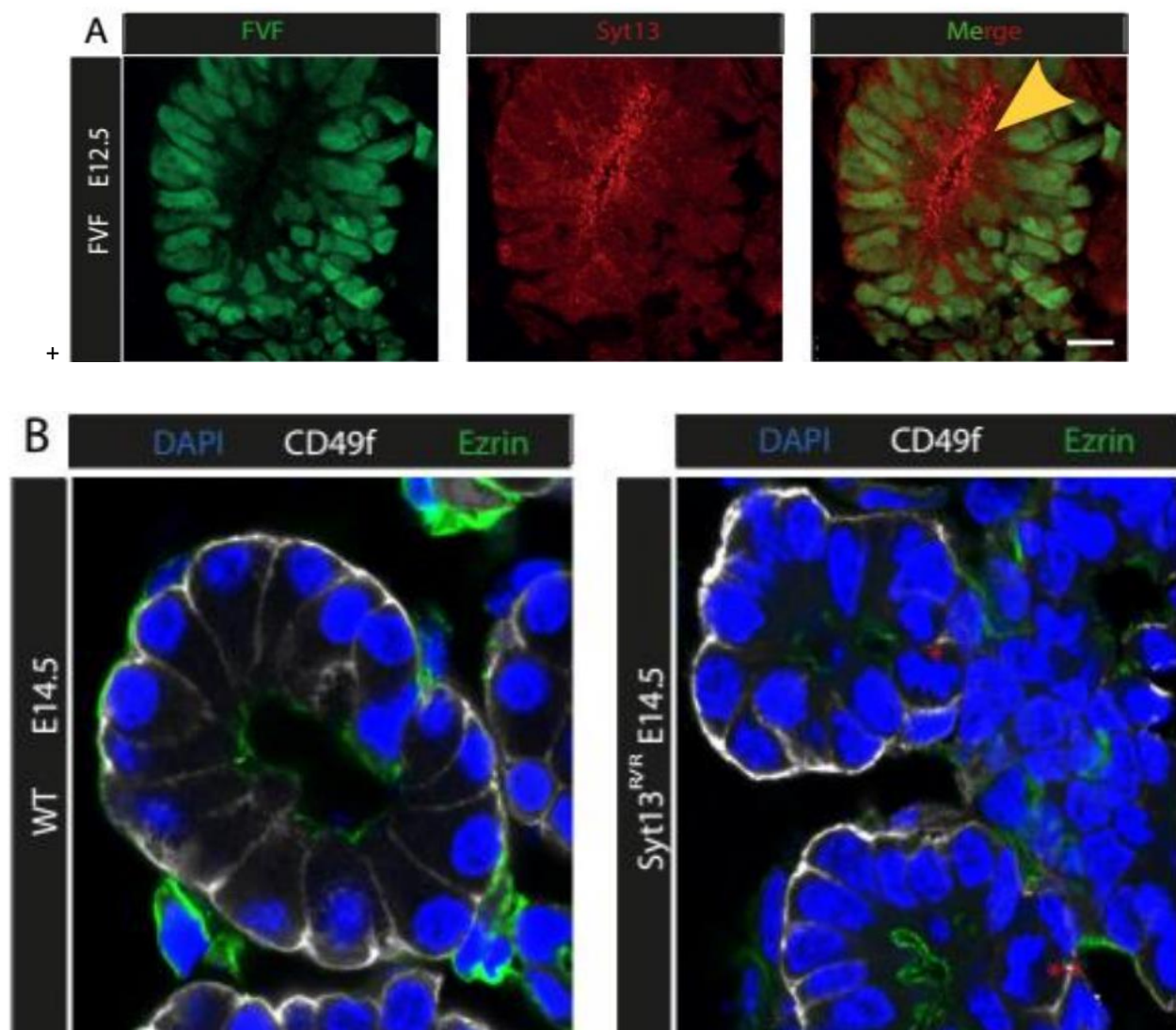


Figure 3.46: *Syt13* is expressed in the MPP with multinucleated rosette-like structures in the PE at E14.5

- (A)** IHC on coronal pancreatic sections at E12.5 identified apical localization of endogenous Syt13 in the PE (yellow arrow). FVF characterizes the PE including basal orientated nuclei, Syt13 indicates the PL at the apical surface.
- (B)** The *WT* at E14.5 illustrates a monolayered sheet with rosette-like structures, the nuclei (DAPI) basally located (Cd49f<sup>+</sup>) and lumen initiation at the apical membrane (Ezrin<sup>+</sup>). Contrary, *Syt13<sup>R/R</sup>* mutants exhibit a multilayered PE at E14.5. The Cd49f<sup>+</sup> basal and apical Ezrin<sup>+</sup> surface in the rosette-like structures are established, however polarity cues to be altered. Also, nuclei within the rosette-like structures divide perpendicular to the division plane (indicated with \*) and on a planar division mode (\*\*).

Scale is set for 10µm

Abbreviations: DAPI = 4',6-Diamidin-2-phenylindol, Syt13 = Synaptotagmin 13; R = Rosa; PE = pancreatic epithelium; WT = wild type; IHC = immunohistochemistry; Cd49f = (Itga6; Integrin alpha 6); E = embryonic stage; FVF<sup>+</sup> = Foxa2-Venus-Fusion positive; FVF<sup>-</sup> = Foxa2-Venus-Fusion negative; PL = primary lumen.

In line with previous results, SEM analysis illustrated shortened zonula adherens in the *Syt13<sup>R/R</sup>* pancreatic sample compared to the *WT* (accomplished by Dr. M. Aichler and Prof. Dr. A. Walch). The TJ, respective AB polarity appears to be established however not continuous and maintained (Figure 3.47, A yellow arrow). Furthermore, the *WT* represents a monolayered epithelial sheet including distinct cell-cell boundaries, indicating polarization within the PE and thus spatio-temporally controlled cell proliferation (Martin-Belmonte et al., 2008; Shih et al., 2013) (Figure 3. 47, A yellow arrow). The AB polarity is illustrated by basal located nuclei and apical distributed mitochondria (Figure 3. 47, B *WT*). Notably, the mitochondria in the region of interest are mainly in the cristae type (Figure 3. 47, B *WT* \*). Contrary, the SEM section of the genotype *Syt13<sup>R/R</sup>* shows randomly distributed nuclei and mitochondria (Figure 3. 47, B *Syt13<sup>R/R</sup>* \*). The larger diameter between L and BM and intermittent membranes (Figure 3. 47, B *Syt13<sup>R/R</sup>* yellow arrows), indicating a multilayered lumen and thus impairment in lumen formation, illustrated by the smaller L. Previously published by Sato et al., the initial step in lumen formation implicates the formation of the apical membrane surface. The polarity complexes will be recruited to the JAM, respective TJ (Sato et al. 2007). From the results already discussed, we assume that the endocytotic vesicle transport towards apical membrane surfaces is impaired and therefore establishment of AB polarity in the PE impeded.

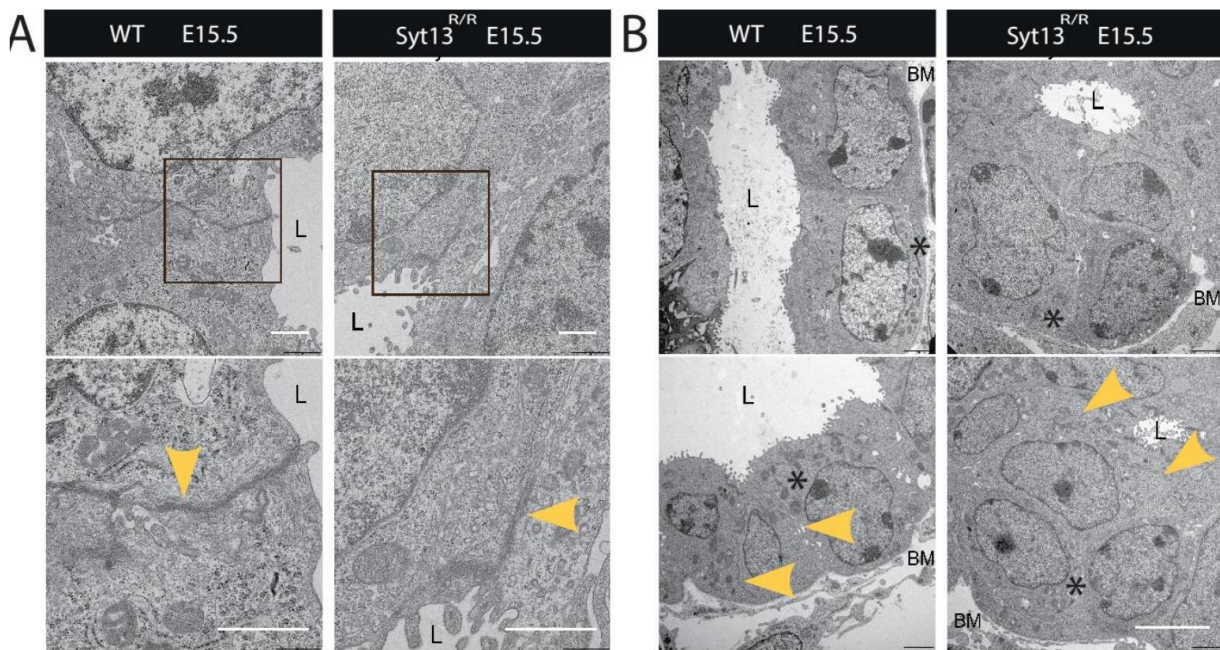


**Figure 3.47: *Syt13* deficiency results in a multinucleated PE and affects AB polarity**

- (A)** SEM images in the PE at E15.5 of pancreatic sections at TJ, respective zonula adherens (ZA) in the WT illustrates continuous boundary between the neighboring cells. Indicated region in the box is highlighted below (yellow arrow), Lumen (L) marked by L. Contrary, the *Syt13*<sup>R/R</sup> shows truncated ZA and shortened L.
- (B)** The WT reflects continuous L, junctional complexes separate the cells from each other in the PE at E15.5 (yellow arrow) and nuclei are located basally at the BM in a monolayer. In addition, mitochondria are represented as cristae proxy to the basal cell surface (\*). The genotype *Syt13*<sup>R/R</sup> is characterized through shortened L at E15.5, cell-cell boundaries are discontinuous (yellow arrow). The nuclei and mitochondria are randomly distributed within the cells with mitochondria represented by saculus and cristae type (\*).

Scale unknown

Abbreviations: L = lumen; WT = wild type, *Syt13* = Synaptotagmin 13; R = Rosa; ZA = zonula adherens; PE = pancreatic epithelium; E = embryonic stage; SEM = secondary raster electron microscopy; TJ = tight junctions; BM = basement membrane.

Taken together, we could observe polarity defects in *Syt13* mutants, indicating that *Syt13* is expressed in the PE at E14.5. Further mining on function and mechanism will reveal the role of *Syt13* in the PE, respective in endocrine lineage segregation.

## 4. Discussion

### 4.1 FVF marks the multipotent progenitors in the pancreas

The advantage of the *Foxa<sup>Venus</sup>* (FVF) mouse line represent our GRN of the pancreas in the secondary transition. Data was obtained for the MPP in the PE, respective the *FVF<sup>+</sup>* cell compartment. In the secondary transition the lineages segregate in the PE, therefore we characterized the MPP if a niche is maintaining the MPP characteristics (Pan and Wright, 2011). Remarkably, subpopulations of MPP in the PE were identified, represented by different protein levels stated as *FVF<sup>high</sup>* and *FVF<sup>low</sup>*. In the bi-potent trunk pattern in the PE in the secondary transition, the *FVF<sup>high</sup>* subpopulation indicates lineage commitment of the endocrine lineage, highlighted by the fact of *FVF<sup>high</sup>Nkx6-1<sup>+</sup>Pax6<sup>+</sup>Ecad<sup>-</sup>* expressing cells. Contrary, the *FVF<sup>low</sup>Sox9<sup>+</sup>HNF1 $\beta$ <sup>+</sup>Cpa1<sup>+</sup>* indicates exocrine, respective ductal fate of the lineage determined cells. The marker onset implicates for *Foxa2* a major role as the MPP segregates into the different lineages in the secondary transition. Remarkably, *Foxa2* protein levels correlates to the *Pdx1<sup>+</sup>* PE between E12.5-E15.5, which references to *Foxa2* as a upstream regulator of *Pdx1* and key factor in pancreas organogenesis (Gao et al., 2007; Burtscher et al. 2013; Scarce et al. 2002). We made the observation, that after E15.5 *FVF<sup>high</sup>* characterizes the *Gcg<sup>+</sup>* cells, whereas *Pdx1<sup>high</sup>* the *Ins<sup>+</sup>* cell pool, respective  $\alpha$ - and  $\beta$ -cells in the precursor and adult Islets of Langerhans. Thus, the FVF mice is a valuable tool for dissecting the marker onset in the lineage segregation phase of pancreas organogenesis and maturation into adult Islets of Langerhans. We suggest sorting of the different subpopulations of FVF in the PE at E14.5, improving de-differentiation protocols and mimicking *in vivo* conditions in *in vitro* models. Also,  $\alpha$ -cells in the adult Islets of Langerhans are shown to be converted in  $\beta$ -cells (Ng et al. 2014) emphasizing the role of *Foxa2* for  $\beta$ -cells neogenesis. In summary, the FVF mouse line is a good tool for live-imaging of pancreas lineage segregation and maturation of the Islets of Langerhans in addition to the improvement of de-differentiation protocols.

### 4.2 The FVF mouse line is a valuable tool for genome wide expression profiles

Pancreas lineage commitment is not well understood, mainly the TF hierarchy is described in the context of Gain/Loss of function, whereas complex tissue interactions and signaling via the mesenchyme remains elusive. In the transcriptome profile, we separated non-endodermal and the endodermal compartments of the pancreas in the secondary transition between E12.5-E15.5. The main purpose was improving the understanding of neighboring tissue interactions, metabolic

pathways and lineage determining factors in the steps of lineage segregation. As expected, we identified in the ongoing secondary transition an increasing rate of differentially regulated genes between both tissue compartments. Thus, the expression profile was inspected for metabolic pathways, key transcription factors as MODY, signaling and growth factors. Furthermore, pathway analysis reflected the relationship between mid-hindbrain boundary and axon guidance for endocrine progenitors, indicating a conserved mechanism for neuro-endocrine cells (Van Arensbergen et al. 2010; Schwartz et al. 2013). We suggest a role in coordinated cell autonomous asymmetry and tubulogenesis in the cell-fate decisions during organogenesis (Kesavan et al. 2009). Additionally, we clustered for ECM, focal adhesions, AJTJ, regulation of actin cytoskeleton and Calcium signaling pathways. Our results indicate remodeling of polarity complexes in the PE in line with lineage segregation of the cells. Apparently, the non-endodermal compartment seems to be more stable due to a lesser account of variation in the pathways mentioned above (Willmann et al., 2015). In addition, MODY and T2D already appears as early as E12.5 in the PE, implicating congenital diseases. Thus, *Foxa2* deficiency might affect Insulin, respective Glucagon secretion. As *Foxa2* is expressed in the node, common endoderm progenitors during gastrulation as *Sox17* are likely to be expressed in the pancreas (Burtscher et al., 2009; Burtscher et al. 2013; Engert et al. 2013). Although, *Sox17* suggests a role in insulin trafficking and secretion in  $\beta$ -cells of normal and pathologic mouse models (Jonatan et al. 2014). Recently, Odom *et al.* combined chromatin immunoprecipitation assays (ChIP) with promoter microarrays for the identification of the transcriptional regulatory network of *HNF1 $\alpha$* , *HNF4 $\alpha$* , and *HNF6* in liver and pancreatic tissue of the Islets of Langerhans (Odom et al. 2004). The results implicate that misregulation of *HNF4 $\alpha$*  may contribute to late onset of T2D. The core members of the endodermal program as *HNF1 $\alpha$*  (*Foxa1*), *Foxa2* (*HNF3 $\beta$* ), *HNF1 $\beta$*  (*Tcf2*), *HNF6* (*Onecut1*) and *Gata4* are assigned to the MPP in pancreas organogenesis at E12.5-E15.5. *Foxa2* is a speculative MODY gene, as MODY1, MODY3 and MODY5 are determined by mutations in *HNF1 $\alpha$* , *HNF1 $\beta$*  and *HNF4 $\alpha$* . Interestingly, *Foxa2* controls expression of *HNF1 $\alpha$*  and *HNF4 $\alpha$*  and *Foxa2* itself is induced by activation of phosphatidylinositol 3-kinase-Akt through insulin (Wolfrum et al. 2003). As Akt/protein kinase B might be involved in  $\beta$ -cell proliferation and insulin secretion this may point out the importance of *Foxa2* in the pancreatic  $\beta$ -cells maturation (Kulkarni 2002; Jhala et al. 2003). In addition, *HNF1 $\alpha$*  and *Foxa2* act upstream in regulatory domains of the *Pdx1* gene, implicating that pancreas induction is initiated through *HNF1 $\alpha$* /*Foxa2* (Gao et al. 2008). Smukler et al. lately identified pancreatic-derived multipotent precursor (PMP) in human adult Islets of Langerhans. The PMP are *Ins*<sup>+</sup>, combined to *Pdx1*<sup>+</sup> and *Foxa2*<sup>+</sup> expression. This might be interesting in aspects of a 'stem cell niche' and thereby a cell progenitor pool for  $\beta$ -cell neogenesis (Seaberg et al. 2004; Smukler et al. 2011). Further expression profiling in the adult Islets of Langerhans will shed light on the importance of *Foxa2* as a factor in  $\alpha$ - and  $\beta$ -cell de-differentiation and maturation (Murtaugh and Kopinke 2008; Murtaugh 2007; Murtaugh 2011).

### 4.3 Molecular pathways guiding pancreas organogenesis

Growing evidence suggest that the miR pathways are important in embryonic development and pancreas organogenesis. *Dicer1*, the enzyme that generates miRs is essential for normal pancreatic development, Pdx1 Cre mediated deletion of *Dicer1* exhibits impaired Islet of Langerhans genesis with a dramatic reduction of Ngn3<sup>+</sup> endocrine progenitors at E15.5. In line with endocrine defects, expression of the Notch signaling target gene *hairy and enhancer of split 1 (Hes1)* increases. Thus, implying that *Hes1* is a direct target gene of miR-23a in the developing pancreas or miR targets several Notch pathway components upstream of *Hes1*, facilitation thereby *Hes1* transcription (Lynn et al., 2007). Overexpression of miR-7 in  $\beta$ -cells show defects in insulin secretion in glucose-stimulated insulin secretion (GSIS) experiments and miR-7 deficient mice impairment in SNARE complex fusion and exocytosis (Latreille et al., 2014). Also, miR -19b and miR -18a have been shown to directly target the 3'UTR of *NeuroD1* and *Ptf1a*, thus affecting all the lineages in the adult pancreas (Zhang et al., 2011; Yang et al., 2012). The miR -15, miR -15b, miR -16 and miR -195 are upregulated in neo-Islets of Langerhans and potentially bind to *Ngn3*, implying regulation of endocrine lineage segregation in pancreas development and regeneration of  $\beta$ -cells in the adult Islets of Langerhans (Bonner-Weir et al., 1993; Joglekar et al., 2007). Previous results highlight that miRs are critical regulators of pathways underlying the pathophysiology of T2D, thus the GRN in the secondary transition may reflect miRs which negatively regulate gene expression at the post-transcriptional level causing T2D.

Various studies have shown the significant role of Notch signaling in pancreas organogenesis and lateral inhibition of Notch signaling in pancreatic progenitor differentiation and maintenance (Apelqvist et al., 1999; Horn et al., 2012; Cras-Meneur et al., 2009; Pan and Wright, 2011). The lateral inhibition model describes endocrine lineage segregation by Ngn3<sup>+</sup> cells and activation of Delta, a Notch ligand. In a next step, binding of Delta to Notch receptors in neighboring cells leads to the initiation of the Notch signaling cascade and release of the NICD (Notch intracellular domain). Subsequently, the NCID translocates into the nucleus to activate the target gene *Hes1*, which inhibits expression of *Ngn3* (Qu et al., 2013). Thus, repression of the Notch signaling pathway accelerates the endocrine progenitor Ngn3<sup>+</sup> cell pool (Fujikura et al., 2006; Zecchin et al., 2007). Contrary, Ptf1 $\alpha$ -mediated control of *Delta like 1 (Dll1)* promotes endocrine lineage segregation by an increase of Ngn3<sup>+</sup> cells and expression of upstream regulator of *Ngn3*, *Sox9*, is induced by Notch signaling (Ahnfelt-Ronne et al., 2012; Shih et al., 2012; Seymour et al., 2008; Seymour et al., 2014). In addition, Afelik et al., demonstrated that Notch-dependent activation of *Nkx6-1* by direct binding of *Rbp-j* to the proximal promoter is essential for ductal and endocrine lineage segregation (Afelik et al., 2013). Therefore,

dissecting Notch pathway components in the GRN of the secondary transition in pancreas organogenesis might be a good tool for deciphering the impact of Notch on the MPP characteristics in the PE and endocrine cell fate decision.

The Notch and Wnt signaling pathways are essential in the direct differentiation of embryonic stem cells into specific adult organs. In pancreas organogenesis, Wnt pathway components inhibit pancreas initiation, whereas Wnt signaling is required for proliferation of the PE (Baumgartner et al., 2013). The Wnt effector gene *TCF7L2*, also known as *Tcf4*, has been recently reported in GWAS studies as a locus for T2D (Migliorini and Lickert 2015; Migliorini et al., 2014). Thereby, the Wnt/ $\beta$ -catenin pathway and components suggest to be upregulated in T2D patients (Lee et al. 2008). In line with previous results, Wnt signaling implicates to be involved in GSIS in the  $\beta$ -cells of the adult Islets of Langerhans in mice. The Wnt co-receptor, lipoprotein receptor-related protein 5 (LRP5) stimulates GSIS through Wnt3a and Wnt5a via crosstalk to PI3K/AKT signaling (Gui et al., 2013; Fujino et al., 2003). Contrary, in pancreata of  *$\beta$ -catenin<sup>-/-</sup>* mice almost a complete loss of the acinar cell compartment was observed, pointing to the comprehensive role of Wnt pathway components not only in endocrine lineage segregation (Baumgartner et al., 2014). Also, ectopic expression in the pancreas at the late E18.5 induces proliferation and results in an enlarged organ size (Heiser et al., 2004). Lately reported by Tian et al., the blockade of Notch component derepresses the Wnt signaling pathway in intestinal stem cells, as well as in a subset of ductal cells in the pancreas, hypothesized to be the pancreatic stem cell compartment (Tian et al., 2015; Belo et al., 2013). Thus, *Dvl2* as an activator of the Wnt signaling pathway directly inhibits Notch signaling by binding to the C-terminus of the Notch-Delta-receptor (Collu et al., 1996). The antagonistic crosstalk of Notch and Wnt is conserved in vertebrates likely due to the fact that *Dvl2* in the Wnt/PCP, respective *Rbp-j* in Notch are core pathway members. Taken the previous results in account, the GRN of the *FVF<sup>+</sup>* cell compartment suggests to obtain transcriptional profiling of the Wnt/Notch family members in the PE in the different E of the secondary transition and thereby expose the convergence of the signaling pathways in pancreas organogenesis.

The signaling cascade in the secondary transition involves FGF, mainly as paracrine factor in the surrounding mesenchyme of the growing pancreas. Landmark studies by Golosow and Grobstein showed that the pancreatic bud 'stripped of' from the mesenchyme fails to proliferate (Golosow et al., 1962). Recent studies highlight the epitheliomesenchymal interactions, the default state of the PE is the lineage segregation into endocrine cells whereas the mesenchyme induces segregation of the exocrine lineage in the PE via an inductive signaling cascade (Gittes et al., 1996; Miralles et al., 1998). Thereby, *Fgf10<sup>-/-</sup>* embryos show a reduced PE, marked by a *Pdx1<sup>+</sup>* cell pool along with perturbed differentiations and morphogenesis (Sudheer et al., 2001). Vice versa, persistent expression of *Fgf10* in the PE stimulates proliferation and affects the Notch-mediated lateral inhibition pathway (Hart et

al., 2003). Thus, *Fgf10* is crucial for maintaining expression of *Sox9*, the upstream regulator of endocrine progenitors (Seymour et al., 2007; Seymour et al., 2012; Seymour et al., 2014). However, the GRN illustrated FGF signaling pathway components peaking in at E15.5 in the PE (*Fgf15*, *Fgf20*, *Fgf23*, *Fgf8*, *Fgf6*), pointing to a more complex signaling cascade as previously described (Willmann et al., 2015). We suggest the detailed register of the FGF pathway components in the *FVF*<sup>+</sup>, respective *FVF*<sup>-</sup> cell compartment for specifying epitheliomesenchymal interactions, in line with Notch and Wnt signaling components. Thus, an illustrated landscape of the signaling pathways in the secondary transition of the pancreas will improve the understanding of tissue interactions and lineage segregation.

#### 4.4 The pancreas gene selection for known and unfamiliar genes

As an additional benefit of the GRN, functionally described and yet not functionally described genes in pancreas organogenesis were selected. In particular, we aimed to select functionally not described genes, to establish mouse models associated with pancreas-related diseases as T1D/ T2D, cancer and cystic fibrosis.

The use of the digital database GenePaint.org provided us with *in silico in situ* expression pattern. GenePaint.org serves as a rich resource for expression profiles of known and unknown transcripts. Therefore, expression pattern of the *in silico in situs* were inspected on whole mount embryos at E14.5, zooming into the pancreatic region determined the more specific expression pattern in the pancreas, respective surrounding mesenchyme. The *in situs* of the digital database Genepaint.org originated from different backgrounds as C57BL/6 and NMRI which did not affect the expression pattern. The database itself is a rich resource as it offered only for 11% out of the 884 gene no expression pattern at the specific time point E14.5. Temporal and spatial analyses in the secondary transition of the selected genes already suggested for a majority, a role in pancreas organogenesis due to clear detectable pattern in the pancreatic region. The Affymetrix® expression profile confirmed the probe sets of the selected genes even between E12.5 – E15.5 and highlighted the transcriptional regulation. To a minor extend, genes illustrating epithelial *in situ* patterns were progressively detected in the non-endodermal GRN. Concerning the pattern exclusively at E14.5 contrary to expression profiling between E12.5-E15.5 and statistical analysis might reflect the error rate.

In a next step, pancreatic *in situ* patterns of representative genes were classified into specific expression patterns termed as tip, epithelium/trunk and mesenchyme, respective the exocrine progenitors, MPP and endocrine progenitors and the surrounding tissue of the pancreas. Thus, the

novel pancreatic candidate genes *Grb7* represents likely the MPP in the PE at E14.5 including a *Foxa2<sup>+</sup>Pdx1<sup>+</sup>Grb7<sup>+</sup>* hybridization pattern. Recently, expressed sequence tag (EST) library screening already identified pancreatic expression with indicated role in insulin secretion as a member of the Grb-IR/Grb-10/Grb7/Grb14 family (Frantz et al., 1997). It may be speculative, if *Grb7* is co-expressed in *Foxa2<sup>+</sup>* cells in embryogenesis, further localization studies will determine the function and mechanism of *Grb7*. In addition, the gene *Vwa5b2* reflects an epithelial hybridization pattern exclusively in the PE at E14.5, pointing to a specific role in pancreas organogenesis. Thus, the MPP at E14.5 suggest to be characterized by *FVF<sup>low</sup>Grb7<sup>+</sup>Vwa5b2<sup>+</sup>* in the PE. Furthermore, we identified several Riken clones (*1700011H14Rik*, *5330417C22Rik*, *1700086L119Rik*) functionally not described. The gene *5330417C22Rik* suggests to have a Mannose-6-phosphate receptor binding and a Growth factor receptor cysteine-rich domain ([www.informatics.jax.org](http://www.informatics.jax.org)), which might implicate a novel receptor isoform in the family of insulin receptor (Hernandez-Sanchez et al., 2008; Raducanu et al., unpublished). Currently, we are analyzing the gene *1810019J16Rik*, respective *keratinocyte differentiation factor 1 (Kdf1)* in pancreas organogenesis. Preliminary results already highlight endocrine lineage segregation in the PE and  $\beta$ -cell co-localization in the adult Islets of Langerhans of *1810019J16Rik<sup>GT/</sup>* mice (Engert et al., unpublished).

Temporal and spatial expression of the classical tip hybridization pattern exhibited the functionally not described gene *2210010C04Rik*, thus implying bi-potent pancreatic progenitors expressing *2210010C04Rik<sup>+</sup> FVF<sup>low</sup>Cpa1<sup>+</sup>Sox9<sup>+</sup>* (Zhou et al., 2007; Pin et al., 2001). Also, *Slc38a3*, *Rbm47*, *Cldn10* illustrate a pattern referred as tip, indicating a *Slc38a3<sup>+</sup>Rbm47<sup>+</sup>Cldn10<sup>+</sup>2210010C04Rik<sup>+</sup> FVF<sup>low</sup>Cpa1<sup>+</sup>Sox9<sup>+</sup>* subpopulation in the PE at E14.5.

Finally, the 'mesenchymal' hybridization pattern suggests to be characterized by the genes *Syt6*, *Tenc1*, *Il11ra2* and *SrpX2*. Tang and colleagues described the role of *SRPX2* in tumor progression and metastasis. Thus, *SRPX2* serves as a biomarker for Glioblastoma (GBM) associated with fatal perspectives for the affected patients. The gene itself suggests to enhance EMT via the MAPK cascade as it is not classified to the classical EMT players likely due to the fact that *SRPX2<sup>-/-</sup>* GBM cells are still capable of cell invasion and migration (Tang et al., 2015). Interestingly, EMT in pancreas organogenesis is predominantly described in the context of endocrine lineage segregation in the PE (Rukstalis et al., 2007; Rukstalis et al., 2006; Gouzi et al., 2011). Remodeling of cells in the mesenchymal compartment indicated by *SrpX2<sup>+</sup>* cells might hint to a temporal and fine-tuned mechanism in mouse embryogenesis.

Taken together, the selected pancreatic candidate genes suggests to be useful for the scientific community to elucidate the factors in lineage segregation of the formerly MPP in the PE. In addition, the MPP can be characterized more precise which will be helpful identifying the 'stem cell niche' in pancreas organogenesis and in the adult Islet of Langerhans. Preliminary results may be achieved by

promoter analysis, respective enhancer analysis as described for the synergistic induction of the *Pdx1* promoter by *Foxa2* (Lee et al., 2005). Thus, up- or downstream regulation of the pancreatic candidate genes by *Pdx1*, respective *Foxa2* can be determined in line with the MPP state of the genes in the PE. In addition, a bioinformatics approach regarding a scheme of the transcriptional network and the various signaling pathways could define the factors in the maturation of the pancreas more detailed. Especially in regard that global expression profiles in general defined genetic pathways that regulate endocrine development (Searce et al. 2002). Our GRN of the secondary transition has the advantage of either focusing on endocrine lineage segregation or dissecting tissue epitheliomesenchymal interactions which are necessary for cytodifferentiation and morphogenesis of the pancreas (Golosow and Grobstein, 1962; Levine et al., 1973).

#### 4.5 Generation of different mouse lines

We generated in this thesis chimeras by *CD1* morula aggregation of *Grb7<sup>GT</sup>*, *Tmem171<sup>GT</sup>*, *Vwa5b2<sup>GT</sup>*, *Srpx2<sup>GT</sup>*, *Syt13<sup>GT</sup>*, *5330417C22Rik<sup>GT</sup>*, *1810019J16Rik<sup>GT</sup>* and *1700011H14Rik<sup>GT</sup>*. As germline transmission was only achieved for chimeras of *Tmem171<sup>GT/-</sup>*, *Srpx2<sup>GT/-</sup>*, *Syt13<sup>GT/-</sup>*, *5330417C22Rik<sup>GT/-</sup>*, *1810019J16Rik<sup>GT/-</sup>* and *1700011H14Rik<sup>GT/-</sup>* these mouse models are currently in focus for function and mechanism of the pancreatic gene candidates. In addition, we generated next to the knock-out first allele (*GT*), conditional alleles (post-*Flp-e*) and Reporter-tagged deletion alleles (post-*Cre*). The final aim is generating a deletion allele (post-*Flp-e* and *Cre* with no reporter) in line with crossing to inducible Reporter-lines as the *Foxa2-Cre*, *Pdx1-Cre* and *Ins-Cre*. Thus, spatial and temporal expression in the PE will be investigated more precise. The analysis of the different genes was additionally impeded by the strong background dependency, mice are either on a *C57Bl/6J*, *CD1* or mixed background.

For example the *Syt13<sup>GT/GT</sup>* mouse line was generated in the *C57Bl/6J* and *CD1* background and showed low penetrance hydrocephalus in the *C57Bl/6J* background, whereas none was observed in the maintained *CD1* mouse line. In addition, P lethality was observed in intercrosses of *Syt13<sup>R/R</sup>* on the *C57Bl/6J* background. Contrary, occasional embryonic lethality of embryos with the genotype *Syt13<sup>R/R</sup>* on *CD1* background was most likely due to the extended litter mates and natural selection. Also, we did not observe embryonic lethality in the *Syt13<sup>GT/GT</sup>* intercrosses, either on the *C57Bl/6J* or *CD1* background. Maintaining the mendelian ratios will determine the observed phenotypes more accurate. The background dependency is already illustrated in the *Bardel-Biedl Syndrome<sup>-/-</sup>* (*BBS4<sup>-/-</sup>*) mouse lines, mice generated via homologous recombination showed none of the phenotypes described in *BBS4<sup>GT/GT</sup>* mice on a *C57Bl/6J* background (Ross et al., 2005; Zhang et al., 2012).

#### 4.6 Generation of the *Syt13*<sup>GT/GT</sup> mouse line

The gene *Syt13* was identified in the GRN with a trunk pattern comparable to the endocrine progenitor *Ngn3*. Thus, we focused our analyses on localization, function and predicted mechanism of *Syt13* in pancreas organogenesis. First, we generated the *Syt13*<sup>GT/GT</sup> mouse line in the *CD1*, respective *C57Bl/6J* background. Intercrosses of *Syt13*<sup>GT/-</sup> produced the expected mendelian ratio with a slight increase in the offspring of the *Syt13*<sup>GT/GT</sup> mice. Preliminary data suggests that intercrosses of the *Syt13*<sup>R/-</sup> mice are P lethal which will be observed closer in oncoming offspring.

The advantage of the *Syt13*<sup>GT/GT</sup> mouse line was the application of the *LacZ* reporter gene expression cassette for comparison to *Syt13*<sup>GT/-</sup> mice. We did observe the dose of both targeted alleles in the *Syt13*<sup>GT/GT</sup> paraffin sections. Our first intention was the generation of a null mutation of the *Syt13* gene, but promoter analyses (Berkeley Drosophila Genome Project) showed an alternative promoter in front of exon 3 and therefore an alternative transcript of *Syt13* downstream of the CE2. Therefore, we suggest for *Syt13*<sup>GT/GT</sup> a truncated protein product which does not harbor the N-terminal transmembrane domain (Sudhof 2002; Bacaj et al. 2013; Xu et al. 2009). Nevertheless, the benefit of this mouse line had been the first results of the *LacZ* reporter gene expression and indication of *Syt13* as a gene involved in endocrine formation.

The crossing of *Syt13*<sup>GT/GT</sup> into the *Flpe-e* and *R26R Cre* reporter line was initiated to generate the *CKO* mouse line. As a suitable tool, the mouse lines *Foxa2-Cre* and *Pdx1-Cre* are used for either conditional gene inactivation in the DE or tissue specific in the pancreas, in neurogenic regions of the brain or in enteroendocrine cells of the duodenum. Additionally, the Insulin specific *Cre* mouse line suggests to be useful to specifically delete *Syt13* in the  $\beta$ -cells of the adult Islets of Langerhans. Furthermore, we suggest for future purpose generation of a *Venus* reporter line of *Syt13* for real-time labeling of the pancreas, neural lines and gastro-intestinal tract. In line with these recommendations, we generated successfully the new mouse lines *Syt13*<sup>GT</sup> and *Syt13*<sup>R</sup> for further research on function and mechanism of the gene *Syt13*.

#### 4.7 *Syt13* expression in a distinct subset of tissue

The reporter gene expression analysis and *in silico in situ* showed expression for *Syt13* in a distinct subset of mono- and multiciliated tissue. We did observe *LacZ* pattern in the ganglion precursors, limbs, olfactory epithelium, opticle ventricle and the pancreas during the development of the mouse embryo. In the adult mouse, we did exclusively observe expression in the brain and the pancreas and did not favor the other organs. We assured pancreatic cysts formation P 30 days, apparently in the kidney the expected polycystic kidney disease (PKD) was not observed (data not shown). *Syt13* may control AB polarity only in a subset of organs. Other reasons could be due to the fact of the large *Synaptotagmin* family which complements deficiency of *Syt13* especially in the kidney. As many proteins involved in cystic diseases localize to the cilium or the BB at the base of the cilium we might suggest a role of *Syt13* in vesicular trafficking in the process of PCP establishment (Jones et al. 2008; Veland et al. 2009).

#### **4.8 Pancreatic multipotent progenitors and endocrine cells marked by *Syt13***

Exocrine and endocrine cells have a common origin, mainly cells that start to express  $Pdx1^+/Foxa2^+/Ptf1\alpha^+$ . Initiation of pancreas outgrowth is therefore composed of MPP which will segregate in the secondary phase to the different lineages. We identified *lacZ* Reporter gene expression in the PE as early as E11.5, suggesting that *Syt13* although marks the MPP in the PE. Segregation into the defined tip and trunk of the different lineages point to different subpopulations of *Syt13* - *Syt13<sup>high</sup>*, respective *Syt13<sup>low</sup>* expressing cells. The *Syt13<sup>low</sup>* represents the classical tip pattern with bi-potent progenitors in the PE, thus characterizing a  $FVF^{low}Cpa1^+Syt13^{low}$  progenitor pool. Interestingly, *Synaptotagmin 1, 3, 6* and *7* expression are already described in pancreatic acinar cells as  $Ca^{2+}$  sensor to stimulate exocytosis at the apical cell surface (Falkowski et al. 2011). Lineage tracing by using either *CreERT2* lines of early pancreatic progenitors which will differentiate into acinar cells as *Cpa1*, *Ptf1 $\alpha$* , *Mist1/Bhlal5* or *Nr5a2* would highlight our results of the *Syt13<sup>low</sup>* expression in the PE and the MPP characteristics of *Syt13* in pancreas development.

Segregation into the ductal/endocrine lineage leads to a trunk pattern, as illustrated for *Ngn3* and *Syt13* (Zhou et al. 2007). Formerly MPP will be restricted to a specified subset of cells. We identified apical localization presumably at the BB (Gegg et al., 2014). Furthermore, basal localization of *Syt13* in *Ngn3<sup>high</sup>* cells indicates a transition of polarity during endocrine formation. This is in line with *Ecad<sup>low</sup>* combined to *Syt13<sup>high</sup>* suggesting the classical model of EMT at least partially needed for the delamination of endocrine progenitors out of the ductal cord (Rukstalis et al. 2006; Rukstalis and Habener 2007). Loss of the epithelial program leads to the repression of *Ecad*, initiated by the transcriptional module of TF family *Snail* and *ZEB*, front-rear polarity and cell migration (Nelson 2009;

Bahmanyar et al. 2008). Zhang et al. proposed regulation of *ZEB2* by *Foxa2* in breast cancer cells, highlighting the results of Bartscher and Lickert (Bartscher and Lickert 2009) for establishment of the polarity program through *Foxa2*. In line with this observation upstream TF *Foxa2/Pdx1/Sox9* activate transcription of *Ngn3* (Lee et al. 2001; Oliver-Krasinski et al. 2009), implicating for *Syt13*<sup>high</sup> a function in re-establishment of the polarity complexes during the *Ngn3* activated endocrine program. Impairment in polarity establishment will led to failure in delamination out of the duct cord. As we observed impairment of endocrine progenitors leaving the ductal cord, we propose for *Syt13* a role in endocrine formation through failure in polarity establishment. Moreover, we suggest asymmetric cell division along with partial EMT in the process of endocrine formation.

#### **4.9 *Syt13* initiates morphogenesis in the pancreatic epithelium**

It has been shown that the protein *Syt13* is already expressed at E7.0 in the embryo, suggesting a role in embryonic development (Fukuda and Mikoshiba 2001). These results strongly indicate a correlation to *Foxa2* in the organizer tissue and thereby expression in endodermal-derived organs.

Thus, we observed impaired Rosette-like structures and multinucleated cells in the PE of *Syt13*<sup>R/R</sup> mice. Next to it, AJ are altered by structure, due to failure of recruitment of the AJ complex. Our results implicate a role of *Syt13* in the morphological remodeling of the pancreas leading to a tubular network. Expression and function in the PE for *Synaptotagmin 1, 3, 6* and *7* had been validated by Falkowski et al.. The Synaptotagmins attending the SNARE complexes and regulate Ca<sup>2+</sup> dependent exocytosis of proenzymes in the pancreatic acinar cells (Falkowski et al. 2011). As *Syt13* lacks of the Ca<sup>2+</sup> binding sites, we speculate about the role of *Syt13* in tubulogenesis in anterograde vesicle transport for establishment of the apical polarity. Impairment of *Syt13* thereby leads to nonlinear vesicle transport and failure of establishing polarity in the epithelial cells, particularly in fusion of the microlumen to a continuous L. In addition, we observed misorientation of the spindle through incorrect positioning which accompanies to multinucleated phenotypes.

Pancreatic initial morphogenesis in the hypomorph *Syt13*<sup>GT/GT</sup> mice appears not to be affected, as we could observe the stratified ductal tree in paraffin section. We assume that in the hypomorphic allele, remaining protein expression might annul the phenotype. Contrary, the sphere-forming assay illustrated defects in L formation, as the cells of the PE rather cluster as aggregates than in spherelike structures.

In general, Cdc42 is involved in assigning polarity cues to the  $\alpha$ PKC complex (Gotta et al. 2001; Hutterer et al. 2004). Therefore, the complex, consisting of Par3, Par6, Cdc42 and  $\alpha$ PKC, regulates in mammalian cells TJ formation (Togawa et al. 2010). Although, localization to the apical surface and involvement in intraflagellar transport (IFT) was lately shown mediated through KIF3A (Yamazaki et al. 1995; Nishimura et al. 2004; Boehlke et al. 2013). As we observed similarity to Cdc42, we speculate about the role of *Syt13* in polarity recruitment to the apical membrane surfaces. KIF3A is described as microtubule motor protein in vesicle transport, implicating that *Syt13* accompanies the transport by vesicle docking (Takeda 2000; Fukuda & Mikoshiba 2001; Gálvez-Santisteban et al. 2012; Fukuda et al. 2000). Moreover, KIF3A depletion leads to deficiency in central lumen formation, equally to the observed phenotype of *Syt13*. Ongoing experiments as pulldown assays will determine the interaction profile of *Syt13* and thereby define the putative interaction of *Syt13* to KIF3A. We further suggest protein interaction domain mapping for determining the specific interaction domains. Additional experiments regarding doxycycline or tetracycline inducible depletion of *Syt13* of Madin-Darby Canine kidney (MDCK) cells might reflect the slow down of cell migration and thereby a suggested role of *Syt13* in the dynamics of microtubules. We already observed lumen dysformation *in vivo* and in MDCK cells (Bakthi observed) and in *Syt13* deficient mice endocrine progenitors failed to separate perpendicularly in the ductal region, implicating indeed a coherence to KIF3A depletion. Further studies will highlight the possible functions of *Syt13* in lumen formation, respective morphogenesis of the pancreatic epithelium.

#### **4.10 The subcellular localization of *Syt13* suggests a role in polarity membrane complexes along with BB positioning**

The conserved function of epithelial cells are the establishment of polarity, mitotic spindle orientation and the formation of a layer rather than a bulk of cells. The AB basal polarity functions as a barrier between the inner lumen and the ECM, neurons polarize into axons and dendrites and thereby pass forward signals in one direction (Yamada et al. 2007). Recruitment of the polarity complex relies on temporal and spatial regulation of polarized trafficking within a tissue (Galic and Matis 2015). Exocytosis and synaptic vesicle function are described in the context of *Synaptotagmins*, which in general mediate synaptic vesicle exocytosis through interaction with the SNARE complex followed by fusion with the target membrane (Sudhof 2002). In exocytosis process of Insulin secretion,  $Ca^{2+}$ -binding of *Synaptotagmins* as *Syt1*, *2*, *6* and *7* leads to membrane fusion and release of Insulin (Gauthier and Wollheim, 2008). As *Syt13* does not harbour of  $Ca^{2+}$ -binding sites, we suggest a role in vesicle transport. The conserved WHXL motif in the C terminus of *Synaptotagmins* functions as vesicle

docking to the plasma membrane/ protein complex (Fukuda et al. 2000). Thus, we assume that *Syt13* may not be involved in exocytosis, more likely in vesicle docking and trafficking on the microtubule network.

Lately published by Xu et al. mapping of the *INS1* promoter in the Human chromosome 11 revealed positive regulation of *SYT8* (Xu et al. 2011). The function of *SYT8* suggests the regulation of insulin and glucagon secretion via governing different *Synaptotagmins*. Interestingly, *SYT13* locates approximately 50 MB of the *INS* promoter, but expression of *SYT13* in human Islets of Langerhans is not affected by glucose-stimulation or inactivation of the *INS* promoter. These results further determining the function of *Syt13* rather in vesicle trafficking than in exocytotic vesicle fusion. Contrary to published results, SNP analysis likely points to insulin secretion defects. We have to further evaluate the impact of GSIS regarding our mouse model and human Islets of Langerhans.

We identified localization of *Syt13* in polarized epithelial cells at the apical site presumably at the BB. Next to these results, we could observe *Syt13* endogenous protein distribution in endocrine cells in the cytoplasm. Ciliogenesis is accomplished by IFT through delivering proteins to the BB and ciliary axonemes. Thus, we suggest for *Syt13* a role in possible IFT vesicle transport, which is in line with observed ciliopathies in the *Syt13<sup>GT/GT</sup>* mouse as hydrocephalus and pancreatic cysts. The AB axis is generated and maintained by the Par complex, encoding Par3-Par6- $\alpha$ PKC and Cdc42 at TJ. In addition, the mentioned polarity proteins likely controlling ciliogenesis through microtubule motor interaction to KIF3a (Takeda 2000). Therefore, contradictory roles of *Syt13* in AJ maintenance and ciliogenesis might be explained.

Recent studies have also indicated a role of phosphoinositides by establishment of polarity, the apical surface is determined by phosphatidylinositol 4,5-bisphosphate (PI(4,5)P<sub>2</sub>) which interact with Synaptotagmins (Martin-Belmonte and Mostov 2008; Martin-Belmonte et al. 2007; Wiedemann and Cockcroft 1998). Furthermore, RNAi screening in MDCK cells identified apical transport proteins involved in regulation of luminal space, respective ciliogenesis (Gálvez-Santisteban et al. 2012; Torkko et al. 2008). In line with published data we therefore propose for *Syt13* vesicular transport of polarity complexes along the microtubules either to apically located protein complexes or to the axonemes of the cilium.

For determining if *Syt13* is involved in IFT and polarity establishment we recommend live-imaging of *Syt13*-fluorescence tagged transfected MDCK cells or even knock-in models using the recently in our laboratory generated *Ar13-RFP*. In addition, mating to the lately published *Ftpt-Cre* line suggests a good tool for deciphering the molecular function of *Syt13* (Gegg et al. 2014). Furthermore, fractioning

of subcellular components by sucrose gradient would determine expression of *Syt13* in the different cell compartments more precise.

#### **4.11 Potential mechanism of *Syt13* in endocrine lineage formation**

Taken the results together, we postulate a role of *Syt13* in IFT transport in line with establishment of apical polarity complexes. Thereby, *Syt13* reveals subpopulations, stated as *Syt13*<sup>high</sup> and *Syt13*<sup>low</sup>. Subcellular localization appears contrary; either apically in the L, in endocrine progenitors basal and in endocrine precursors and differentiated cytoplasmic. We further support the concept, that expression level and subcellular localization defines the function of *Syt13* within the cell.

Focusing on endocrine lineage formation during pancreatic tubulogenesis, the branching tree of the ductal system is formed. In line with morphogenetic changes, expression of *Pdx1* in the ductal compartment peaks in, confirmed by co-expression of the subpopulation *FVF*<sup>high</sup> of upstream regulator *Foxa2* (Wescott et al., 2009). We suggest that *Syt13* is co-expressed and thus might be part in mechanism regarding the endocrine lineage segregation.

Endocrine lineage formation is postulated as remodeling of AB polarity, rearrangement of the cytoskeleton and asymmetric cell division. In general, the polarized epithelial cells will abandon the epithelial sheet and discharge their junctional complexes. Hence, a hallmark of EMT is the downregulation of *Ecad*. Interestingly, loss of *Ecad*, which binds  $\beta$ -catenin, changes components of the Par-complex and oriented cell division. Although  $\beta$ -catenin likely as nima-related kinase-2 (*Nek-2*) substrate, indicates involvement in centrosome separation (Bahmanyar et al. 2008). However, we did not look for the Wnt/ $\beta$ -catenin pathway in pancreas organogenesis. Recently, Dupin and colleagues published that *Cdc42* activity and the actin cytoskeleton are involved in polarized positioning of centrosomes by AJ (Dupin et al. 2009). Thus, loss of *Ecad* may lead to alterations in orientation of the mitotic spindle and chromosome segregation.

We did observe the correlation between *Syt13*<sup>high</sup> and *Ecad*<sup>low</sup>, pointing to the classical EMT program. Further support was acquired as *Syt13*<sup>high</sup> is restricted to endocrine progenitors, precursors and differentiated cells in the Islets of Langerhans. Additionally, the PE at E18.5 of *Syt13*<sup>R/R</sup> mice showed impairment of the endocrine precursors in delamination from the ductal region.

Which cellular mechanism in detail will lead to the formation of the endocrine lineage remains elusive, but we propose the model of asymmetric cell division. We could already observe in the *FVF* pancreas, *Ngn3*<sup>+</sup> cell in mitosis on a perpendicular division, suggesting that primed endocrine progenitor cells

(Ngn3<sup>+</sup>) generate endocrine precursors (Nkx6-1<sup>+</sup>) (Shih et al. 2013). Thus, following up experiments include lineage tracing of the endocrine progenitor pool in the ductal compartment, which might determine the division plane. We recommend using a fluorescence-tagged *Ngn3* mouse model for live imaging. As we already defined subcellular localization of Syt13<sup>high</sup> on the basal surface of Ngn3<sup>high</sup> cells, we suggest that delamination accompanies with a variation in polarity. The mechanisms which convert epithelial cells and leads to migration of 'primed' precursors are well described in the context of cancer as EMT (Morris and Machesky 2015).

We have currently pulse-labelled at E16.5 *Syt13<sup>R/R</sup>* mouse embryos using Bromdeoxyuridine (BrdU) for determining the speculated asymmetric cell division in the endocrine lineage. Furthermore, we utilize the FACS approach for sorting of the different pancreatic cell populations and identifying the Syt13<sup>+</sup> lineages. As we propose our model for the endocrine lineage, we have to consider the competence window of Ngn3<sup>+</sup> endocrine precursors and timing for the different subtypes of the Islets of Langerhans (Johansson et al. 2007), concurrent for determining *Syt13* expression in the adult Islets of Langerhans.

The EMT characteristic TF *Snail2* anti-correlates with *Ecad* expression in the endocrine lineage differentiation, hence IHC for Syt13 will display correlation and subcellular localization. Additionally, the signaling cascade affecting the endocrine lineage can be determined, by sorting the endocrine subpopulation during secondary transition. Especially of interest may be the Wnt/ $\beta$ -catenin pathway, as studies suggest localization of  $\beta$ -catenin at the BB (Corbit et al. 2008). The function of the canonical Wnt/ $\beta$ -catenin pathway is presumably depending on cilia and thus on PCP. PCP is characterized through Frizzled (Fz) and disheveled (Dsh), both proteins are recruited to the plasma membrane upon Wnt binding (Baek et al. 2003; Sokol et al. 2015). The molecular role for these proteins suggests participation in processes including actin-remodeling and ciliary-vesicle transport indicating that *Syt13* is involved in PCP of the cells (Delaval et al. 2011; Gray et al. 2011).

In determining the protein complex and interaction profile, additional information will be achieved about the function of Syt13 in the different lineages of endocrine cells and localization within a cell. It will be interesting regarding the recommended roles of *Syt13* especially in  $\beta$ -cell development and the implication of T2D susceptibility. Next to previous described, Syt13 may be used as a mouse model for duct ligation, as a model for proliferation and reprogramming in the embryonic stage and in the adult mutants, regarding the partial duct ligation (PDL) and the indication for  $\beta$ -cell proliferation. We might especially point to the potential of 'stemness' in the ductal inherited cells in the adult pancreas, which represents a common hypothesis in the pancreatic community. With this in mind, we further suggest deciphering the function of *Syt13* regarding *Sox9*, as *Sox9* controls *Ngn3* and *Pdx1* expression (Kopp et al. 2011). Taken together, the future perspectives for determining the role of Syt13 in duct/endocrine

formation suggest a more closer marker lineage analysis along with suitable tools as the lately in our laboratory generated fluorescent *Ngn3*-mouse line.

#### **4.12 Hypothetical molecular function of *Syt13***

We are only beginning to understand the role of *Syt13* in cellular processes and the biological influence. As we postulate that *Syt13* is involved in vesicle transport and docking to the BB, the comprehensive role of *Syt13* might be the delivery of proteins necessary for polarity. Prior the first analysis of the phenotype, we assume coherence to the exocyst complex. The master regulator of cell polarity and cytoskeletal dynamics, *Cdc42* has been shown to be component of the exocyst complex (Otani et al. 2006; Kesavan et al. 2009; Tuncay et al. 2015). As we observed closely related phenotypical changes in the mutant mice, we assume that *Syt13* might be part of the exocyst complex in establishing polarity.

The hypothesis further suggests localization to the BB, where the exocyst complex will be stabilized by the Par complex. Thus, the hypothetical function of *Syt13* relies on vesicle mediated transport of components in the process of polarity establishment. In line with our observation, we propose the model of *Syt13* in the context with the exocyst complex, by retrograde transport through KIF3 kinesine motor proteins to the apical surface. Rather polarity establishment within the cells is organized through the CDC42-PAR proteins, co-localization to *Syt13* at the BB might lead to polarity failure in mutants. The precise molecular function remains unknown, and is currently under investigation. First pulldown assays showed association to the actin cytoskeleton, highlighting the different localizations of *Syt13* for the polarity within a cell (Mostafa Bahkti, unpublished). During endocrine lineage formation as the cortical actin cytoskeleton undergo the process of EMT, the actin architecture reorganizes indicated by F-Actin remodeling. Thus, *Syt13* co-localizes to the actin rearrangement and remains ubiquitously expressed in the endocrine differentiated cells, indicating that endocrine precursor Islets of Langerhans have not established a defined polarity. It might be still elusive if delamination occurs or the classical EMT, as approaches for the last mentioned are lacking in experimental design. We recommend determining regulation of MAPK/ERK cascade in mutant mice as these pathways promote EMT in carcinoma cells (Wu et al., 2015). We already could determine protein overexpression of Ezrin in IHC analysis, indicating pancreatic adenocarcinoma (Piao et al., 2015). Elevated rates of reactive oxygen species in mitochondria (ROS) might implicate possible EMT mechanism in the *Syt13* mice – respective in the endocrine progenitors. Thus, SEM imaging of mitochondria in endocrine precursors which delaminate out of the epithelial cord could determine if

classical EMT or other mechanism might regulate endocrine commitment in the secondary transition. In addition, we might look for Syt13 localization in the adult Islets of Langerhans as junctional arrangement lead to polarity recruitment within the different subtypes of the cells in the Islets of Langerhans.

## 5 Material and Methods

### 5.1 Material

#### 5.1.1 Equipment

Agarose gel chamber	Midi 450 (Harnischmacher, Kassel)
Balances	Scout™ Pro (Sartorius)
Centrifuges	5417 R (Eppendorf AG, Hamburg) 5417 C (Eppendorf AG, Hamburg) 5804 R (Eppendorf AG, Hamburg) Haereus Rotanta 460R (Thermo Fisher Scientific Inc., Waltham) Hettich Universal 30F (Andreas Hettich GmbH & Co. KG, Tuttlingen) 1-14 (Sigma Laborzentrifugen GmbH, Osterode am Harz) Galaxy Mini (VWR International GmbH, Darmstadt)
Counting chamber	Neubauer (LO - Laboroptik GmbH, Friedrichsdorf)
Cryotome	Leica CM 3050S
Developing machine	AGFA Curix 60 developing machine (AGFA HealthCare GmbH, Bonn)
Electroporation system	BioRad Gene Pulser Xcell (BioRad Laboratories, München)
FACS	FACS Calibur (Becton and Dickinson and Company, Franklin Lakes)
Film cassettes	Hypercassette (Amersham, GE Healthcare GmbH, München)
Freezer -20°C	(Liebherr Hausgeräte Ochsenhausen GmbH, Ochsenhausen)
Fridge 4°C	(Liebherr Hausgeräte Ochsenhausen GmbH, Ochsenhausen)
Gel documentation system	UV-Transilluminator (Biorad, München) Gene Flash (Syngene Bio Imaging, Synoptics Ltd, Cambridge)
Glassware	Schott-Duran (Schott, Mainz)
Microscopes	Axiovert 200M (Carl Zeiss AG, Göttingen) Lumar.V12 (Carl Zeiss AG, Göttingen) MS5 (Leica Microsystems GmbH, Wetzlar) TCS SP5 and SP9 (Leica Microsystems GmbH, Wetzlar) Cameras AxioCam MRc5 (Carl Zeiss AG, Göttingen) AxioCam HRm (Carl Zeiss AG, Göttingen)
Microwave	700W (Severin Elektrogeräte GmbH, Sundern)
Power suppliers	Power Pack Basic (BioRad Laboratories, München)
Pipettes	1000 µl / 100 µl / 20 µl / 10 µl Eppendorf Research (Eppendorf AG, Hamburg)
Pipettboy	accu-jet and accu-jet® pro (Brand GmbH & Co. KG, Wertheim)
Photometer	BioPhotometer (Eppendorf) ND-1000 Spectrophotometer NanoDrop, (Thermo Fisher Scientific Inc., Waltham)
Polyacrylamid gel	(BioRad)
Polyacrylamid gel chamber	Mini Trans-Blot® Cell (BioRad GmbH, Heidelberg)
PCR machines	Px2 ThermoHybaid (Thermo Fisher Scientific Inc., Waltham) PXE0.2

pH meter	Thermo Cycler (Thermo Fisher Scientific Inc. Waltham) pH211 Microprocessor pH Meter (HANNA Instruments Deutschland GmbH, Kehl am Rhein)
Plastic ware	(VITLAB GmbH, Großostheim)
Pump	LABOPORT <sup>®</sup> (neoLab Migge Laborbedarf-Vertriebs GmbH, Heidelberg)
Rotator/tumbler	VSR 23 (Grant BOEKEL, VWR international GmbH, Darmstadt)
Roller	SRT1 (Bibby Scientific (Stuart), Staffordshire, GB)
Stirrer	STIR (VWR international GmbH, Darmstadt)
Vortexer	Vortexer (VWR international GmbH, Darmstadt)
Water bath	VWR
Western Blot	semi-dry system Trans-Blot <sup>®</sup> SD, Semi-Dry Transfer cell (Biorad, Heidelberg)

### 5.1.2 Consumables

Blotting paper	Whatman paper (GE Healthcare Buchler GmbH & Co. KG, München)
dishes 15 cm/ 10 cm/ 6 cm	nunc (Thermo Scientific Fisher, Wiesbaden)
Embedding cassettes	(Carl Roth GmbH & Co. KG, Karlsruhe)
Embedding moulds	(Carl Roth GmbH & Co. KG, Karlsruhe)
Films Kodak BioMax MS	(Sigma-Aldrich GmbH, Hamburg), Amersham
Hyperfilm ECL	(GE Healthcare Buchler GmbH & Co. KG, München)
Nitrocellulose membrane	(GE Healthcare Buchler GmbH & Co. KG, München)
Pasteur pipettes	(Carl Roth GmbH & Co. KG, Karlsruhe)
Plastic transfer pipettes	(Carl Roth GmbH & Co. KG, Karlsruhe)
Pasteur pipettes, glass	(LABOR-BRAND, Gießen; Hirschmann Laborgeräte GmbH & Co. KG, Eberstadt)
Parafilm	(Pechiney Plastic Packaging, Menasha)
PVDF membrane Immun-Blot	(BioRad Laboratories, Hercules)
Scalpels	surgical disposable scalpels B/Braun (Aesculap AG & Co. KG Tuttlingen)

Tubes 50 ml/ 15 ml	(Becton and Dickinson and Company, Franklin Lakes; Sarstedt, Nürnbergrecht)
Tubes 14 ml	BD Labware (Becton Dickinson GmbH, Heidelberg)
Tubes 2 ml/ 1.5 ml	safe-lock reaction tubes (Eppendorf AG, Hamburg)
Tubes 0.2 ml tubes	(Eppendorf AG, Hamburg)
Plates 6- well / 12- well / 24- well /48-well plates/ 96-well	(straight/conical) nunc (Thermo Scientific Fisher, Wiesbaden)
pipettes 50ml/ 25ml/ 10ml/ 5ml/ 2ml/ 1ml	(Greiner bio-one, Frickenhausen)

### 5.1.3 Kits

ECL Detection Kit	(Millipore Cooperation, Billerica, MA)
QIAquick Gel Extraction Kit	(Qiagen Holding, Hilden)
QIAgen Maxi Kit	(Qiagen Holding, Hilden)
QIAgen Mini Kit	(Qiagen Holding, Hilden)
Labelling Kit	(Roche Holding GmbH, Applied Science, Mannheim)
RNeasy Mini Kit	(Qiagen Holding, Hilden)
EdU labeling Kit	(Invitrogen™ Cooperation, Carlsbad, CA)
SuperScriptIII Reverse Transcriptase	(Invitrogen™ Cooperation, Carlsbad, CA)

### 5.1.4 Chemicals

(Sigma-Aldrich GmbH, Hamburg, Merck KGaA, Darmstadt, Carl Roth GmbH & Co. KG, Karlsruhe)

#### A

Acetic acid (Merck)  
Activin A, human (R&D Systems)  
Acrylamide/bisacrylamide (Rotiphorese)  
Agarose (Biozym Scientific)  
Ampicillin (Roche)  
Antifade (Invitrogen™ Cooperation, Carlsbad, CA)  
APS (Roche)

#### B

Big Dye (Life technologies)  
Blocking (Roche Diagnostic)  
BSA

Bradford reagent (Sigma-Aldrich)

**C**

Calcium chloride (Roth)

Chloroform, 99% (Sigma-Aldrich)

Cl (Chloroform-Isoamylalcohol: 24:1)

**D**

Diethylpyrocarbonate (DEPC), approx. 97% (Invitrogen™ Cooperation, Carlsbad, CA)

Dimethylsulfoxide (DMSO), >99,9% (Sigma-Aldrich)

Dithiothreitol (DTT) (Sigma)

dNTPs (Fermentas)

**E**

EDTA (Roth)

Ethanol, 96% (Merck)

Ethidiumbromide (Roth)

**F**

Formaldehyde (Roth)

Formamide (Roth)

**G**

Gelatine (Applichem)

Glutamine

Glutaraldehyde (Sigma-Aldrich)

Glycerol (Sigma)

**H**

HCl (Roth)

HEPES (Gibco)

Heparin (Sigma-Aldrich)

**I**

Isopropanol, (100%) (Merck)

**K**

Kanamycin (Sigma)

**L**

L-glutamine (200mM, Gibco)

**M**

Magnesium chloride (VWR)

Methanol, 100% (Merck)

MEMs non essential amino acids (100x, Gibco)

Milk powder (Becton Dickinson GmbH, Heidelberg )

Mounting medium

MOPS

$\beta$ -mercaptoethanol (50mM, Gibco, Invitrogen™ Cooperation, Carlsbad, CA)

**N**

Nitrogen(I) (Linde AG, München)

Nuclear Fast Red (powder)

NP-40 (Roche Diagnostic, Mannheim)

**O**

Oligo-dT-primer (Promega GmbH, Mannheim)

**P**

Paraformaldehyde (Sigma-Aldrich)

PBS (Gibco, Invitrogen™ Cooperation, Carlsbad, CA)

PCI (Phenol-Chloroform-Isoamylalcohol: 25:24:1; Carl Roth GmbH + Co. KG, Karlsruhe)

Penicillin/Streptomycin (Gibco, Invitrogen™ Cooperation, Carlsbad, CA)

Polyacrylamide/Rotiphorese (Roth)

Potassium acetate

Proteinladder (Fermentas)

Proteinase K (Roche)

Puromycin

**Q**

**R**

RNaseZAP (Invitrogen™ Cooperation, Carlsbad, CA)

Rotihistol Roti-Phenol (Roth)

**S**

Sodium chloride

Sodiumdodecylsulphate (SDS)

Sodium hydrogenic phosphate ( $\text{Na}_2\text{HPO}_4$ )  
Sodium hydroxide

**T**

TEMED (Roth)  
TWEEN20 (Invitrogen™ Cooperation, Carlsbad, CA)  
Tris (Merck)  
Triton X-100 (Merck)  
Trizol (Gibco, Invitrogen™ Cooperation, Karlsruhe)  
Trypsin (Gibco, I Invitrogen™ Cooperation, Karlsruhe)

**V**

Vectashield (Vector Laboratories)

**X**

X-Gal  
Xylene

**5.1.5 Buffer and solutions**

**Immunostaining**

Permeabilisation:	0.2% TritonX-100 0.01 M Glycine in 1x PBS
Blocking solution:	for serum either donkey/goat 10% FCS 0.1% BSA 3% serum in 1x PBST (0.1% Tween20 in 1x PBS)
Washing solution:	PBST (0.1% Tween20 in 1x PBS)

**Isolation of genomic DNA**

Proteinase K lysis buffer for tail clips:	0.05 M EDTA 0.1 M Tris, pH8.0-8.5 0.2 M Sodium chloride, pH8.0 2% SDS
---	--

Yolc sac lysis buffer:                    0.01 M Tris-HCl, pH8.3  
   0.45% NP-40  
   0.45% Tween-20  
   0.02 M MgCl<sub>2</sub>  
   0.05 M KCl

### DNA/RNA agarose gels

TAE buffer (50x stock):                0.05 M Glacial acetic acid  
   0.05 M EDTA  
   2 M Tris

Loading buffer DNA:                    0.2% Bromine phenol blue  
   2% SDS  
   60% Glycerol  
   0.1 M EDTA

Loading buffer RNA (2x):               0.025% Bromine phenol blue  
   0.025% Ethidium bromide  
   0.0005 M EDTA  
   95% Formamide  
   0.025% SDS  
   0.025% Xylene cyanol

### Western blot

Lysisbuffer (RIPA)                      sterile filtration  
   0.05 M Tris/HCl, pH7.4  
   0.15 M Sodium chloride  
   0.002 M EDTA, pH8  
   1% NP-40  
   Add H<sub>2</sub>O  
   Add PI (1:200) freshly

APS:                                         sterile filtration  
   10% APS

4x Tris/SDS pH8.8:                    0.4% SDS  
   1.5 M Tris (pH8.8)

	Add H <sub>2</sub> O
4x Tris/SDS pH6.8:	0.4% SDS 0.5 M Tris (pH6.8) Add H <sub>2</sub> O
10x Tris-Glycine:	1.0% SDS 2 M Glycine 0.25 M Tris Add H <sub>2</sub> O
4x SDS-loading dye:	8% SDS 0.2 M Tris/HCl, pH6.8 40% Glycerol 0.4% bromine phenol blue 0.05 M DTT Add H <sub>2</sub> O
Buffer cathode:	10% Methanol 0.025 M Tris/HCl, pH9.4 0.04 M Glycine Add H <sub>2</sub> O
Buffer anode I:	10% Methanol 0.3 M Tris/HCl, pH10.4 Add H <sub>2</sub> O
Buffer anode II:	10% Methanol 0.025 M Tris/HCl, pH10.4 Add H <sub>2</sub> O
10x TBST:	1.5 M Sodium chloride 0.1 M Tris/HCl, pH7.4 1.0% Tween20 Add H <sub>2</sub> O
Ponceau-solution:	0.2% PonceauS

3% TCA  
Add H<sub>2</sub>O

Blocking solution: 1 g BSA in 1x TBST  
1:10 (v/v) milk powder;  
Add H<sub>2</sub>O

ECL-solution: Solution A and B (1:1)

### LacZ-staining

Fixation buffer: 0.002 M MgCl<sub>2</sub> x 6H<sub>2</sub>O  
0.02% NP-40  
0.005 M EGTA, pH8.0  
1% Formaldehyde  
0.2% Glutaraldehyde in 1x PBS

Washing buffer: 0.02% NP-40 in 1x PBS

Staining buffer: 0.005 M K<sub>4</sub>[Fe(CN)<sub>6</sub>] x 6H<sub>2</sub>O  
0.002 mM MgCl<sub>2</sub> x 6H<sub>2</sub>O  
0.02% NP-40  
0.005 mM K<sub>3</sub>[Fe(CN)<sub>6</sub>]  
0.01% Natriumdesoxycholat  
1 mg/ml X-Gal in 1x PBS

### Nuclear Fast Red staining

NFR: sterile filtration  
25g AlSO<sub>4</sub>  
Add H<sub>2</sub>O

#### 5.1.6 Enzymes

DNA-Polymerases: DNA Taq Polymerase (Invitrogen TM Cooperation, Carlsbad, CA)  
DNA Taq Polymerase (Qiagen, Hilden)

Proteaseinhibitor

Sigma Aldrich GmbH, Seelze

### 5.1.7 Sera and Antibodies

#### Sera

Donkey serum (Sigma-Aldrich, Hamburg)

Goat serum (Sigma-Aldrich, Hamburg)

#### Primary antibodies

Primary antibodies:

ID	name	host species	dilution	company	order number
8	GFP	goat	WB 1:1000 ; IHC 1:500	Abcam	600-101-215
358	Pdx1	goat	IHC 1:500	Abcam	ab47383
365	Pdx1	rabbit	IHC 1:500	Abcam	47267
218	CD49f	rat	IHC 1:3000	gift Kämmerer	555734
188	E-cadherin	rabbit	IHC 1:1000	gift Kämmer lab	GP84
156	Cpa1	rabbit	IHC 1:1000	Biozol	1810-0006
223	HNF-1 $\beta$	goat	IHC 1:500	Santa Cruz	sc-7411
6	Foxa2	goat	WB 1:200; IHC 1:1000	Santa Cruz	sc-9187
23	Foxa2	goat	WB 1:800; IHC 1:1000	Santa Cruz	sc-6554
249	Sox9	rabbit	WB 1:2000	Millipore	AB5535
198	Nkx6-1	mouse	IHC 1:1000	Mouse Hybridoma	F55A10
213	NKX6-1	goat	IHC 1:1000	R&D Sytems	AF5857
215	Nkx6-1	rabbit	WB 1:250; IHC 1:1000	Acris	NBP1-82553
30	acetylated-Tubulin	mouse	IHC 1:1000	Sigma	T7451
259	SYT13 N-term	rabbit	WB 1:100; IHC 1:1000	Aviva	OAAB02896
335	Syt13	rabbit	WB 1:500; IHC 1:1000	Abcam	ab154695

347	Strep-Tag	mouse	WB 1:500; IHC 1:1000	Novagen	71590-3
84	Epcam	rat	IHC 1:500	Mouse Hybridoma	4G1
149	Ezrin	mouse	WB 1:2000-4000	Sigma	E8897
	Ngn3	guinea-pig	IHC 1:1000	gift Sander lab	

**Table 6: List of primary antibodies used in this thesis.**

Abbreviations: WB = Western Blot; IHC: Immunohistochemistry

### Secondary antibodies

Secondary antibodies:

ID	name	host species	dilution	company	order number
18	donkey anti-goat IgG 633	Fluorescent	IHC 1:800	Invitrogen	A21082
23	donkey anti-mouse IgG 488	Fluorescent	IHC 1:800	Invitrogen	A21202
24	donkey anti-rabbit IgG 555	Fluorescent	IHC 1:800	Invitrogen	A31572
25	donkey anti-goat IgG 488	Fluorescent	IHC 1:800	Invitrogen	A11055
26	donkey anti-rabbit IgG 488	Fluorescent	IHC 1:800	Invitrogen	A21206
27	donkey anti-chicken IgY	Cy3	IHC 1:400	Dianova	703-165-155
28	donkey anti-chicken IgY	Cy2	IHC 1:400	Dianova	703-225-155
32	donkey anti-mouse IgG 555	Fluorescent	IHC 1:800	Invitrogen	A31570
35	donkey anti-goat IgG 555	Fluorescent	IHC 1:800	Invitrogen	A21432
76	Donkey anti-guinea pig Alexa 488	Fluorescent	IHC 1:400	Dianova	706-545-148
30	goat anti-chicken IgY	DyLight 488	IHC 1:400	Dianova	103-545-155
33	goat anti-guinea pig IgG 633	Fluorescent	IHC 1:800	Invitrogen	A21105
61	goat anti guinea pig IgG 546	Fluorescent	IHC 1:400	Invitrogen	A11074
58	goat anti-rabbit IgG 546	Fluorescent	IHC 1:800	Invitrogen	A11010

**Table 7: List of secondary antibodies used in this thesis.**

Abbreviations: IHC = Immunohistochemistry

### 5.1.8 Oligonucleotides

#### Oligonucleotides for Genotyping

For genotyping oligonucleotides in the list below were used. The oligonucleotides are stated from 5' to 3' direction.

- EP176: 5'-CTAATGTTGTGGGAAATTGGAGC-3'
- EP177: 5'-CTCGAGGATAACTTGTTTATTGC-3'
- EP485: 5'-ATGCCCAAGAAGAAGAGGAAGGT-3'
- EP486: 5'-GAAATCAGTGC GTTCGAACGCTAGA-3'
- EP 397: 5'- CTACTACCAAGGAGTGTACTCC-3'
- EP 398: 5'- CTGTGGCCCATCTATTTAGGG-3'
- EP 399: 5'- CGGACTTGAAGAAGTCGTG-3'
- EP 1300: 5'-ACGCAGACTACACCTTGGAG-3'
- EP1301: 5'-TACTAAGCCCTGGTTCAAGC-3'
- EP1322: 5'- AGACCAGTTGTGGTGAGGAGAGG-3'
- EP1323: 5'- TGTAATGGAGTGGGCCATAATCC-3'
- EP1324: 5'- CACAACGGGTTCTTCTGTTAGTCC-3'
- Srpx2 fw: 5'- CAGACATAGATCCACCCAAGATCC-3'
- Srpx2 rev: 5'- AGCAGGGTTTCCTTCTCTCTAC-3'
- Vwa5b2 fw: 5'- GCAGCGACGGTTCATAAGG-3'
- Vwa5b2 rev: 5'- CACCAGAGATGGTGGCATAAC-3'
- Grb7 fw: 5'- GTCGATCTGGCCTCTACTAC -3'
- Grb7 rev: 5'- CACAAGCAGAGGCTGATTCC -3'
- Scgn fw: 5'- AGAGCTGGATGCCTTCTTTG -3'
- Scgn rev: 5'- CTGGCCTTTGGCATCTCTGG -3'

#### Oligonucleotides for RT-PCR

For RT-PCR following oligonucleotides had been generated. The oligonucleotides are stated from the 5' to 3' direction.

Ex1,2 fw: 5'-TGCTGTCGGTGCCTGTGATCG-3

Exon1,2 rev: 5'- CCTCTGTGGTCTCCAAGGTGTAGTC-3

Exon 3,4 fw: 5'- CTCCACTTCCGCCTGGACTATG-3

Exon 3,4 rev:5'- GCAGGGTGAGTGTCAGGGTAGC-3

Exon 5,6 fw: 5'- AAGAACCTCCACTCCAACCAATCC-3

Exon 5,6 rev: 5'- AGCAAGTCATCCGGTAGCTCAAAC-3

#### 5.1.9 Cell lines

IDG3.2: murine ES cell line (F1); genetic background 129S6/SvEvTac x C57BL/6J (Hitz et al., 2007)

MEF: primary murine embryonic fibroblasts isolated on E13.5

#### 5.1.10 Culture media

**MEF:** DMEM (Gibco, Invitrogen™ Cooperation, Carlsbad, CA)  
2 mM L-glutamine (200 mM Gibco, Invitrogen™ Cooperation, Carlsbad, CA)  
15% FCS (PAN Biotech GmbH, Aidenbach)  
0.1 mM β-mercaptoethanol (50 mM, Gibco, Invitrogen™ Cooperation, Carlsbad, CA)  
1x MEM (non-essentiell amino acids, 100x; Gibco, Invitrogen™ Cooperation, Carlsbad, CA)

**IDG3.2:** DMEM (Gibco, Invitrogen™ Cooperation, Carlsbad, CA)  
2mM L-glutamine (200x, Gibco, Invitrogen™ Cooperation, Carlsbad, CA)  
15% FCS (PAN Biotech GmbH, Aidenbach)

0.1 mM  $\beta$ -mercaptoethanol (50 mM, Gibco, Invitrogen™ Cooperation, Carlsbad, CA)

ESGRO® (LIF) (107 U/ml; Chemicon, Millipore, Schwalbach)

1x MEM (non-essential amino acids, 100x Gibco, Invitrogen™ Cooperation, Carlsbad, CA)

2mM HEPES (200 mM, Gibco, Invitrogen™ Cooperation, Carlsbad, CA)

**Freezing media:** 5ml FCS (PAA)

4ml DMEM

1ml DMSO

**Solutions for cells culture:**

1x PBS without  $Mg^{2+}/Ca^{2+}$  (Gibco, Invitrogen™ Cooperation, Carlsbad, CA)

1x Trypsin-EDTA                      0.05 % Trypsin and 0.25% Trypsin

0.53 mM EDTA\*4Na, Gibco, Invitrogen™ Cooperation, Carlsbad, CA)

**5.1.11 Molecular weight markers**

RNA ladder: RNA ladder high Range (Fermentas GmbH, St. Leon-Roth)

DNA ladder: 100bp; 1kb (NEB GmbH, Frankfurt a. M.)

Protein ladder: SeeBlueR Plus2 Standard Pre-Stained (Invitrogen, Frankfurt a. M.)

### 5.1.12 Mouse lines

<i>129S6/SvEvTac</i>	embryonic stem cell line (ES) for knockout mice (Taconic)
<i>C57BL/6NJ</i>	(Charles River)
<i>CD1</i>	outbred strain (Helmholtz Center Munich)
<i>Syt13<sup>GT</sup></i>	mouse line generated in this thesis ( <i>129S2, Bl6, CD1</i> background)
<i>Syt13<sup>R</sup></i>	mouse line generated in this thesis ( <i>129S2, Bl6, CD1</i> background)
<i>R26R Cre</i>	(Soriano et al. 1999)
<i>Flp-e</i>	(Dymecki et al. 1996)
<i>Foxa2<sup>Venus</sup></i>	(Burtscher et al., 2009)
<i>Grb7<sup>GT</sup></i>	mouse line generated in this thesis ( <i>129S2, Bl6, CD1</i> background)
<i>Tmem171<sup>GT</sup></i>	mouse line generated in this thesis ( <i>129S2, Bl6, CD1</i> background)
<i>Vwa5b2<sup>GT</sup></i>	mouse line generated in this thesis ( <i>129S2, Bl6, CD1</i> background)
<i>Slc38a3<sup>GT</sup></i>	mouse line generated in this thesis ( <i>129S2, Bl6, CD1</i> background)
<i>Rbm47<sup>GT</sup></i>	mouse line generated in this thesis ( <i>129S2, Bl6, CD1</i> background)
<i>Cldn10<sup>GT</sup></i>	mouse line generated in this thesis ( <i>129S2, Bl6, CD1</i> background)
<i>2210010C04Rik<sup>GT</sup></i>	mouse line generated in this thesis ( <i>129S2, Bl6, CD1</i> background)
<i>5330417C22Rik<sup>GT</sup></i>	mouse line generated in this thesis ( <i>129S2, Bl6, CD1</i> background)
<i>1700011H14Rik<sup>GT</sup></i>	mouse line generated in this thesis ( <i>129S2, Bl6, CD1</i> background)
<i>Scgn<sup>GT</sup></i>	mouse line generated in this thesis ( <i>129S2, Bl6, CD1</i> background)
<i>Srpx2<sup>GT</sup></i>	mouse line generated in this thesis ( <i>129S2, Bl6, CD1</i> background)

## 5.2 Methods

### 5.2.1 Bioinformatics methods

#### 5.2.1.1 Affymetrix®Gene 1.0 ST Array

The experimental setup contained analysis of FACS-sorted cell populations at E12.5, E13.5, E14.5 and E15.5. In total there are 3 populations: The *Foxa2*<sup>Venus</sup>(positive), non-endodermal (negative) and total pancreatic (control) population. The Agilent 2100 Bioanalyzer assessed only high RNA quality (RIN>7) for further quantification. On the Affymetrix®mouse Gene 1.0 ST Array card an average of 27 probes/gene are applied. Only perfect match probes were taken for the following setup.

#### 5.2.1.2 Affymetrix®Gene 1.0 ST Array card

The array format accounted for 169 with the featured size of 5µm/sample. Each well carries a 25-mer oligonucleotide probe with a total number of 770.317 probes for the array card. The interrogated strand of the oligonucleotide probes consists of an sense strand with 27 (median) probes/gene for better resolution. With an estimated number of genes for the mouse 1.0 ST Array card of 28.853, the gene-level probe sets with Ensembl support contains 27.543 genes. For gene-level probe sets with putative full-length transcript support (GenBank and RefSeq) Affymetrix®offers 19.434 genes. The Genome assembly taken are dated from February 2006 (UCSC mm8; NCBI build 36). The RefSeq NM transcripts are dated from 3th April, 2007, and the GenBank putative full-length transcript are from 13 November, 2006. Controls served for positives in total 1.324 putative exon-level probes sets from putative constitutive genes and for negative 5.222 putative intron-level probes sets from putative constitutive genes. For Hybridization control bioB, bioC, bioD and cre was applied. Antigenomic Set was used for background probes with additional control for the PoyA tail including dap, lys, phe, thr. We accomplished the 1.0 ST Array with the recommended starting material of 100ng (without RiboMinus).

#### 5.2.1.3 Affymetrix®Gene 1.0 ST Array card quality control

For quality control Log probe cell intensity and relative Log Probe cell intensity prior analysis identified the quality of the Array. As some differences in the distribution of the different samples are normal, the divergent probe intensity distribution across all arrays are in the median level. RMA data was filtered for expression >200log and Agglomerative clustering excluded E13.5 negative sample from the dataset. We thereby separated the positive, negative and total pancreas samples. In the next step, heatmap generating with RMA data filtered for expression >200 in at least one group (19k probe sets remaining), sorted by ratio for positive and negative population. In this statistical analysis we excluded E13.5 positive population. In total one sample of 13.5 negative and positive population was excluded and E15.5 cDNA was in low range.

#### 5.2.1.4 Affymetrix®Gene 1.0 ST Array card analysis

The Affymetrix®Expression console was used for gene-level preprocessing (including quantile normalization). For statistical analysis we applied the Limma t-test (rawp) and although Benjamini-Hochberg (BH) multiple testing correction (FDR<5%). The analysis identified 2921 probe sets out of the dataset in the positive versus negative population with FDR<5% and ratio>2.

**Rainer, J., Sanchez-Cabo, F., Stocker, G., Sturn, A. and Trajanoski, Z. (2006).** CARMAweb: comprehensive R- and bioconductor-based web service for microarray data analysis. *Nucleic Acids Res* **34**, W498-503

positive population	rawp <0.005	rawp <0.005 ratio>2	FDR <5%	FDR <5% ratio>2
vs negative			11888	2921
E13.5 vs E12.5	528	14		
E13.5/14.5 vs E12.5	817	56		
E14.5 vs E13.5			743	238
E14.5 vs E13.5/12.5			4096	435
E15.5 vs E14.5			4390	253

**Table 8: Statistical analysis of the Affymetrix®Gene Array dataset.**

Applied rawp <0.005 calculated for the positive population in comparison of E13.5 to E12.5 528 probe sets and for E13.5/E14.5 in comparison to E12.5 817 different probe sets. Further mining with ratio>2 offered in the

positive population of E13.5 to E12.5 14 probe sets and for E13.5/E14.5 in comparison to E12.5 56 different probe sets. Applying FDR<5% showed 11888 different regulated genes between the positive and negative population. In detail for the E14.5 in contrast to E13.5 743 probe sets. For E14.5 versus E13.5/E12.5 4096 differentially regulated probe sets and for the time point E15.5 versus E14.5 4390 probe sets. In using FDR<5% and the ratio<2 we detected 2921 different regulated probe sets between positive and negative population. For the comparison of E14.5 and E13.5 there are 238 probe sets, for E14.5 versus E13.5/E12.5 435 probe sets and correlation between E15.5 and E14.5 showed 253 different regulated probe sets.

Group averages comparison (6 comparisons) and ratio>2, respective ratio>3 identified 1394 probe sets for the positive population and 1645 probe sets for the negative population. GO term analysis by Genomatix for these probe sets sorted the probe sets into specific term. The terms depicted are TF, signaling pathway, extracellular/located at Plasmamembrane; cilium related (Kim et al., PMID 2039563 screen for ciliogenesis modulators) and Riken. Probe sets which are not defined by GO term analysis are clustered to the term unclassified. It is to note that no statistic is applied.

#### **4.2.1.5 Pancreas gene selection using the digital database Genepaint.org**

The digital *in situ* atlas genpaint.org offers *in silico in situs* at E14.5. Comparison of the transcriptome dataset with the *in silico in situs* confirmed RNA expression. Applying the GO term analysis, sorted the probe sets into different clusters. For both tissue compartments we classified for the GO signaling (247), extracellular/located at PM (348), cilium related (43), TF (228) and unknown (20) in total for the both tissue compartments 886 non-redundant genes .

Additionally, function of the genes were annotated and RNA expression at E12.5, E13.5, E14.5 and E15.5. analyzed. Genes which are functionally not analyzed with RNA expression and *in silico in situ* expression at E14.5 had been selected as putative pancreatic genes. Further mining lead to a subset of candidate genes for knock in/knock out studies in mice.

#### **5.2.2 Cell culture**

For the purpose of gene targeting stable murine embryonic stem cells (ES) are needed. Mouse embryonic cells (MEF) which are mitotically inactivated prior ES cell addition allow stem cell culture without LIF (leukemia inhibitory factor).

### **5.2.2.1 Embryonic stem cell culture and spheres culture**

The MEF used for ES culture were cultured in 15 cm dishes in and supplied every 2-3 days with Feeder medium. Every 3-5 days the confluent MEFs had been splitted in a ratio 1:5 after washing with 10ml DPBS (-MgCl<sub>2</sub>) and 7ml Trypsin-EDTA treatment at 37°C for 4min. After resuspension for single cell suspension with 6ml medium, the suspension was transferred to 50ml falcon tube and centrifuged at 1200 rpm for 4min. The pellet with the cells was resuspended in using an appropriate volume of MEF medium and plated on new dishes.

### **5.2.2.2 Culture of primary murine embryonic fibroblasts**

For mitotical inactivation of the MEF cells treatment with mytomycin (MMC) was used.

MEF culturing until at least passage 4 assured confluency. After washing of five 5 cm dishes with 15ml DPBS (-MgCl<sub>2</sub>) and trypsination (0.05% Trypsin-EDTA) with 37°C for 4min we transferred the cells with 6ml into 50ml falcons. The supernatant of the centrifugation at 1200 rpm for 4min had been discarded. The pellet itself was washed twice and the cells plated on dishes for further use in ES cell culturing or freezing.

### **5.2.2.3 Treatment of MEF with mytomycin**

MEF out of the 15cm dishes had been transferred with freezer medium (2.5ml) into appropriate tubes and quickly frozen. By needs, 15cm dishes were coated with 0.1% gelatin and dried. The prepared ES cells were cultured on theses plates including MEF at 5-7% Co<sub>2</sub> in a humid incubator.

### **5.2.2.4 Freezing –Thawing of MEFs**

MEF out of the 15cm dishes had been transferred with freezer medium (2.5ml) into appropriate tubes and quickly frozen. By needs, 15cm dishes were coated with 0.1% gelatin and dried. The prepared ES cells were cultured on theses plates including MEF at 5-7% Co<sub>2</sub> in a humid incubator.

#### **5.2.2.5 Freezing –Thawing of ES cells**

Cryopreservation in liquid nitrogen of ES cells was implemented for long-term storage. Cells were trypsinized (see 5.2.1.1.2.), centrifuged and the resuspended pellet transferred to pre-cooled cryovial. The cryovials had been kept at least for 4h at -80°C to slowly lower the temperature before storage in the liquid nitrogen tank.

The thawing of the cryovial of ES cells was performed in a 37°C waterbath. After thawing the ES cells were transferred to a falcon with pre-warmed 10ml ES cell medium and centrifuged with 1200 rpm for 4min. The pellet was resuspended in an appropriate volume of ES cell medium and cultured on MEF at 5-7% CO<sub>2</sub> in a humid incubator.

#### **5.2.2.6 Passaging of ES cells**

For the passage of the ES cells medium was removed and cells washed with DPBS (-MgCl<sub>2</sub>). In the trypsination step (0.05% Trypsin-EDTA) after incubation for 5min at 37°C in the humid chamber, colony dissociation was confirmed by the microscope. ES cell medium was added to stop the reaction and pipetting by several times up and down should retained single cell suspension. The ES cells were transferred to a falcon tube and centrifuged with 1200rpm for 4min. The pellet was then resuspended in ES cell medium and plated on dishes. The splitting of the ES cells was in the range 1:5 – 1:20 depending on the calculated division rate. As mentioned in section 5.2.1.1.4. ES cells were cultured on MEF at 5-7% CO<sub>2</sub> in a humid incubator.

#### **5.2.2.7 Electroporation of ES cells**

For the generation of knock in mice the method of homologous recombination is used. The linearized targeting vector needs to be electroporated into ES cells. The ES cells with integrated targeting vector are selected by their resistance (neo) of the targeting vector (EUCOMM targeting strategy).

ES cells are trypsinized (see 5.2.1.1.6.) and half of a 10cm dish was transferred to a falcon tube. The single cell suspension was washed DPBS (-MgCl<sub>2</sub>), centrifuged with 1200rpm for 4min and resuspended

in 1.5ml ice-cold DPBS on ice. For the electroporation, 0.7ml of the cells was mixed with 100 $\mu$ l linearized targeting vector (25 $\mu$ g). After transferring the single cell suspension into an ice-cold cuvette, electroporation was carried out with following program:

pulses (on ice after the first pulse for 1min)

program: 220V

500 $\mu$ F

Resistance:  $\infty$

The cuvette was placed on ice after electroporation for additional 5min. Targeted ES cells had been transferred to pre-warmed dishes on MEF with ES cell medium. One electroporation step had been plated (0.4ml) on two 10cm dishes. The ES cell medium was changed daily. Selection for neomycin (300 $\mu$ g) started after 24h and after 6-8 days the clones could be picked.

### 5.2.2.8 Picking of ES cell clones

For the picking the selected ES cell clones, one conical 96-well plates with 60 $\mu$ l DPBS (-MgCl<sub>2</sub>)/well, one 96-well plates coated with 0.1% gelatin and one 96-well plate with MEF and 100 $\mu$ l ES selection media were prepared.

The 10cm dishes with ES clones were washed with 10ml DPBS (-MgCl<sub>2</sub>) and colonies picked under the stereomicroscope. Only roundish and compact ES cells were picked and transferred into the prepared conical 96-well plates with 60 $\mu$ l DPBS (-MgCl<sub>2</sub>). In the next step 30 $\mu$ l Trypsin-EDTA was added to the 96-well plate and incubated at 37°C for 15min. After the incubation, the ES cells had been pipetting up and down to assure single cell suspension. A volume of 50 $\mu$ l was transferred to the 96-well plates coated with 0.1% gelatin for DNA preparation and 50 $\mu$ l to the 96-well plate with MEF for Cryopreservation.

## 5.2 Molecular biology

### **5.3.1 DNA extraction**

#### **Isolation of genomic DNA from mouse tails**

For genotyping of the mice tails were clipped at approximately 4 week old mice. The 2mm tail had been transferred into a single tube with the corresponding number. After tail clipping, lysis followed by Lysisbuffer (500µl including ProteinaseK 50µg/500µl) and incubation for 55°C overnight. If the lysis was accomplished, the tail had been digested on the next day. In the next step, centrifugation at 14.000rpm for 10min spinned down undigested tissue and hair. The supernatant was transferred into a new tube and the DNA precipitated with 1x volume isopropanol. After centrifugation for 20min with 14.000rpm at 4°C, supernatant was discarded and the pellet washed twice with 1.5 volume 70% ethanol. Following the next centrifugation step with 12.000 rpm for 10min, the supernatant was discarded and the pellet air dried. The pellet was resuspended in 200-500µl H<sub>2</sub>O and 0.5-1.5µl were taken for genotyping of the mouse lines.

As an additional technique, the hot shot method was used for extraction of genomic DNA out of mouse tails. On the clipped tails 100 µl 0.5M NaOH had been pipetted and boiled for 10 min at 98°C. After cooling on ice for 5min, 30 µl of Tris pH 7.5 neutralized the solution. The further wash steps above are not applied in this methods as for genotyping at least 1-2µl were directly pipetted into the PCR reaction.

### **5.3.2 RNA preparation**

For RNA preparation, the Quiagen miRNeasy kit was used. As an additional method, Trizol had been used. In this case all solutions had been treated with diethylpyrocarbonate (DEPC) to ensure inactivation of RNAses, and therefore clean RNA extraction. The tissue was covered with 1ml Trizol (50-100mg tissue/ml Trizol) before homogenization with the Turax/Ultrasound. After homogenization, incubation for 5min at RT followed. In detail 0.2ml chloroform/1ml Trizol was added and the tube shaken vigorously. Centrifugation at 12.000rpm for 15min at 4°C followed after 2-3min incubation at RT. The first phase (aqueous) was then transferred to a new tube and RNA precipitation passed by adding 0.5ml isoprop/1ml Trizol. In the next step the supernatant was removed after 10min incubation at RT and centrifugation with 12.000rpm at 4°C. The pellet was washed in 1ml 75%EtOH/ml Trizol and vortexed. The washing included centrifugation at 7500rpm for 5min at 4°C and the supernatant was discarded. The pellet was air dried and resuspended in TE-buffer for stability of the RNA.

### 5.3.3 DNA/RNA concentration

The nanodrop determined the concentration of DNA and RNA by measuring the extinction photometrically. Purity of the samples are ensured by the quotient  $E_{260\text{nm}}/E_{280\text{nm}}$ , indicating by a range of 1.8-2.0 for DNA and RNA.

### 5.3.4 Reverse transcription

For reverse transcriptase reaction, the Superscript™ III Reverse Transcriptase Kit was used.

For first strand cDNA synthesis the following reaction was set up:

10pg-5µg RNA  
1.0 µl Oligo-dT-primer (50µM)  
Add to 13µl with DEPC-treated H<sub>2</sub>O

The solution was heat mixed at 65°C for 5 min and then put on ice. Afterwards the following solutions had been pipetted to the mixture:

4.0 µl 5x First strand buffer  
2.0 µl 0.1M DTT  
1µl RNaseOUT™ RNase Inhibitor  
1.0 µl 10mM dNTP Mix  
1.0 µl SuperScript™ III RT (200U/µl)

The tube was incubated for 5 min at 25°C. The next step contained incubation for 30-60min at 50°C. Afterwards the reaction was inactivated by heating up to 70°C for 15min. The cDNA was then ready for PCR reaction.

### 5.3.5 Gelelectrophorese

#### Analytical agarose gelelectrophoresis

Agarose was weighed out and transferred in a beaker with TAE (Tris-acetate, EDTA) buffer. The solution was heated up in the microwave, cooled down and 1:10.000 dilution of EtBr added. After mixing, the solution was poured into a gel tray with combs. When the agarose gel finally got solid, the tray was loaded into a gel chamber with TAE buffer. The pockets of the agarose gel were loaded with DNA marker and the DNA loading buffer mixture and voltage was turned on for a variable time (30-50min). Quantification of the agarose gel had been accomplished by using the UV lamp.

For the RNA agarose gel we used the same procedure except that all the material had been treated with RNase ZIP before and DEPC- H<sub>2</sub>O replaced H<sub>2</sub>O.

### 5.3.6 DNA sequencing

DNA sequencing verified the correct sequences in the by reading every single nucleotide.

The master mix for short sequences was pipetted as followed:

- 0.5 µl BigDye (contains polymerase)
- 2.0 µl BigDye-buffer
- 10 pM Primer (sense/antisense)
- (n) bp/100 = x ng
- Σ 5,0 µl

The PCR program used for amplification:

96°C 1 min

96°C 10 s }  
50°C 5 s } 35x  
60°C 4 min }

4°C ∞

Afterwards the sample had been precipitated by using the Qiagen Dye ex Spin Colum and spinning down for 15min at 12.000rpm. The DNA was then solved in 25µl HPLC-H<sub>2</sub>O.

## **5.4 Protein biochemistry**

### **5.4.1 Protein extraction from tissue**

The embryo was dissected and the brain/pancreas transferred to an tube and covered with RIPA buffer (included proteinase inhibitor 1:200). Homogenization and sonification was carefully carried out on ice. After incubation for 5min at RT, the solution was centrifuged at 14.000rpm and 4C for 12min. The supernatant contains the protein and was transferred to a new tube. The protein concentration was measured by Bradford (see 5.2.4.2.)

### **5.4.2 Bradford assay for determining protein concentration**

In the Bradford assay the Coomassie shifts the absorbance to 595nm by building a complex with basic residues of the protein. For determining the specific concentration of each sample, first of all a standard curve with known protein concentrations had to be implemented. The standard row was prepared starting with BSA concentration of 10µg/ml, 20µg/ml, 40µg/ml and 60µg/ml in lysis buffer, whereas the protein sample was diluted 1:10 in lysis buffer. The protein sample and standard curve samples together with the control (only lysis buffer) had been pipetted into cuvettes already prefilled with 990µl Bradford reagenz and incubated for 10min at RT. The concentration of the different samples including the dilution factor was determined by the nanodrop relative to the standard curve.

### **5.4.3 Western blot**

#### **SDS-polyacrylamide gelectrophorese (SDS-PAGE)**

In the SDS-PAGE proteins get separated by their size. For this purpose, already denaturated proteins are applied on a denaturated polyacrylamide gel and run by electrophoresis. After separation and blotting on a membrane, specific antibodies will detect the protein of interest

For 2 separating gels (10%) the following scheme was used:

- 5.0 ml acrylamide/bisacrylamide (ready-to-use, Biorad)
- 3.75 ml 4x Tris/SDS buffer, pH8.8
- 6.25 ml H<sub>2</sub>O
- 20.0 µl TEMED
- 150.0 µl APS

The prepared mixture was immediately poured between two glass plates and covered with Isopropanol. After polymerization the isopropanol was discarded.

In the next step 2 collecting gels were prepared:

- 0.65 ml acrylamide/bisacrylamide (ready-to-use, Biorad)
- 1.25 ml 4x Tris/SDS buffer, pH6.8
- 3.1 ml H<sub>2</sub>O
- 10.0 µl TEMED
- 50.0 µl APS

Again, the mixture was poured immediately between the glass plates and the comb was inserted between the glass plates.

The samples were prepared by mixing in a ratio 1:3 with 4x SDS loading buffer including dithiothreitol (DTT). In the denaturation step at 4min for 96C even the disulfide bridges will be diminished, ensuring denaturated proteins. Afterwards the samples had been cooled on ice.

The gels were placed into the running chamber and filled with 1x Tris-glycine. For loading the collection gel, combs were removed and rinsed with 1x Tris-glycine. Samples were pipetted into the pockets (including 5µl protein weight marker) and separated by 45mA for 1h.

As the protein size differs, the range of Acrylamid concentration changes for separation of proteins. Below shows a table for different protein sizes correlated to the Acrylamid concentration.

Acrylamid concentration (in%) correlates to protein size (kDa)

%	kDa
15.0	12-43
10.0	16-68
7.0	36-94
5.0	57-212

### **Semi-dry blot**

After SDS-PAGE the glass plates were separated and the gel equilibrated in KP buffer for 10 min. The PVDF/Nitrocellulose membrane was activated in methanol for 15 s, washed in H<sub>2</sub>O for 4 min and placed in APII buffer for 5 min.

The scheme of the blot as followed:

Anode

1x blotting paper (thick) soaked with API

1x blotting paper (thin) soaked with APII

PVDF-/Nitrocellulose membrane

SDS-PAGE

1x blotting paper (thick) soaked with KP

Cathode

Blotting was performed at 0.22A/gel for 20min. To ensure the transfer to the membrane, the membrane was put into Ponceaus S solution. Afterwards the membrane was washed out for the Ponceau S solution.

#### **5.4.4 Western blot immunostaining**

The membrane was blocked with blocking solution (1x TBST buffer + 5% milk powder (w/v) for 1.2h. After blocking, primary antibody was added (in blocking solution) and incubated ON at 4C.

On the next day, the membrane was washed 3x with 1x TBST for 10min. The secondary antibody (in blocking solution) was incubated at the membrane for 1-4h at RT/ ON at 4C. Afterwards the membrane was washed 2x with 1x TBST and put on saran foil. The enhanced chemiluminescence (ECL) solution was had been prepared and immediately pipetted onto the membrane. The foil was wrapped and placed in a film cassette. In the darkroom film were exposed between 1s up to 10min with subsequent developing of the films in the developing machine.

#### **5.4.5 Immunohistochemistry**

##### **Immunohistochemistry on Cryo sections**

Dissected pancreata were fixed in 4% paraformaldehyde (PFA) for 1h and subsequently incubated in a sucrose gradient/each gradient at least 1h (7%, 30%, 70%). In the last step tissue was incubated in OCT (optimal cutting temperature) medium and frozen in blocks at -20C. Immunohistochemistry was applied on 7 to 12 µm-thick sections which are mounted on coverslips.

Sections were rehydrated in 1x PBS, permeabilised in 0.1 M glycine/0.1% TritonX100 in PBS for 20min, and blocked for 1 h in blocking solution (see section 5.2.4.5.2.). After blocking, the primary antibody was incubated for at least 1h. The secondary antibody in blocking solution was applied ON at 4C next to the wash steps after primary antibody incubation. Slides were washed with PBS-T, incubated with DAPI in PBS for at least 20min and mounted with ProLong Gold antifade reagent (Invitrogen, P36930). For image acquisition Leica DMI 6000 confocal microscope and image analysis was carried out using Leica LAS AF software.

##### **Immunohistochemistry on whole mount pancreas**

Nakaya et al lately describe whole mount staining which we applied on the pancreas. The pancreas was dissected, fixed in 4% paraformaldehyde (PFA) and permeabilized according to the standard protocol (see section above). Antibody incubation had been accomplished ON for primary and secondary antibody. After immunohistochemistry, the tissue was dried out in a Methanol gradient (5%; 20%, 60%, 100%) and cleared with BABB. For imaging, the pancreas in BABB was embedded between 2 coverslips

(Secure-Seal spacer). Images are taken on the Leica DMI 6000 confocal microscope and analysis of the data by the Leica LAS AF software.

## 5.5 Embryology

### 5.5.1 Genotyping of mice and embryos

The weaning age of mice is defined at 4 weeks. In the weaning age the mice were tail clipped and genotyped by the method Isolation of genomic DNA from mouse tails (see section 5.2.3.1.)

#### Genotyping of *Foxa2*<sup>Venus</sup> mouse line

Genotyping of the *Foxa2*<sup>Venus</sup> intercrosses was performed by using the primer EP 38, Ep 397 and EP398. The 3 primer collection distinguished between *WT* allele (207bp), and mutant allele (506bp).

#### Genotyping of the *Syt13*<sup>GT</sup> mouse line

PCR genotyping of *Syt13*<sup>GT</sup> was accomplished in using Primer EP 1300 and EP 1301. The forward primer in Exon2 (EP1300) in combination with reverse primer in the 3'UTR site in *Syt13*<sup>GT</sup> (1301) distinguished between *WT* and mutant allele. For *WT* 490bp are expected in contrast to 559bp for the mutant allele.

#### Genotyping of the *Syt13*<sup>R</sup> mouse line

The PCR for this mouse line was performed by confirming the LAR site in the mutant allele with Primer EP1322, EP 1232 and EP 1224. After PCR amplification at 64C with 35 cycles *WT* and agarose gelelectrophorese *WT* exhibits 384bp, whereas the mutant allele 307bp. For distinguishing active *Cre*, Primer EP485 and EP486 result in no band (*WT*) and 450bp (mutant allele).

#### Genotyping of the *Grb7*<sup>GT</sup> mouse line

Primer *Grb7* forward (fw) and *Grb7* reverse (rev) were used to distinguish the *Grb7*<sup>GT</sup> allele from the *WT* allele. The PCR was accomplished with 35 cycles and an annealing temperature of 56C. Size differences in agarose electrophorese showed for the *WT* 236bp and for the targeted allele 314bp.

### Genotyping of the *Srpx2*<sup>GT</sup> mouse line

The forward Primer located in Exon 6 (*Srpx2* fwd) and a reverse primer (*Srpx2* rev) in the 3'UTR distinguished between *WT* with 570bp and targeted allele with 609bp. The PCR conditions were set up with 35 cycles and annealing temperature of 45C.

### Genotyping of the *Vwa5b2*<sup>GT</sup> mouse line

PCR genotyping of *Vwa5b2*<sup>GT</sup> mice was performed using the primer *Vwa5b2* fw, respective *Vwa5b2* rev (see oligonucleotide section). Using 35 cycles and the annealing temperature of 56C, PCR products distinguish between *WT* (234bp) and targeted allele (517bp).

### Genotyping of the *Scgn*<sup>GT</sup> mouse line

Was performed using a forward primer in the targeted exon (*Scgn* fw) and reverse primer in the 3'UTR. Amplification of 35 cycles with primer annealing at 55C ended in *WT* band size of 300bp versus targeted allele with 672bp.

### Genotyping of the *Flp-e*

The genotyping of the *Flp-e* mice was performed as previously described (Dymecki et al., 1996). In a PCR cycle of 35 and Primer EP176 and EP 177 the mutant allele exhibits a band in the agarose gel at 600bp.

## 5.5.2 PCR Programs for genotyping

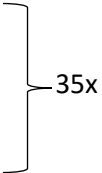
### *Foxa2*<sup>Venus</sup> PCR program

96°C 1 min	}	35x
96°C 10 s		
56°C 5 s		
60°C 4 min		

4°C ∞

**Syt13<sup>GT</sup> PCR program**

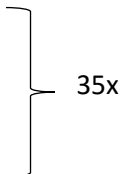
96°C 1 min  
96°C 10 s  
55°C 5 s  
60°C 4 min  
4°C ∞



35x

**Syt13<sup>R</sup> PCR program**

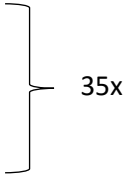
96°C 1 min  
96°C 10 s  
64°C 5 s  
60°C 4 min  
4°C ∞



35x

**Grb7<sup>GT</sup> PCR program**

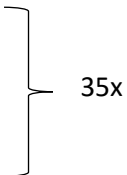
96°C 1 min  
96°C 10 s  
56°C 5 s  
60°C 4 min  
4°C ∞



35x

**Srpx2<sup>GT</sup> PCR program**

96°C 1 min  
96°C 10 s  
45°C 5 s  
60°C 4 min  
4°C ∞



35x

***Vwa5b2*<sup>GT</sup> PCR program**

96°C 1 min  
96°C 10 s  
56°C 5 s  
60°C 4 min  
4°C ∞

} 35x

***Scgn*<sup>GT</sup> PCR program**

96°C 1 min  
96°C 10 s  
55°C 5 s  
60°C 4 min  
4°C ∞

} 35x

***Flp-e* PCR program**

96°C 1 min  
96°C 10 s  
50°C 5 s  
60°C 4 min  
4°C ∞

} 35x

**5.5.3 Isolation of embryos and organs**

The embryos and organs were dissected in line with Nagy and Behringer (Manipulating the mouse embryo: a laboratory manual).

**5.5.4 Tissue clearing with BABB**

For BABB clearing tissue was dried out carrying out a methanol gradient (5%; 20%, 60%, 100%). Each series was at least incubated for 2h. Briefly, BABB solution was prepared including 1:2 benzyl alcohol and benzyl benzoate and the tissue embedded until cleared. Imaging acquisition had been accomplished either on the Zeiss Lumar.V12 Stereo using an AxioCam MRc5 camera or the Leica DMI 6000 confocal microscope.

### 5.5.5 X-gal (5-bromo-4-chloro-3-indolyl $\beta$ -D-galactoside) staining

*$\beta$ -gal* staining of organs and embryos was performed as previously described (Liao et al., 2009). The tissue was fixed in PFA and stored in PBS prior image acquisition. Images are taken at the Zeiss Lumar.V12 Stereo microscope using an AxioCam MRc5 camera. For some samples BABB clearing was accomplished for higher resolution of the  *$\beta$ -gal* staining (see section above).

## 5.6 Histology

### 5.6.1 Paraffin sections

Samples after  *$\beta$ -gal* staining were fixed in PFA and washed in PBS. Subsequent gradient with ethanol/methanol (5%; 20%, 60%, 100%) dehydrated the tissue sample. In the last step 100% ethanol/methanol was repeated before clearing in Xylol for 2x 5min. The sample was embedded in paraffine and incubated ON at 65C. This was accomplished on the next day again. Right after 2 day incubation in paraffin, sample was embedded in a mold and orientated. Shortly after cooling down of the paraffin block, mounting on a grid followed. Sectioning of the sample was accomplished using the microtome, standardized sectioning thickness is thereby dependent on the tissue (range 4 $\mu$ m up to 10 $\mu$ m). For each glass slide approximately 2 sections were mounted. The sections were dried in an incubator at 37C ON, dewaxed in xylol (2x5min) and mounted with mounting media and covered with a cover slip. On the next day sections had been ready for imaging at the Zeiss Lumar.V12 Stereo microscope using an AxioCam MRc5 camera.

### **5.6.2 Counterstaining with Nuclear Fast Red (NFR)**

The paraffin section were dewaxed for 20min in xylene. Rehydration followed by a gradient of ethanol (100%, 60%, 20%, 5%), each step with 10min incubation. The NFR staining started with tab H<sub>2</sub>O for 3min followed by 45sec in NFR staining solution. The slides were washed in dist. H<sub>2</sub>O and dehydrated using the reverse gradient from before (5%; 20%, 60%, 100%). The last step contained incubation for 5-10 min in xylene and 5-10min in rotiphorese and mounting with mounting media. On the next day sections were ready for documentation.

### **5.6.3 Cryosections**

After dissection, tissue was fixed in 4% PFA in between 10min (RT) and ON (4°C) depending on the thickness of the organ. The tissue was washed 2x 5min in 1x PBS and incubated in a sucrose gradient from 7%, 15%, 30%, each step at least for 4h. Saturation of the tissue with sucrose was indicated by the tissue at the bottom of the vial. In the last step 1:2 solution of 30% sucrose and OCT was used as embedding media. After incubation, tissue was transferred to an embedding mold and orientated. Freezing was accomplished by dry ice and stored at -80C. Prior sectioning, tissue samples were deposit at -20 for 1h. Sectioning was carried out at the cryostat with section thickness between 7µm – 12µm.

## 6 Supplement

### 6.1 Abbreviations

% percent

μ micro

AA amino acid

AB apical-basal

ADAMTS adam metalloproteinase

AFF AF4/FMR2 family, member

AGO argonaute

AIP anterior intestinal portal

AJ adherens junctions

AJC adherens junction complex

AL apical-lateral

AMY amylase

AP anterior-posterior

APPL adaptor protein, phosphotyrosine Interaction, PH Domain and leucine zipper containing

APS ammoniumperoxosulfide

ARP actin-related protein

ARX aristaless related homeobox

ATPB sodium/potassium-transporting ATPase subunit beta

AVE anterior visceral endoderm

B bos

BABB bis(dimethylamino-)bis(n-fluosulfonylimodo-)-sulfate

BASO\_ST\_KIN basophilic serine/threonine kinase

BB basal body

BBS bardet-biedl syndrome

BCAP b-cell receptor associated protein

BM basement membrane

BMI body mass index

BMP bone morphogenetic protein

BP base pairs

BRDU bromdeoxyuridine

BSA bovine serum albumine

CA california

CAM cell adhesion molecules

CAMK2G calmodulin dependent Kinase 2

CARMAWEB comprehensive r based microarray analyses web fronted

CBX chromobox protein homolog

CC/C cerebral cortex

CCKAR cholecystokinin a receptor

CD24 small cell lung carcinoma cluster 4

CD49F integrin alpha 6

CDC cell division control

CDNA complementary DNA

CE critical exon

CEL carboxyl ester lipase

CELA chymotrypsin-like elastase family

CHIP-SEQ chromatin immunoprecipitation DNA-sequencing

CIP caudal intestine portal

CIS ciston

CKO conditional knock out

CLCA chloride channel accessory

CLDN caudin

CLPS colipase

CLU clusterin

COL collagen

COL6A collagen type VI alpha

CPA carboxypeptidase a

CPE carboxypeptidase e

CRB crumbs

CRE causes recombination

CSF cerebrospinal fluid  
CT cyst structures  
CTRB chymotrypsinogen b  
CV cavities  
D danio  
D dentate gyrus  
DAPI 4',6-Diamidin-2-phenylindol  
DCN decorin  
DE definitive endoderm  
DEK DEK proto-oncogene  
DLG giant larvae homologue  
DLL delta-like  
DMEM dulbeccos modified eagle medium  
DNA desoxyribonucleine acid  
DSH disheveled  
DT ductal  
DTT dithiotreitol  
DVE distal visceral endoderm  
E embryonic stage  
ECAD e-cadherin  
ECM extracellular matrix  
EDARADD EDAR-associated death domain  
EDTA ethylenediaminetetraacid  
EET epithelial-to-epithelial transition  
EGTA ethyleneglycolaminoethylether  
EMT epithelial-to-mesenchymal transition  
EN1/2 engrailed homeobox 1/2  
EN2 = engrailed homeobox 2  
ENPP ectonucleotide pyrophosphatase/phosphodiesterase  
EP primer  
EPHA EPH receptor a  
EPI epiblast

ES embryonic stem  
EST expressed sequence tag  
EXE extraembryonic tissue  
FACS fluorescent activated cell sorting  
FAG facio-acoustic ganglia  
FB fibrillin  
FCS fetal calf serum  
FDR false discovery rate  
FGF fibroblast growth factor  
FLP flippase  
FLPE enhanced flippase  
FLTP flattop  
FMO flavin containing monooxygenase  
FOX winged helix/forkhead box  
FP floor plate  
FRT flippase recognition target  
FVF foxa2-venus-fusion  
FZD frizzled  
G generation  
GAS growth-arrest-specific *gene*  
GATA gata binding protein  
GBM glioblastoma  
GC group specific component  
GCG glucagon  
GFP green fluorescent protein  
GHRL ghrelin  
GLP glypican  
GO gene ontology  
GPC glypican  
GRB growth factor receptor-bound  
GRN gene regulatory network  
GSIS glucose-stimulated insulin secretion

GT gene trap  
GTT2H general transcription factor IIH, polypeptide  
GWAS genome wide association study  
H homo  
H human  
H3K27ac histone 3 lysine 27 acetylation  
H3K4me histone 3 lysine 4 methylation  
HAHP hyaluronan binding protein  
HBAP human beta act promoter  
HEPACAM HEPACAM family member  
HES hairy and enhancer of split  
HF hair follicle  
HHEX hematopoietically expressed homeobox  
HIGH MAGN higher magnification  
HLXB homeobox protein hHB  
HNF hnf homeobox  
IAPP islet amyloid polypeptide  
ICM inner cell mass  
IFT intraflagellar transport  
IGF insulin-Like Growth Factor  
IGFBP insulin-like growth factor binding protein  
IHC immunohistochemistry  
IL islets of langerhans  
IL11RA interleucin 11 receptor, alpha  
INS Insulin  
INSRR insulin receptor related receptor  
IRES internal ribosome entry-site  
ISL isl lim homeobox  
JAM junctional adhesion molecules  
K thousand/1000  
KB kilo bases  
KD kilo dalton

KEGG kyoto encyclopedia of genes and genome  
KIF kinesine heavy chain member  
KIN\_BIND kinase binding site  
L lumen  
LACZ  $\beta$ -galactosidase  
LEF lymphoid enhancer-binding factor 1  
LIF leukemia inhibitory factor  
LM length marker  
LOG logarithm  
LOXP site-specific recombinase Cre  
LRP lipoprotein receptor-related protein  
LUM lumican  
M month  
M mus  
MAFB maf musculoaponeurotic fibrosarcoma oncogene homolog B  
MAMDC mam domain containing  
MAPK mitogen activated protein kinase  
MAPK1 ERK d-domain  
MATN matrilin  
MDCK madin-darby canine kidney  
MED/GATA gata transcription factor  
MEIS meis homeobox  
MET mesenchymal-to-epithelial transition  
MET MET proto-oncogene  
MGO mago nashi-like protein  
MIR microRNA  
MIST/BHLHA basic helix-loop-helix protein  
MM messenger  
MMC mytomycin  
MNX moto neuron and pancreas homeobox  
MODY maturity onset diabetes of the young  
MOE main olfactory epithelium

MPC multipotent pancreatic cells  
MPP multipotent pancreatic progenitors  
MRNA messenger ribonucleotide acid  
MYT myelin transcription factor  
N nano  
NEK nima-related kinase  
NEO neomycin  
NEUROD neuronal differentiation  
NFIX nuclear Factor I/X  
NFT nuclear fast red  
NGN neurogenin  
NGT normal glucose tolerant  
NICD notch intracellular domain  
NKX nk homeobox x  
NMD nonsense-mediated decay  
NO/N number  
NR5A nuclear receptor subfamily 5 group a  
NWASP neuronal wiskott-aldrich syndrome  
ON over nighth  
ONECUT one cut homeobox  
ORF open reading frame  
OSR odd-skipped related  
OTX/DMBX orthodenticle homolog/diencephalon/mesencephalon homeobox  
OV opticle ventricles  
P postnatal  
PA polyadenylation site/ sv40 large t gene  
PA sc40 large T gen  
PAMR peptidase domain containing associated with muscle regeneration  
PAR partitioning defective protein  
PAX paired homeobox x  
PB pancreatic bud  
PC principal component

PCH/VRK vaccinia related kinase  
PCP planar cell polarity  
PCR polymerase chain reaction  
PD proximal-distal  
PDGFC platelet derived growth factor c  
Pdx pancreatic and duodenal homeobox  
PE pancreatic epithelium  
PFA paraformaldehyde  
PGK phosphor-glycerate kinase  
PIFO pitchfork  
PKD polycystic kidney disease  
PL primary lumen  
PMP pancreatic multipotent progenitors  
PNLIPRP pancreatic lipase-related protein  
PP pancreatic polypeptide  
PRE primitive endoderm  
PRG posterior root ganglions  
PRKCZ PKC $\zeta$   
PRSS protease, serine  
PS primitive streak  
PTDINS(4,5)P<sub>2</sub> phosphatidylinositol-4,5-biphosphate  
PTF pancreas specific transcription factor  
PTPN protein Tyrosine phosphatase non-receptor type  
PYCR pyrroline-5-carboxylate reductase family, member  
R rattus  
R rosa  
R26R Rosa26  
RA retinoic acid  
RAC ras-related C3 botulimum toxin substrate  
RBM RNA binding motif protein  
RBPJ recombining binding protein suppressor of hairless  
REEP receptor accessory protein

RFX regulatory factor X

RIK RIKEN cDNA

RIPA radioimmunoprecipitationbuffer

RMA robust multichip-analyses

RNA ribo nucleotide acid

ROS reactive oxygen species

ROSA26 R26R

RT real time

RUNX runt-related transcription factor

SA splice acceptor

SCGN secretagoin

SCRIB scribble

SD standard deviation

SDS sodium dodecyl sulfide

SEM secondary raster electron microscopy

SEQ sequencing

SERPINA serine/cysteine peptidase inhibitor clade a

SFRP secreted frizzled-related protein

SHH sonic hedgehog

SLC solute carrier family

SMARCA swi/snf family

SNAIL snail family zinc finger

SNARE n-ethylmaleimide-sensitive-factor attachment receptor

SNP single nucleotide polymorphism

SOSTDC sclerostin domain containing

SOX sry related homeobox

SRPR signal recognition particle receptor

SRPX sushi-repeat containing protein, X-linked

$\beta$ -GAL  $\beta$ -galactosidase

SYT synaptotagmin

T1D type 1 diabetes

T2D type 2 diabetes

TAE tris-acetate

TCF4 tcf7l2

TE trophectoderm

TENC tensin-like c domain-containing phosphatase

TF transcription factor

TG trigeminal ganglion

THBS thrombospondin

TINAGL tubulointerstitial nephritis antigen-like

TJ tight junctions

TM trademark

TMD transmembrane domain

TMEM transmembrane protein

TRIS trometamol

TRPS trichorhinophalangeal Syndrome I

TSNARE trans-soluble N-ethylmaleimide-sensitive-factor attachment receptor

TSS/R transcriptional start site/region

TWIST twist family bhlh transcription factor

UTR untranslated region

VMAFB v-maf musculoaponeurotic fibrosarcoma oncogene homolog B

VTN vitronectin

VWA von Willebrand factor A domain containing

W week/s

WNT wingless-type MMTV integration site family

WT wild type

XGAL 5-bromo-4-chloro-3-indolyl  $\beta$ -D-galactoside

ZA zonula adherens

ZEB zinc finger e-box binding homeobox

ZO zonula occludens

## 6.2 Figures and tables

Figure 2.1: Early stages of mouse development.....	9
Figure 2.2: Tubulogenesis of the embryonic pancreas.....	13
Figure 2.3: Lineage hierarchy of the pancreatic lineages with cell specific genes for the adult pancreas (A) and the embryonic pancreas from multipotent state to the mature $\beta$ cell (B).....	15
Figure 2.4: The epithelial polarity program players.....	20
Figure 2.5: Model of <i>Synaptotagmin 1</i> promoting membrane fusion.....	22
Figure 3.1: Targeting strategy of the <i>FVF</i> allele.....	25
Figure 3.2: <i>FVF</i> and <i>Cpa1</i> co-localize in the PE.....	26
Figure 3.3: <i>FVF</i> and <i>Pax6</i> co-localize in the PE.....	27
Figure 3.4: <i>FVF</i> and <i>Nkx6-1</i> co-localize in the PE.....	28
Figure 3.5: <i>FVF</i> and <i>Hnf1<math>\beta</math></i> co-localize in the PE.....	29
Figure 3.6: <i>FVF</i> and <i>Sox9</i> co-localize in the PE.....	29
Figure 3.7: <i>FVF</i> expression after secondary transition correlates to the endocrine lineage commitment.....	31
Figure 3.8: Experimental setup for the gene regulatory network (GRN).....	33
Figure 3.9 : The GRN in the pathway analysis.....	34
Figure 3.10: The GRN in endodermal and non-endodermal tissue populations.....	36
Figure 3.11: The TF of EMT in the GRN.....	38
Figure 3.12: Experimental setup for expression pattern analysis. ....	40
Figure 3.13: Representative pancreatic genes classified into specific expression patterns.....	41
Figure 3.14: Temporal and spatial expression of depicted known pancreatic genes and the classical PE/trunk <i>in silico in situ</i> pattern obtained by Genepaint.....	44
Figure 3.15: Temporal and spatial expression of depicted known pancreatic genes and the classical trunk <i>in silico in situ</i> pattern obtained by Genepaint.....	45
Figure 3.16: Temporal and spatial expression of depicted known pancreatic genes and the classical mesenchymal <i>in silico in situ</i> pattern obtained by Genepaint.....	46
Figure 3.17: Temporal and spatial expression of depicted genes functionally not described in pancreas organogenesis and the <i>in silico in situ</i> pattern classified as PE/trunk obtained by Genepaint.....	48
Figure 3.18: : Temporal and spatial expression of depicted functionally not described genes reflecting a classical tip <i>in silico in situ</i> pattern hybridization pattern.....	49
Figure 3.19: Temporal and spatial expression of genes, functionally not described in pancreas organogenesis, selected due to a comparabel mesenchymal hybridization pattern in Genepaint.....	51
Figure 3.20: Spatial expression of the <i>Syt</i> isoforms ( <i>Syt1-17</i> ) in whole mount embryo and in the pancreatic region.....	53

Figure 3.21: Spatial expression of the <i>Ngn3</i> and <i>Syt13</i> in the pancreatic region.....	54
Figure 3.22: Profile-profile alignment of SYT13 sequences to the references database scansite.org.....	55
Figure 3.23: ChIP-seq of maturity Islet of Langerhans transcription factor (TF) with corresponding RNA seq data of <i>PDX1</i> and <i>SYT13</i> .....	56
Figure 3.24: The complementary deoxyribonucleic acid (cDNA) sequence of the gene <i>Syt13 mus musculus</i> .....	58
Figure 3.25: The aa sequence of <i>Syt13</i> in <i>mus musculus</i> . .....	59
Figure 3.26: The orthologous of the protein <i>Syt13</i> .....	59
Figure 3.27: Targeting strategy of the <i>Syt13</i> allele.....	60-61
Figure 3.28: Verification of the <i>Syt13<sup>GT</sup></i> allele by PCR, Western blot and RT-PCR.....	61
Figure 3.29: Whole mount <i>LacZ</i> staining of the embryo at E9.5.....	66
Figure 3.30: The $\beta$ -gal activity reflects distinct expression pattern in the early mouse embryo at E11.5.....	67
Figure 3.31: <i>LacZ</i> - reporter analyses in the crown at E14.5 (A - B) and E15.5 (C - D).....	68
Figure 3.32: Reporter gene expression in the crown of 10 w mice (A-D), respective <i>WT</i> and <i>Syt13<sup>GT/GT</sup></i> illustrating a hydrocephalus (E).....	69
Figure 3.33: <i>Syt13</i> reporter gene expression in the Islets of Langerhans and in cystic structures.....	71
Figure 3.34: Islets of Langerhans in <i>Syt13<sup>GT/GT</sup></i> are streaked along the pancreatic duct and enlarged.....	72
Figure 3.35: <i>Syt13</i> shows periductal accumulation in the pancreas.....	74
Figure 3.36: The precursor Islets of Langerhans in <i>Syt13</i> deficient mice illustrate Superislets along with a lower quantity of the $\beta$ -cell mass.....	76
Figure 3.37: In the secondary transition of the pancreas the endocrine precursor pool is characterized through <i>Syt13<sup>high</sup></i> .....	78-79
Figure 3.38: After secondary transition of the pancreas the endocrine progenitors and endocrine cells are expressing <i>Syt13</i> .....	80
Figure 3.39: In the <i>Syt13<sup>R/R</sup></i> mutants precursor Islets of Langerhans are disorganized with a decreased quantity of $Ins^+$ cells.....	81
Figure 3.40 SNP in rs1038374 and rs28374189 correlate to T2D susceptibility.....	83
Figure 3.41: FVF, Pdx1 and <i>Syt13</i> co-localize in the PE.....	84
Figure 3.42: The endocrine precursors fail to delaminate into the PE in <i>Syt13<sup>R/R</sup></i> pancreata.....	85-86
Figure 3.43: <i>Syt13</i> co-localizes to <i>Ngn3</i> in the PE at E14.5.....	87
Figure 3.44: Sphere-forming assay of the different genotypes <i>WT</i> , <i>Syt13<sup>GT/-</sup></i> and <i>Syt13<sup>GT/GT</sup></i> .....	89-90
Figure 3.45: Cell Polarity is altered in the PE of <i>Syt13</i> deficient mice.....	91
Figure 3.46: <i>Syt13</i> is expressed in the MPP with multinucleated rosette-like structures in the PE at E14.5.....	92
Figure 3.47: <i>Syt13</i> deficiency results in a multinucleated PE and affects AB polarity.....	94
Figure 6.1 <i>Syt13</i> co-localizes to F-Actin and reveals anti-correlated expression in the process of endocrine formation.....	214

Figure 6. 2 FVF, Ngn3 and Nkx6-1 co-localize in the PE in the process of lineage segregation at E14.5.....215

Table 1: *Syt13*<sup>GT/-</sup> CD1 G2 intercrosses.....63

Table 2: *Syt13*<sup>GT/-</sup> C57Bl/6J G2 intercrosses.....63

Table 3: *Syt13*<sup>GT/-</sup> C57Bl/6J G1 intercrosses.....64

Table 4: *Syt13* C57Bl/6J G2 intercrosses.....64

Table 5: *Syt13*<sup>R/R</sup> C57Bl/6J G2 dead pups at P1.....65

Table 6: List of primary antibodies used in this thesis. ....122

Table 7: List of secondary antibodies used in this thesis.....123

Table 8 Statistical analysis of the Affymetrix®Gene Array dataset.....129

Table 9: Associations of *SYT13* tagging SNPs with insulin secretion *in vivo*.....159-161

Table 10: GenePaint *in silico in situs* of whole mount embryos at E14.5 and a higher magnification of the pancreatic region.....162-196

Table 9: Associations of *SYT13* tagging SNPs with insulin secretion *in vivo* (N =2100).

	Genotype	N	Insulinogenic index (*10 <sup>-9</sup> )	AUC <sub>Ins0-30</sub> /AUC <sub>Glc0-30</sub> (*10 <sup>-9</sup> )	AUC <sub>C-pep0-30</sub> /AUC <sub>Glc0-30</sub> (*10 <sup>-9</sup> )	AUC <sub>C-pep0-120</sub> /AUC <sub>Glc0-120</sub> (*10 <sup>-9</sup> )
rs6416129	CC	1,513	172 ±164	47.0 ±33.1	201 ±76	314 ±100
	CA	477	167 ±144	48.7 ±38.0	203 ±82	317 ±105
	AA	37	167 ±187	45.4 ±39.8	195 ±101	305 ±133
pAssociation	-	-	0.3	0.8	0.7	0.9
pGender interaction	-	-	0.8	0.5	<b>0.0207</b>	0.1
pBMI interaction	-	-	0.5	0.9	0.7	0.8
pIS interaction	-	-	0.1	0.5	0.4	0.6
pGlc interaction	-	-	<b>0.0449</b>	0.6	0.08	0.06
rs1077490	GG	998	168 ±176	46.3 ±34.0	199 ±78	311 ±103
	GA	907	170 ±133	48.1 ±34.5	204 ±76	320 ±98
	AA	191	184 ±181	47.7 ±33.0	200 ±82	311 ±106
pAssociation	-	-	0.06	0.1	0.5	0.3
pGender interaction	-	-	0.1	0.4	0.07	<b>0.0385</b>
pBMI interaction	-	-	0.5	1.0	0.9	0.4
pIS interaction	-	-	0.8	0.7	0.7	0.4
pGlc interaction	-	-	0.2	0.1	0.5	0.7
rs11038371	GG	617	171 ±194	45.3 ±32.3	197 ±75	310 ±100
	GA	1,041	168 ±132	48.1 ±34.5	204 ±77	317 ±100
	AA	442	174 ±164	47.7 ±35.6	200 ±82	315 ±105
pAssociation	-	-	0.7	0.2	0.9	0.6
pGender interaction	-	-	0.3	0.8	0.8	0.3
pBMI interaction	-	-	0.1	0.8	0.7	0.4
pIS interaction	-	-	0.3	0.9	0.2	0.3
pGlc interaction	-	-	0.5	0.2	0.1	0.4

	Genotype	N	Insulinogenic index (*10 <sup>-9</sup> )	AUC <sub>Ins0-30</sub> /AUC <sub>Glc0-30</sub> (*10 <sup>-9</sup> )	AUC <sub>C-pep0-30</sub> /AUC <sub>Glc0-30</sub> (*10 <sup>-9</sup> )	AUC <sub>C-pep0-120</sub> /AUC <sub>Glc0-120</sub> (*10 <sup>-9</sup> )
rs2863176	GG	647	170 ±147	47.1 ±32.0	199 ±72	313 ±95
	GA	1,032	172 ±157	47.8 ±34.8	203 ±79	318 ±103
	AA	417	167 ±182	45.9 ±35.6	199 ±82	309 ±106
pAssociation	-	-	0.2	0.3	0.9	0.6
pGender interaction	-	-	0.2	0.2	<b>0.0291</b>	<b>0.0334</b>
pBMI interaction	-	-	0.5	0.4	0.3	0.9
pIS interaction	-	-	0.4	0.2	0.2	0.6
pGlc interaction	-	-	0.3	0.3	0.9	0.5
rs7942231	GG	565	173 ±199	45.7 ±32.7	198 ±76	311 ±102
	GC	1,000	168 ±132	48.0 ±34.7	204 ±77	317 ±100
	CC	459	176 ±163	47.9 ±35.8	200 ±82	316 ±106
pAssociation	-	-	0.3	0.1	0.8	0.5
pGender interaction	-	-	0.2	0.8	0.8	0.3
pBMI interaction	-	-	0.1	0.9	0.8	0.4
pIS interaction	-	-	0.1	0.6	0.2	0.2
pGlc interaction	-	-	0.4	0.2	0.3	0.8
rs4755307	TT	1,578	172 ±164	46.8 ±32.9	200 ±76	313 ±100
	TC	473	167 ±141	48.9 ±37.6	205 ±81	320 ±104
	CC	37	166 ±188	44.2 ±39.1	195 ±100	305 ±131
pAssociation	-	-	0.3	0.6	0.9	0.5
pGender interaction	-	-	0.5	0.3	<b>0.0170</b>	0.2
pBMI interaction	-	-	0.7	0.7	0.4	0.4
pIS interaction	-	-	0.2	0.8	0.4	0.8
pGlc interaction	-	-	<b>0.0155</b>	0.8	0.07	0.08

	Genotype	N	Insulinogenic index (*10 <sup>-9</sup> )	AUC <sub>Ins0-30</sub> /AUC <sub>Glc0-30</sub> (*10 <sup>-9</sup> )	AUC <sub>C-pep0-30</sub> /AUC <sub>Glc0-30</sub> (*10 <sup>-9</sup> )	AUC <sub>C-pep0-120</sub> /AUC <sub>Glc0-120</sub> (*10 <sup>-9</sup> )
rs11601021	TT	999	168 ±147	47.1 ±34.2	199 ±76	314 ±100
	TC	909	175 ±159	48.3 ±34.0	205 ±79	318 ±103
	CC	189	163 ±215	42.3 ±33.6	192 ±76	299 ±98
pAssociation	-	-	0.5	0.1	1.0	0.5
pGender interaction	-	-	0.3	0.4	0.5	0.2
pBMI interaction	-	-	0.8	0.2	0.1	0.6
pIS interaction	-	-	0.8	0.4	0.4	0.8
pGlc interaction	-	-	0.4	0.2	0.1	0.4
rs7482931	GG	1,680	173 ±165	47.3 ±33.9	201 ±77	314 ±102
	GA	320	162 ±131	48.0 ±37.2	202 ±80	318 ±101
	AA	26	179 ±198	43.9 ±36.2	197 ±98	311 ±138
pAssociation	-	-	0.2	0.9	0.7	0.7
pGender interaction	-	-	0.5	0.4	0.9	0.4
pBMI interaction	-	-	0.2	0.3	0.8	1.0
pIS interaction	-	-	<b>0.0306</b>	0.1	0.2	0.6
pGlc interaction	-	-	0.3	0.5	0.3	0.4
rs11038374	TT	1,772	168 ±149	47.2 ±33.5	200 ±77	313 ±101
	TG	308	183 ±210	47.5 ±37.7	203 ±81	320 ±103
	GG	8	151 ±101	38.9 ±19.9	209 ±83	335 ±110
pAssociation	-	-	<b>0.0169</b>	<b>0.0427</b>	<b>0.0096</b>	<b>0.0026</b>
pGender interaction	-	-	<b>0.0258</b>	0.09	1.0	0.6
pBMI interaction	-	-	0.3	0.08	0.1	1.0
pIS interaction	-	-	0.4	0.2	0.2	0.8
pGlc interaction	-	-	0.5	0.1	0.07	0.1

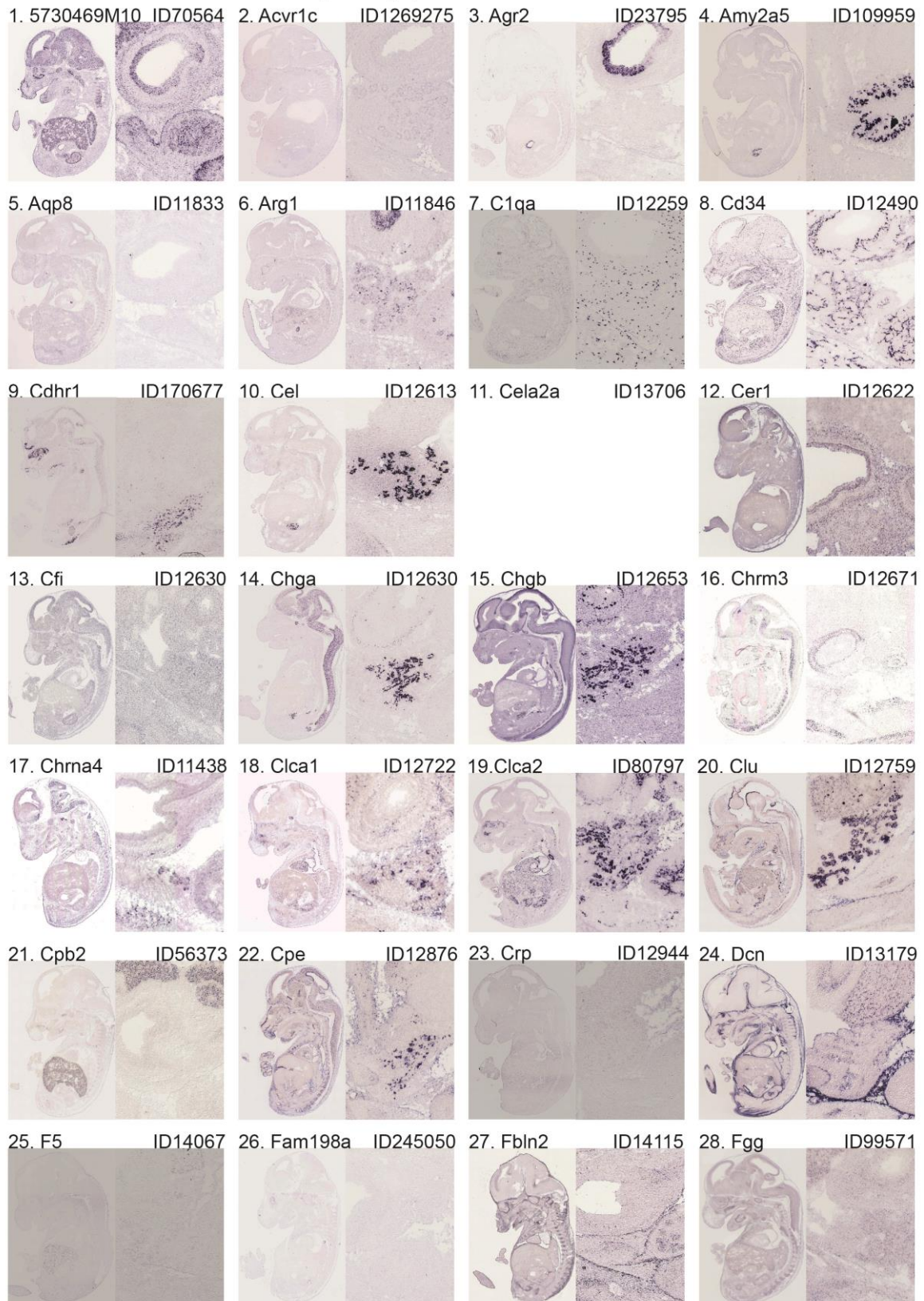
	Genotype	N	Insulinogenic index (*10 <sup>-9</sup> )	AUC <sub>Ins0-30</sub> /AUC <sub>Glc0-30</sub> (*10 <sup>-9</sup> )	AUC <sub>C-pep0-30</sub> /AUC <sub>Glc0-30</sub> (*10 <sup>-9</sup> )	AUC <sub>C-pep0-120</sub> /AUC <sub>Glc0-120</sub> (*10 <sup>-9</sup> )
rs10838436	CC	785	167 ±147	46.5 ±33.8	199 ±77	313 ±99
	CT	1,012	174 ±152	48.6 ±34.6	204 ±79	317 ±103
	TT	294	164 ±206	43.9 ±33.0	196 ±75	308 ±100
pAssociation	-	-	0.5	0.3	0.9	0.7
pGender interaction	-	-	0.2	0.4	0.5	0.1
pBMI interaction	-	-	0.4	1.0	0.8	0.7
pIS interaction	-	-	0.3	0.9	1.0	0.8
pGlc interaction	-	-	1.0	0.07	<b>0.0386</b>	0.1
rs26374189	GG	1,849	170 ±153	47.4 ±34.6	202 ±78	315 ±102
	GA	175	186 ±227	47.0 ±33.1	200 ±76	311 ±102
	AA	1	107	18.0	192	323
pAssociation	-	-	0.4	1.0	0.9	0.6
pGender interaction	-	-	<b>0.0381</b>	0.09	<b>0.0053</b>	<b>0.0006</b>
pBMI interaction	-	-	0.6	0.9	1.0	0.9
pIS interaction	-	-	0.3	0.7	0.8	0.7
pGlc interaction	-	-	0.4	0.6	0.8	0.5
rs2863181	AA	1,475	170 ±164	47.2 ±34.6	200 ±77	314 ±102
	AG	564	171 ±148	47.0 ±32.9	203 ±78	316 ±98
	GG	56	180 ±137	49.3 ±34.2	199 ±86	310 ±116
pAssociation	-	-	0.5	0.7	0.9	0.9
pGender interaction	-	-	0.7	0.9	0.8	0.3
pBMI interaction	-	-	0.1	0.5	0.7	0.3
pIS interaction	-	-	1.0	0.8	0.7	0.6
pGlc interaction	-	-	0.3	0.1	0.1	0.4

	Genotype	N	Insulinogenic index (*10 <sup>-9</sup> )	AUC <sub>Ins0-30</sub> /AUC <sub>Glc0-30</sub> (*10 <sup>-9</sup> )	AUC <sub>C-pep0-30</sub> /AUC <sub>Glc0-30</sub> (*10 <sup>-9</sup> )	AUC <sub>C-pep0-120</sub> /AUC <sub>Glc0-120</sub> (*10 <sup>-9</sup> )
rs34074764	CC	1,754	172 ±164	47.7 ±34.6	202 ±78	316 ±103
	CT	334	161 ±135	44.4 ±31.5	196 ±73	307 ±94
	TT	8	193 ±118	55.5 ±28.3	211 ±64	323 ±59
pAssociation	-	-	0.6	0.2	0.7	0.4
pGender interaction	-	-	0.7	0.8	0.8	0.8
pBMI interaction	-	-	0.6	0.7	0.9	0.8
pIS interaction	-	-	0.2	0.5	0.4	0.6
pGlc interaction	-	-	0.5	0.7	0.4	0.4

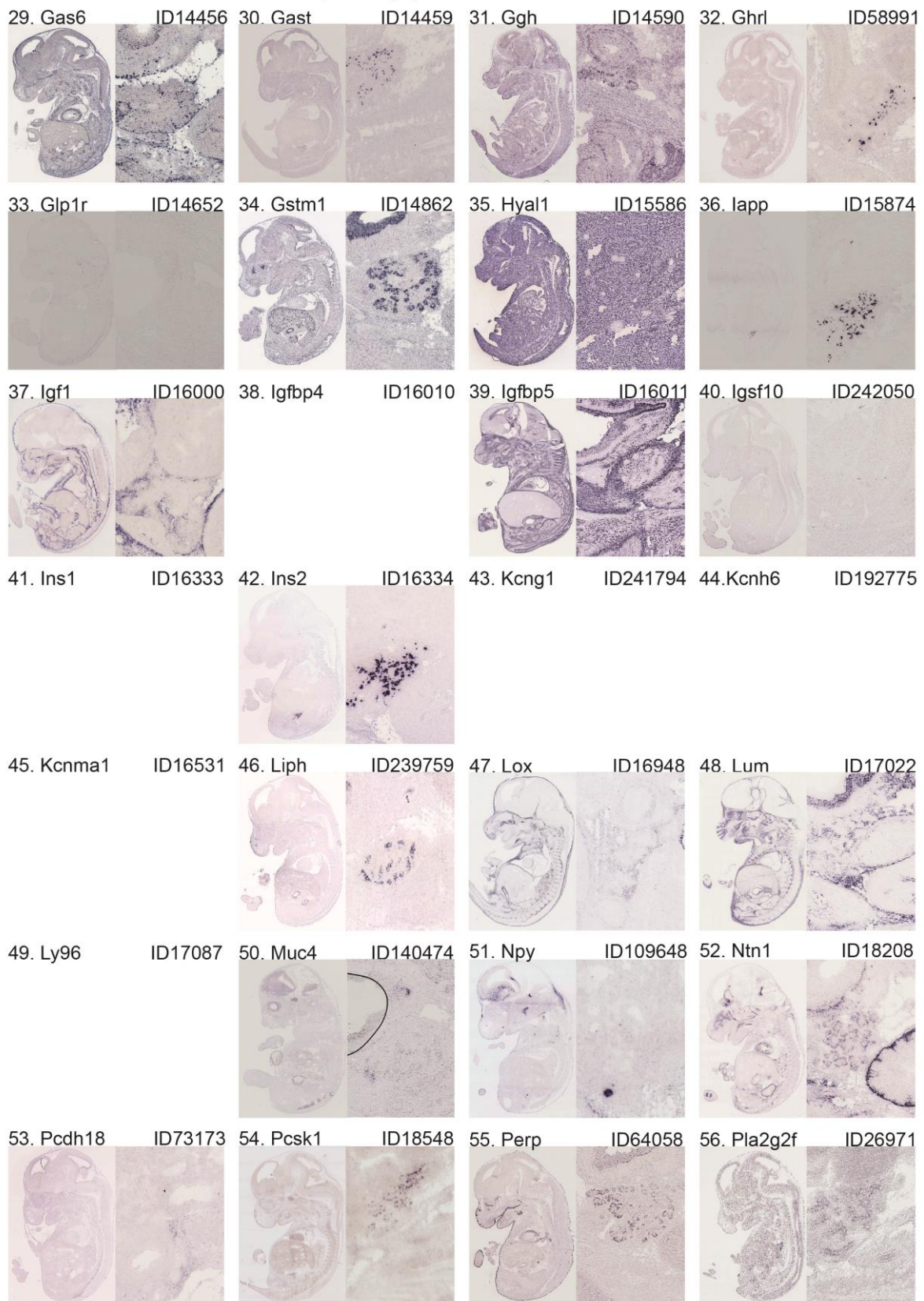
Metabolic data are shown as unadjusted raw data (means ±SD). Associations between SNP genotypes and insulin secretion parameters were tested by multiple linear regression analyses (standard least squares method) with gender, age, BMI, and (OGTT-derived) insulin sensitivity as covariates. Cross effects were tested by multiple linear regression analyses with (i) gender, age, BMI, and insulin sensitivity as covariates when assessing SNP-gender, SNP-BMI and SNP-insulin sensitivity interactions, and with (ii) gender, age, BMI, insulin sensitivity, and AUC<sub>Glc0-120</sub> as covariates when assessing SNP-AUC<sub>Glc0-120</sub> interactions. p<sub>Association</sub> – p-value for association between SNP and insulin secretion (additive inheritance model); p<sub>Gender/BMI/IS/Glc interaction</sub> – p-values for interaction effects between SNP and gender, BMI, insulin sensitivity, or AUC<sub>Glc0-120</sub>, respectively, on insulin secretion. Nominal associations (p<0.05) are marked by using bold fonts; associations significant after Bonferroni correction for multiple testing (p<0.0040) are marked by using bold fonts and underlining. BMI – body mass index; C-pep – C-peptide; Glc – glucose; Ins – insulin; IS – insulin sensitivity; OGTT – oral glucose tolerance test; SNP – single nucleotide polymorphism

**Table 10: GenePaint *in silico in situs* of whole mount embryos at E14.5 and a higher magnification of the pancreatic region.**

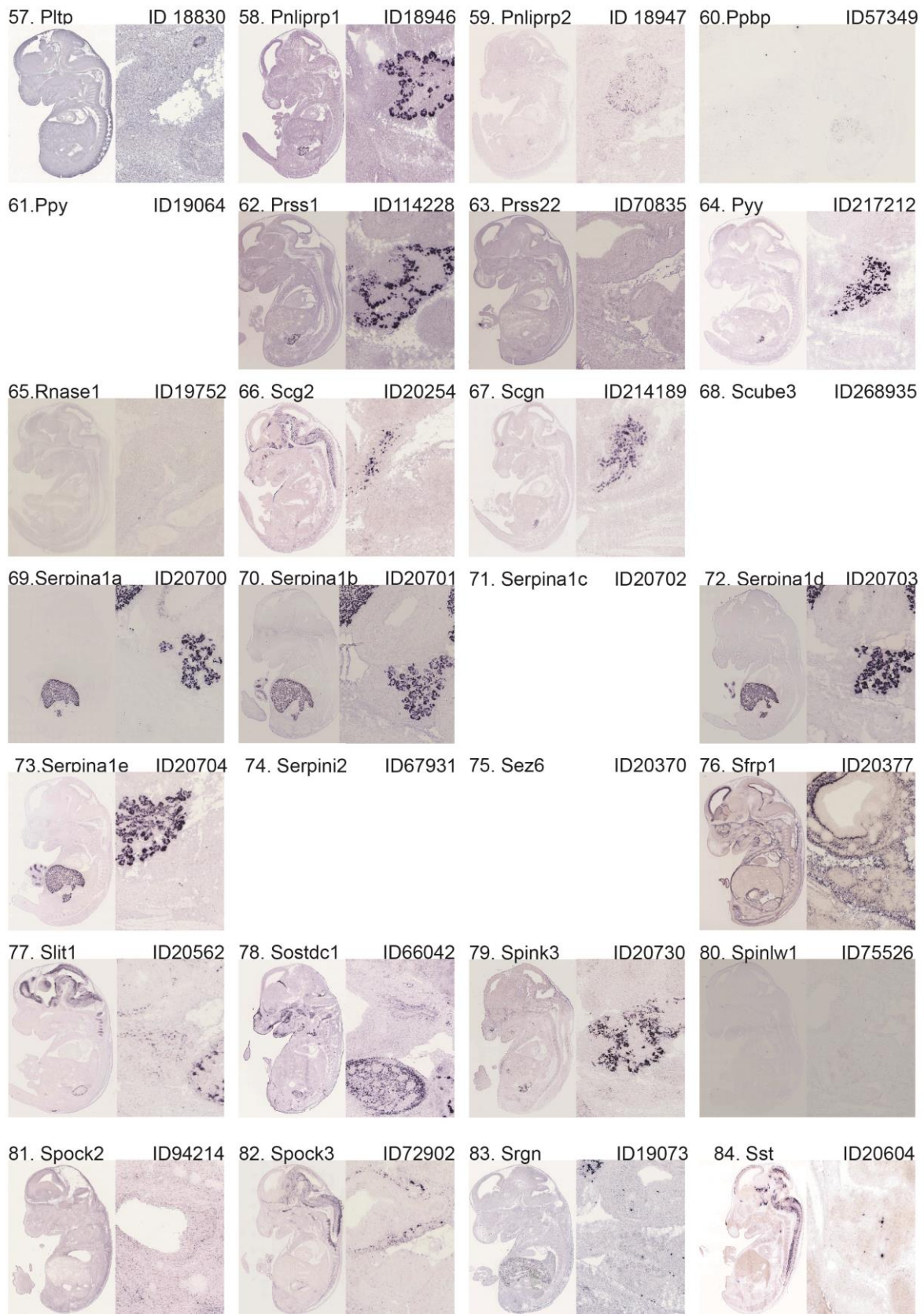
GO term extracellular located at PM epithelial population 1-28



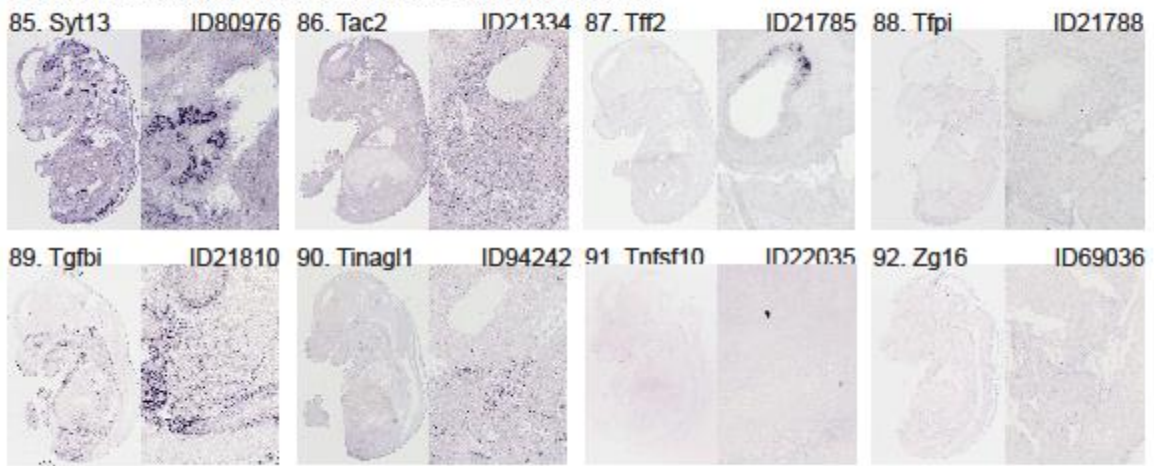
GO term extracellular located at PM epithelial population 28-56



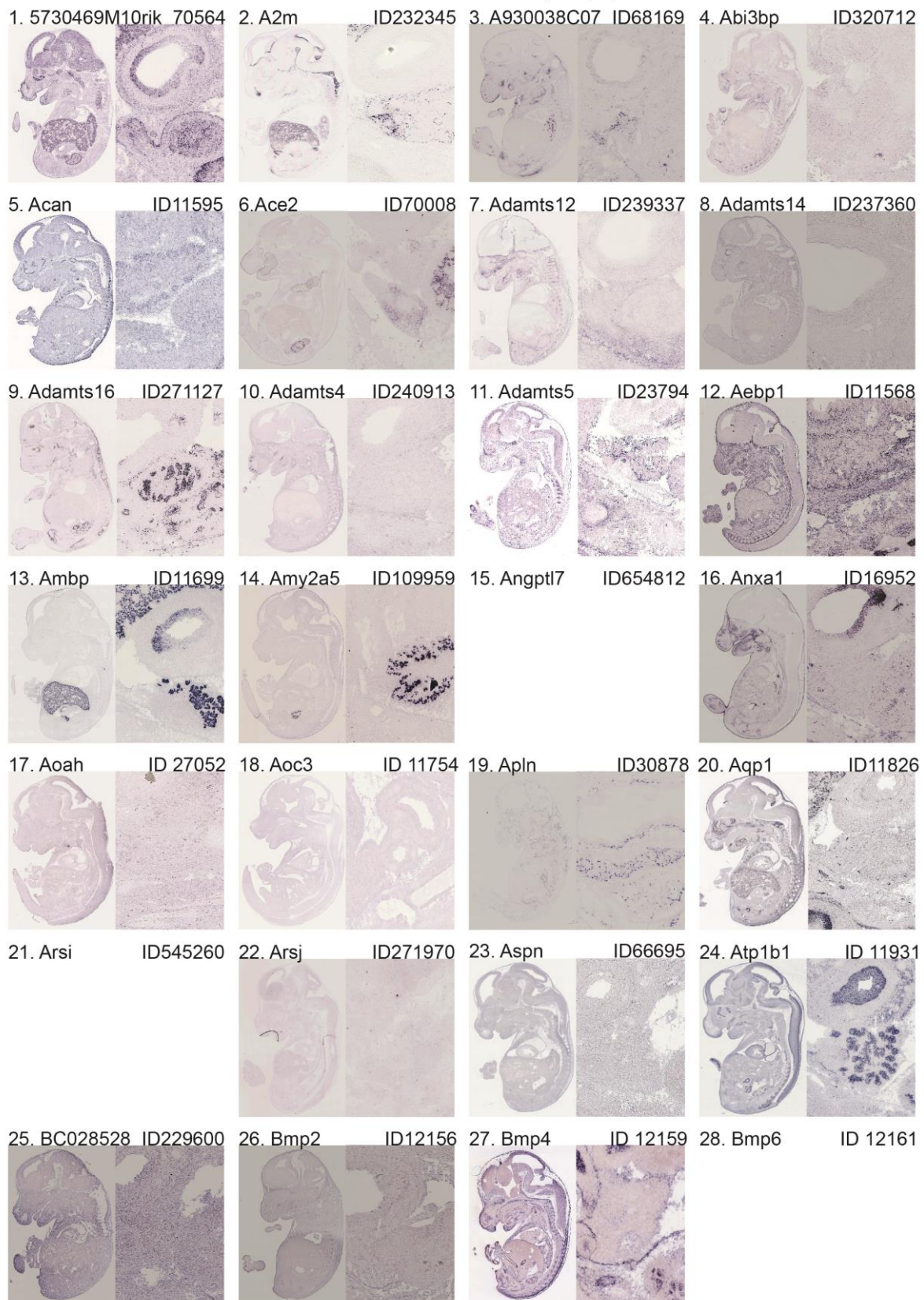
GO term extracellular located at PM epithelial population 57-84



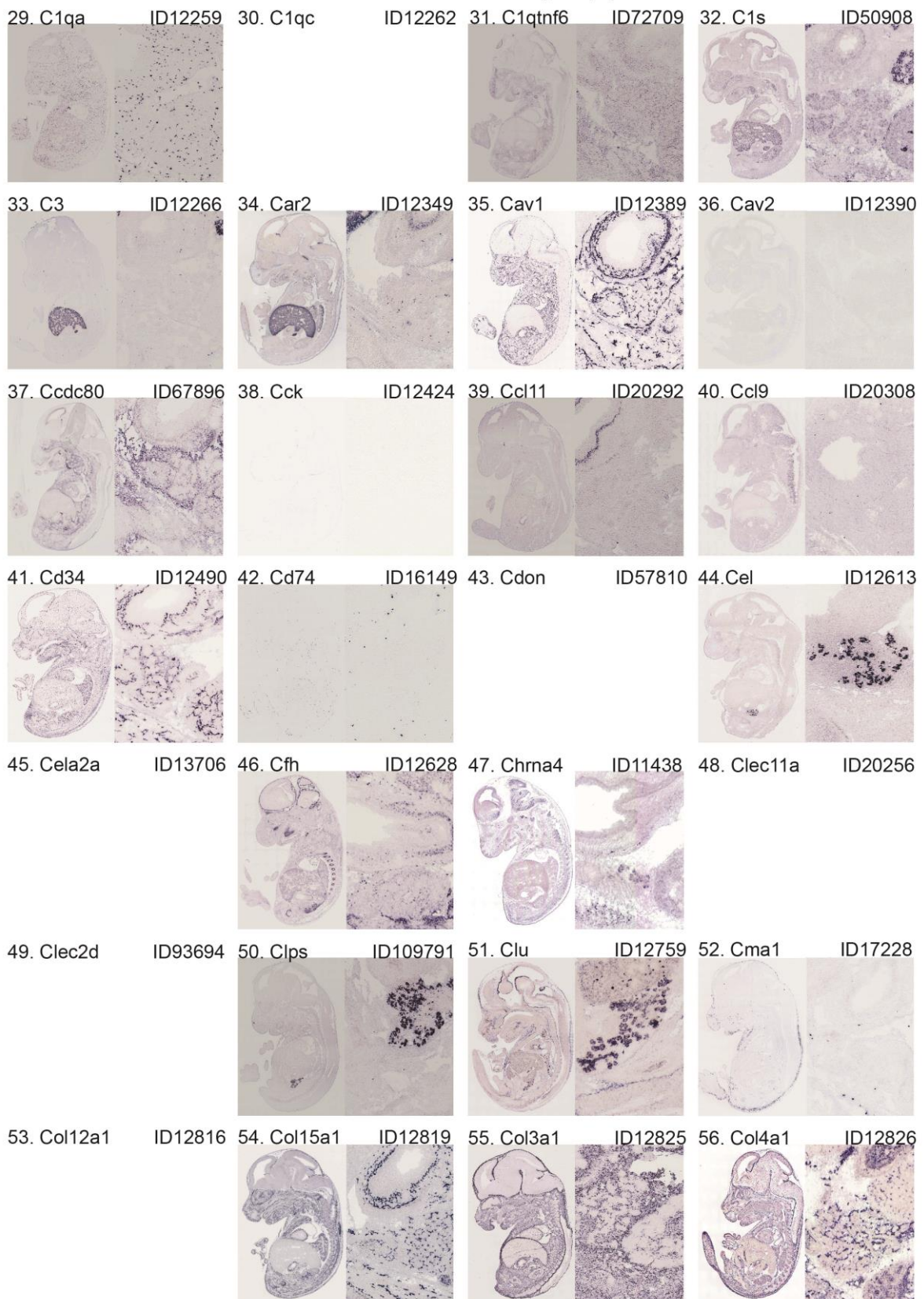
GO term extracellular located at PM epithelial population 85-92



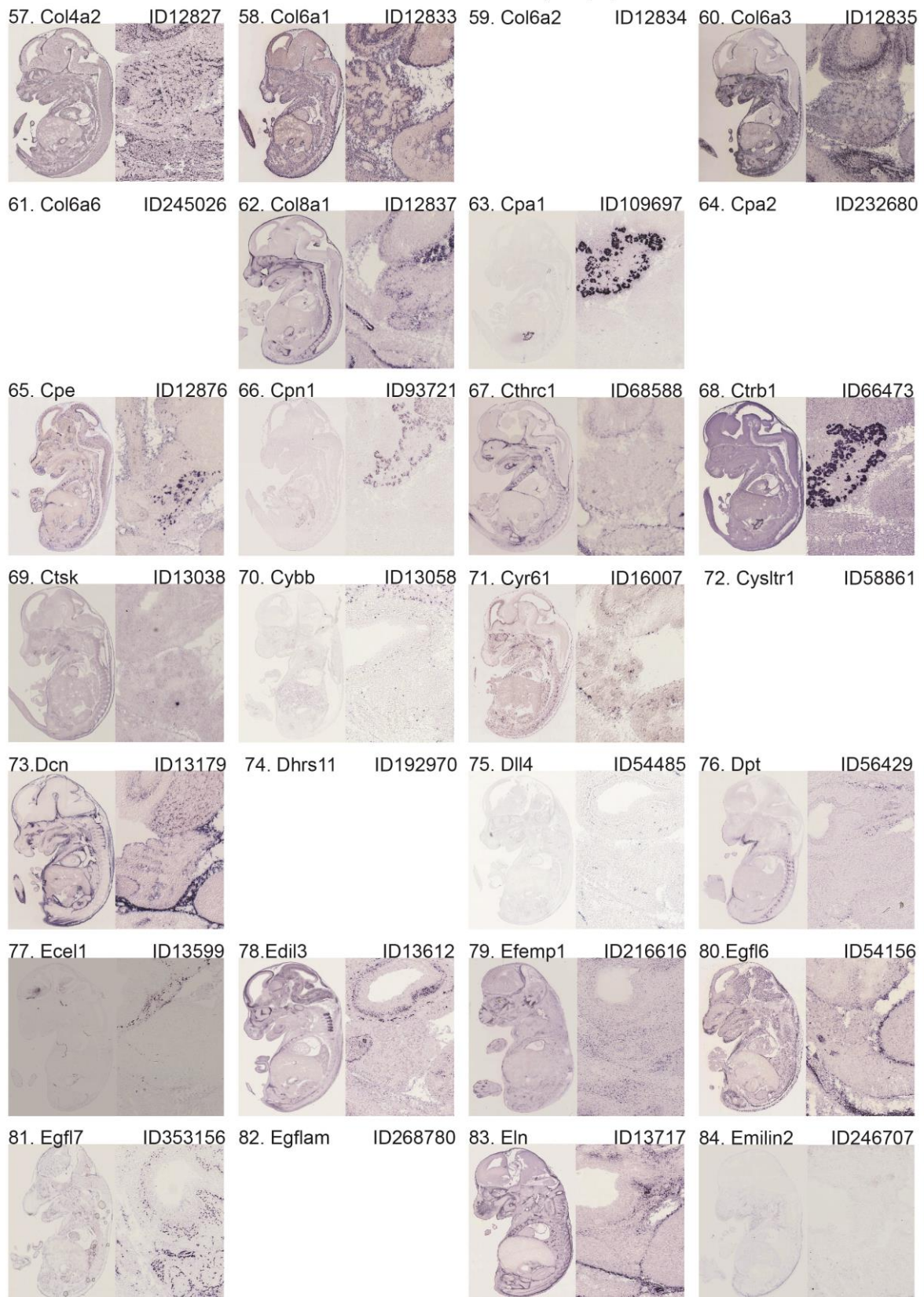
GO term extracellular located at Plasmamembrane in mesenchymal population 1-28



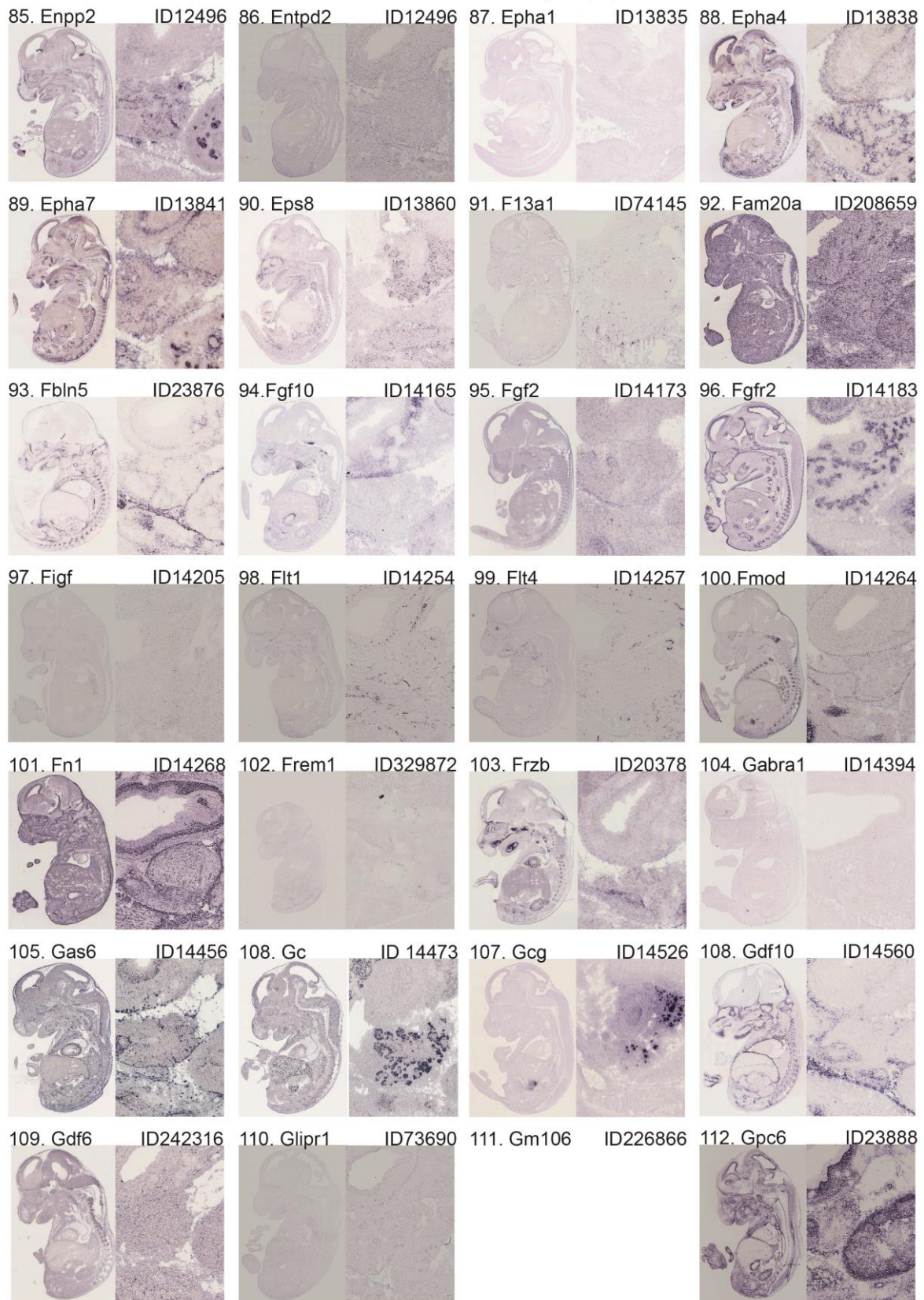
GO term extracellular located at Plasmamembrane in mesenchymal population 29-56



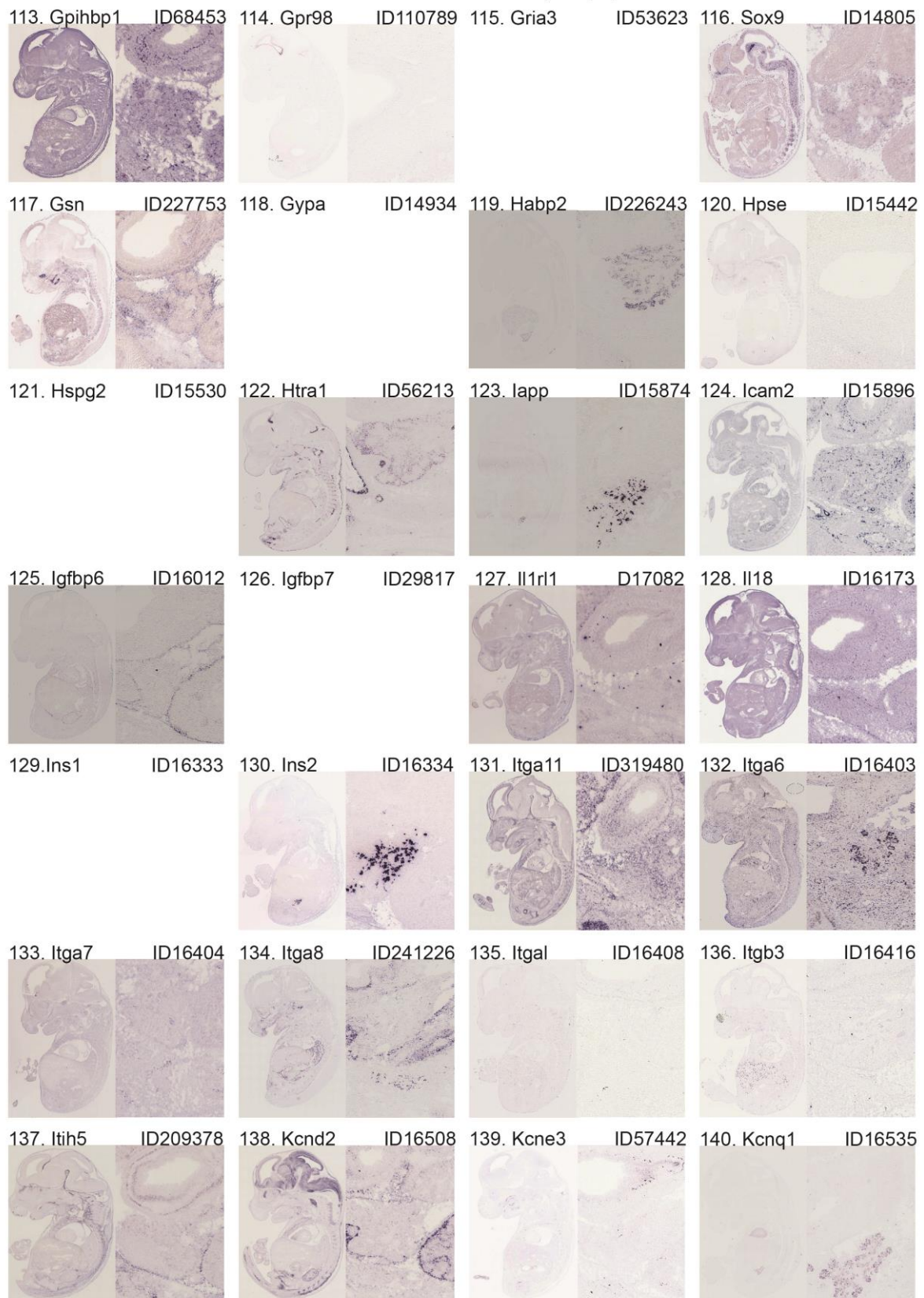
GO term extracellular located at Plasmamembrane in mesenchymal population 57-84



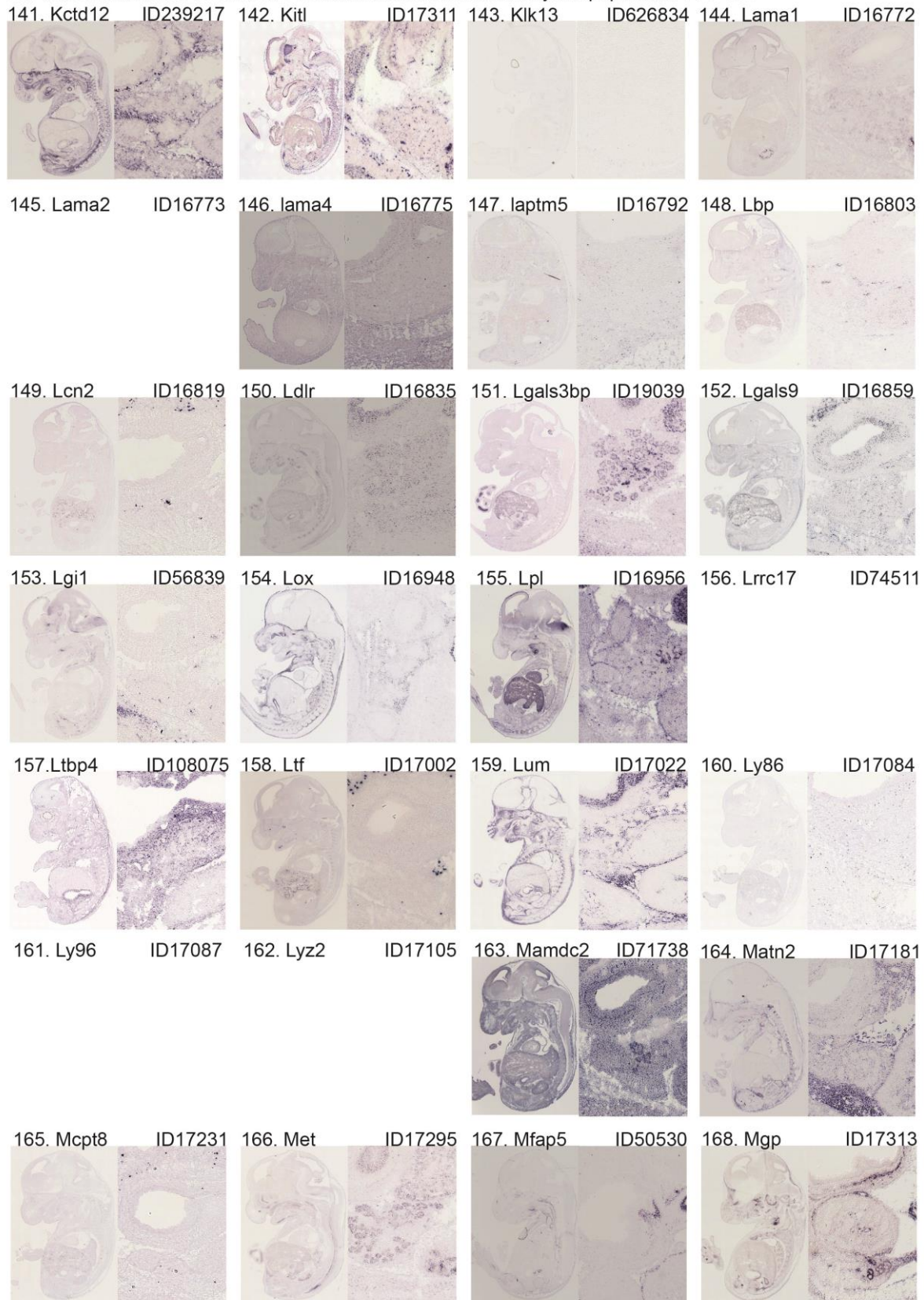
GO term extracellular located at Plasmamembrane in mesenchymal population 85-112



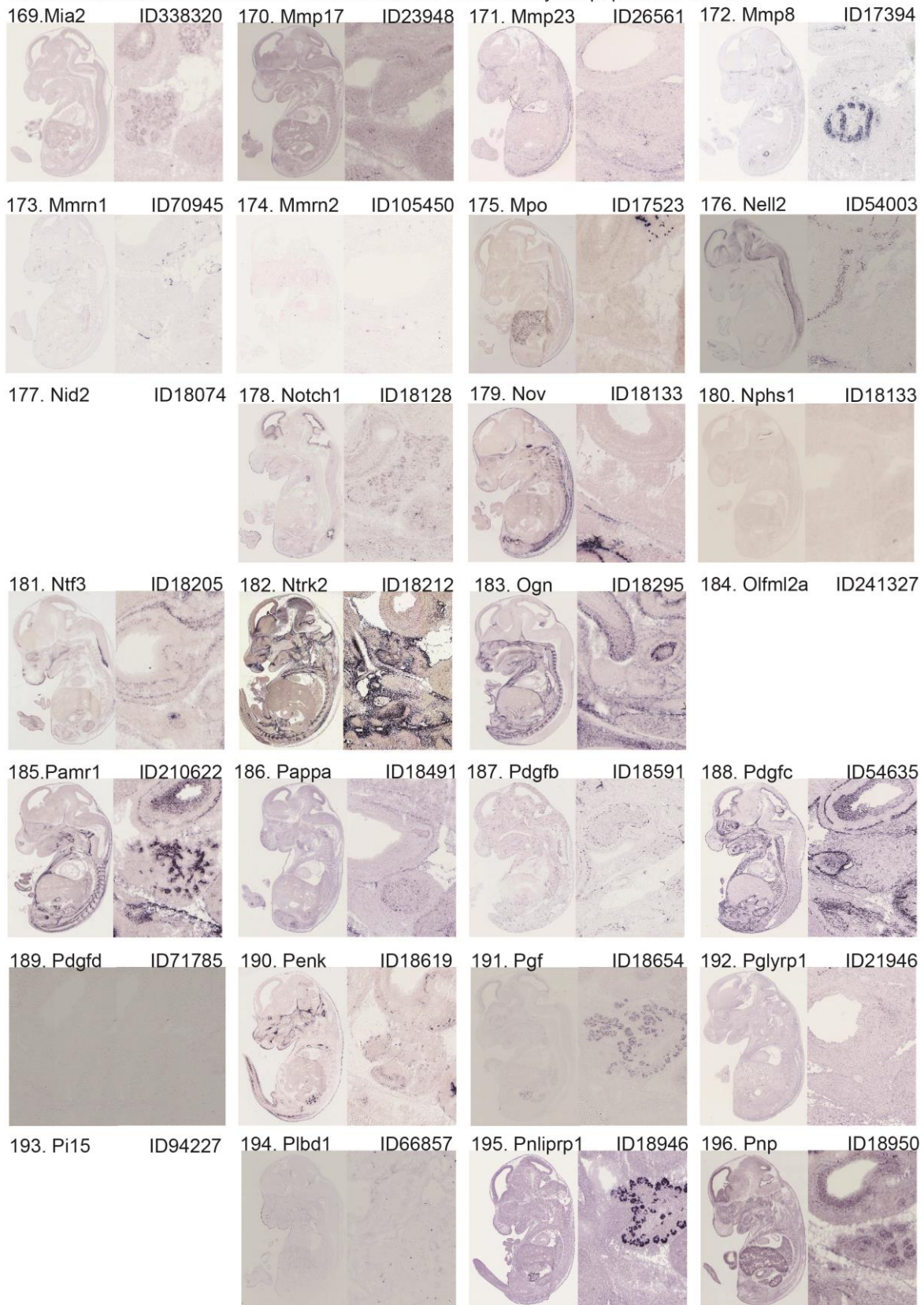
GO term extracellular located at Plasmamembrane in mesenchymal population 113-140



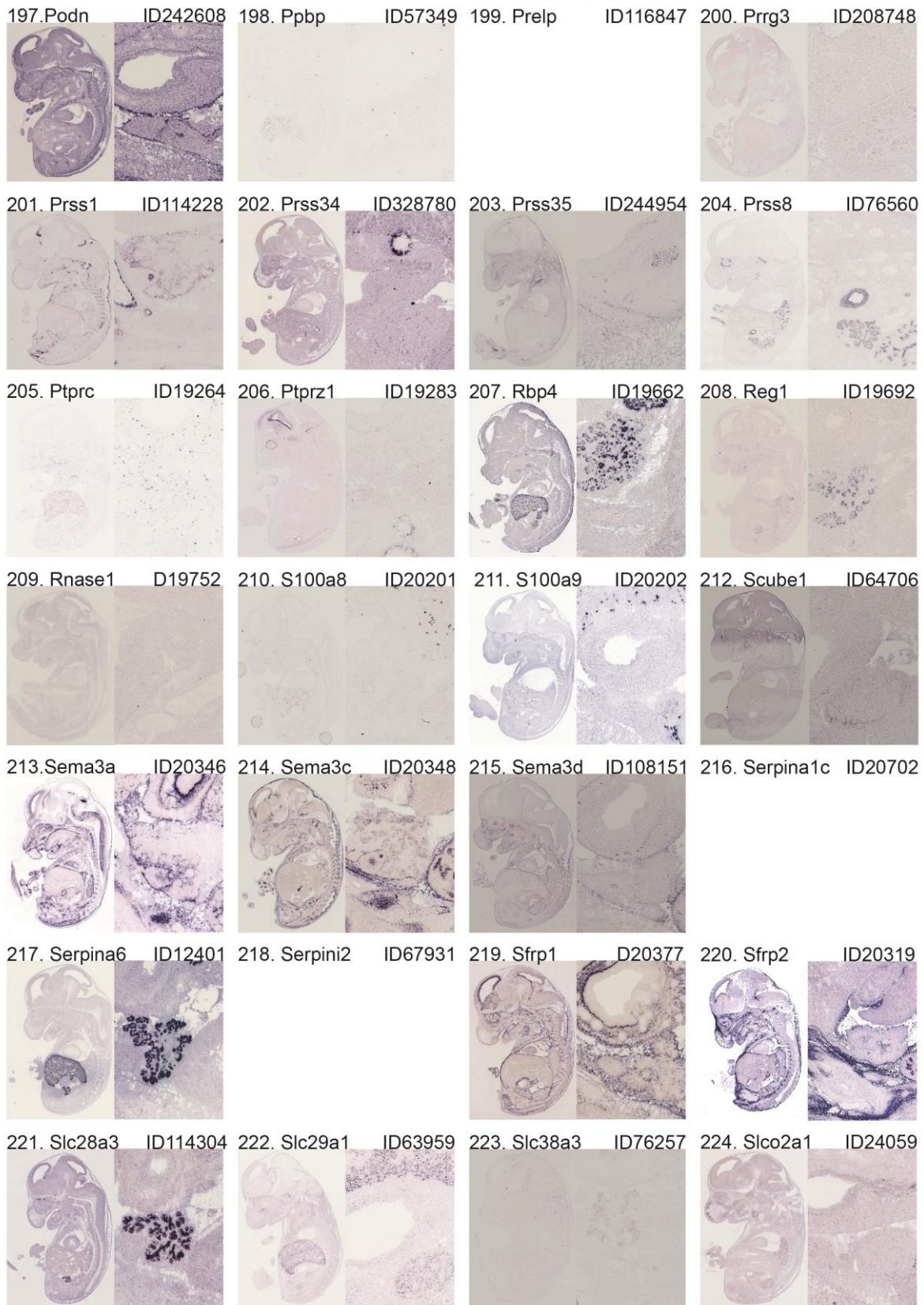
GO term extracellular located at Plasmamembrane in mesenchymal population 141-168



GO term extracellular located at Plasmamembrane in mesenchymal population 169-196

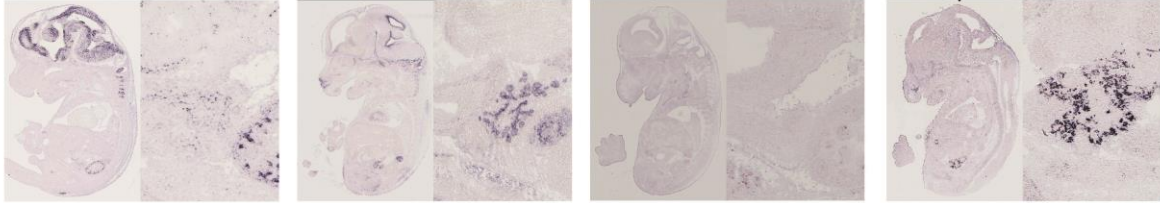


GO term extracellular located at Plasmamembrane in mesenchymal population 197-224



GO term extracellular located at Plasmamembrane in mesenchymal population 225-252

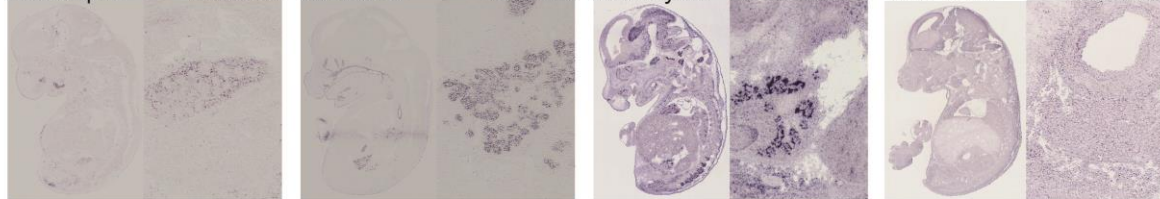
225. Slit1 ID20562 226. Smoc1 ID64075 227. Sod3 ID20657 228. Spink3 ID20730



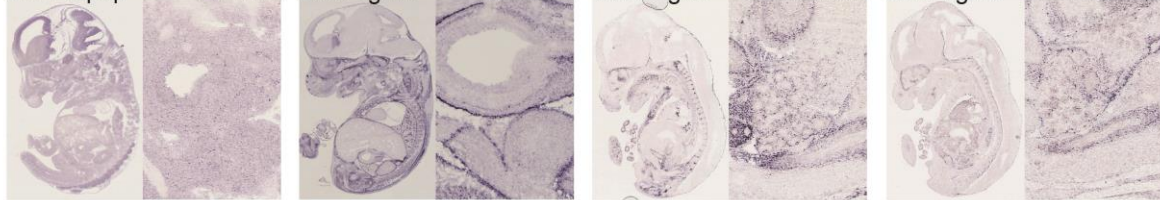
229. Spon1 D233744 230. Spon2 ID100689 231. Spp1 ID20750 232. Srgn ID19073



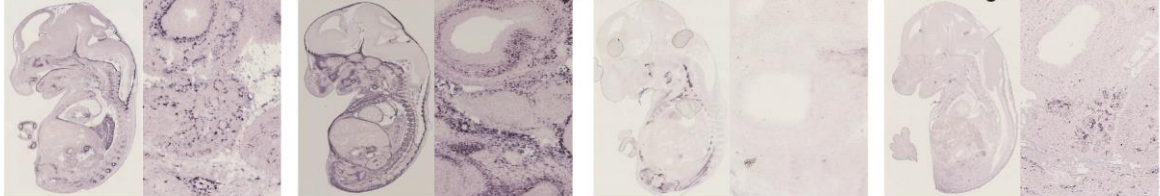
233. SrpX2 ID68792 234. St14 ID19143 235. Syt13 ID80976 236. Tac2 ID21334



237. Tapbp ID21356 238. Tgfb3 ID21809 239. Tgfb1 ID21810 240. Tgm2 ID21817



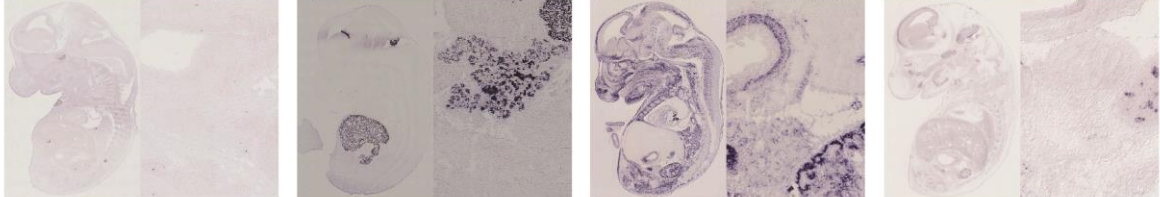
241. Thbd ID21824 242. Thbs2 ID21826 243. Thbs4 ID21828 244. Tinagl1 ID94242



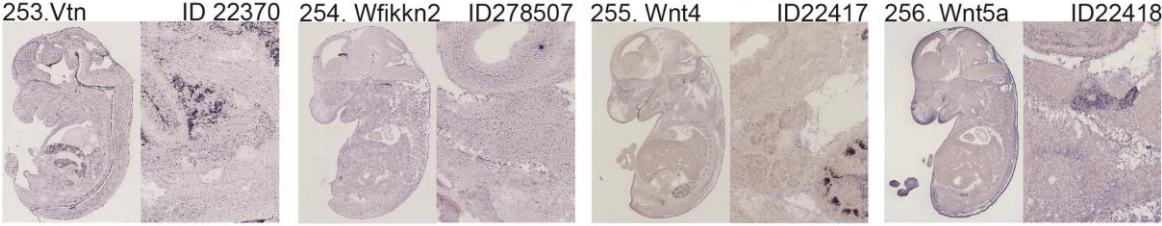
245. Tll1 ID21892 246. Tnxb ID81877 247. Tpsb2 ID17229 248. Trf ID22041



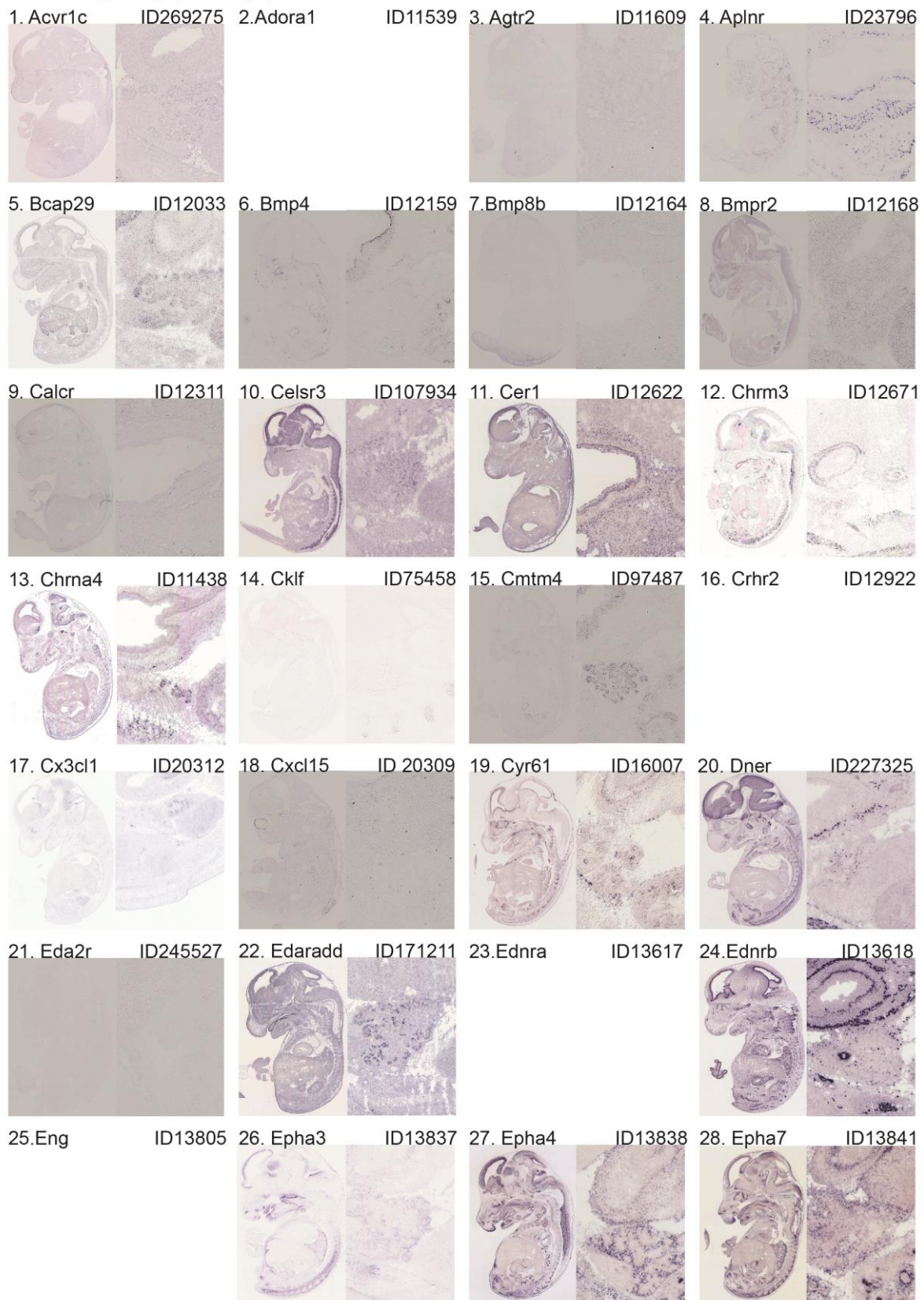
249. Trh ID22044 250. Ttr ID22139 251. Vcan ID13003 252. Vldlr ID22359



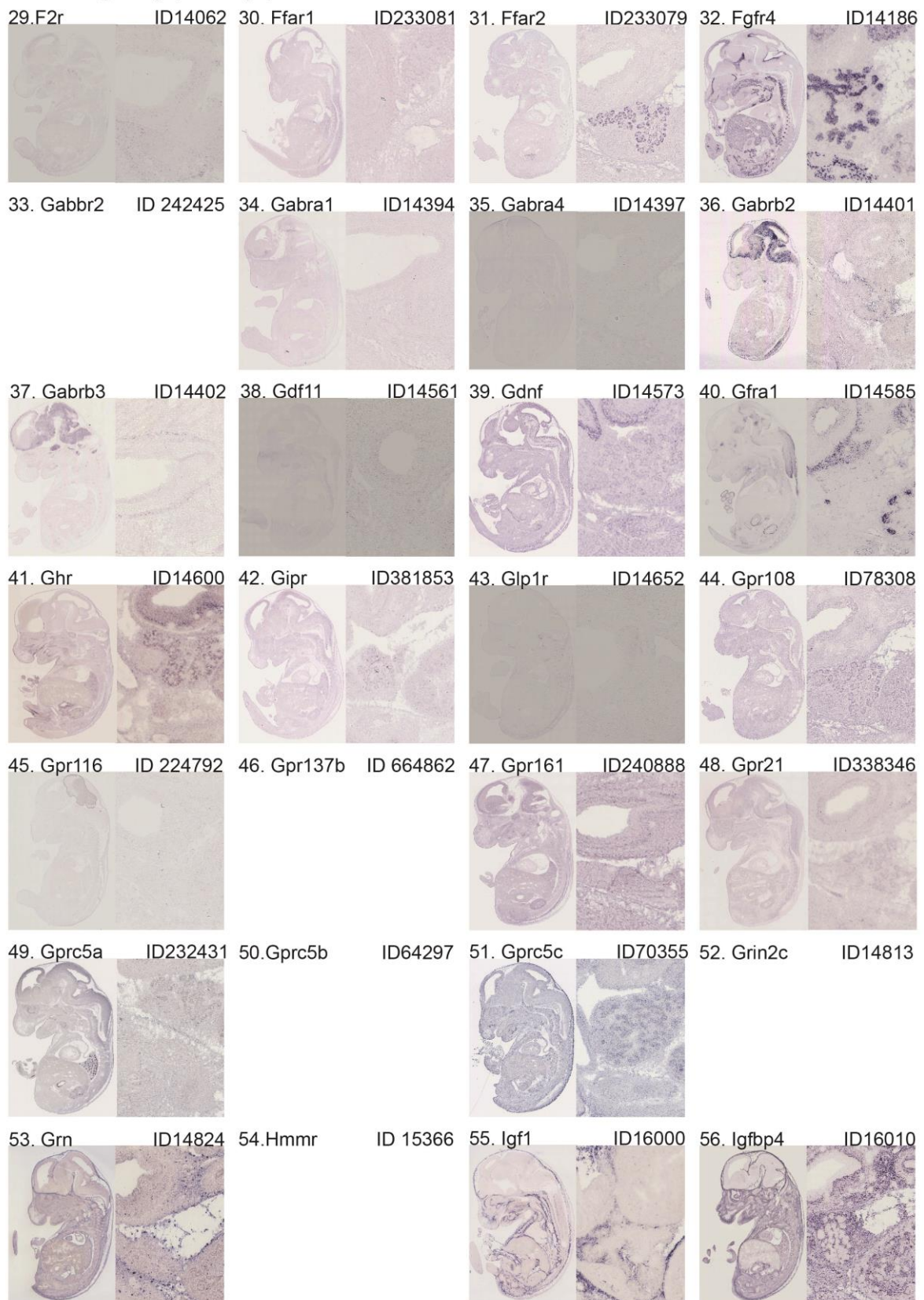
GO term extracellular located at Plasmamembrane in mesenchymal population 253-256



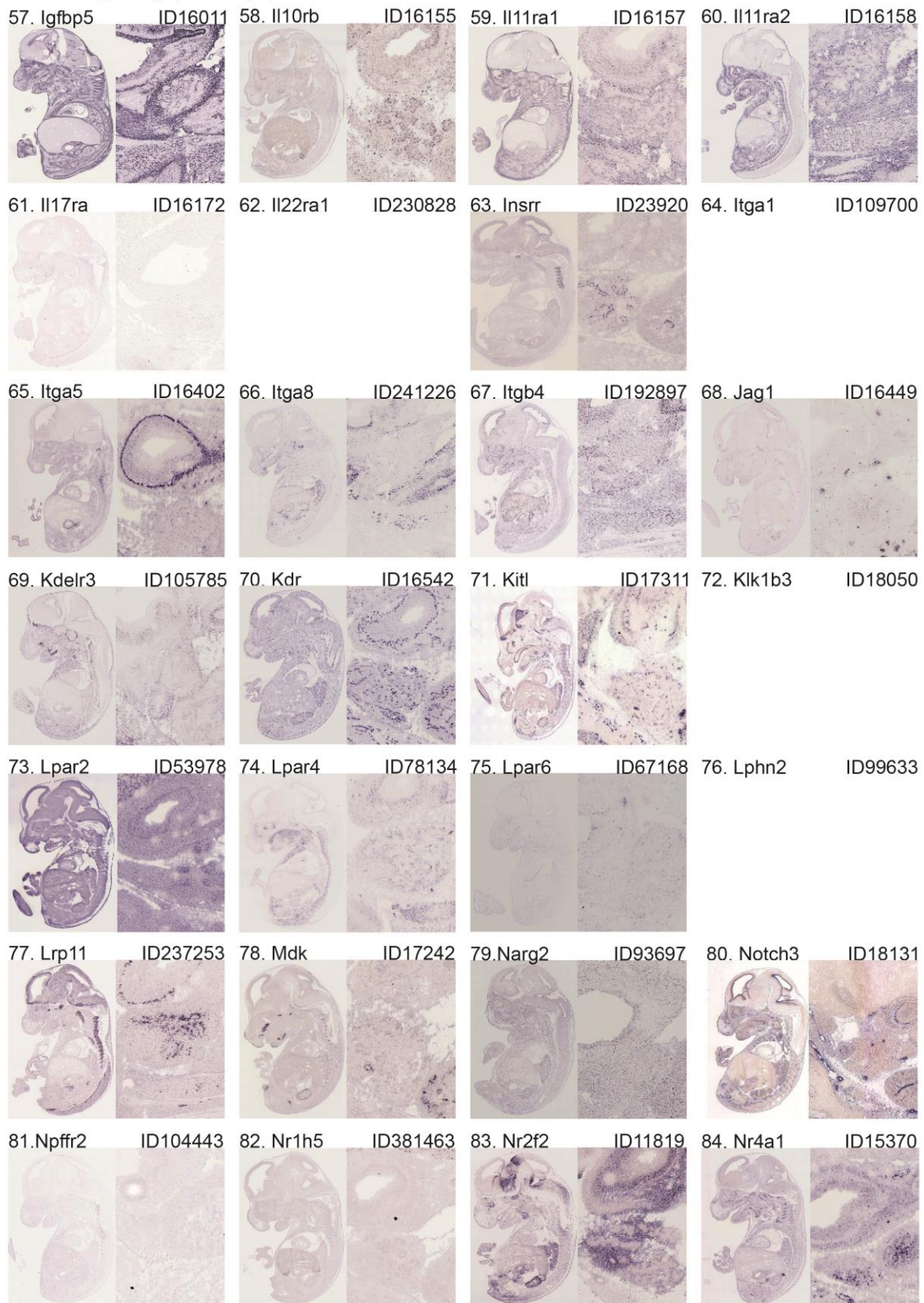
GO term signaling epithelial population 1-28



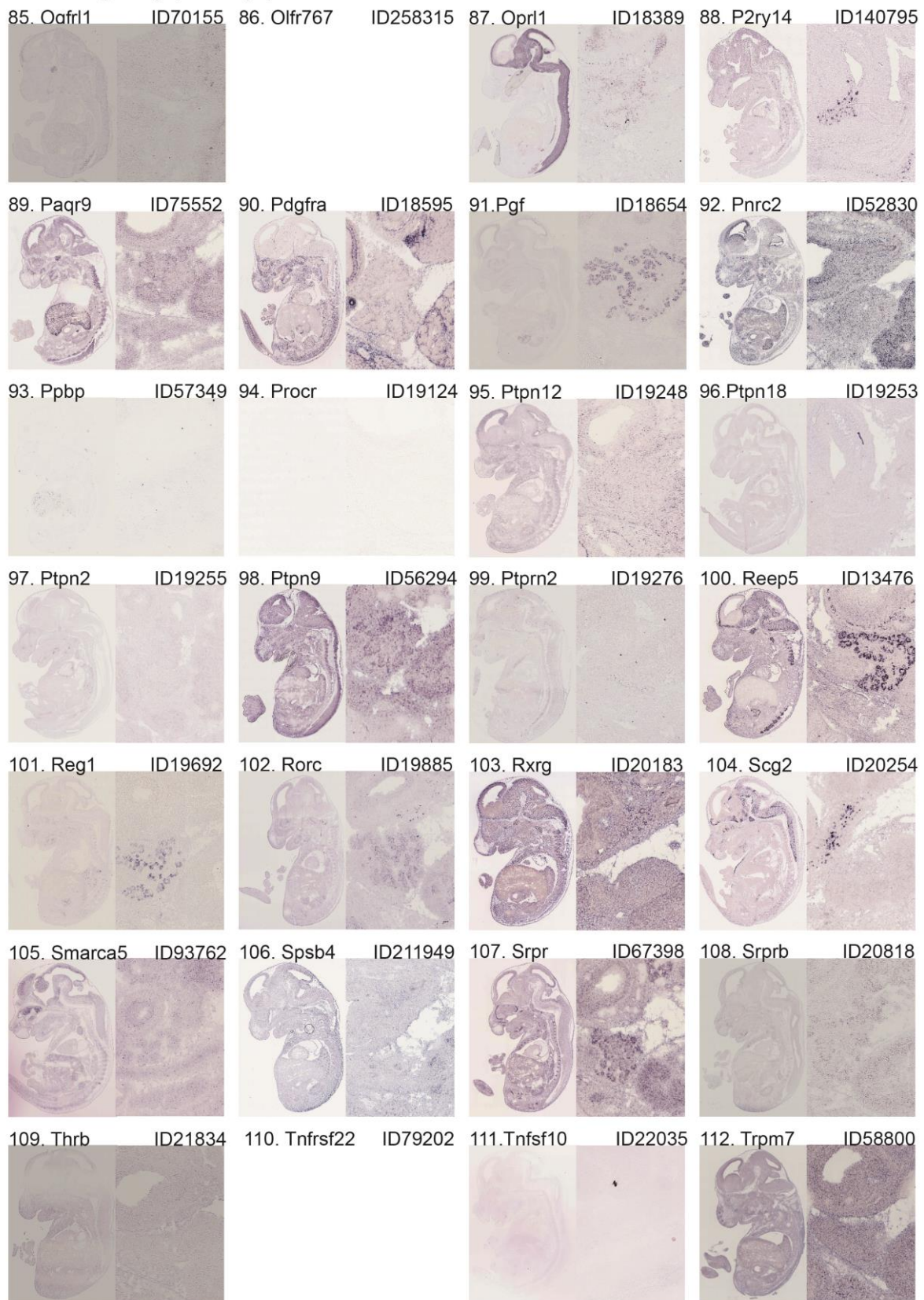
GO term signaling epithelial population 29-56



GO term signaling epithelial population 57-84



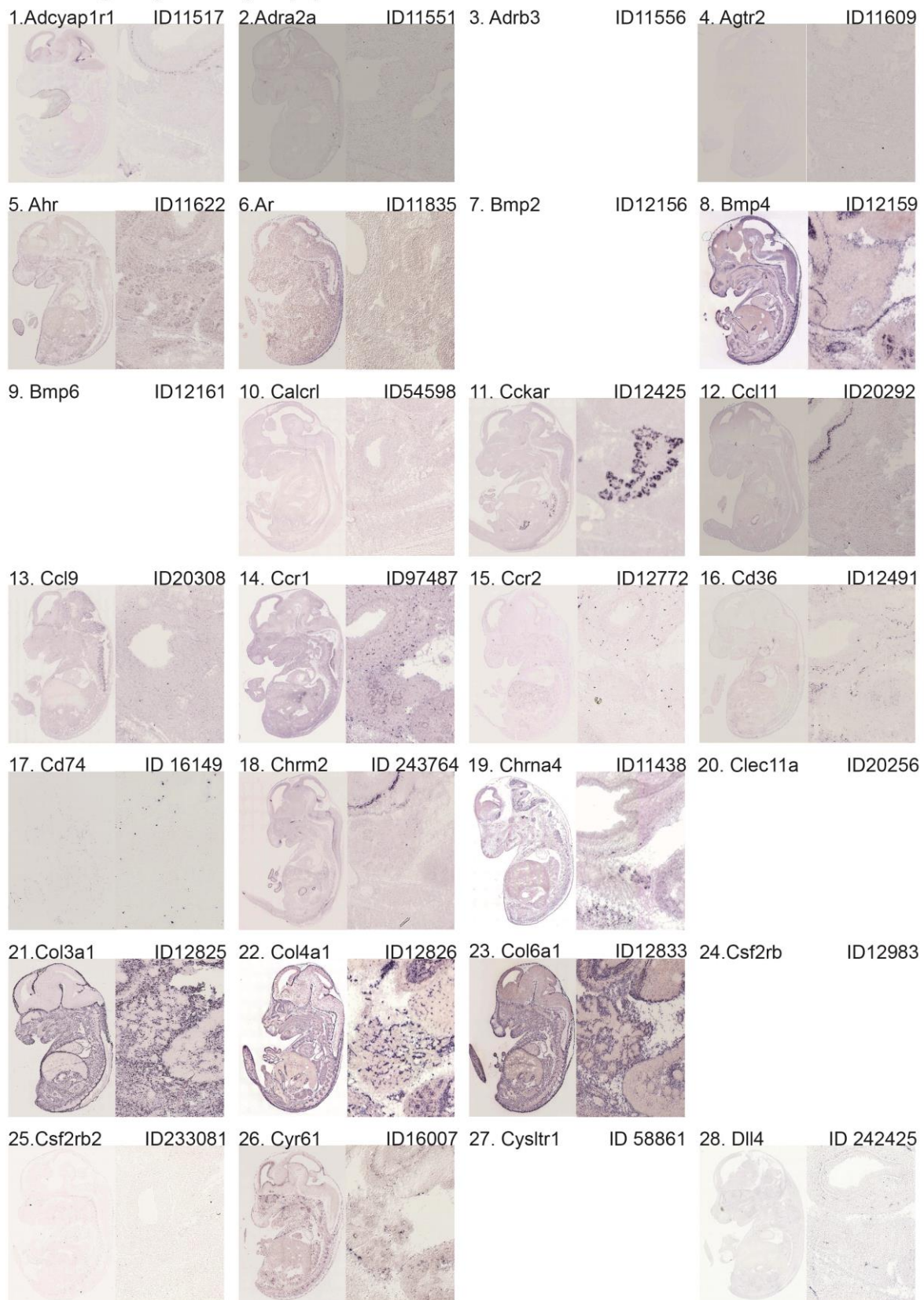
GO term signaling epithelial population 85-112



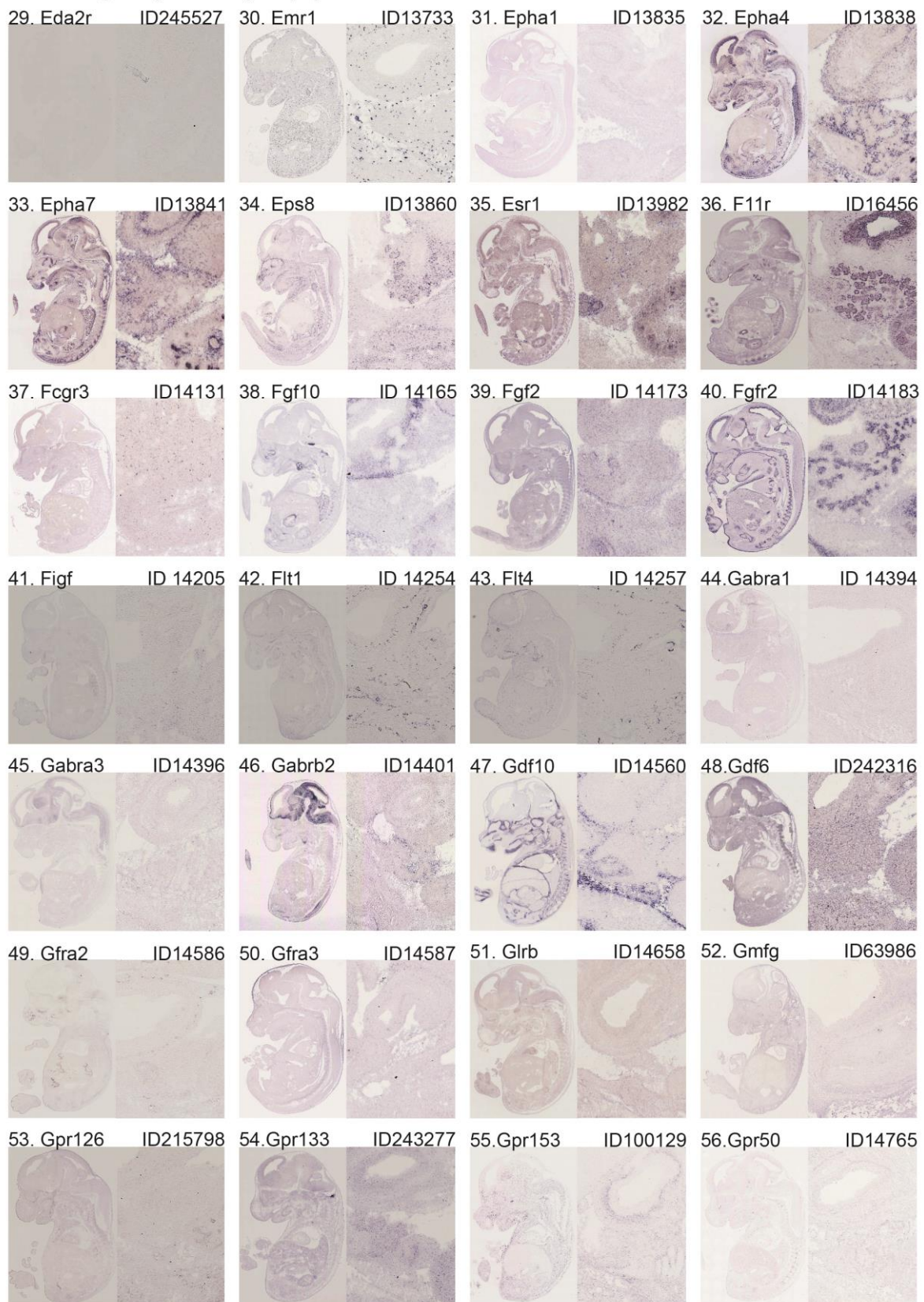
GO term signaling epithelial population 113-116



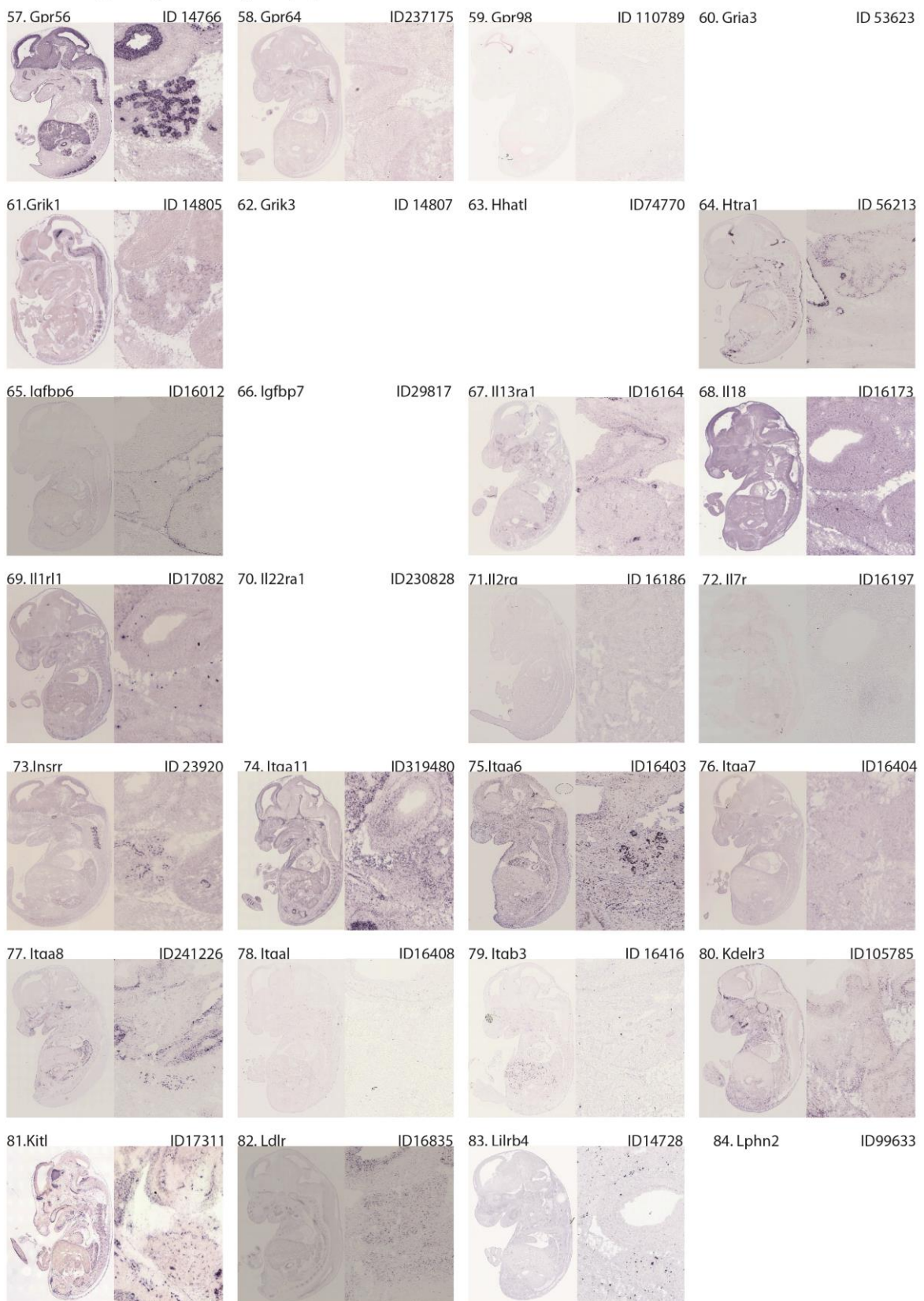
GO term signaling mesenchymal population 1-28



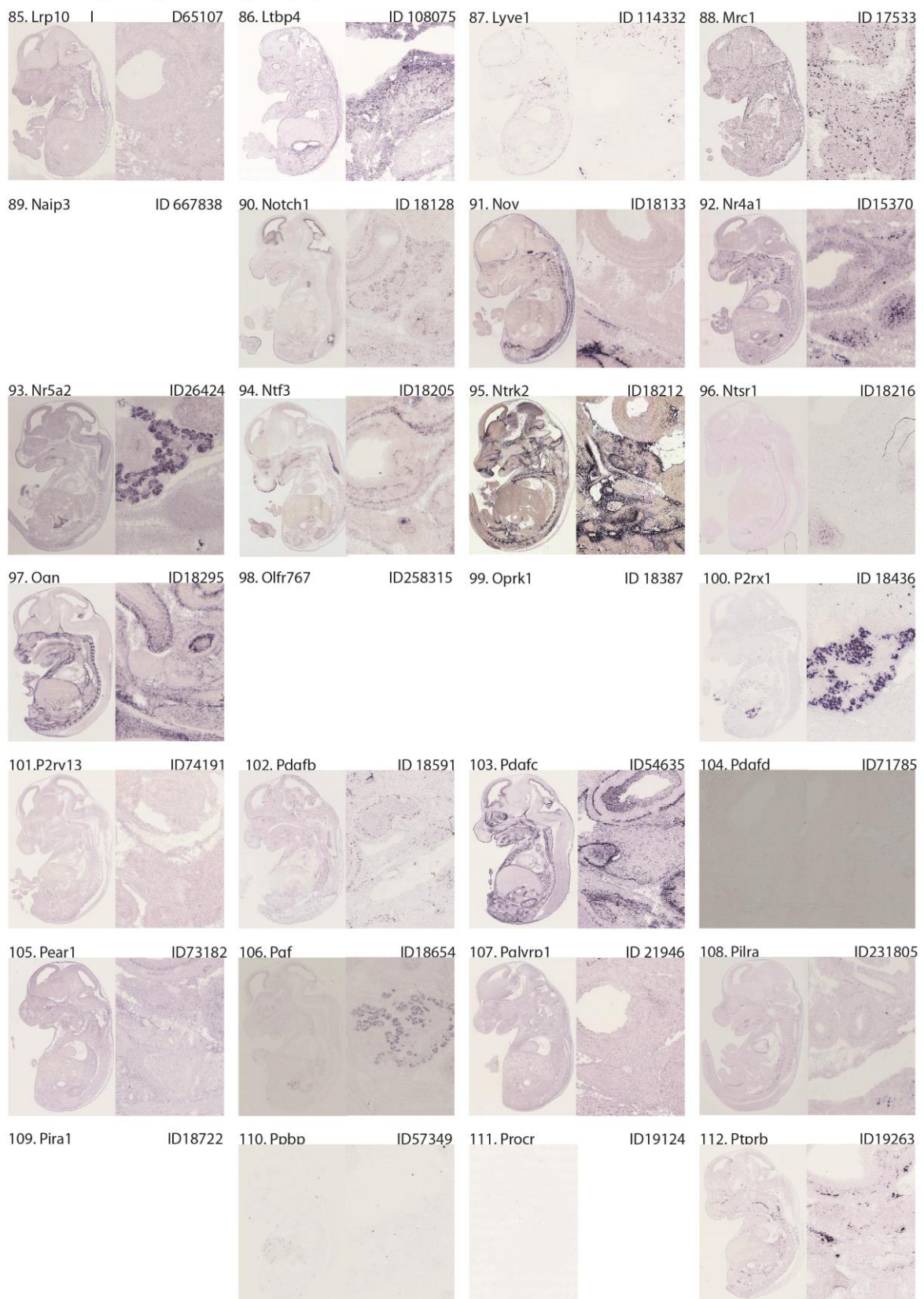
GO term signaling mesenchymal population 29-56



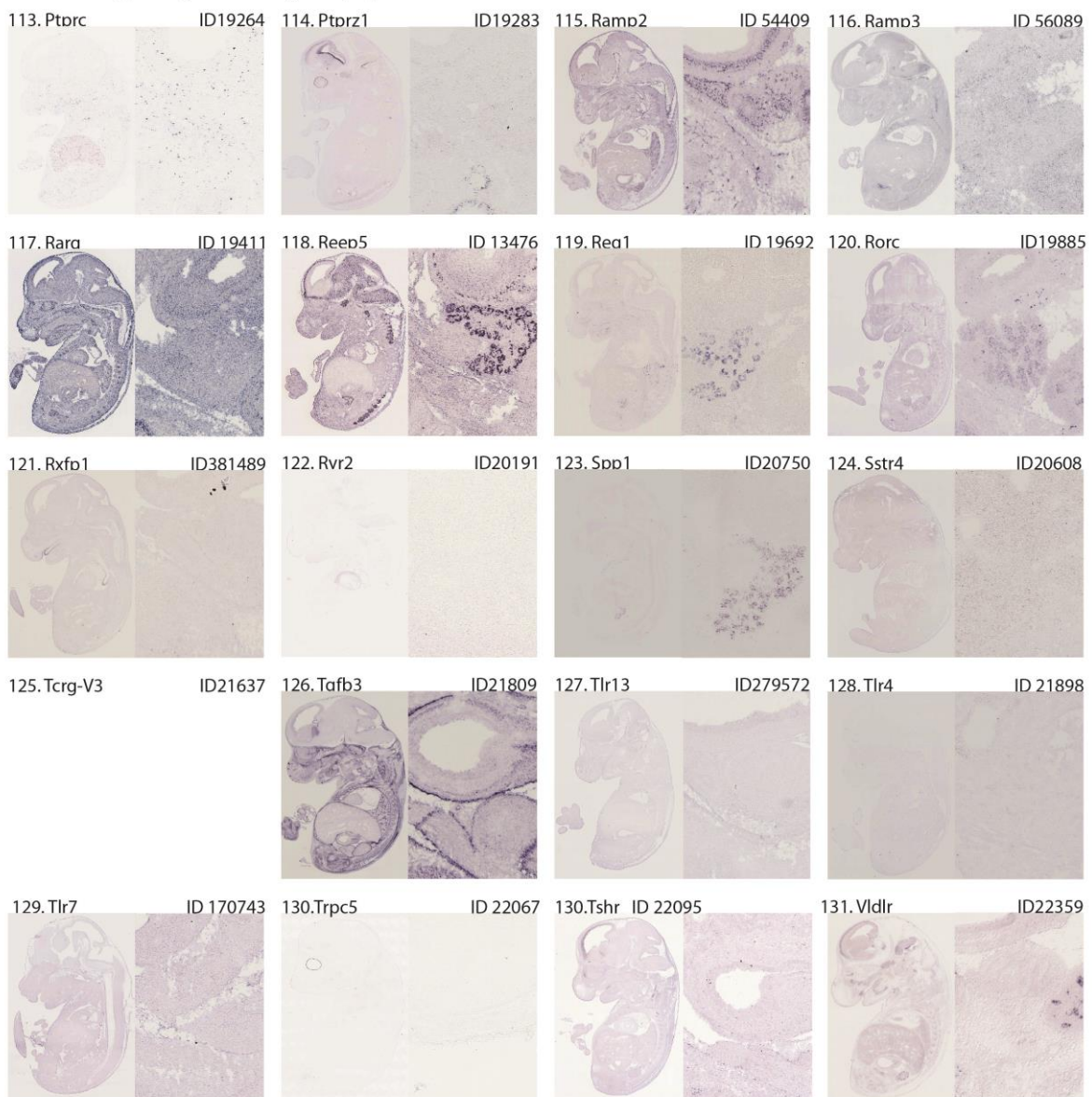
GO term signaling mesenchymal population 57-84



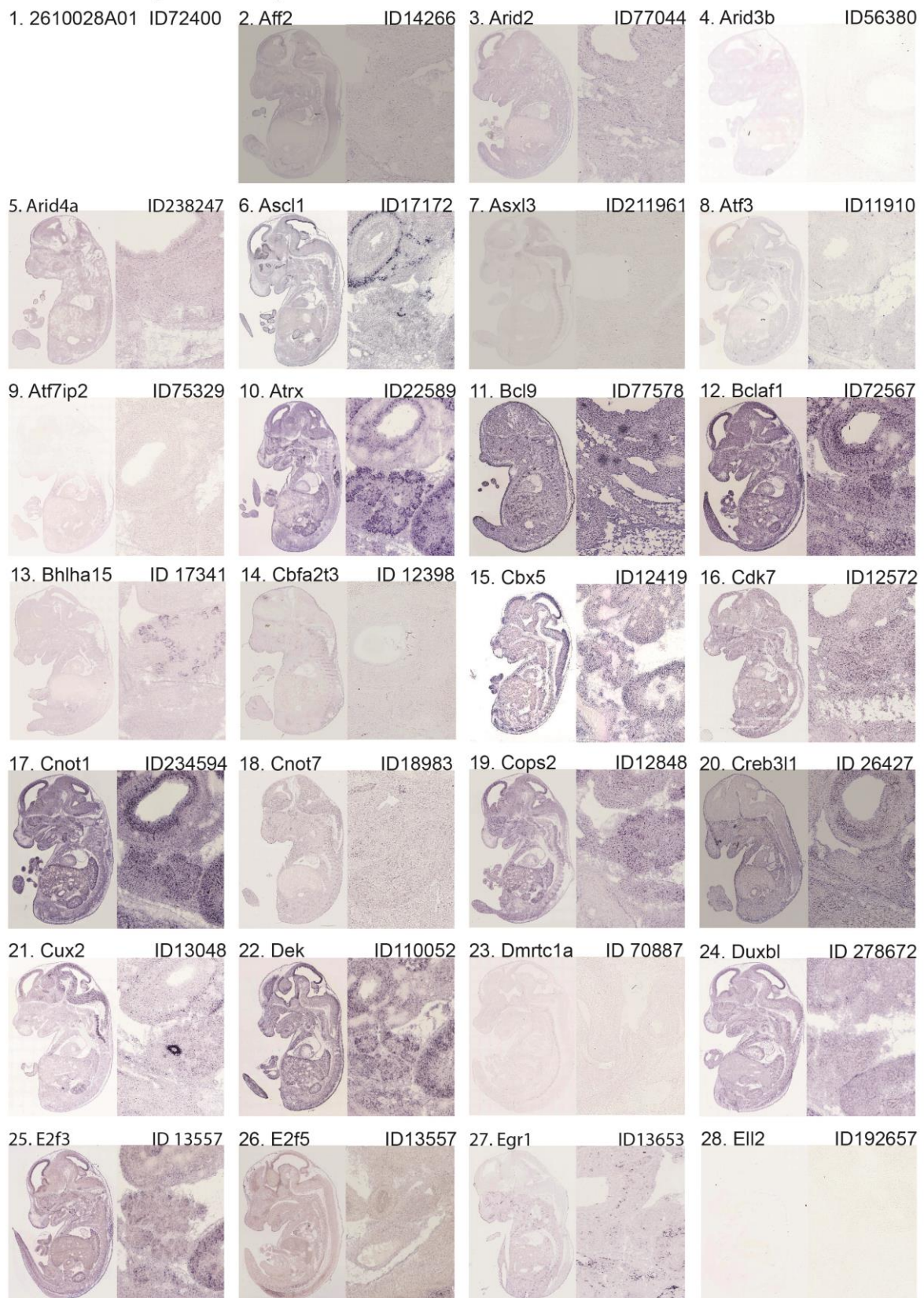
GO term signaling mesenchymal population 85-112



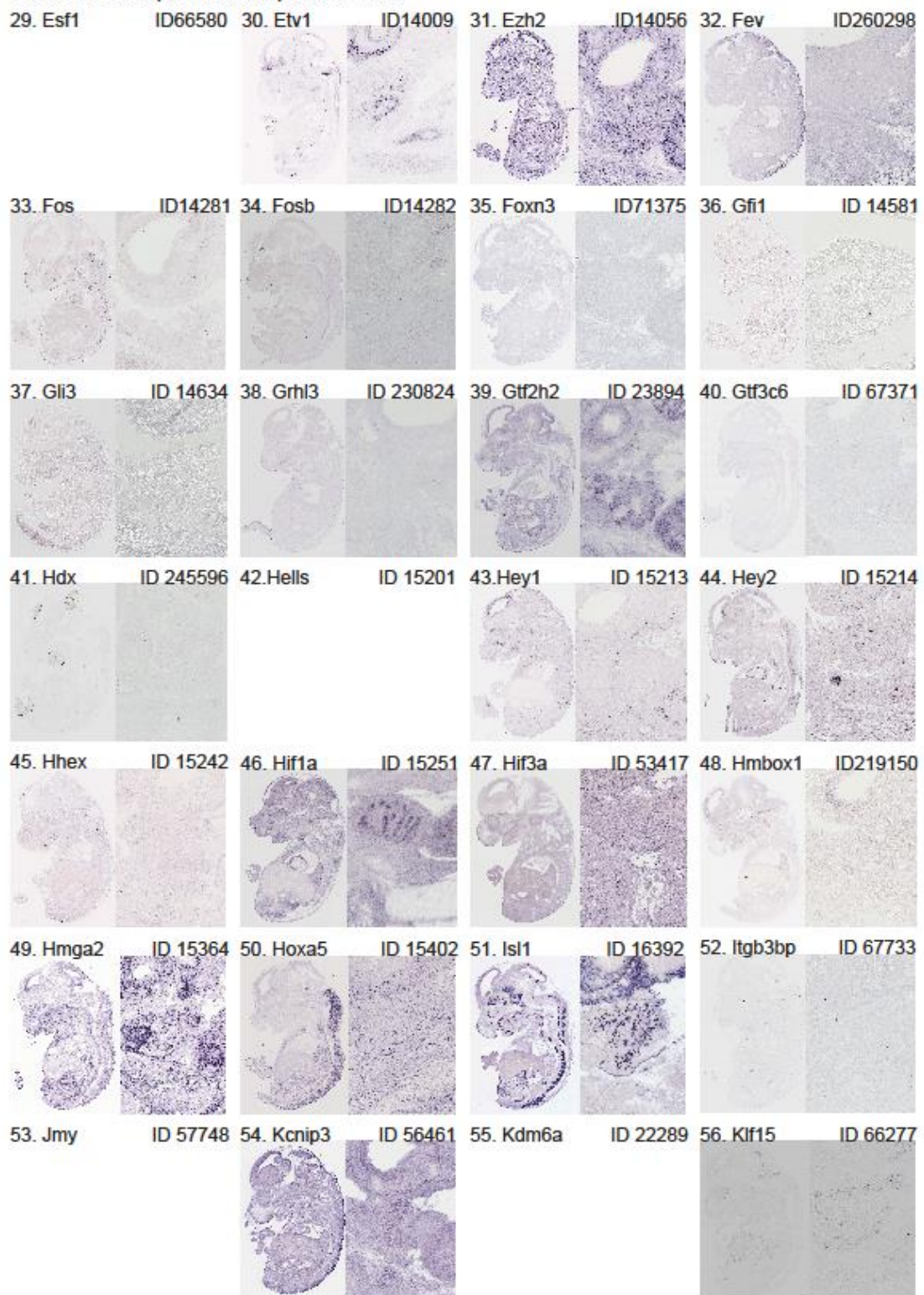
GO term signaling mesenchymal population 113-131



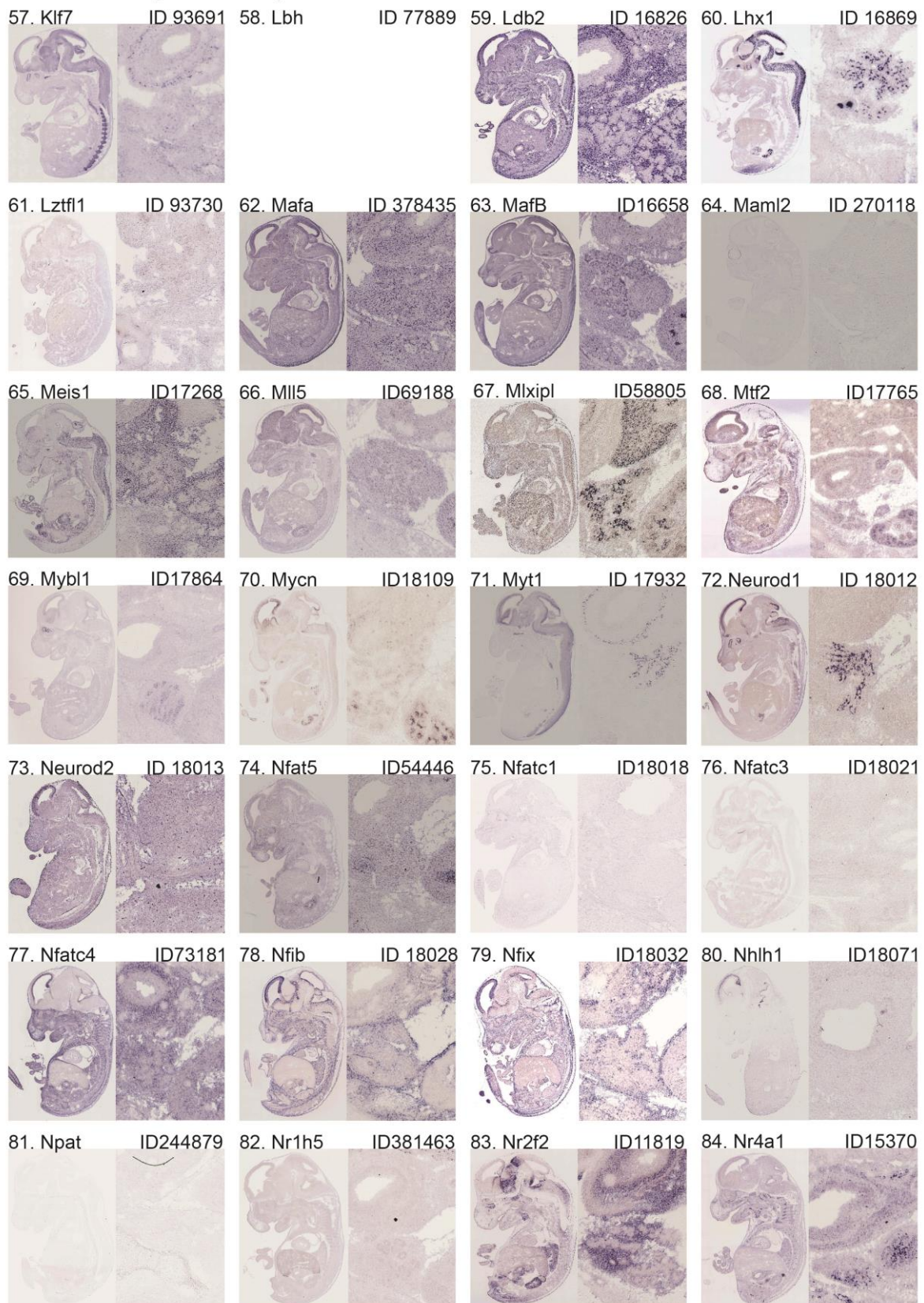
GO term Transcription factors epithelial 1-28



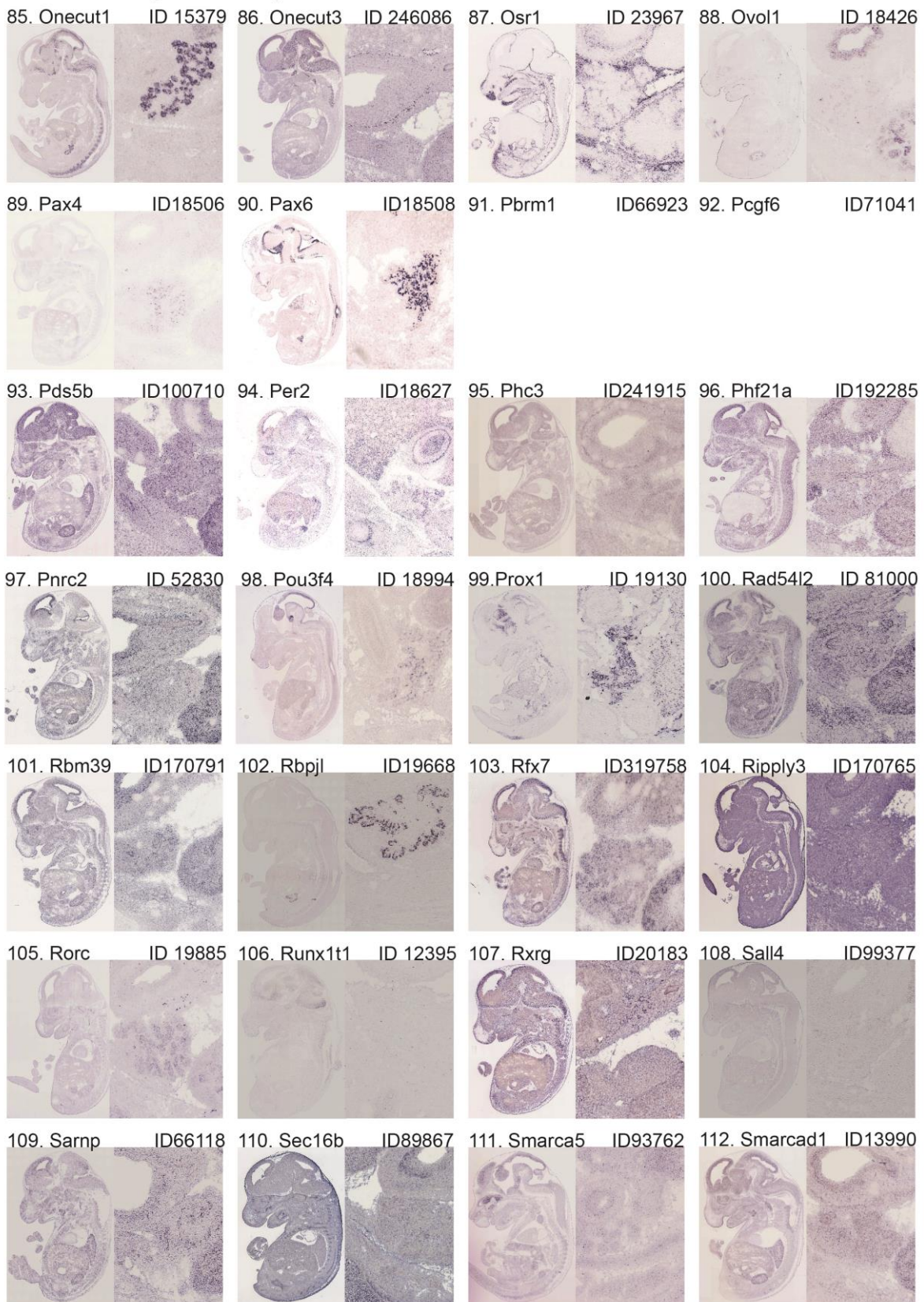
GO term Transcription factors epithelial 29-56



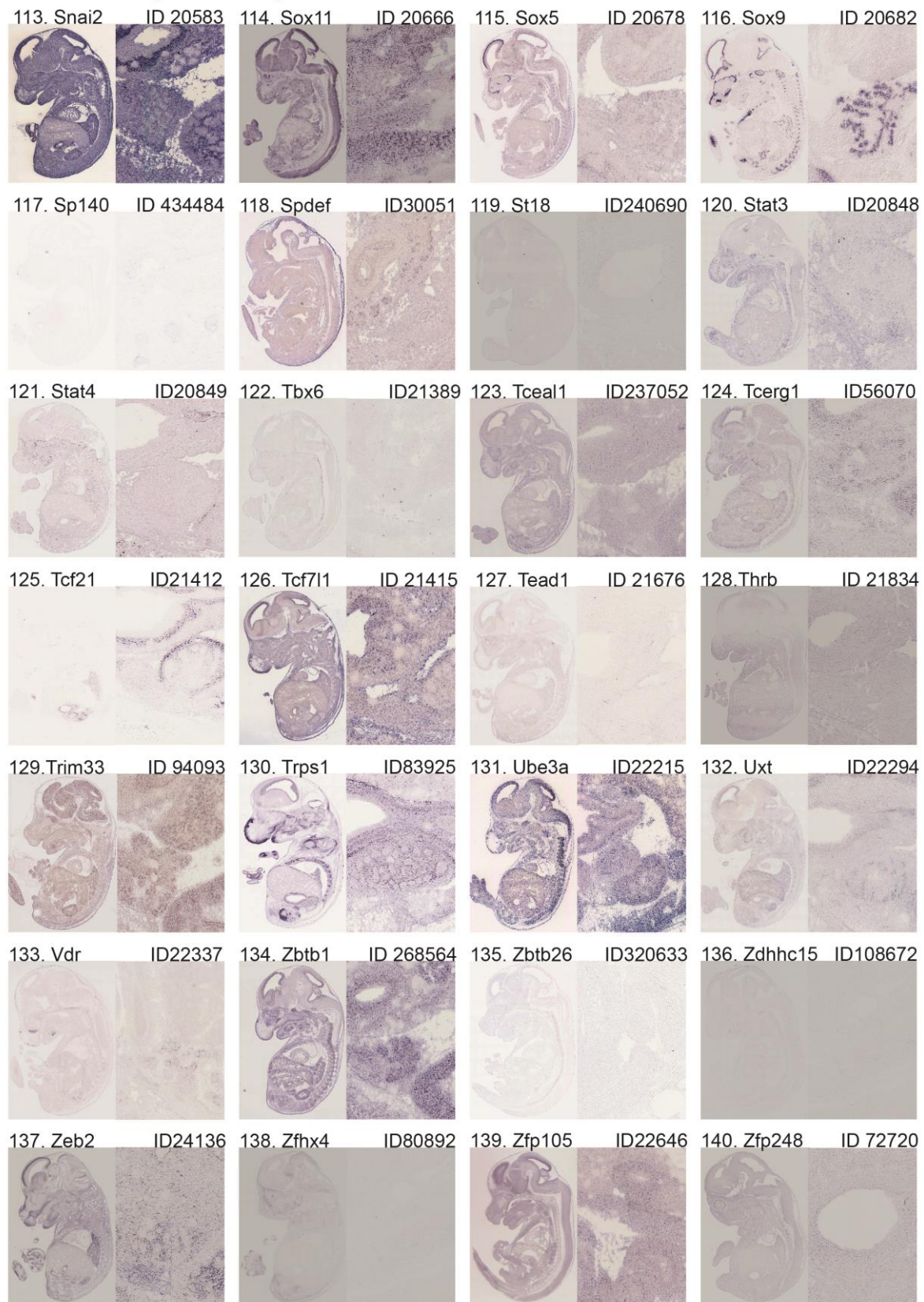
GO term Transcription factors epithelial 57-84



GO term Transcription factors epithelial 85-112

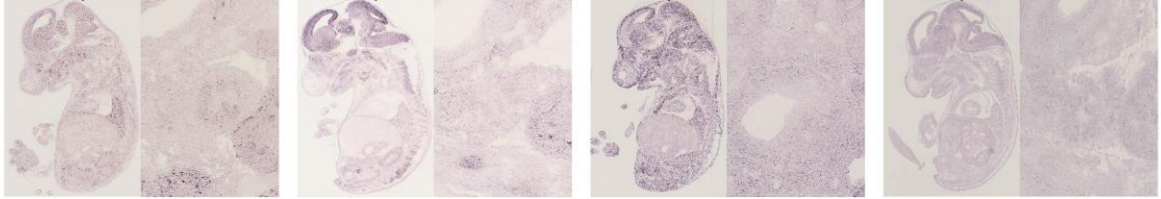


GO term Transcription factors epithelial 113-140

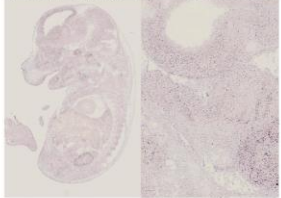


GO term Transcription factors epithelial 141-145

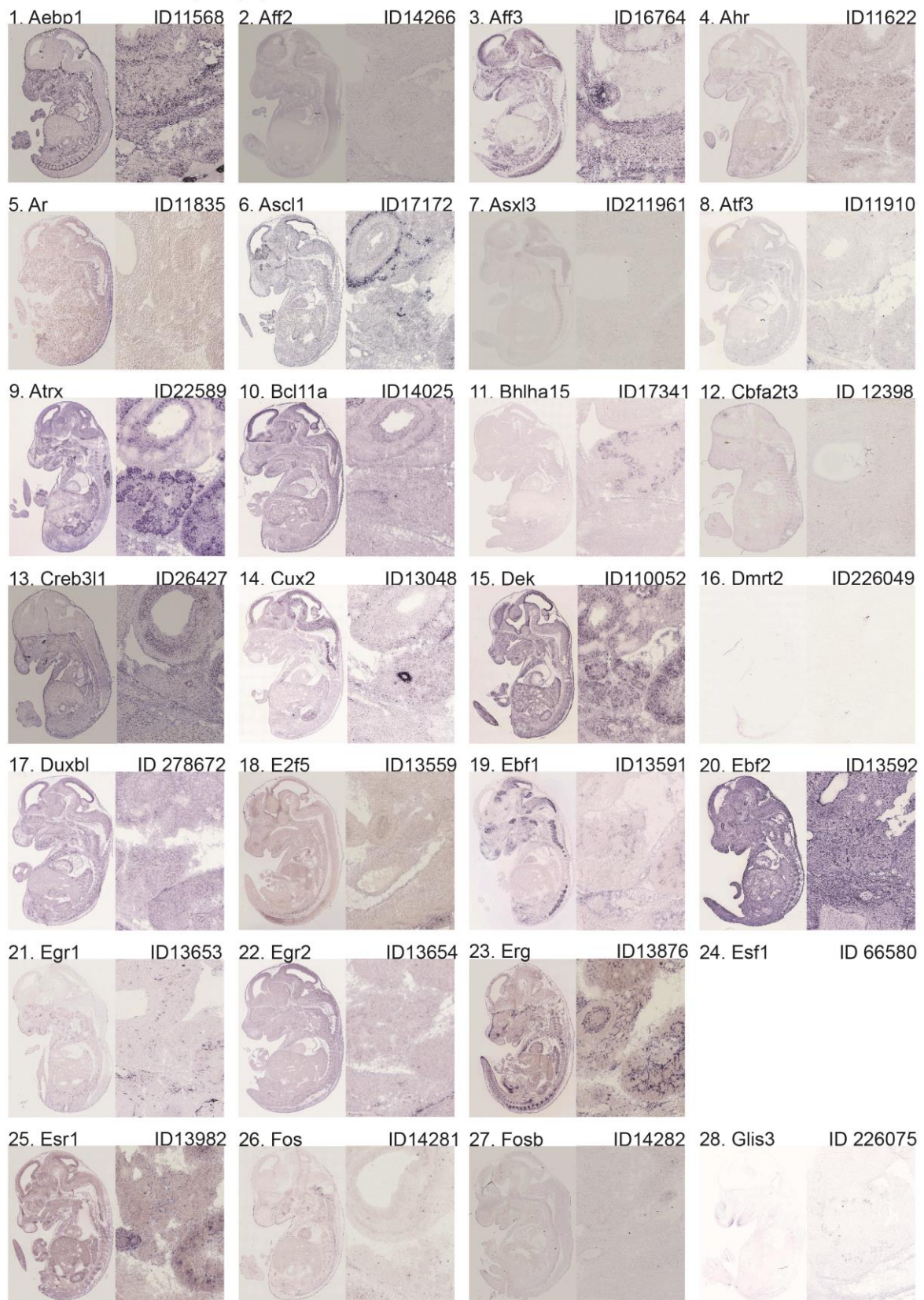
141. Zfp281 ID 226442 142. Zfp462 ID 242466 143. Zfp521 ID 225207 144. Zfp558 ID 72230



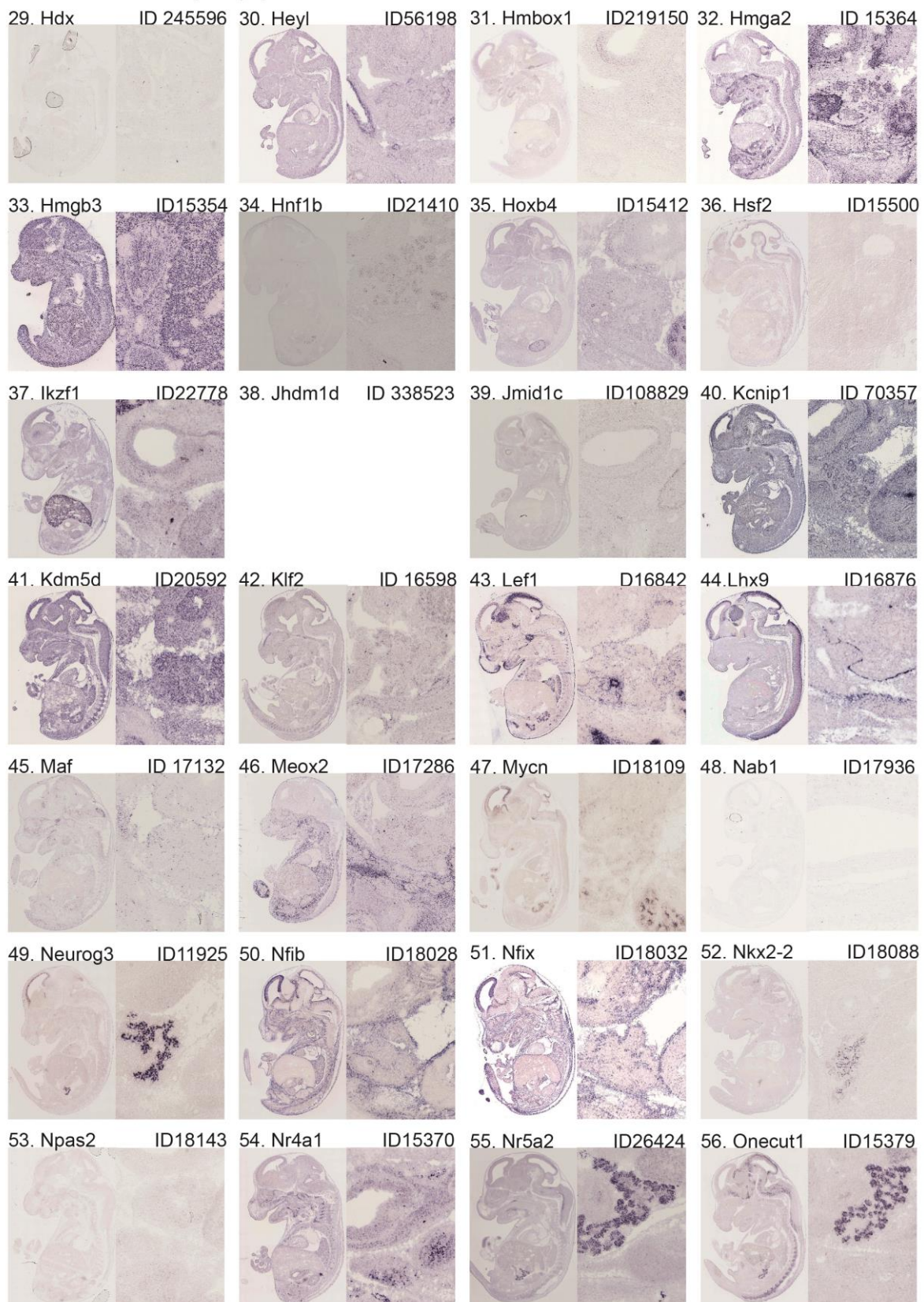
145. Zranb2 ID53861



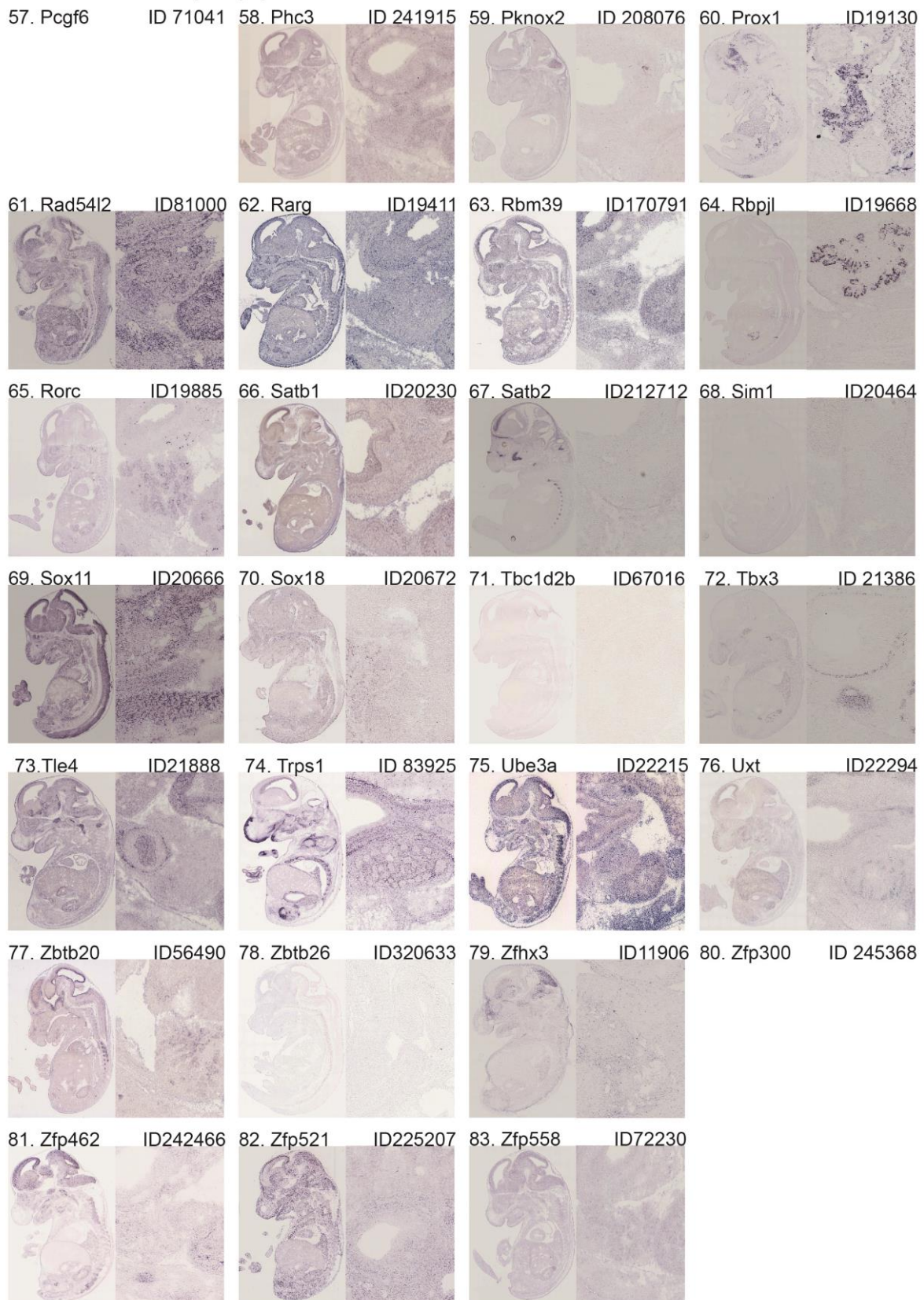
GO term TF mesenchymal population 1-28



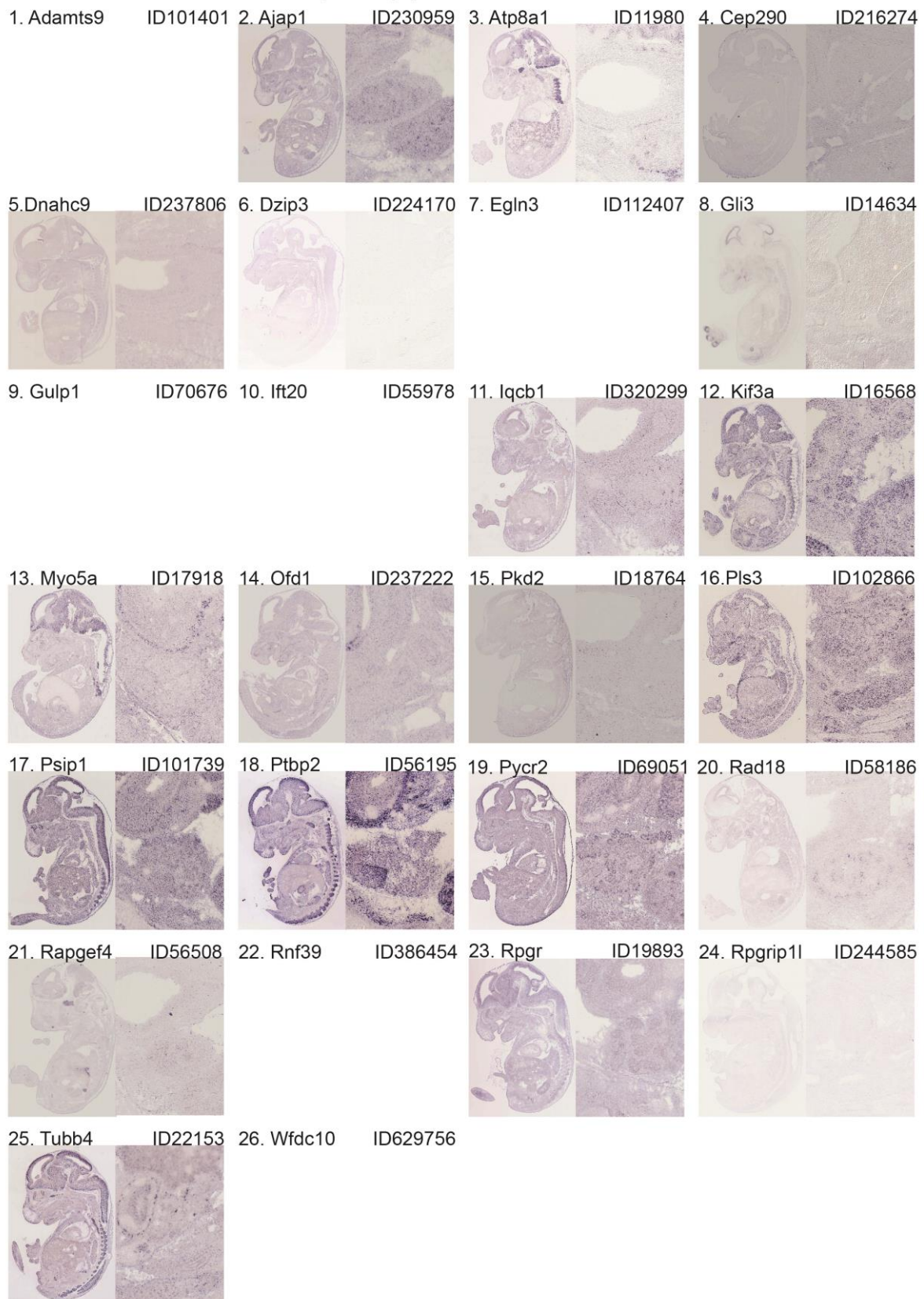
GO term TF mesenchymal population 29-56



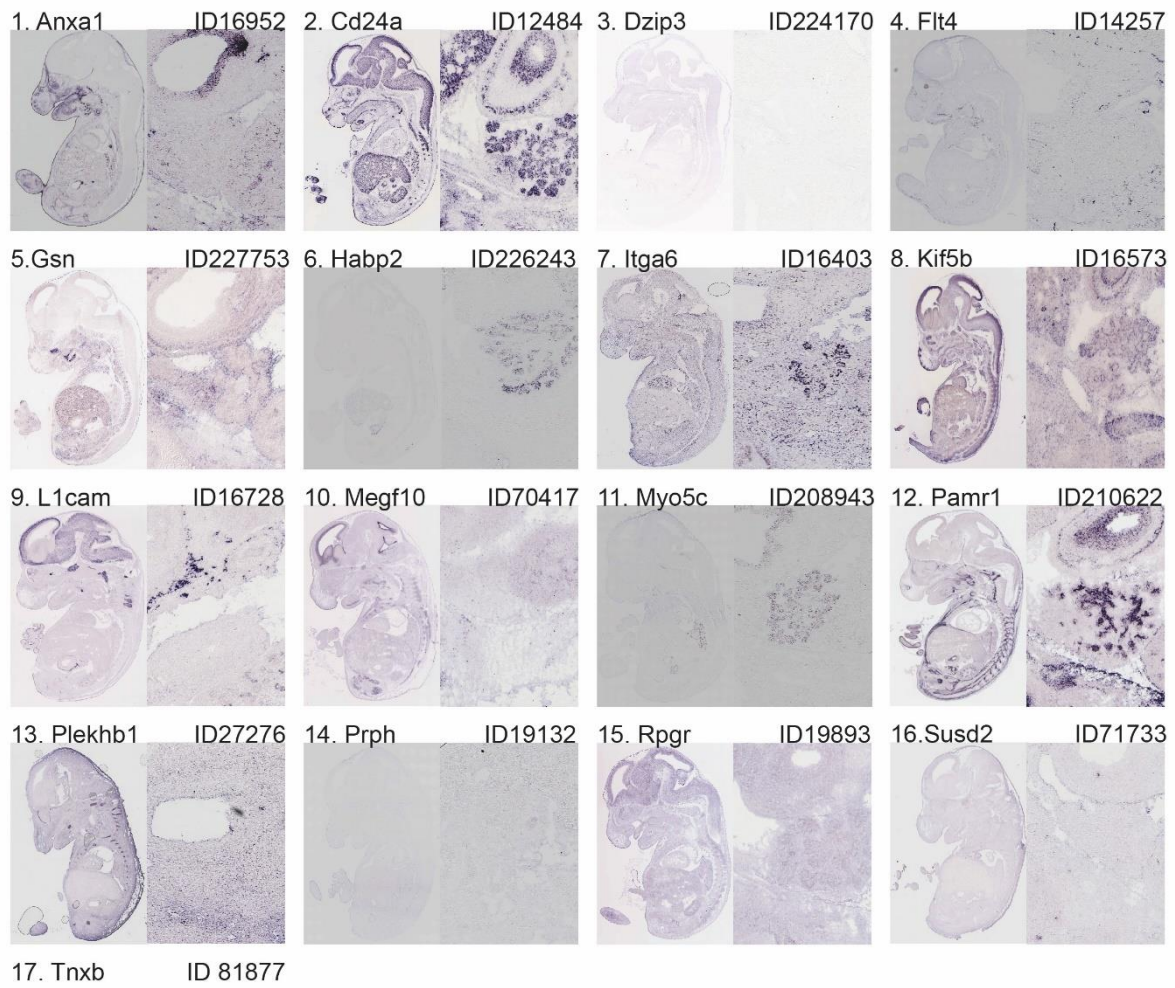
GO term TF mesenchymal population 57-83



GO term extracellular cilium related epithelial population 1-26

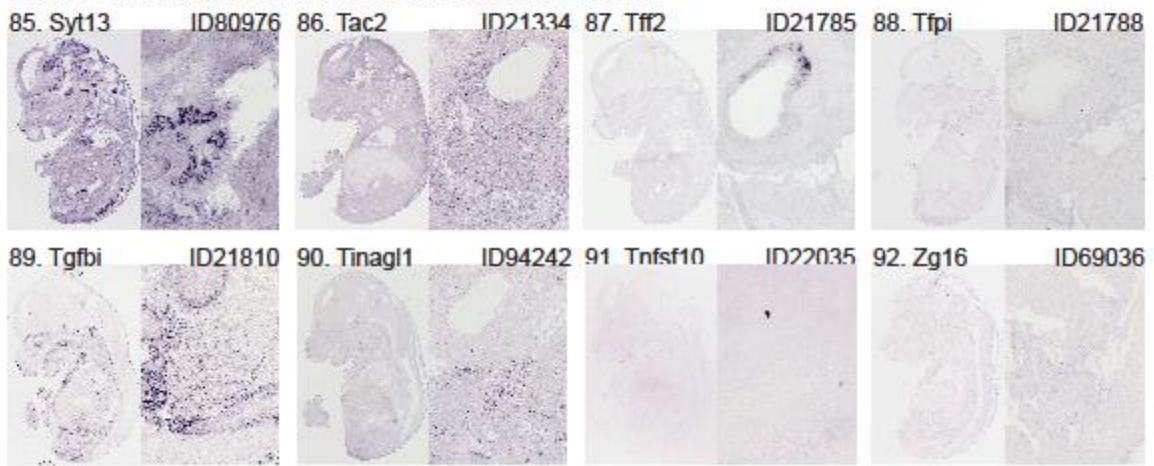


GO term extracellular cilium related mesenchymal population 1-17



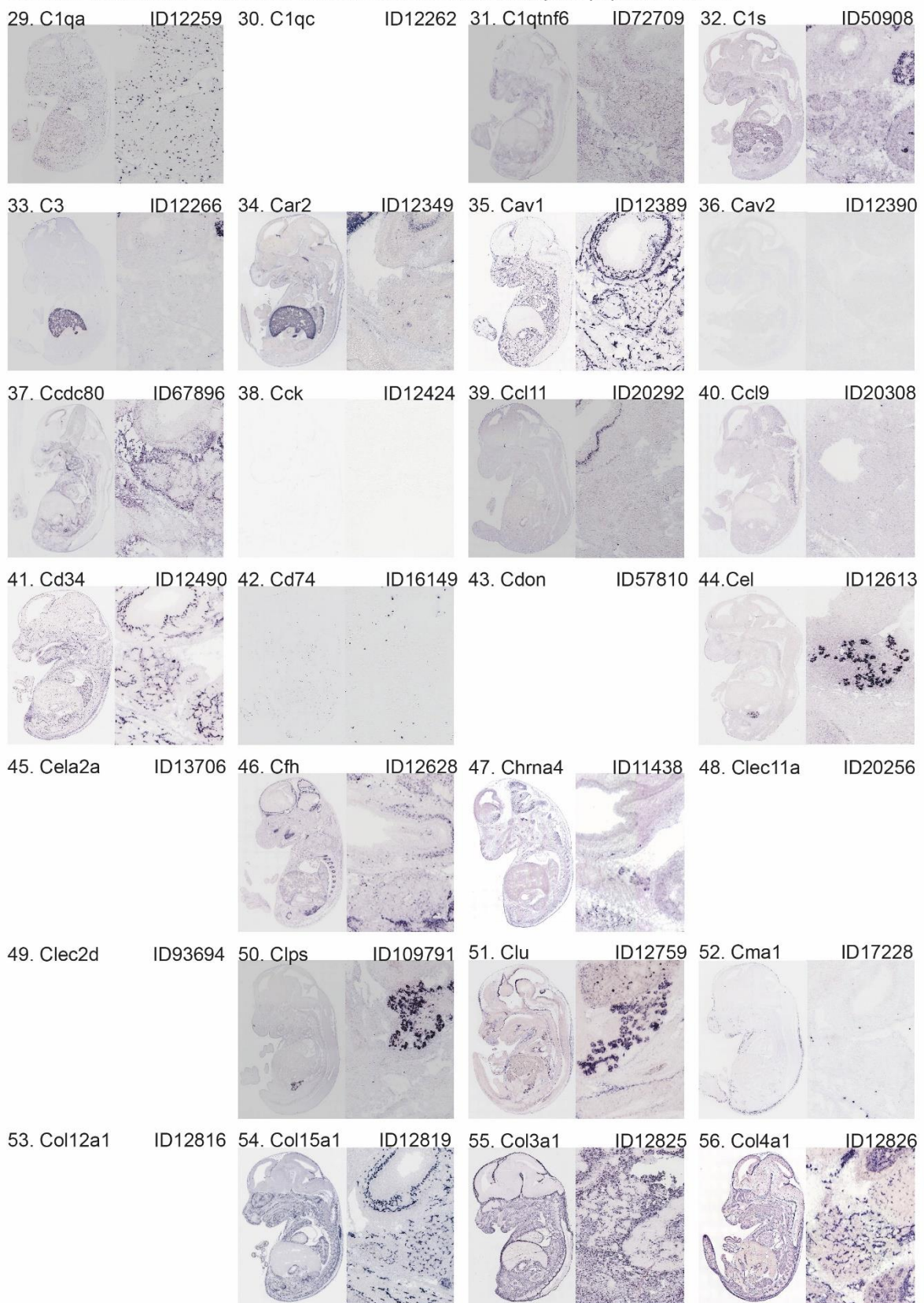


GO term extracellular located at PM epithelial population 85-92





GO term extracellular located at Plasmamembrane in mesenchymal population 29-56





### 6.3 Literature

- Adolfson, B. & Littleton, J.T., 2001. Genetic and molecular analysis of the synaptotagmin family. *Cell Molecular Life Science*, 58(3), pp.393-402.
- Afelik, S., Chen, Y. & Pieler, T., 2006. Combined ectopic expression of Pdx1 and Ptf1a/p48 results in the stable conversion of posterior endoderm into endocrine and exocrine pancreatic tissue. *Genes & development*, 20(11), pp.1441–6. Available at: <http://genesdev.cshlp.org/content/20/11/1441.long>.
- Afelik, S. et al., 2013. Notch signaling in the pancreas: patterning and cell fate specification. Wiley Interdisciplinary reviews: *Developmental Biology*, 2(4), pp. 531-44
- Ahnfelt-Ronne, J. et al., 2012. Ptf1a-mediated control of Dll1 reveals an alternative to the lateral inhibition mechanism. *Development*, 139(1), pp. 33-45
- Andersson, S.A. et al., 2012. Reduced insulin secretion correlates with decreased expression of exocytotic genes in pancreatic islets from patients with type 2 diabetes. *Molecular and cellular endocrinology*, 364(1-2), pp.36–45. Available at: <http://www.sciencedirect.com/science/article/pii/S0303720712004042> [Accessed September 15, 2015].
- Apeqvist, A. et al., 1999. Notch signaling controls pancreatic cell differentiation. *Nature*, 400(6747), pp877-81
- Apodaca, G., Gallo, L.I. & Bryant, D.M., 2012. Role of membrane traffic in the generation of epithelial cell asymmetry. *Nature Cell Biology*, 14(12), pp.1235–1243. Available at: <http://eutils.ncbi.nlm.nih.gov/entrez/eutils/elink.fcgi?dbfrom=pubmed&id=23196841&retmode=ref&cmd=prlinks\npapers2://publication/doi/10.1038/ncb2635>.
- Augustine, G.J., 2001. How does calcium trigger neurotransmitter release? *Current Opinion in Neurobiology*, 11(3), pp.320-6
- Van Arensbergen, J. et al., 2010. Derepression of polycomb targets during pancreatic organogenesis allows insulin-producing beta-cells to adopt a neural gene activity program. *Genome Research*, 20(6), pp.722–732.
- Artner, I. et al., 2007. MafB is required for islet beta cell maturation. *Proceedings of the National Academy of Sciences of the United States of America*, 104(16), pp.3853–3858.
- Bacaj, T. et al., 2013. Synaptotagmin-1 and synaptotagmin-7 trigger synchronous and asynchronous phases of neurotransmitter release. *Neuron*, 80(4), pp.947–59. Available at: <http://www.sciencedirect.com/science/article/pii/S0896627313009306> [Accessed September 30, 2015].
- Baek, S.H. et al., 2003. Regulated subset of G1 growth-control genes in response to derepression by the Wnt pathway. *Proceedings of the National Academy of Sciences of the United States of America*, 100(6), pp.3245–3250.
- Bahmanyar, S. et al., 2008.  $\beta$ -catenin is a Nek2 substrate involved in centrosome separation. *Genes and Development*, 22(1), pp.91–105.
- Baumgartner, B.K. et al., 2014. Distinct requirements for beta-catenin in pancreatic epithelial growth and patterning. *Developmental Biology*, 391(1), pp.89-98
- Beddington, R.S.P. & Robertson, E.J., 1999. Axis development and early asymmetry in mammals. *Cell*, 96(2), pp.195–209.
- Belo, J. et al., 2013. The role of SOX9 transcription factor in pancreatic and duodenal development. *Stem Cells and Development*, 22(22), pp. 2935-43
- Blanco, M.J. et al., 2002. G????????? ?? ????? ?????????? ??? ?????????????? ????? ??? ????? ????? ?????? ?? ?????? ?????????? *Oncogene*, pp.3241–3246.
- Boehlke, C. et al., 2013. Kif3a Guides Microtubular Dynamics, Migration and Lumen Formation of MDCK Cells. *PLoS ONE*, 8(5), p.e62165. Available at: <http://dx.plos.org/10.1371/journal.pone.0062165>.
- Bonner-Weir, S., 2000. Life and death of the pancreatic beta cells. *Trends in endocrinology and metabolism: TEM*, 11(9), pp.375–378. Available at: <http://www.ncbi.nlm.nih.gov/pubmed/11042468>.
- Bonner-Weir, S. et al., 1993. A second pathway for regeneration of adult exocrine and endocrine pancreas. A possible recapitulation of embryonic development. *Diabetes*, 42(12), pp.1715-20
- Boyer, D.F. et al., 2006. Complementation rescue of Pdx1 null phenotype demonstrates distinct roles of proximal and distal cis-regulatory sequences in pancreatic and duodenal expression. *Developmental Biology*, 298(2), pp.616–631. Available at: <http://linkinghub.elsevier.com/retrieve/pii/S0012160606010268>.
- Burtscher, I., Barkey, W. & Lickert, H., 2013. Foxa2-venus fusion reporter mouse line allows live-cell analysis of endoderm-derived organ

- formation. *Genesis*, 51(8), pp.596–604.
- Burtscher, I. & Lickert, H., 2009. Foxa2 regulates polarity and epithelialization in the endoderm germ layer of the mouse embryo. *Development*, 136(6), pp.1029–1038. Available at: <http://dev.biologists.org/cgi/doi/10.1242/dev.028415>.
- Cano, D. a., Sekine, S. & Hebrok, M., 2006. Primary Cilia Deletion in Pancreatic Epithelial Cells Results in Cyst Formation and Pancreatitis. *Gastroenterology*, 131(6), pp.1856–1869. Available at: <http://linkinghub.elsevier.com/retrieve/pii/S0016508506022840>.
- Carpino, G. et al., 2016. Peribiliary Glands as a Niche of Extra-Pancreatic Precursors Yielding Insulin-Producing Cells in Experimental and Human Diabetes. *Stem Cells*. Feb 6. doi: 10.1002/stem.2311
- Caveoer, D.R., 1987. volume 15 Number 4 1987 *Nucleic Acids Research*, 15(4), pp.1353–1361.
- Chapman, ER., 2008. How does synaptotagmin trigger neurotransmitter release? *Annual Review of Biochemistry*, 77, pp. 615-41
- Chakravarti, S., 1998. Lumican Regulates Collagen Fibril Assembly: Skin Fragility and Corneal Opacity in the Absence of Lumican. *The Journal of Cell Biology*, 141(5), pp.1277–1286. Available at: <http://jcb.rupress.org/content/141/5/1277.abstract> [Accessed June 25, 2015].
- Ciruna, B. & Rossant, J., 2001. FGF signaling regulates mesoderm cell fate specification and morphogenetic movement at the primitive streak. *Developmental Cell*, 1(1), pp.37–49. Available at: [http://www.ncbi.nlm.nih.gov/entrez/query.fcgi?cmd=Retrieve&db=PubMed&dopt=Citation&list\\_uids=11703922](http://www.ncbi.nlm.nih.gov/entrez/query.fcgi?cmd=Retrieve&db=PubMed&dopt=Citation&list_uids=11703922).
- Cockburn, K. & Rossant, J., 2010. Making the blastocyst: lessons from the mouse. *The Journal of clinical investigation*, 120(4), pp.995–1003. Available at: <http://www.pubmedcentral.nih.gov/articlerender.fcgi?artid=2846056&tool=pmcentrez&rendertype=abstract>.
- Collu, GM. et al., 2014. Wnt-Notch signaling crosstalks in development and disease. *Cellular and molecular life sciences*, 71(18), pp.3553-67
- Corbit, K.C. et al., 2008. Kif3a constrains  $\beta$ -catenin-dependent Wnt signalling through dual ciliary and non-ciliary mechanisms. *Nature Cell Biology*, 10(1), pp.70–76. Available at: <http://www.nature.com/doi/10.1038/ncb1670>.
- Cortijo, C. et al., 2012. Planar Cell Polarity Controls Pancreatic Beta Cell Differentiation and Glucose Homeostasis. *Cell Reports*, 2(6), pp.1593–1606. Available at: <http://linkinghub.elsevier.com/retrieve/pii/S2211124712003713>.
- Courtney, M. et al., 2013. The Inactivation of Arx in Pancreatic  $\beta$ -Cells Triggers Their Neogenesis and Conversion into Functional  $\beta$ -Like Cells. *PLoS Genetics*, 9(10), p.e1003934. Available at: <http://dx.plos.org/10.1371/journal.pgen.1003934>.
- Cras-Meneur, C. et al., 2009. Presenilins, Notch dose control the fate of pancreatic endocrine progenitors during a narrow developmental window. *Genes and Development*, 23(17), pp.2088-101
- Crisera, CA. et al., 2000. Expression and role of laminin-1 in mouse pancreatic organogenesis. *Diabetes*, 49(6), pp.936-44
- D'Atri, F. & Citi, S., 2001. Cingulin interacts with F-actin in vitro. *FEBS Lett*, 507(1), pp.21–24. Available at: [http://www.ncbi.nlm.nih.gov/entrez/query.fcgi?cmd=Retrieve&db=PubMed&dopt=Citation&list\\_uids=11682052](http://www.ncbi.nlm.nih.gov/entrez/query.fcgi?cmd=Retrieve&db=PubMed&dopt=Citation&list_uids=11682052).
- Delaval, B. et al., 2011. Centrin depletion causes cyst formation and other ciliopathy-related phenotypes in zebrafish and *developmental cell*, 10(22), pp.3964–3972.
- Dragoi, a.-M. et al., 2014. Novel Strategies to Enforce an Epithelial Phenotype in Mesenchymal Cells. *Cancer Research*, 74(14), pp.3659–3672. Available at: <http://cancerres.aacrjournals.org/cgi/doi/10.1158/0008-5472.CAN-13-3231>.
- Dubois, C.L. et al., 2011. Sox9-Haploinsufficiency Causes Glucose Intolerance in Mice. *PLoS ONE*, 6(8), p.e23131. Available at: <http://dx.plos.org/10.1371/journal.pone.0023131>.
- Dupin, I., Camand, E. & Etienne-Manneville, S., 2009. Classical cadherins control nucleus and centrosome position and cell polarity. *The Journal of Cell Biology*, 185(5), pp.779–786. Available at: <http://www.jcb.org/cgi/doi/10.1083/jcb.200812034>.
- Dymecki, S.M., 1996. Flp recombinase promotes site-specific DNA recombination in embryonic stem cells and transgenic mice. *Proceedings of the National Academy of Sciences of the United States of America*, 93(12), pp.6191–6196.
- Ebnet, K., 2003. The junctional adhesion molecule (JAM) family members JAM-2 and JAM-3 associate with the cell polarity protein PAR-3: a possible role for JAMs in endothelial cell polarity. *Journal of Cell Science*, 116(19), pp.3879–3891. Available at: <http://jcs.biologists.org/cgi/doi/10.1242/jcs.00704>.
- Engert, S. et al., 2013. The Sox17CreERT2 knock-in mouse line displays spatiotemporal activation of Cre recombinase in distinct Sox17 lineage progenitors. *Genesis*, 51(11), pp.793–802.
- Ertaylan, G.ä. et al., 2014. Gene regulatory network analysis reveals differences in site-specific cell fate determination in mammalian brain. *Frontiers in Cellular Neuroscience*, 8(December), pp.1–14. Available at: <http://journal.frontiersin.org/article/10.3389/fncel.2014.00437/abstract>.

- van Eyll, J.M. et al., 2006. Eph receptors and their ephrin ligands are expressed in developing mouse pancreas. *Gene Expression Patterns*, 6(4), pp.353–359.
- Falkowski, M. a et al., 2011. Expression , localization , and functional role for synaptotagmins in pancreatic acinar cells. , 2(4), pp.306–316.
- Frantz, J.D. et al., 1997. Human GRB-IRbeta/GRB10. Splice variants of an insulin and growth factor receptor-binding protein with PH and SH2 domains. *The Journal of Biological Chemistry*, 31(5), pp. 2659-67
- Frydman, H.M. & Spradling, a C., 2001. The receptor-like tyrosine phosphatase lar is required for epithelial planar polarity and for axis determination within drosophila ovarian follicles. *Development (Cambridge, England)*, 128, pp.3209–3220.
- Fujikura, J. et al., 2006. Notch/Rbp-j signaling prevents premature endocrine and ductal cell differentiation in the pancreas. *Cell Metabolism*, 3(1), pp.59-65
- Fujino, T. et al., 2003. Low-density lipoprotein receptor-related protein 5 (LRP5) is essential for normal cholesterol metabolism and glucose-induced insulin secretion. *Proceedings of the National Academy of Sciences of the United States of America*, 100(1), pp.229-34
- Fukuda, M. et al., 2000. Role of the conserved WHXL motif in the C terminus of synaptotagmin in synaptic vesicle docking. *Proceedings of the National Academy of Sciences of the United States of America*, 97(26), pp.14715–9. Available at: <http://www.pubmedcentral.nih.gov/articlerender.fcgi?artid=18984&tool=pmcentrez&rendertype=abstract>.
- Fukuda, M. & Mikoshiba, K., 2001. Characterization of KIAA1427 protein as an atypical synaptotagmin (Syt XIII). *The Biochemical journal*, 354(Pt 2), pp.249–257.
- Fuller, M.T. & Spradling, A.C., 2007. Germline Stem Cells : Two Versions of Immortality. *Science*, (April), pp.402–404.
- Galic, M. & Matis, M., 2015. Polarized trafficking provides spatial cues for planar cell polarization within a tissue. *BioEssays*, p.n/a–n/a. Available at: <http://doi.wiley.com/10.1002/bies.201400196>.
- Gálvez-Santisteban, M. et al., 2012. Synaptotagmin-like proteins control the formation of a single apical membrane domain in epithelial cells. *Nature Cell Biology*, 14(8), pp.838–849. Available at: <http://www.nature.com/doi/10.1038/ncb2541>.
- Gao, N. et al., 2008. Dynamic regulation of Pdx1 enhancers by Foxa1 and Foxa2 is essential for pancreas development. *Genes and Development*, 22(24), pp.3435–3448.
- Gardner, R.L., 2001. Specification of embryonic axes begins before cleavage in normal mouse development. *Development (Cambridge, England)*, 128(6), pp.839–47. Available at: <http://www.ncbi.nlm.nih.gov/pubmed/11222139>.
- Gauthier, B. & Wollheim, C., 2008. Synaptotagmins bind calcium to release insulin. *American Journal of Physiology. Endocrinology and Metabolism*, 295, pp.E1279–E1286. Available at: <http://ajpendo.physiology.org/content/295/6/E1279.short>.
- Gegg, M. et al., 2014. Flattop regulates basal body docking and positioning in mono- and multiciliated cells. *eLife*, 3, pp.1–24. Available at: <http://elifesciences.org/lookup/doi/10.7554/eLife.03842>.
- Geppert, M. et al., 1994. Synaptotagmin I: A major Ca<sup>2+</sup> sensor for transmitter release at a central synapse. *Cell*, 79(4), pp.717–727. Available at: <http://www.sciencedirect.com/science/article/pii/0092867494905568> [Accessed September 30, 2015].
- Gibb, N., Lavery, D.L. & Hoppler, S., 2013. sfrp1 promotes cardiomyocyte differentiation in Xenopus via negative-feedback regulation of Wnt signalling. *Development (Cambridge, England)*, 140(7), pp.1537–49. Available at: <http://www.pubmedcentral.nih.gov/articlerender.fcgi?artid=4074298&tool=pmcentrez&rendertype=abstract>.
- Gittes, G.K., 2009. Developmental biology of the pancreas: A comprehensive review. *Developmental Biology*, 326(1), pp.4–35. Available at: <http://dx.doi.org/10.1016/j.ydbio.2008.10.024>.
- Gittes, G.K. et al., 1996. Lineage-specific morphogenesis in the developing pancreas: role of mesenchymal factors. *Development (Cambridge, England)*, 122(2), pp.439–447.
- Gloyn, AL. et al., 2002. Maturity-onset diabetes of the young caused by a balanced translocation where the 20q12 break point results in disruption upstream of the coding region of the hepatocyte nuclear factor-4alpha (HNF4A) gene. *Diabetes*, 51(7), pp.2313-6
- Golosow, N., 1962. Epitheliomesenchymal interaction in pancreas morphogenesis. *Developmental Biology*, Apr4, pp.242–55
- Gosmain, Y., 2010. Pax6 controls the expression of critical genes involved in pancreatic (alpha) cell differentiation and function. *Journal of biological chemistry*, 285(43), pp. 33381-93
- Gotta, M., Abraham, M.C. & Ahringer, J., 2001. CDC-42 controls early cell polarity and spindle orientation in C. elegans. *Current Biology*, 11(7), pp.482–488.
- Gouzi, M. et al., 2011. Neurogenin3 initiates stepwise delamination of differentiating endocrine cells during pancreas development. *Developmental Dynamics*, 240(3), pp.589–604.

- Gradwohl, G. et al., 2000. Neurogenin3 Is Required for the Development of the Four Endocrine Cell Lineages of the Pancreas. *Proceedings of the National Academy of Sciences of the United States of America*, 97(4), pp.1607–1611.
- Granot, Z. et al., 2009. LKB1 Regulates Pancreatic  $\beta$  Cell Size, Polarity, and Function. *Cell Metabolism*, 10(4), pp.296–308. Available at: <http://linkinghub.elsevier.com/retrieve/pii/S1550413109002587>.
- Gray, R.S., Roszko, I. & Solnica-Krezel, L., 2011. Planar Cell Polarity: Coordinating Morphogenetic Cell Behaviors with Embryonic Polarity. *Developmental Cell*, 21(1), pp.120–133. Available at: <http://linkinghub.elsevier.com/retrieve/pii/S1534580711002450>.
- Gu, G. et al., 2004. Global expression analysis of gene regulatory pathways during endocrine pancreatic development. *Development (Cambridge, England)*, 131(1), pp.165–179.
- Gu, G., Dubauskaite, J. & Melton, D. a, 2002. Direct evidence for the pancreatic lineage: NGN3+ cells are islet progenitors and are distinct from duct progenitors. *Development (Cambridge, England)*, 129(10), pp.2447–2457.
- Gut, a et al., 2001. Expression and localisation of synaptotagmin isoforms in endocrine beta-cells: their function in insulin exocytosis. *J Cell Sci*, 114(Pt 9), pp.1709–1716. Available at: [http://www.ncbi.nlm.nih.gov/entrez/query.fcgi?cmd=Retrieve&db=PubMed&dopt=Citation&list\\_uids=11309201](http://www.ncbi.nlm.nih.gov/entrez/query.fcgi?cmd=Retrieve&db=PubMed&dopt=Citation&list_uids=11309201)  
[\npapers://16a943e3-1d14-4259-a468-c82b7e4def7c/Paper/p326](http://papers://16a943e3-1d14-4259-a468-c82b7e4def7c/Paper/p326).
- Hale, M. a. et al., 2014. The nuclear hormone receptor family member NR5A2 controls aspects of multipotent progenitor cell formation and acinar differentiation during pancreatic organogenesis. *Development*, 141(16), pp.3123–3133. Available at: <http://dev.biologists.org/cgi/doi/10.1242/dev.109405>.
- Han, D. et al., 2011. Detection of differential proteomes associated with the development of type 2 diabetes in the Zucker rat model using the iTRAQ technique. *Journal of proteome research*, 10(2), pp.564–77. Available at: <http://www.ncbi.nlm.nih.gov/pubmed/21117707>.
- Hay, C.W. et al., 2005. Glucagon-like peptide-1 stimulates human insulin promoter activity in part through cAMP-responsive elements that lie upstream and downstream of the transcription start site. *Journal of Endocrinology*, 186(2), pp.353–365.
- Hart, A. et al., 2003. Fgf10 maintains notch activation, stimulates proliferation and blocks differentiation of pancreatic epithelial cells, *Developmental Dynamics*, 228(2), pp.185-93
- Heiser, PW: et al., 2004. Development and cancer: lessons learned in the pancreas. *Cell Cycle*, 3(3), pp.270-2
- Hernandez\_sanchez, C. et al., 2008. Evolution of the insulin receptor family and receptor isoform expression in vertebrates. *Molecular Biology and Evolution*, 25(6), pp.1043-53
- Herrera, P.L., 2000. Adult insulin- and glucagon-producing cells differentiate from two independent cell lineages. *Development (Cambridge, England)*, 127(11), pp.2317–2322.
- Hesselson, D., Anderson, R.M. & Stainier, D.Y.R., 2011. Suppression of Ptf1a Activity Induces Acinar-to-Endocrine Conversion. *Current Biology*, 21(8), pp.712–717. Available at: <http://linkinghub.elsevier.com/retrieve/pii/S0960982211003459>.
- Holland, A.M. et al., 2002. Experimental control of pancreatic development and maintenance. *Proceedings of the National Academy of Sciences of the United States of America*, 99(19), pp.12236–12241.
- Horn, S. et al., 2012. Mind bomb 1 is required for pancreatic  $\beta$ -cell function. *Proceedings of the National Academy of Sciences of the United States of America*, 147(2-3), pp.7356-61
- Hutterer, A. et al., 2004. Sequential roles of Cdc42, Par-6, aPKC, and Lgl in the establishment of epithelial polarity during Drosophila embryogenesis. *Developmental Cell*, 6(6), pp.845–854.
- Ichikawa, D. et al., 2013. Live imaging of whole mouse embryos during gastrulation: migration analyses of epiblast and mesodermal cell. *PLoS One*, 8(7), e64506
- Ikeda, W. et al., 1999. Afadin: A key molecule essential for structural organization of cell-cell junctions of polarized epithelia during embryogenesis. *The Journal of cell biology*, 146(5), pp.1117–32. Available at: <http://www.pubmedcentral.nih.gov/articlerender.fcgi?artid=2169488&tool=pmcentrez&rendertype=abstract>.
- Jensen, J., 2004. Gene Regulatory Factors in Pancreatic Development. *Developmental Dynamics*, 229(1), pp.176–200.
- Jhala, U.S. et al., 2003. cAMP promotes pancreatic  $\beta$  -cell survival via CREB-mediated induction of IRS2. *Genes and Development*, 17(858), pp.1575–1580.
- Jia, D., Sun, Y. & Konieczny, S.F., 2008. Mist1 Regulates Pancreatic Acinar Cell Proliferation Through p21CIP1/WAF1. *Gastroenterology*, 135(5), pp.1687–1697. Available at: <http://linkinghub.elsevier.com/retrieve/pii/S001650850801370X>.

- Joglekar, M.V. et al., 2007. MicroRNA profiling of developing and regenerating pancreas reveal post-transcriptional regulation of neurogenin3. *Developmental Biology*, 311(2), pp.603-12
- Johansson, K. a. et al., 2007. Temporal Control of Neurogenin3 Activity in Pancreas Progenitors Reveals Competence Windows for the Generation of Different Endocrine Cell Types. *Developmental Cell*, 12(3), pp.457-465. Available at: <http://linkinghub.elsevier.com/retrieve/pii/S1534580707000615>.
- Johnson, M.H., Maro, B. & Takeichi, M., 1986. The role of cell adhesion in the synchronization and orientation of polarization in 8-cell mouse blastomeres. *Journal of embryology and experimental morphology*, 93, pp.239-255.
- Jonatan, D. et al., 2014. Sox17 Regulates Insulin Secretion in the Normal and Pathologic Mouse  $\beta$  Cell. *PLoS ONE*, 9(8), p.e104675. Available at: <http://dx.plos.org/10.1371/journal.pone.0104675>.
- Jones, C. et al., 2008. Ciliary proteins link basal body polarization to planar cell polarity regulation. *Nature Genetics*, 40(1), pp.69-77. Available at: <http://www.nature.com/doi/10.1038/ng.2007.54>.
- Kaku, K. et al., 2010. Original Article. *Obesity and Metabolism*, 55(March), pp.341-347.
- Karihaloo, A. et al., 2005. Vascular Endothelial Growth Factor Induces Branching Morphogenesis / Tubulogenesis in Renal Epithelial Cells in a Neuropilin-Dependent Fashion Vascular Endothelial Growth Factor Induces Branching Morphogenesis / Tubulogenesis in Renal Epithelial Cells in . *Society*, 25(17), pp.7441-7448.
- Kawaguchi, Y. et al., 2002. The role of the transcriptional regulator Ptf1a in converting intestinal to pancreatic progenitors. *Nature Genetics*, 32(1), pp.128-134. Available at: <http://www.nature.com/doi/10.1038/ng959>.
- Kesavan, G. et al., 2014. Cdc42/N-WASP signaling links actin dynamics to pancreatic cell delamination and differentiation. *Development*, 141(3), pp.685-696. Available at: <http://dev.biologists.org/cgi/doi/10.1242/dev.100297>.
- Kesavan, G. et al., 2009. Cdc42-Mediated Tubulogenesis Controls Cell Specification. *Cell*, 139(4), pp.791-801. Available at: <http://linkinghub.elsevier.com/retrieve/pii/S0092867409011891>.
- Kim, H.J. et al., 2005. Wnt5 signaling in vertebrate pancreas development. *BMC biology*, 3, p.23.
- Kim, S.K. et al., 2000. Activin receptor patterning of foregut organogenesis. *Genes & Development*, 14(15), pp.1866-1871. Available at: <http://www.pubmedcentral.nih.gov/articlerender.fcgi?artid=316826&tool=pmcentrez&rendertype=abstract>.
- Kim, S.K. & Melton, D. a, 1998. Pancreas development is promoted by cyclopamine, a hedgehog signaling inhibitor. *Proceedings of the National Academy of Sciences of the United States of America*, 95(22), pp.13036-41. Available at: <http://www.pubmedcentral.nih.gov/articlerender.fcgi?artid=23700&tool=pmcentrez&rendertype=abstract>.
- Kinder, S. J., Tsang, T. E., Quinlan, G. A., Hadjantonakis, A. K., Nagy, A. and Tam, P. P. (1999). The orderly allocation of mesodermal cells to the extraembryonic structures and the anteroposterior axis during gastrulation of the mouse embryo. *Development* 126, 4691-4701.
- Kinder, S. J., Tsang, T. E., Wakamiya, M., Sasaki, H., Behringer, R. R., Nagy, A. and Tam, P. P. (2001). The organizer of the mouse gastrula is composed of a dynamic population of progenitor cells for the axial mesoderm. *Development* 128, 3623-3634.
- Kinzel, D. et al., 2010. Pitchfork Regulates Primary Cilia Disassembly and Left-Right Asymmetry. *Developmental Cell*, 19(1), pp.66-77. Available at: <http://linkinghub.elsevier.com/retrieve/pii/S1534580710002959>.
- Kitamura, T. et al., 2002. The forkhead transcription factor Foxo1 links insulin signaling to Pdx1 regulation of pancreatic  $\beta$  cell growth. *Journal of Clinical Investigation*, 110(12), pp.1839-1847.
- Koh, T.W. et al., 2003. Synaptotagmin I, a Ca<sup>2+</sup> sensor for neurotransmitter release. *Trends in Neurosciences*, 26(8), pp.413-22
- Kone, M. et al., 2014. LKB1 and AMPK differentially regulate pancreatic  $\beta$ -cell identity. *The FASEB Journal*, 28(11), pp.4972-4985. Available at: <http://www.fasebj.org/cgi/doi/10.1096/fj.14-257667>.
- Kopp, J.L. et al., 2011. Progenitor cell domains in the developing and adult pancreas. *Cell Cycle*, 10(12), pp.1921-1927.
- Krapp, a et al., 1996. The p48 DNA-binding subunit of transcription factor PTF1 is a new exocrine pancreas-specific basic helix-loop-helix protein. *The EMBO journal*, 15(16), pp.4317-4329.
- Kulkarni, R.N., 2002. Receptors for insulin and insulin-like growth factor-1 and insulin receptor substrate-1 mediate pathways that regulate islet function. *Biochemical Society transactions*, 30(2), pp.317-322.
- Kyriakides, T.R., 1998. Mice That Lack Thrombospondin 2 Display Connective Tissue Abnormalities That Are Associated with Disordered Collagen Fibrillogenesis, an Increased Vascular Density, and a Bleeding Diathesis. *The Journal of Cell Biology*, 140(2), pp.419-430. Available at: <http://jcb.rupress.org/content/140/2/419.abstract> [Accessed October 8, 2015].

- Latreille, M. et al., 2014. MicroRNA-7a regulates pancreatic  $\beta$  cell function. *The Journal of Clinical Investigation*, 124(6), pp. 2722–35
- Lawson, K. a, Meneses, J.J. & Pedersen, R. a, 1986. Cell fate and cell lineage in the endoderm of the presomite mouse embryo, studied with an intracellular tracer. *Developmental biology*, 115(2), pp.325–39. Available at: <http://www.ncbi.nlm.nih.gov/pubmed/3709966>.
- Lawson, K. a & Pedersen, R. a, 1987. Cell fate, morphogenetic movement and population kinetics of embryonic endoderm at the time of germ layer formation in the mouse. *Development (Cambridge, England)*, 101(3), pp.627–52. Available at: <http://www.ncbi.nlm.nih.gov/pubmed/3502998>.
- Lechler, T. & Fuchs, E., 2005. Asymmetric cell divisions promote stratification and differentiation of mammalian skin. *Nature*, 437(7056), pp.275–80. Available at: <http://www.pubmedcentral.nih.gov/articlerender.fcgi?artid=1399371&tool=pmcentrez&rendertype=abstract>.
- Lee, CS. 2005. Foxa2 is required for the differentiation of pancreatic alpha-cells. *Developmental Biology*, 278(2), pp.484–95.
- Lee, J.C. et al., 2001. Regulation of the pancreatic pro-endocrine gene neurogenin3. *Diabetes*, 50(May), pp.928–936.
- Lee, S.-H. et al., 2008. Islet Specific Wnt Activation in Human Type II Diabetes. *Experimental Diabetes Research*, 2008, pp.1–13. Available at: <http://www.hindawi.com/journals/jdr/2008/728763/>.
- Levine, S. et al., 1973. Control of cell proliferation and cytodifferentiation by a factor reacting with the cell surface. *Nature*, 246(150), pp.49–52
- Lewis, S.L. & Tam, P.P.L., 2006. Definitive endoderm of the mouse embryo: Formation, cell fates, and morphogenetic function. *Developmental Dynamics*, 235(9), pp.2315–2329. Available at: <http://doi.wiley.com/10.1002/dvdy.20846>.
- Li, Y. et al., 2005. Structure of the Conserved Cytoplasmic C-terminal Domain of Occludin: Identification of the ZO-1 Binding Surface. *Journal of Molecular Biology*, 352(1), pp.151–164. Available at: <http://linkinghub.elsevier.com/retrieve/pii/S0022283605008041>.
- Li, Y. et al, 2007. Regulation of insulin secretion and GLUT4 trafficking by the calcium sensor synaptotagmin VII. *Biochemical and Biophysical Research Communication*, 362(3), pp.658–64
- Li, Z. et al., 2004. Multifaceted pancreatic mesenchymal control of epithelial lineage selection. *Developmental Biology*, 269(1), pp.252–263. Available at: <http://linkinghub.elsevier.com/retrieve/pii/S001216060400096X>.
- Lin, D. 2000. A mammalian PAR-3-PAR6 complex implicated in Cdc42/Rac1 and aPKC signalling and cell polarity. *Nature Cell Biology*, Aug;2(8):540–7
- Lickert, H., 2005. Dissecting Wnt/ -catenin signaling during gastrulation using RNA interference in mouse embryos. *Development*, 132(11), pp.2599–2609. Available at: <http://dev.biologists.org/cgi/doi/10.1242/dev.01842>.
- Liebner, S. et al., 2008. Wnt/ -catenin signaling controls development of the blood-brain barrier. *The Journal of Cell Biology*, 183(3), pp.409–417. Available at: <http://www.jcb.org/cgi/doi/10.1083/jcb.200806024>.
- Liu, B. et al., 2014. A ciliopathy with hydrocephalus, isolated craniosynostosis, hypertelorism, and clefting caused by deletion of Kif3a. *Reproductive Toxicology*, 48, pp.88–97. Available at: <http://www.sciencedirect.com/science/article/pii/S089062381400094X> [Accessed October 9, 2015].
- Lo, B. et al., 2012. Lkb1 regulates organogenesis and early oncogenesis along AMPK-dependent and -independent pathways. *The Journal of Cell Biology*, 199(7), pp.1117–1130. Available at: <http://jcb.rupress.org/content/199/7/1117.abstract> [Accessed October 8, 2015].
- Lun, M.P., Monuki, E.S. & Lehtinen, M.K., 2015. Development and functions of the choroid plexus–cerebrospinal fluid system. *Nature Reviews Neuroscience*, 16(8), pp.445–457. Available at: <http://www.nature.com/doi/10.1038/nrn3921>.
- Lynn, FC. et al, 2007. MicroRNA expression is required for pancreatic islet cell genesis in the mouse. *Diabetes*, 56(12), pp. 2938–45
- Mandai, K. et al., 1997. Afadin: A Novel Actin Filament-binding Protein with One PDZ Domain Localized at Cadherin-based Cell-to-Cell Adherens Junction. *The Journal of Cell Biology*, 139(2), pp.517–528. Available at: <http://jcb.rupress.org/content/139/2/517.abstract> [Accessed October 8, 2015].
- Scearce, L. et al., 2002. Functional genomics of the endocrine pancreas: The pancreas clone set and PancChip, new resources for diabetes research. *Diabetes*, 51(7), pp.1997–2004.
- Martens, S. et al., 2007. How synaptotagmins promotes membrane fusion. *Science*, 316(5282), pp. 1205–8
- Martin-Belmonte, F. et al., 2007. PTEN-Mediated Apical Segregation of Phosphoinositides Controls Epithelial Morphogenesis through Cdc42. *Cell*, 128(2), pp.383–397. Available at: <http://linkinghub.elsevier.com/gosmain/retrieve/pii/S0092867407000050>.
- Martin-Belmonte, F. et al., 2008. Cell-Polarity Dynamics Controls the Mechanism of Lumen Formation in Epithelial Morphogenesis. *Current Biology*, 18(7), pp.507–513.

- Martin-Belmonte, F. & Mostov, K., 2008. Regulation of cell polarity during epithelial morphogenesis. *Curr Opin Cell Biol*, 20(2), pp.227–234. Available at: [http://www.ncbi.nlm.nih.gov/entrez/query.fcgi?cmd=Retrieve&db=PubMed&dopt=Citation&list\\_uids=18282696](http://www.ncbi.nlm.nih.gov/entrez/query.fcgi?cmd=Retrieve&db=PubMed&dopt=Citation&list_uids=18282696).
- Martin-Belmonte, F. & Perez-Moreno, M., 2011. Epithelial cell polarity, stem cells and cancer. *Nature Reviews Cancer*.
- May-Simera, H.L. & Kelley, M.W., 2012. Cilia, Wnt signaling, and the cytoskeleton. *Cilia*, 1(1), p.7. Available at: <http://www.ciliajournal.com/content/1/1/7>.
- McClintock, T.S. et al., 2008. Tissue expression patterns identify mouse cilia genes. *Physiological genomics*, 32(2), pp.198–206.
- Mehta, S. & Gittes, G.K., 2005. Pancreatic differentiation. *Journal of Hepato-Biliary-Pancreatic Surgery*, 12(3), pp.208–217. Available at: <http://link.springer.com/10.1007/s00534-005-0981-4>.
- Migliorini, A., Bader, E. & Lickert, H., 2014. Islet cell plasticity and regeneration. *Molecular Metabolism*, 3(3), pp.268–274. Available at: <http://linkinghub.elsevier.com/retrieve/pii/S2212877814000155>.
- Migliorini, A. & Lickert, H., 2015. Beyond association: A functional role for Tcf7l2 in  $\beta$ -cell development. *Molecular Metabolism*, 4(5), pp.365–366. Available at: <http://linkinghub.elsevier.com/retrieve/pii/S2212877815000575>.
- Miralles, F. et al., 1998. TGF- $\beta$  plays a key role in morphogenesis of the pancreatic islets of Langerhan by controlling the activity of the matrix metalloproteinase MMP-2. *The Journal of Cell Biology*, 143(3), pp. 827–36
- Miwa, H., 2015. Generation and characterization of PDGFR $\alpha$ -GFP $\text{CreERT2}$  knock-In mouse line. *Genesis*.53(5), pp.329–36
- Morán, I. et al., 2012. Human  $\beta$  Cell Transcriptome Analysis Uncovers lncRNAs That Are Tissue-Specific, Dynamically Regulated, and Abnormally Expressed in Type 2 Diabetes. *Cell Metabolism*, 16(4), pp.435–448. Available at: <http://linkinghub.elsevier.com/retrieve/pii/S1550413112003610>.
- Morris, H.T. & Machesky, L.M., 2015. Actin cytoskeletal control during epithelial to mesenchymal transition: focus on the pancreas and intestinal tract. *British Journal of Cancer*, 112(4), pp.613–620. Available at: <http://www.nature.com/doi/10.1038/bjc.2014.658>.
- Murtaugh, L.C., 2007. Pancreas and beta-cell development: from the actual to the possible. *Development (Cambridge, England)*, 134(3), pp.427–438.
- Murtaugh, L.C., 2011. Stem Cells and  $\beta$  Cells: The Same, but Different? *Cell Stem Cell*, 8(3), pp.244–245. Available at: <http://linkinghub.elsevier.com/retrieve/pii/S1934590911000610>.
- Murtaugh, L.C. & Kopinke, D., 2008. Pancreatic stem cells. , pp.1–16. Available at: <http://www.ncbi.nlm.nih.gov/books/NBK27059/>.
- Nagy, A., 2000. Cre recombinase: The universal reagent for genome tailoring. *Genesis*, 26(2), pp.99–109.
- Nakai, H. et al., 2008. Conditional ablation of Notch signaling in pancreatic development. *Development*, 135(16), pp. 2757–65
- Nelson, W.J., 2009. Remodeling epithelial cell organization: transitions between front-rear and apical-basal polarity. *Cold Spring Harbor perspectives in biology*, 1(1), p.a000513. Available at: <http://www.pubmedcentral.nih.gov/articlerender.fcgi?artid=2742086&tool=pmcentrez&rendertype=abstract>.
- Ng, M.C.Y. et al., 2014. Meta-Analysis of Genome-Wide Association Studies in African Americans Provides Insights into the Genetic Architecture of Type 2 Diabetes. *PLoS Genetics*, 10(8), p.e1004517. Available at: <http://dx.plos.org/10.1371/journal.pgen.1004517>.
- Nieto, MA. et al., 2013. Epithelial plasticity: a common theme in embryonic and cancer cells. *Science*, 342(6159)
- Nishimura, T. et al., 2004. Role of the PAR-3–KIF3 complex in the establishment of neuronal polarity. *Nature Cell Biology*, 6(4), pp.328–334. Available at: <http://www.nature.com/doi/10.1038/ncb1118>.
- Nostro, MC. et al., 2011. Stage-specific signaling through TGF $\beta$  family members and WNT regulates patterning and pancreatic specification of human pluripotent stem cells. *Development*. 138(5)pp.861–71
- Nomme, J. et al., 2011. The Src homology 3 domain is required for junctional adhesion molecule binding to the third PDZ domain of the scaffolding protein ZO-1. *The Journal of biological chemistry*, 286(50), pp.43352–60. Available at: <http://www.pubmedcentral.nih.gov/articlerender.fcgi?artid=3234847&tool=pmcentrez&rendertype=abstract>.
- Odom, D.T. et al., 2004. Control of pancreas and liver gene expression by HNF transcription factors. *Science (New York, N.Y.)*, 303(5662), pp.1378–1381.
- Oliver-Krasinski, J.M. et al., 2009. The diabetes gene Pdx1 regulates the transcriptional network of pancreatic endocrine progenitor cells in mice. *Journal of Clinical Investigation*, 119(7), pp.1888–1898.
- Ostenson, CG., 2006. Impaired gene and protein expression of exocytotic soluble N-ethylmaleimide attachment protein receptor complex

- proteins in pancreatic islets of type 2 diabetic patients. *Diabetes*, 55(2), pp.435–40
- Osterhoff, M. et al., 2003. Ca<sup>2+</sup>/calmodulin-dependent protein kinase regulates the junctional configuration delta2 regulates gene expression of insulin in INS-1 rat insulinoma cells. *Cell Calcium*, 33(3), pp.175–84
- Otani, T. et al., 2006. Cdc42 GEF Tubulation of simple epithelial cells. *The Journal of Cell Biology*, 175(1), pp.135–146. Available at: <http://www.jcb.org/cgi/doi/10.1083/jcb.200605012>.
- Pan, F.C. & Wright, C., 2011. Pancreas organogenesis: From bud to plexus to gland. *Developmental Dynamics*, 240(3), pp.530–565.
- Pasquali, L. et al., 2014: Pancreatic islet enhancer clusters enriched in type 2 diabetes risk-associated variants. *Nature Genetics*, 46(2), pp.136–43
- Pettitt, S.J. et al., 2009. Agouti C57BL/6N embryonic stem cells for mouse genetic resources. *Nature Methods*, 6(7), pp.493–495. Available at: <http://www.nature.com/doifinder/10.1038/nmeth.1342>.
- Pictet, R.L. et al., 1972. An ultrastructural analysis of the developing embryonic pancreas. *Developmental biology*, 29(4), pp.436–467.
- Pin, CL. et al., 2001. The bHLH transcription factor Mist1 is required to maintain exocrine pancreas cell organization and acinar cell identity. *The Journal of Cell Biology*, 155(4), pp.519–30
- Piotrowska, K. & Zernicka-Goetz, M., 2001. Role for sperm in spatial patterning of the early mouse embryo. *Nature*, 409(January), pp.517–521.
- Piotrowska-Nitsche, K. & Zernicka-Goetz, M., 2005. Spatial arrangement of individual 4-cell stage blastomeres and the order in which they are generated correlate with blastocyst pattern in the mouse embryo. *Mechanisms of Development*, 122, pp.487–500.
- Poser von, C., 2001. Synaptotagmin 13: Structure and expression of a novel synaptotagmin. *European Journal of Cell Biology*, 80(1), pp.41–47. Available at: <http://www.sciencedirect.com/science/article/pii/S0171933504701168> [Accessed September 30, 2015].
- Qu, X. et al., 2013. Notch mediated post-transcriptional control of Ngn3 protein stability regulates pancreatic patterning and cell fate commitment. *Developmental Biology*, 376(1), pp.1–12
- Raducanu, A. & Lickert, H., 2012. Understanding Pancreas Development for  $\beta$ -Cell Repair and Replacement Therapies. *Current Diabetes Reports*, 12(5), pp.481–489. Available at: <http://link.springer.com/10.1007/s11892-012-0301-8>.
- Rankin, S. a. et al., 2012. Suppression of Bmp4 signaling by the zinc-finger repressors Osr1 and Osr2 is required for Wnt/  $\beta$ -catenin-mediated lung specification in Xenopus. *Development*, 139(16), pp.3010–3020. Available at: <http://dev.biologists.org/cgi/doi/10.1242/dev.078220>.
- Rodriguez-Fraticelli, a. E. et al., 2012. Cell confinement controls centrosome positioning and lumen initiation during epithelial morphogenesis. *The Journal of Cell Biology*, 198(6), pp.1011–1023. Available at: <http://www.jcb.org/cgi/doi/10.1083/jcb.201203075>.
- Rodriguez-Seguel, E., 2013. Mutually exclusive signaling signatures define the hepatic and pancreatic progenitor cell lineage divergence. *Genes and Development*, 27(17), pp.1932–46
- Ross, AJ. et al., 2005. Disruption of Bardet-Biedl syndrome ciliary proteins perturbs planar cell polarity in vertebrates. *Nature Genetics*, 37(10), pp. 1135–40
- Rudnick, a et al., 1994. Pancreatic beta cells express a diverse set of homeobox genes. *Proc. Natl. Acad. Sci. USA*, 91(December), pp.12203–12207.
- Rukstalis, J.M. et al., 2006. Transcription Factor Snail Modulates Hormone Expression in Established Endocrine Pancreatic Cell Lines. *Endocrinology*, 147(6), pp.2997–3006. Available at: <http://press.endocrine.org/doi/abs/10.1210/en.2005-1396>.
- Rukstalis, J.M. & Habener, J.F., 2007. Snail2, a mediator of epithelial-mesenchymal transitions, expressed in progenitor cells of the developing endocrine pancreas. *Gene Expression Patterns*, 7(4), pp.471–479. Available at: <http://linkinghub.elsevier.com/retrieve/pii/S1567133X06001931>.
- Sanitarias, I. et al., 2002. The Epithelial Mesenchymal Transition Confers Resistance to the Apoptotic Effects of Transforming Growth Factor  $\beta$  in Fetal Rat Hepatocytes. *Molecular Cancer Research*, 1(November), pp.68–78.
- Sato, T. et al., 2007. The Rab8 GTPase regulates apical protein localization in intestinal cells. *Nature*, 448(7151), pp.366–369. Available at: <http://www.nature.com/doifinder/10.1038/nature05929>.
- Schaffer, A.E. et al., 2013. Nkx6.1 Controls a Gene Regulatory Network Required for Establishing and Maintaining Pancreatic Beta Cell Identity. *PLoS Genetics*, 9(1), p.e1003274. Available at: <http://dx.plos.org/10.1371/journal.pgen.1003274>.
- Schwartz, M.W. et al., 2013. Cooperation between brain and islet in glucose homeostasis and diabetes. *Nature*, 503(7474), pp.59–66. Available at: <http://www.ncbi.nlm.nih.gov/pubmed/24201279>.

- Schwitzgebel, V.M. et al., 2000. Expression of neurogenin3 reveals an islet cell precursor population in the pancreas. *Development*, 127(16), pp.3533–3542. Available at: [http://www.ncbi.nlm.nih.gov/entrez/query.fcgi?cmd=Retrieve&db=PubMed&dopt=Citation&list\\_uids=10903178](http://www.ncbi.nlm.nih.gov/entrez/query.fcgi?cmd=Retrieve&db=PubMed&dopt=Citation&list_uids=10903178)<http://dev.biologists.org/content/127/16/3533.full.pdf>.
- Scott Heller, R. et al., 2004. The role of Brn4/Pou3f4 and Pax6 in forming the pancreatic glucagon cell identity. *Developmental Biology*, 268(1), pp.123–134. Available at: <http://linkinghub.elsevier.com/retrieve/pii/S0012160603007887>.
- Seaberg, R.M. et al., 2004. Clonal identification of multipotent precursors from adult mouse pancreas that generate neural and pancreatic lineages. *Nature biotechnology*, 22(9), pp.1115–1124.
- Seymour PA, et al. 2007. SOX9 is required for maintenance of the pancreatic progenitor cell pool. *Proceeding of the National Academ of Sciences of the United States of America*, 104(6), pp.1865–70
- Seymour, P. a. et al., 2008. A dosage-dependent requirement for Sox9 in pancreatic endocrine cell formation. *Developmental Biology*, 323(1), pp.19–30. Available at: <http://linkinghub.elsevier.com/retrieve/pii/S0012160608010828>.
- Seymour, P. a. et al., 2012. A Sox9/Fgf feed-forward loop maintains pancreatic organ identity. *Development*, 139(18), pp.3363–3372. Available at: <http://dev.biologists.org/cgi/doi/10.1242/dev.078733>.
- Seymour, P. a. et al., 2014. Sox9: a master regulator of the pancreatic program. *The Review of Diabetic Studies*, 11(1), pp.51–83
- Sherwood, R.I., Chen, T.Y. a & Melton, D. a., 2009. Transcriptional dynamics of endodermal organ formation. *Developmental Dynamics*, 238(1), pp.29–42.
- Shih, H.P. et al., 2015. A Gene Regulatory Network Cooperatively Controlled by Pdx1 and Sox9 Governs Lineage Allocation of Foregut Progenitor Cells. *Cell Reports*, pp.1–11. Available at: <http://linkinghub.elsevier.com/retrieve/pii/S2211124715010074>.
- Shih, H.P. et al., 2012. A Notch-dependent molecular circuitry initiates pancreatic endocrine and ductal cell differentiation. *Development*, 139(14), pp.2488–2499. Available at: <http://dev.biologists.org/cgi/doi/10.1242/dev.078634>.
- Shih, H.P., Wang, A. & Sander, M., 2013. Pancreas Organogenesis: From Lineage Determination to Morphogenesis. *Annual Review of Cell and Developmental Biology*, 29(1), pp.81–105. Available at: <http://www.annualreviews.org/doi/abs/10.1146/annurev-cellbio-101512-122405>.
- Smukler, S.R. et al., 2011. The Adult Mouse and Human Pancreas Contain Rare Multipotent Stem Cells that Express Insulin. *Cell Stem Cell*, 8(3), pp.281–293. Available at: <http://linkinghub.elsevier.com/retrieve/pii/S1934590911000166>.
- Sobrado, VR., 2009. The class I bHLH factors E2-2A and E2-2b regulate EMT. *Journal of Cell Science*.122(7), pp. 1014-24
- Sokol, S.Y., 2015. Spatial and temporal aspects of Wnt signaling and planar cell polarity during vertebrate embryonic development. *Seminars in Cell & Developmental Biology*, 42, pp.78–85. Available at: <http://www.sciencedirect.com/science/article/pii/S1084952115000993> [Accessed October 8, 2015].
- Solar, M. et al., 2009. Pancreatic exocrine duct cells give rise to insulin-producing beta cells during embryogenesis but not after birth. *Developmental Cell*, 17(6), pp.849-60
- de Sousa Lopes, S. M. C., Roelen, B. A. J., Monteiro, R. M., Emmens, R., L. & H. Y., Li, E., Lawson, K. A. and Mummery, C.L., 2004. BMP signaling mediated by ALK2 in the visceral endoderm is necessary for the generation of primordial germ cells in the mouse embryo. *Genes and Development*, 18, pp.1838–1849.
- Stanger, B.Z., Tanaka, A.J. & Melton, D. a., 2007. Organ size is limited by the number of embryonic progenitor cells in the pancreas but not the liver. *Nature*, 445(7130), pp.886–891. Available at: <http://www.nature.com/doi/10.1038/nature05537>.
- St-Onge, L., 1997. Pax6 is required for differentiation of glucagon-producing alpha-cell in mouse pancreas. *Nature*, 387(6631), pp.406-9
- Strate, I., Tessadori, F. & Bakkers, J., 2015. Glypican4 promotes cardiac specification and differentiation by attenuating canonical Wnt and Bmp signaling. *Development*, 142(10), pp.1767–1776. Available at: <http://dev.biologists.org/cgi/doi/10.1242/dev.113894>.
- Sudheer, S. et al., 2012. FGF inhibition directs BMP4-mediated differentiation of human embryonic stem cells to syncytiotrophoblast. *Stem cells and Development*, 21(16), pp. 2987-3000
- Sudhof, T.C., 2002. Synaptotagmins: Why So Many? *Journal of Biological Chemistry*, 277(10), pp.7629–7632. Available at: <http://www.jbc.org/cgi/doi/10.1074/jbc.R100052200>.
- Sugiyama, T. et al., 2006. Conserved markers of fetal pancreatic epithelium permit prospective isolation of islet progenitor cells by FACS. *Proceedings of the National Academy of Sciences of the United States of America*, 104(1), pp.175-80
- Sumi, T. et al., 2008. Defining early lineage specification of human embryonic stem cells by the orchestrated balance of canonical

- Wnt/beta-catenin, Activin/Nodal and BMP signaling. *Development (Cambridge, England)*, 135(17), pp.2969–2979.
- Sumi, T. et al., 2013. Epiblast ground state is controlled by canonical Wnt/ $\beta$ -catenin signaling in the postimplantation mouse embryo and epiblast stem cells. *PLoS one*, 8(5), p.e63378. Available at: <http://www.pubmedcentral.nih.gov/articlerender.fcgi?artid=3653965&tool=pmcentrez&rendertype=abstract>.
- Suzuki, M. et al., 2015. Plasma FGF21 concentrations, adipose fibroblast growth factor receptor-1 and  $\beta$ -klotho expression decrease with fasting in northern elephant seals. *General and comparative endocrinology*, 216, pp.86–9. Available at: <http://www.sciencedirect.com/science/article/pii/S0016648015000878> [Accessed October 8, 2015].
- Tachibana, K. et al., 2000. Two Cell Adhesion Molecules, Nectin and Cadherin, Interact through Their Cytoplasmic Domain-Associated Proteins. *The Journal of Cell Biology*, 150(5), pp.1161–1176. Available at: <http://jcb.rupress.org/content/150/5/1161.abstract> [Accessed October 8, 2015].
- Takeda, S., 2000. Kinesin Superfamily Protein 3 (KIF3) Motor Transports Fodrin-associating Vesicles Important for Neurite Building. *The Journal of Cell Biology*, 148(6), pp.1255–1266. Available at: <http://jcb.rupress.org/content/148/6/1255.abstract> [Accessed October 9, 2015].
- Tam, P.P.L. & Loebel, D.A.F., 2007. Gene function in mouse embryogenesis: get set for gastrulation. *Nature Reviews Genetics*, 8(5), pp.368–381. Available at: <http://www.nature.com/doi/10.1038/nrg2084>.
- Tamplin, O.J. et al., 2008. Microarray analysis of Foxa2 mutant mouse embryos reveals novel gene expression and inductive roles for the gastrula organizer and its derivatives. *BMC Genomics*, 9(1), p.511. Available at: <http://www.biomedcentral.com/1471-2164/9/511>.
- Tang, H. et al., 2015. SRPX2 Enhances the Epithelial-Mesenchymal Transition and Temozolomide Resistance in Glioblastoma Cells. *Cellular and Molecular Neurobiology*, Epub ahead of print.
- Tian, L. et al., 2016. Activation of pancreatic stellate cells involves an EMT-like process. *International Journal of Oncology*, 48(2), pp.783-92
- Togawa, A. et al., 2010. Hepatocyte Growth Factor stimulated cell scattering requires ERK and Cdc42-dependent tight junction disassembly. *Biochemical and Biophysical Research Communications*, 400(2), pp.271–277. Available at: <http://linkinghub.elsevier.com/retrieve/pii/S0006291X1001555X>.
- Torkko, J.M. et al., 2008. Depletion of apical transport proteins perturbs epithelial cyst formation and ciliogenesis. *Journal of Cell Science*, 121(8), pp.1193–1203. Available at: <http://jcs.biologists.org/cgi/doi/10.1242/jcs.015495>.
- Tsuboi, T. & Rutter, G. a, 2003. Insulin secretion by “kiss-and-run” exocytosis in clonal pancreatic islet beta-cells. *Biochemical Society transactions*, 31(Pt 4), pp.833–836.
- Tuncay, H. et al., 2015. JAM-A regulates cortical dynein localization through Cdc42 to control planar spindle orientation during mitosis. *Nature Communications*, 6(May), p.8128. Available at: <http://www.nature.com/doi/10.1038/ncomms9128>.
- Uetzmann, L., Burtscher, I. & Lickert, H., 2008. A mouse line expressing Foxa2-driven Cre recombinase in node, notochord, floorplate, and endoderm. *Genesis*, 46(10), pp.515–522. Available at: <http://doi.wiley.com/10.1002/dvg.20410>.
- Ullrich, B. et al., 1994. Functional properties of multiple synaptotagmins in brain. *Neuron*, 13(6), pp.1281–91. Available at: <http://www.ncbi.nlm.nih.gov/pubmed/7993622>.
- Ullrich, B. & Südhof, T.C., 1995. Differential distributions of novel synaptotagmins: Comparison to synapsins. *Neuropharmacology*, 34(11), pp.1371–1377. Available at: <http://www.sciencedirect.com/science/article/pii/002839089500132P> [Accessed September 30, 2015].
- Veland, I.R. et al., 2009. Primary Cilia and Signaling Pathways in Mammalian Development, Health and Disease. *Nephron Physiology*, 111(3), pp.p39–p53. Available at: <http://www.karger.com/doi/10.1159/000208212>.
- Velazquez-Garcia, S. et al., 2011. Activation of Protein Kinase C- in Pancreatic -Cells In Vivo Improves Glucose Tolerance and Induces -Cell Expansion via mTOR Activation. *Diabetes*, 60(10), pp.2546–2559. Available at: <http://diabetes.diabetesjournals.org/cgi/doi/10.2337/db10-1783>.
- Villasenor, A. et al., 2010. Epithelial dynamics of pancreatic branching morphogenesis. *Development*, 137(24), pp.4295–4305. Available at: <http://dev.biologists.org/cgi/doi/10.1242/dev.052993>.
- Wang, J. et al., 2005. Prox1 activity controls pancreas morphogenesis and participates in the production of “secondary transition” pancreatic endocrine cells. *Developmental Biology*, 286, pp.182–94
- Wang, S., et al. 2010. Neurog3 gene dosage regulates allocation of endocrine and exocrine cell fates in the developing mouse pancreas. *Developmental Biology*, 339, pp.26–37
- Weaver, S. a. et al., 2014. Basal localization of MT1-MMP is essential for epithelial cell morphogenesis in 3D collagen matrix. *Journal of Cell Science*, 127(6), pp.1203–1213. Available at: <http://jcs.biologists.org/cgi/doi/10.1242/jcs.135236>.

- Weinstein, D.C. et al., 1994. The winged-helix transcription factor HNF-3 $\beta$  is required for notochord development in the mouse embryo. *Cell*, 78(4), pp.575–588. Available at: <http://www.sciencedirect.com/science/article/pii/0092867494905231>.
- Wells, J.M. & Melton, D. a, 1999. Vertebrate endoderm development. *Cell Differentiation*, pp.393–410.
- Wen, H. et al., 2010. Distinct roles for two synaptotagmin isoforms in synchronous and asynchronous transmitter release at zebrafish neuromuscular junction.
- Wiedemann, C. & Cockcroft, S., 1998. The Role of Phosphatidylinositol Transfer Proteins (PITPs) in Intracellular Signalling. *Trends in endocrinology and metabolism: TEM*, 9(8), pp.324–8. Available at: <http://www.ncbi.nlm.nih.gov/pubmed/18406297>.
- Willmann, S.J. et al., 2015. The global gene expression profile of the secondary transition during pancreas development. *Mechanism of Development*, Nov 28. pii: S0925-4773(15)30037-X. doi: 10.1016/j.mod.2015.11.004
- Wittchen, E.S., Haskins, J. & Stevenson, B.R., 1999. Protein Interactions at the Tight Junction. , 274(49), pp.35179–35185.
- Wolfrum, C. et al., 2003. Insulin regulates the activity of forkhead transcription factor Hnf-3 $\beta$ /Foxa-2 by Akt-mediated phosphorylation and nuclear/cytosolic localization. *Proceedings of the National Academy of Sciences of the United States of America*, 100(20), pp.11624–11629.
- Wu, Z. et al., 2015. miR-497 inhibits epithelial mesenchymal transition in breast carcinoma by targeting Slug. *Tumour Biology*, Epub ahead of printing
- Xu, J. et al., 2009. Synaptotagmin-1 functions as a Ca<sup>2+</sup> sensor for spontaneous release. *Nature Neuroscience*, 12(6), pp.759–766. Available at: <http://www.nature.com/doi/10.1038/nn.2320>.
- Xu, J. et al., 2014. Structure and Ca<sup>2+</sup>-binding properties of the tandem C2 domains of E-Syt2. *Structure*. 22(2), pp.269-80
- Xu, Z. et al., 2011. Mapping of INS promoter interactions reveals its role in long-range regulation of SYT8 transcription. *Nature Structural & Molecular Biology*, 18(3), pp.372–378. Available at: <http://www.nature.com/doi/10.1038/nsmb.1993>.
- Xuan, S. et al., 2012. Pancreas-specific deletion of mouse Gata4 and Gata6 causes pancreatic agenesis. *Journal of Clinical Investigation*, 122(10), pp.3516–3528.
- Yang, Y. et al., 2012. MIR-18a regulates expression of the pancreatic transcription factor Ptf1a in pancreatic progenitor and acinar cell. *FEBS Letter*, 586(4), pp. 422-7
- Yamada, M. et al., 2007. Origin of Climbing Fiber Neurons and Their Developmental Dependence on Ptf1a. *Journal of Neuroscience*, 27(41), pp.10924–10934. Available at: <http://www.jneurosci.org/cgi/doi/10.1523/JNEUROSCI.1423-07.2007>.
- Yamazaki, H. et al., 1995. KIF3A/B: A heterodimeric kinesin superfamily protein that works as a microtubule plus end-directed motor for membrane organelle transport. *Journal of Cell Biology*, 130(6), pp.1387–1399.
- Yoshihara, M. & Littleton, J.T., 2002. Synaptotagmin functions as a calcium sensor to synchronize neurotransmitter release. *Neuron*, 36(5), pp.897–908.
- Zecchin, E., et al 2007. Distinct delta and jagged genes control sequential segregation of pancreatic cell types from precursor pools in zebrafish. *Developmental Biology*, 301(1), pp.192-204
- Zhadanov, A.B. et al., 1999. Absence of the tight junctional protein AF-6 disrupts epithelial cell-cell junctions and cell polarity during mouse development. *Current Biology*, 9, pp.880–888.
- Zhang, Q. et al., 2012. Intrinsic protein-protein interaction-mediated and chaperonin-assisted sequential assembly of stable bardet-biedl syndrome protein complex, the BBSome. *The Journal of Biological Chemistry*, 287(24), pp. 20625-35
- Zhang, ZW: et al., 2011. MicroRNA-19b downregulates insulin 1 through targeting transcription factor NeuroD1. *FEBS letter*, 585(16), pp. 2592-8
- Zhang, Z. et al., 2015. WNT/  $\beta$ -Catenin Signaling Is Required for Integration of CD<sub>24</sub><sup>+</sup> Renal Progenitor Cells into Glycerol-Damaged Adult Renal Tubules. *Stem Cells International*, 2015, pp.1–11. Available at: <http://www.hindawi.com/journals/sci/2015/391043/>.
- Zhou, J.X. & Huang, S., 2011. Understanding gene circuits at cell-fate branch points for rational cell reprogramming. *Trends in Genetics*, 27(2), pp.55–62. Available at: <http://dx.doi.org/10.1016/j.tig.2010.11.002>.
- Zhou, Q. et al., 2007. A Multipotent Progenitor Domain Guides Pancreatic Organogenesis. *Developmental Cell*, 13(1), pp.103–114.
- Zorn, A.M. & Wells, J.M., 2009. Vertebrate Endoderm Development and Organ Formation. *Annual Review of Cell and Developmental Biology*, 25(1), pp.221–251. Available at: <http://www.annualreviews.org/doi/abs/10.1146/annurev.cellbio.042308.113344>.
- Zorn, A.M. & Wells, J.M., 2010. Vertebrate endoderm development. , pp.221–251.



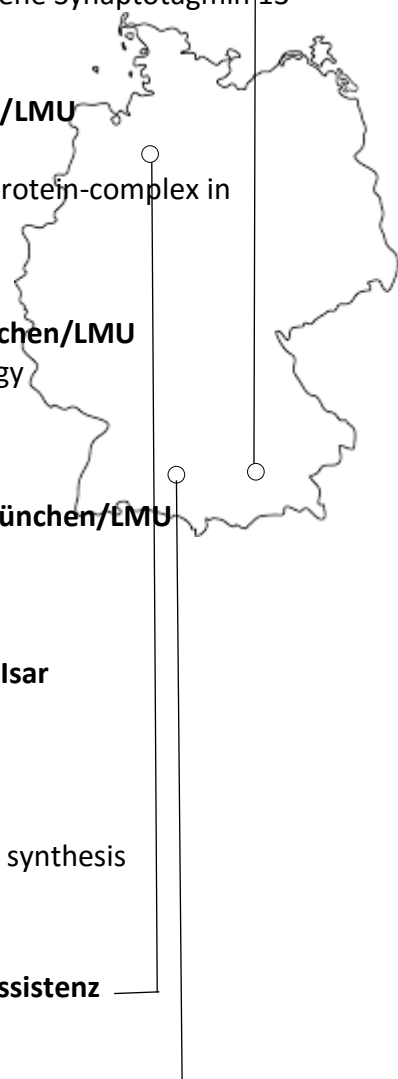
## 6.4 Curriculum Vitae

**Diploma biol. uni. Stefanie Julia Willmann**

Türkenstr. 21, 80799 München

Tel.: 0173 3277 430

Mail: SJWillmann@gmx.de

- 11/2015 - **ATV Life Science Management Seminar**  
Projectmanagement, Health management, QM and GxP, Regulatory Affairs, Pharmaceutical product approval
- 12/2010 – 12/2015 **scientific assistant/PhD candidate at the Institut für Diabetes/IDR Research/Helmholtz Center**  
Group: Heiko Lickert  
Titel: ‚Screen to identify the novel pancreatic gene Synaptotagmin 13‘
- 5/2009 – 06/2010 **diploma thesis at the Adolf Butenandt Institut/LMU**  
Group: Axel Imhof  
Titel: ‚Characterization of a heterochromatin-protein-complex in *Drosophila melanogaster*.‘
- 08/2006 – 06/2010 **Biology Ludwig-Maximilians-Universität München/LMU**  
Main courses: genetic, biochemistry, cell biology  
Certificate: Diplom
- 10/2003 – 07/2006 **Chemistry Ludwig-Maximilians-Universität München/LMU**  
Main courses: biochemistry, chemistry
- 12/2001 – 03/2003 **Institut of Humangenetic/Klinikum rechts der Isar**  
Technical Assistant in the field of Proteomics
- 08/2000 – 11/2001 **metaBion**  
Technical Assistant in the field Oligonucleotide synthesis
- 08/1998 – 07/2000 **Berufsfachschule für biologisch-technische Assistenz**  
Certificate: Biological-Technical Assistant
- 07/1996 – 07/1998 **Gymnasium für Wirtschaftswissenschaften Tuttlingen/Washington College Academy A)**  
Certificate: matriculation standard/High School Diploma
- 

## 6.6 Congresses and Publications

**Willmann SJ**, Müller NS, Engert S, Sterr M, Burtscher I, Raducanu A, Irmeler A, Beckers J, Sass S, Theis FJ, Lickert H.: The global gene expression profile of the secondary transition during pancreas development.. *Mechanism of Development*. 2015

*In preparation*: **Willmann SJ**, Müller N, Burtscher I, Raducanu A, Lickert H.: Gene regulatory networks during secondary transition of the pancreas. *Data in Brief*. 2016

*In preparation*: Bakhti M, **Willmann SJ**, Burtscher I, Lickert H.: SytXIII – a novel player in endocrine specification. *Cell Biology*. 2015

Zischka H, Gloeckner CJ, **Willmann SJ**, Swiatek-de Lange M, Ueffing M.: Improved mass spectrometric identification of gel-separated hydrophobic membrane proteins after sodium dodecyl sulfate removal by ion-pair extraction. *Proteomics*. 2004

- 03/2015           **,Pancreatic Islet workshop/DZD/Bremen – talk**
- 02/2015           **,Endoderm lineages in Development and Disease ‘/Keystone/USA – poster**
- 06/2013           **,Pancreatic Islet workshop‘/DZD/Dresden – talk**
- 03/2013           **Helmholtz Diabetes Day/ Helmholtz Zentrum/München – talk**
- 09/2013           **,Oktoberfest Symposium 2013‘/DZD/München**
- 09/2013           **,Nature Medicine Diabetes Conference‘/Nature Medicine/ München**
- 11/2013           **,International Symposium on Insulin Receptors‘/ DZD/ Barcelona – poster**
- 09/2011           **,Stem Cells in Development and Disease‘/MDC/Berlin**

## 6.7 Additional Figures

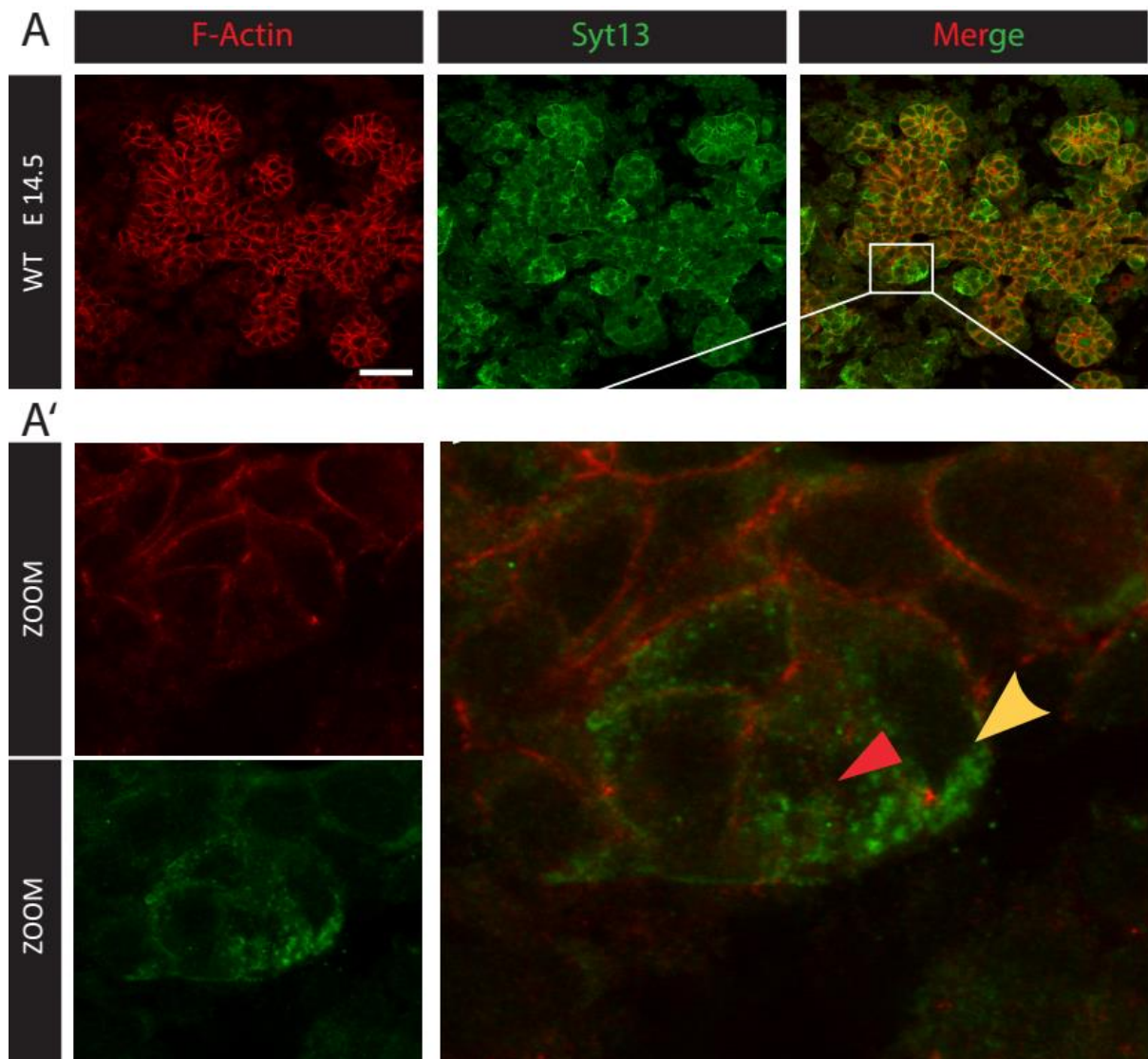


**Figure 6.1 Syt13 co-localizes to F-Actin and reveals anti-correlated expression in the process of endocrine formation**

**(A)** IHC against F-Actin and Syt13 on coronal PE section at E14.5 in the WT. All F-Actin<sup>+</sup> expressing cells in the PE express Syt13 at the onset of pancreas lineage segregation. Remarkably, F-Actin<sup>low</sup> are Syt13<sup>high</sup>, contrary F-Actin<sup>high</sup> cells express Syt13<sup>low</sup>, thus highlighting the fact that Syt13 suggests to be involved in endocrine lineage segregation (Kesavan et al., 2014; Villasenor et al., 2010).

**(A')** The Syt13<sup>high</sup>F-Actin<sup>low</sup> cells illustrate diverse Syt13 distribution within the cells in the process of lineage segregation. The apical localization shifts to random (red arrow), respective basal localization (yellow arrow) indicating that Syt13 is involved in the polarity recruitment of the endocrine progenitors. This first result highlighting the fact of EMT to MET in the process of endocrine lineage segregation, implicating a shift from AB polarity.

Scale: unknown

Abbreviations: WT = wild type; MET = mesenchymal-to-epithelial transition; EMT = epithelial-to-mesenchymal transition; Syt13 = Synaptotagmin 13; IHC = immunohistochemistry; AB = apical-basal.

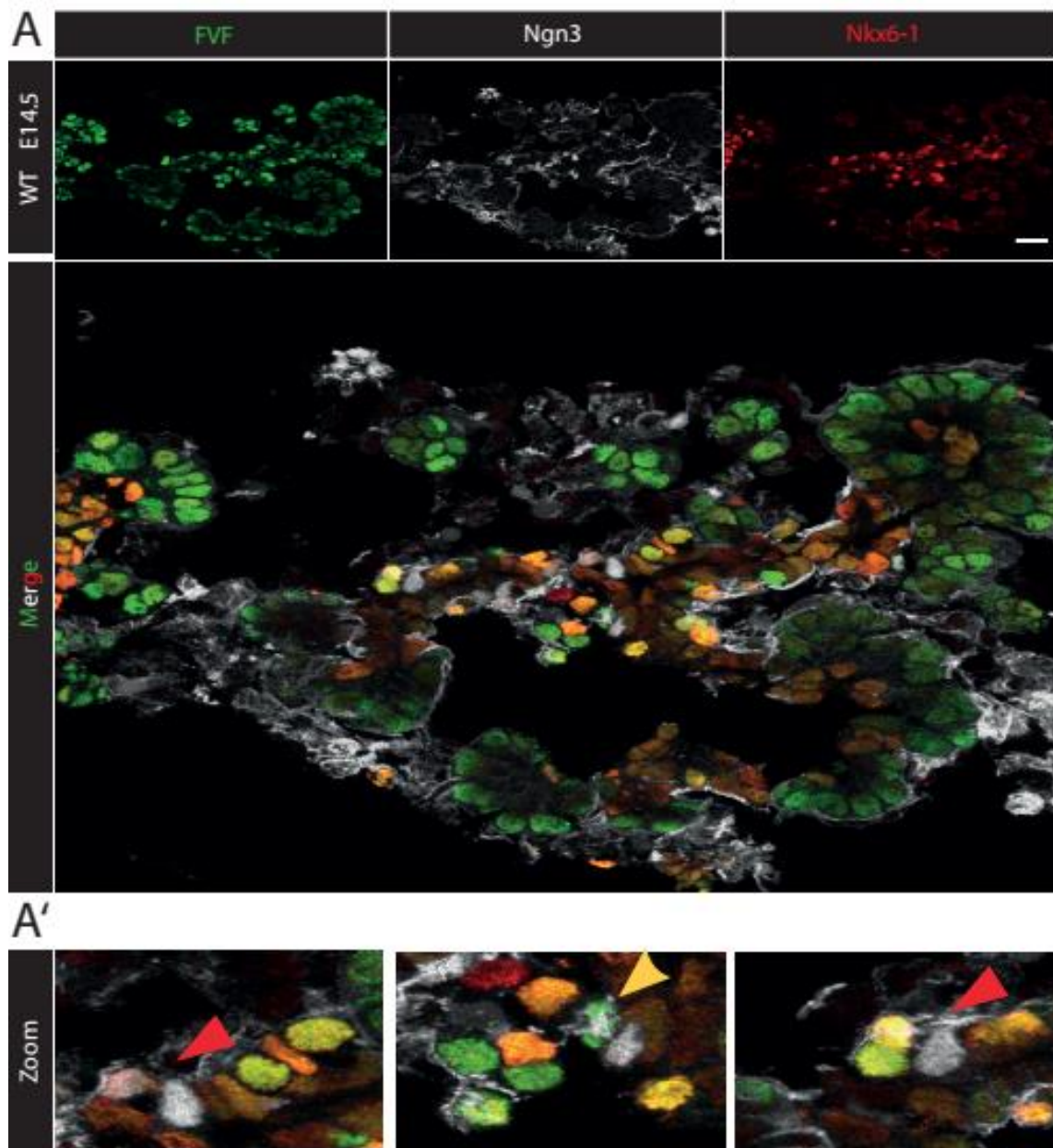


**Figure 6.1** Syt13 co-localizes to F-Actin and reveals anti-correlated expression in the process of endocrine formation

**Figure 6.** FVF, Ngn3 and Nkx6-1 co-localize in the PE in the process of lineage segregation at E14.5

(A) IHC on coronal pancreatic sections of the WT at E14.5 illustrate  $FVF^{low}Ngn3^{-}Nkx6-2^{-}$  expressing cells in the PE, whereas an endocrine precursor pool illustrates  $FVF^{high}Ngn3^{-}Nkx6-2^{+}$ , thus highlighting the fact that Syt13 is already expressed in Ngn3 lineage that endocrine progenitors are marked by  $Ngn3^{+}Syt13^{basal}$ .

(A') The Zoom into selected regions illustrate subpopulations of  $FVF^{low}Ngn3^{-}Nkx6-2^{+}$  (red arrow),  $FVF^{high}Ngn3^{-}Nkx6-2^{-}$  (yellow arrow);  $FVF^{high}Ngn3^{-}Nkx6-2^{+}$  (red arrow) suggesting on the one hand that endocrine progenitors are  $FVF^{low}Nkx6-2^{low}$ , contrary endocrine precursors are marked by the marker onset  $FVF^{high}Ngn3^{-}Nkx6-2^{+}$ . In addition, bi-potent trunk cells in the MPP of the PE at E14.5 suggests to

express  $FVF^{low}Sox9^{+}Ngn3^{-}Ecad^{+}Nkx6-1^{+}Ngn3^{-}Syt13^{apical}$ , whereas endocrine progenitors are  $FVF^{low}Sox9^{-}Ngn3^{+}Ecad^{-}Nkx6-1^{-}Syt13^{basal}$ , contrary to endocrine progenitor which are implicated by the marker onset  $FVF^{high}Sox9^{-}Ngn3^{-}Ecad^{-}Nkx6-1^{-}Syt13^{random}$ .

Scale: unknown

Abbreviations: IHC = immunohistochemistry; WT = wild type; FVF = Foxa2-Venus fusion; Ngn3 = neurogenin 3; Nkx6-1 = NK homeobox x6-1; PE = pancreatic epithelium; WT = wild type; Syt13 = Synaptotagmin 13; MPP = multipotent pancreatic progenitors; E = embryonic stage; Sox9 = Sry related homeobox 9; Ecad = E-cadherin.

At last: Syt13 is involved in remodeling and establishing polarity cues within a cell, thus it may be interesting to investigate the process of Syt13<sup>high</sup> in endocrine lineage segregation in endodermal derived organs and in the stem cell niche of the adult organs. In addition, Syt13<sup>low</sup> suggests to be involved in lumen formation, respective pancreas morphogenesis. Future experiment and collaborations, eventually with the Semb laborators with the Syt13 mouse model for PDL will bring fortune and glory, fame and eventually the nobel prize.